Masters   Engineering

2012-9

Probabilistic Analysis of Indeterminate Highway Bridges Considering Material Nonlinearity

Liam McCarthy
Technological University Dublin

Follow this and additional works at: https://arrow.tudublin.ie/engmas

Part of the Civil Engineering Commons, and the Structural Engineering Commons

Probabilistic Analysis of Indeterminate Highway Bridges Considering Material Nonlinearity

by

Liam McCarthy B.E.

School of Civil and Building Services Engineering

Dublin Institute of Technology, Bolton St, Dublin 1, Ireland

Supervisor:

Dr. Colin Caprani

MPhil Thesis

September 2012

Abstract

With ever-reducing maintenance budgets and ever-deteriorating bridge infrastructure, the assessment of existing bridges is vital. Reliability analysis techniques are becoming increasingly popular in the structural safety assessment of existing bridge structures. Commonly, a component based approach is used in reliability analysis techniques. Traditional reliability procedures often employ a conservative definition of failure, in that the component is deemed to have failed when the strength capacity has been exceeded at a single cross section. As a result, the component's degree of redundancy and ductility is ignored, giving an often conservative estimate of the load carrying capacity of the bridge component. Therefore, this dissertation is focused on the development of a reliability analysis procedure which accounts for material behaviour for indeterminate beams.

The structural safety of a representative group of steel composite bridge beams is examined. The material response of each beam subjected to a combination of both dead load and live load is assessed using a one-dimensional nonlinear finite element analysis (NFEA) model. The Response Surface Method (RSM) is then used to replace the NFEA model with an approximated explicitly-known polynomial function. This allows a First Order Reliability Method (FORM) analysis to be performed. The developed procedure is compared to the traditional approach with regard to three limit states. These limit states are defined as elastic member failure, first formation of a plastic hinge and ultimate failure. Ultimate failure occurs when a collapse mechanism has formed. The live load on each structure consists of annual maximum traffic loading events determined from Monte Carlo Simulation (MCS) of Weigh-in Motion (WIM) data. The modelling of realistic live loads highlights the practicality of the procedure developed. This procedure may act as a foundation for the development of an evaluation method accounting for material nonlinearity for existing bridge structures.

Declaration

The author hereby declares that this thesis, in whole or part, has not been used to obtain any degree in this, or any other, university. Except where reference has been given in the text, it is entirely the author's own work.

The author confirms that the library may lend or copy this thesis upon request, for academic purposes.

_____

Liam McCarthy

September 2012

Acronyms

AASHTO-LRFD   American Association of State Highway and Transportation Officials-Load and Resistance Factor Design

AS   Axle Scenario

BB   Box-Behnken

CCC   Central Composite Inscribed

CCD   Central Composite Design

CCF   Central Composite Face

CDF   Cumulative Density Function

ED   Experimental Design

FEA   Finite Element Analysis

FORM   First Order Reliability Method

FOSM   First Order Second Moment

GEV   Generalized Extreme Value

GVW   Gross Vehicle Weight

LM1   Load Model 1

MCS   Monte Carlo Simulation

MPP   Most Probable Point

NFEA   Nonlinear Finite Element Analysis

PDF   Probability Density Function

RSM   Response Surface Method

SEV   Standard Extremal Variate

VaP   Variables Processor

WIM   Weigh in Motion

Nomenclature

Unless the additional specification appears in the text, the physical or mathematical definitions of the symbols in this thesis are as follows:

Variable	Definition
β	Reliability index
β_n	Cumulative reliability index
β_{LT}	Life-time reliability index
D_1	Dead load due to factory made elements
D_2	Dead load due to cast in place elements
D_3	Dead load due to surfacing
E	Young's modulus
f_x	Probability density function
F_x	Cumulative density function
F	External force vector
g	Limit state function
$\breve{g}$	Taylor series expansion of the limit state function
h	Response surface method experiment design dispersion
h_v	Importance sampling function
$I[\ ]$	Indicator function

I	Second moment of area
K	Global stiffness matrix
k_e	Local stiffness matrix
L	Length
L_S	Span length
L_T	Total bridge length
M_Y	Initial yield moment capacity
M_P	Plastic moment capacity
N	Number of samples
P_f	Probability of failure
P_{fn}	Cumulative probability of failure
P	Point load
q	Strain hardening
R	Resistance
S	Load
U^*	Most probable point of failure
u	Displacement vector
w	Universally distributed load
x_m	Response surface method centre point
x_d	Response surface method design point

α_D	Dead load safety factor
α_L	Live load safety factor
ε	Convergence tolerance
Γ	Yield function
μ	Location parameter
μ_x^e	Equivalent-normal location parameter
σ	Scale parameter
σ_x^e	Equivalent-normal scale parameter
ξ	Shape parameter
λ_{LT}	Life-time load factor
ϕ	Resistance factor

Acknowledgements

This work has been carried out under the supervision of Dr. Colin Caprani. I would like to thank him for his guidance and advice throughout. His enthusiasm, experience and attention to detail contributed greatly to this work. He has gone above and beyond the role of a supervisor and for this I am extremely appreciative.

I would also like to thank Professor Eugene O'Brien, whose recommendations helped steered the direction of this work.

I would like to express my appreciation to all the staff in the Dublin Institute of Technology, in particular John Turner and Dr Marek Rebow, whom without this work would never have been completed. I owe special thanks to Michael Faherty for use of the computer labs in DIT.

Special thanks are given to Colm Carey, Joe Keogh, Conor Briody and Neal Renehan for their help and encouragement throughout the last two years. I wish them all the best in their future careers.

I would like to express my sincere gratitude to my parents, Alex and Frances. Thank you for supporting me throughout my education. For this I am truly grateful.

To Laura, Catríona and Brian, thank you for the encouragement over the last two years.

Finally I would like to extend my deep appreciation to Emer Skelly, her positivity, kindness and patience are outstanding and for that I am forever thankful.

Table of Contents

Chapter 1

Introduction

1.1   Background

Highway bridge structures are a fundamental component of today's infrastructure. These bridge structures allow people and goods to move freely between locations allowing both economic and social development. As bridge stock is ever-deteriorating, appropriate assessment techniques and procedures are vital. Better assessment of existing highway bridge structures can prolong the life of such structures with consequent and significant savings to rehabilitation and replacement budgets. Currently there are over one million bridge structures in Europe with a total estimated replacement cost of €400 billion (Cost 345, 2004).

Many European bridges are nearing the end of their design lives and hence require regular maintenance or even replacement. Bridge maintenance and assessment is a growing concern due to reducing financial budgets. Accurate bridge assessment is therefore a necessity, as it is no longer acceptable to assess a bridge structure using excessive conservatism.

Parsons Brickenhoff carried out a survey entitled "A Review of Bridge Assessment Failures on the Motorway and Trunk Road Network" in 2003. This survey was the appraisal of assessment results from 294 bridge structures in the United Kingdom. The modes of failure examined in the bridge assessments included longitudinal flexure, transverse flexure and shear. This survey found that the most common reason for assessment failure was "conservative or inappropriate methods of assessment" (Parsons Brickenhoff, 2003). This finding highlights the requirement for a less conservative assessment procedure. Traditionally in bridge assessment failure is deemed to occur when the load effects calculated using a linear elastic structural model exceed the resistance of a particular cross section. Whilst this is

a safe approach by virtue of the well-known Lower Bound Theorem, it may lead to unacceptably conservative results. Many bridges are redundant structures and so if the resistance of one element in the structure has been reached, the bridge may yet be able to redistribute the load elsewhere. This is dependent on the nonlinear behaviour of materials such as steel (Imhof, 2004).

1.2   Research Objectives

This research embodies three main subject areas: structural reliability, nonlinear finite element modelling, and response surface methodology. These subject areas are combined to achieve three objectives;

1.2.1   Objective 1: Live Load Application in a Nonlinear Assessment

A nonlinear assessment procedure of a moving load is developed. Typically live loads are modelled as static loads positioned according to an elastic analysis. Since the principle of superposition is not valid for a nonlinear assessment, load must be applied incrementally, so as the spread of plasticity can be accounted for. The proposed moving procedure also applies the load incrementally but also incrementally moves the load across the structure. This allows for the spread of plasticity as the load traverses the structure. The common approach is compared to the proposed moving approach in terms of a load factor. The load factor is the multiple of axle loads required to cause failure. Failure is defined as the formation of a mechanism. This comparison indicates the effects of accounting for load redistribution as the load is moving across the structure.

1.2.2 Objective 2: Deterministic Safety Assessment

A deterministic safety assessment of existing bridge beams is performed. Safety is described in terms of a load factor required to cause failure. Only flexural limit states describing failure are examined. Three limit states which are used in this study are:

1. The exceedance of the initial yield capacity at any section.

2. The formation of a plastic hinge at any section.

3. The formation of a collapse mechanism.

A number of representative bridge structures are designed to the required minimum flexural capacity. These bridges are subjected to a lifetime of annual maximum loading events. These traffic events are determined using MCS of WIM data. A load factor for each definition of failure for each loading event is found. These results are then combined in a semi-probabilistic manner to determine the lifetime load factor. This is done using a limit state extrapolation technique. The Eurocode for bridge loading suggests that a return period of 1000 years is suitable. The annual load factors are converted to limit state values and extrapolated to find the 1000 year value. From this the 1000 year load factor is found. A value less than unity indicates failure of the corresponding limit state. In particular, a lifetime load factor for the initial yield capacity limit state below unity signifies that material nonlinearity is present thus an elastic structural model is inappropriate for a reliability analysis for such cases.

1.2.3 Objective 3: Probabilistic Safety Assessment

This research aims to develop a structural safety assessment procedure which incorporates a nonlinear structural model into a probabilistic assessment of an existing highway bridge structure. By doing so, the structure may be assessed in terms of true collapse rather than failure at a single cross section. This allows for the longitudinal redistribution of loads due to

the redundant capabilities of the structure, thus providing a more accurate assessment of the true structural safety. RSM is used to link a NFEA model with a conventional reliability analysis. RSM is used because a closed form limit state function cannot be expressed and failure can only be identified using a NFEA model. This method replaces the NFEA model by approximating a polynomial function, allowing a FORM calculation to be completed. The reliability indices found using the proposed approach are compared to those found using the conventional approach thus describing the importance of accounting for material behaviour.

1.3   Research Methodology

To address the objectives of this research the following approach is used. A one-dimensional NFEA model is developed. A representative group of steel composite bridge structures is designed according to the minimum prescribed Eurocode flexural capacity. Two-span and three span configurations of bridge lengths 30, 40, 50 and 60 m are examined. The proposed nonlinear moving load procedure is compared to the commonly used approach of applying the live load statically at positions identified using the elastic analysis in terms of a load factor needed for a collapse mechanism to form (Objective 1). Using a grillage model of each structure, lane distribution factors for each longitudinal beam are calculated. Critical beams are identified as those carrying the majority of the bending moment. Using MCS based on WIM data a lifetime of annual maximum loading events are determined. A load factor for each limit state is found for each annual maximum loading event (Objective 2). The lifetime load factor is then found using extrapolation techniques (Objective 2). A FORM model which is commonly used to assess structural safety is developed (Objective 3). The NFEA is connected to a FORM model using RSM. A reliability analysis accounting for material behaviour is performed for each critical beam identified in the representative group of steel composite bridge structures.

1.4   Thesis Structure

The second chapter of this thesis consists of a literature review of typical reliability assessments, system reliability assessments and probabilistic assessments considering nonlinear material behaviour. An introduction into structural reliability theory is outlined in Chapter 3. This chapter also contains the FORM model developed and demonstrated on three bench mark examples. Chapter 4 presents the development of a one dimensional NFEA model. The model is validated and its accuracy checked against the established results. The RSM is introduced in Chapter 5. The model developed in this study is outlined. Three benchmark examples from the structural reliability literature are used to validate the model. Chapter 6 describes the bridge models used complete with simple flexural capacity design and the identification of a critical beam using a grillage model. Chapter 7 outlines the experiments, methodology and results obtained in achieving Objective 1 which assesses the application of live load in a nonlinear assessment used in reliability analysis. The deterministic structural safety assessment procedure and the results found for the representative group of steel composite bride structures are explained in Chapter 8. Chapter 9 describes the methodology used to incorporate a nonlinear structural model into a reliability assessment and compares this technique to the commonly used approach. Conclusions found for each of the objectives are outlined in Chapter 10. Suggestions for possible further work are also discussed in this chapter. Figure 1.1 shows how each Chapter is connected in achieving the desired objectives.
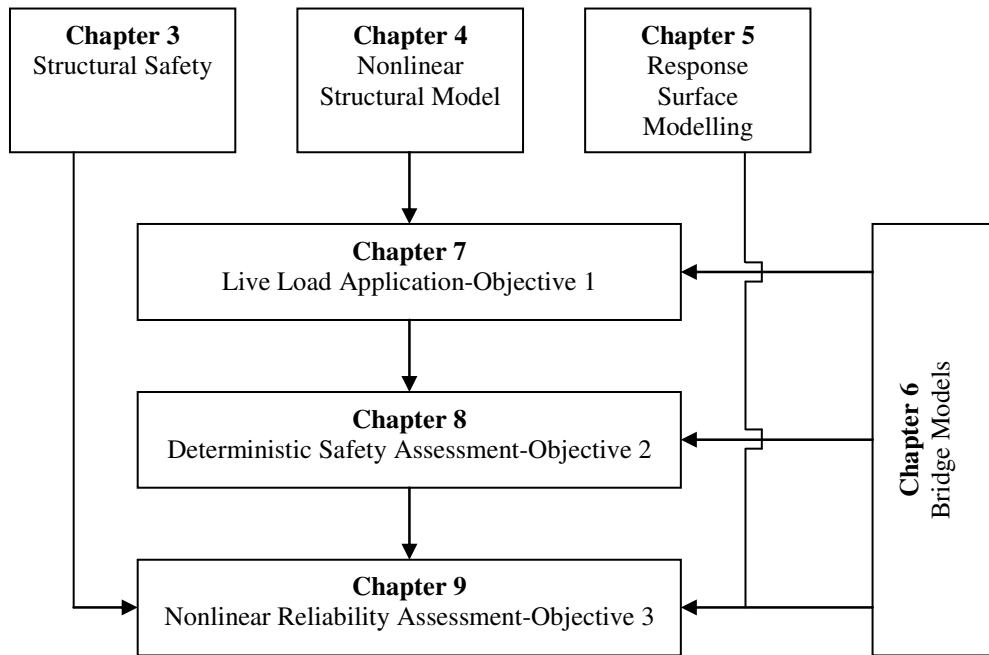
Figure 1.1: Chapter Interrelation

Chapter 2

Literature Review

2.1 Introduction

In this chapter a literature review of probabilistic assessments of existing bridge structures is given. Reliability assessments, system reliability assessments and probabilistic assessments considering nonlinear material behaviour are reviewed. All studies examine the probability of flexural failure. The application of live load in probabilistic assessments of existing bridge structures is also discussed.

2.2 Reliability Analysis of Existing Bridge Structures

Parsons & Brickenhoff (2003) investigated assessment failures of 294 bridge structures located throughout the United Kingdom and confirmed that longitudinal flexure is a predominant mode of bridge failure. This form of failure has been studied extensively in probabilistic assessments of existing highway bridge structures. Nowak et al (2001) compared the reliability of the flexural capacity of prestressed concrete bridge beams designed using three design codes (Spanish Norma IAP-98 1998, AASHTO LRFD 1998, EN 1991-3 Eurocode). Similarly Du et al (2005) repeated this study examining Chinese, Hong Kong and AASHTO-LRFD design codes. Ferreira et al (2008) examines moment capacity of various structures in Brazil and uses reliability theory to develop truck weights restrictions. Park et al (1998) examined how different rates of corrosion can affect the moment limit state over time.

Importantly, in the probabilistic assessments mentioned, elastic structural models are typically used to determine the moment applied to the structure. These studies used a component-based approach because each structure is deemed to have failed when the applied

moment exceeds the resistance at a single cross section of a component (i.e. longitudinal beam). Since ultimate flexural failure occurs when a collapse mechanism forms, this approach is correct for these studies (Park et al, 1998; Nowak et al, 2001; Du et al, 2005; Ferreira et al, 2008) which consider only single span structures. However, if these studies were extended to indeterminate structures, the use of an elastic structural model would ignore load redistribution due to nonlinear material behaviour and ultimate failure would not occur (i.e. the formation of a collapse mechanism) due to the Lower Bound Theorem (Ghali et al, 2009). Load redistribution can be accounted for by incorporating a nonlinear structural model into a probabilistic assessment. The valuable extra capacity offered by redistribution of moments could then be realised, and this may make the difference between retention or replacement of a bridge.

2.3   System Reliability Analysis

A nonlinear structural model can be used to determine the resistance of a structure accounting for longitudinal and transverse load redistribution. This resistance can then be used in a probabilistic assessment. This methodology, known as system reliability, is based on the fact that structural components of a bridge do not act independently; rather they interact to form a structural system. This system may have a high level of redundancy and so it is still capable of carrying a load even after one member or section has failed.

Design codes tend to ignore the concept of system reliability, instead adopting an understandably conservative approach to design. However, such conservatism is not warranted when assessing existing bridges as it may result in bridge replacement when bridge rehabilitation would suffice. Consequently, substantial savings can be made to bridge maintenance if system reliability is employed in bridge assessment. The resistance of the

bridge as a whole combines the resistances of the individual bridge girders, the slab and a contribution from the secondary components such as footpaths, kerbs and barriers.

Nonlinear material behaviour is accounted for in system reliability when determining the resistance of the structure. The resistance of a structural system is defined as the maximum load that the bridge can carry before a defined failure has occurred. Ghosn et al (1998) uses the formation of a collapse mechanism as the definition of failure. Czarnecki et al (2007) defines failure to occur when deflection exceeds an arbitrary limit (0.0075 of the span length). Other studies describe failure to occur when the ultimate capacity has been reached in a number of bridge girders (Tabsh et al, 1991; Estes et al 1999; Liu et al, 2001). Once a structure's resistance is found, it can be combined with an assessment load model to determine the probability of failure. It is beneficial to account for the load redistribution in structural reliability calculations as a truer representation of the structures safety can be established (Czarnecki et al, 2007).

The drawback with system reliability is that a linear elastic structural model has been used in the referenced studies to calculate the desired load effect. This presumes that a structure behaves elastically for all loading events which may not be true when examining extreme traffic loading events. This study aims to incorporate a nonlinear structural model to assess loading rather than to determine the resistance as used in system reliability.

2.4   Probabilistic Studies Considering Nonlinear Material Behaviour

Methods of incorporating a nonlinear structural model into a probabilistic assessment can be categorized following Haldar et al (2000) to be:

1. Monte Carlo Simulations (MCS)

2. Sensitivity Analysis

3. Response Surface Method (RSM)

2.4.1 Monte Carlo Simulation

MCS including efficient sampling methods such as Importance Sampling, can produce high levels of accuracy (Choi et al, 2007). Biondini et al (2004) applied this technique to assess the probability of failure of an existing arch bridge accounting for material and geometrical nonlinearities. However, only notional live loads are applied to the structure. A disadvantage to MCS is that it requires extensive computational expense when dealing with low probabilities of failure (Melchers, 1999). Low probabilities of failure are expected with structural collapse and for this reason other methods of incorporating a nonlinear structural model in a probabilistic assessment are examined.

2.4.2 Sensitivity Analysis

Sensitivity analysis can be used in a probabilistic assessment accounting for nonlinearities, but is not easily adaptable to practical problems (Wisniewski et al, 2009). Despite this, it has been successfully implemented by Val et al (1997b) when examining the structural safety of reinforced concrete slab bridges considering material nonlinearity. However, the work of Val et al (1997b) is limited to notional live load models.

2.4.3 Response Surface Method

The RSM uses a polynomial function to approximate an unknown limit state function representing a nonlinear structural model, thereby allowing a closed-form probabilistic analysis such as FORM to be carried out. The method results in significantly-reduced computational expense but may prove ineffective when dealing with highly nonlinear limit states, or for problems with multiple modes of failure (Wisniewski et al, 2009). Despite this, the RSM is the chosen method for incorporating a nonlinear structural model into a probabilistic assessment for this work. The drawbacks are mitigated by only considering one mode of failure at a time, and by using stringent convergence checks on the limit state.

Since the introduction of RSM in the 1950s, it has been used in a wide variety of fields; for example, chemical engineering, agriculture, chemistry, and mechanical engineering (Box, 1978; Bucher et al, 2008). Rackwitz (1982) was one of the first to suggest applying the RSM to structural reliability. Since then its use in structural problems has increased and has been used in many recent studies (Neves et al, 2006; Soares et al, 2002).

An example where the RSM has proven efficient in assessing a bridge structure is Wong et al (2005) in which the probability of failure of a five-beam reinforced concrete single span bridge considering transverse load redistribution is calculated. This study by Wong et al (2005) is limited to notional live load models but provides an introduction into the methodology required to conduct a probabilistic assessment of existing structures subjected to realistic traffic events for collapse.

2.5   Live Load Application

2.5.1   Linear Structural Models

When linear elastic structural models have been used in reliability assessments, the live load on a structure has been applied as a notional load (Jeong et al, 2003; Estes et al, 2005; Marková, 2010); for example, as the AASHTO HS20 design truck (Tonias, 2007) or as the Eurocodes Load Model 1(LM1) (EC1.2, 2003). These notional load models are necessarily conservative since they must give sufficient safety for a wide geographical area, which can include vastly different traffic regimes. A more accurate approach to representing the live load is to apply site-specific traffic data to a published load model, such as was done by Ghosn et al, 1986; Cooper, 1997; and Nowak, 1999. Using Weigh-In-Motion (WIM) the necessary statistical parameters can be found to develop site-specific loading models (Cost 345, 2004). From WIM systems truck configurations (number of axles and axle spacing) and weights (axle weights and gross vehicle weight) are recorded. By fitting statistical

distributions to this WIM data and using MCS, traffic loading events can be generated. For each loading event, generated load effects are calculated using a linear elastic structural model. Maximum load effects in the bridge lifetime are determined using extrapolation techniques. Studies employing this approach include Park et al, 1998; Nowak et al, 2001; Du et al, 2005; and Ferreira et al, 2008. Similarly to these studies, this work will also examine realistic traffic loading events generated from WIM data. However, each event will be assessed using a nonlinear structural model.

2.5.2   Nonlinear Structural Models

Traditionally in a nonlinear structural analysis, live loads are applied as static loads. An example of this is the work of Choudhury et al (1986). The author presents a numerical procedure for the analysis of curved nonprismatic reinforced and prestressed concrete box girder bridges considering material nonlinearity. Choudhury demonstrates the procedure on a three-span prestressed structure subjected to an overloaded vehicle typical of California's highway traffic at that time. While the author does investigate the effect of transverse load positioning, the load is applied longitudinally as a static load located in the centre of the middle span of the structure.

Generally live loads are applied as static loads positioned using an elastic analyses, i.e. the loads are positioned to cause maximum desired load effect determined using an elastic analysis. Studies using this approach include Val et al, 1997a; Ghosn et al, 1998; and Czarnecki et al, 2007. The choice of load effect is under the discretion of the author. Val et al (1997b) investigates four longitudinal positions of a HS20 design truck, located to cause maximum bending moment at defined cross sections of the bridge. They incorporate a nonlinear structural model into a reliability assessment of a three-span reinforced concrete slab bridge with corroded reinforcement. Similarly, Zona et al, (2010) deems the positions of

the two bogey axles in Eurocode LM1 causing maximum elastic bending moment in a three-span beam at the first interior support as critical. They perform a probabilistic analysis of a three span continuous steel-concrete composite girder considering nonlinear material behaviour to efficiently design a continuous steel composite bridge girder. Ghosn et al (1998) developed a framework for considering structure redundancy in a load capacity evaluation. The framework employs system reliability to account for nonlinear behaviour of the structure. An essential step to this framework is the identification of critical load positions of the HS20 design truck causing maximum desired load effects, which is done using an elastic analysis. Similarly Czarnecki et al (2007) applies a similar approach when examining the system reliability of a single-span steel composite structure.

Casas et al (2007) highlights that a linear elastic structural model may not always identify important loading positions as resistance properties of the structure are ignored. Nonetheless the study locates the static loads according to an elastic analysis in the reliability assessment of railway bridge structures. Likewise, Wisniewski et al (2009) apply the load due to train traffic at positions causing overall maximum bending moment in a three-span structure.

All of these studies apply live loads as statically-located loads. This approach therefore assumes that load redistribution, as a load traverses across the structure, is negligible. The first objective of this work is to assess this assumption. A proposed moving load approach is developed and compared to the commonly-used approach of applying the live loads as static loads, located according to an elastic analysis, to cause a 'critical' (by some definition) value of load effect.

Chapter 3

Structural Reliability

3.1   Introduction

This chapter provides an introduction to reliability theory. A basic description of popular simulation techniques and reliability index methods is provided. Also given is the development and validation of a FORM model.

Structural reliability is a measure of the safety level of a structure and is concerned with the calculation of the probability of a defined failure. This involves the selection of a limit state function, the identification of the variables involved in that function, a description of the statistical parameters of each variable (usually mean and variance) and the calculation of the probability of violation of that limit state function.

3.1.1   Limit States

A limit state is a function which describes the performance of a structure or a component. Failure is often deemed to occur when an applied load effect (S) is greater than the structural resistance (R) giving a limit state function (g) of:

$$g = R - S \leq 0 \tag{3.1}$$

Generally limit states are divided into two categories (Melchers, 1999): The first category is ultimate limit states which relate to collapse of part or all of the structure. Examples include corrosion, deterioration, and collapse mechanism formation. These limits states should have a low probability of failure as there are significant consequences, if failure occurs, such as loss of life. The second category is serviceability limit states which include limit states which may cause a disruption to the regular use of the structure such as excessive deflection or vibration.

3.1.2 Probability of Failure

For the basic structural problem outlined in Equation (3.1), the probability of failure can be defined as follows (Melchers, 1999):

$$P_f = \int \cdots \int_{g(x) \leq 0} f_x(x)\, dx \qquad (3.2)$$

This can be rewritten as:

$$P_f = \iint I\left[g(r,s) \leq 0\right] f_R(r) f_S(s)\, drds \qquad (3.3)$$

where $I[\ ]$ is an indicator function which takes on a value of unity if the term in the brackets is true, or zero if the term in the brackets is false, f_R and f_S are the probability density functions of resistance and load respectively. In essence therefore, Equation (3.3) sums the joint probability of violating the limit state function over the design space, i.e. over the full range of the variables R and S.

Equation (3.3) can be solved quite easily when only one load and one resistance parameter are present. However, practical problems typically consist of more than two variables; therefore either a simulation technique or a reliability index technique is needed to solve the integral. Simulation techniques use direct experimentation to obtain probabilistic information of the defined problem. Generally simulation techniques such as MCS are associated with high computational expense but improved sampling methods such Importance Sampling have been developed to increase efficiency. Reliability index techniques such as FORM simplify the integral in Equation (3.2) and the limit state function (Equation (3.1)) by converting both into standard normal space. This simplification allows for an accurate estimation of the probability of failure to be made with a reduction in computational expense.

3.2 Simulation Techniques

3.2.1 Monte Carlo Simulation

The MCS method is the most direct method of calculating the probability of failure. Samples of the random variables are generated and the limit state function evaluated for each set. The probability of failure is calculated as a ratio of the number of fails to the number of trials, and can thus be given by:

$$P_f = \frac{1}{N}\sum_{j=1}^{N} I[g(x) \le 0] \tag{3.4}$$

where N is the total number of samples, $I[\ ]$ is the indicator function and $g(x)$ is the limit state function value. The accuracy of the MCS method increases with the number of trials (Melchers, 1999). However, this becomes unpractical when the indicator function in Equation (3.4) requires a computationally expensive numerical analysis such as a finite element calculation. Thus, this approach is inefficient when dealing with low probabilities of failure because a very large sample set is required. However, it has been implemented in numerous structural problems (Biondini et al, 2004).

3.2.2 Importance Sampling

Importance Sampling is an extension of MCS and can produce an accurate estimate of the probability of failure with a significantly reduced number of samples. If sampling occurs around random variables that are more likely to contribute to the probability of failure fewer samples are required. This is achieved by using a biased sampling distribution. This bias is then corrected for by weighting the outputs of the simulation. The probability integral is therefore:

$$P_f = \int \ldots \int I[g(x) \le 0] \frac{f_X(x)}{h_v(x)} h_v(x) dx \tag{3.5}$$

where $h_v(x)$ is the importance sampling function. It is common to use a normal distribution for the importance sampling function with the mean shifted to the Most Probable Point (MPP) of failure. The MPP is the point with the highest probability of occurrence on the limit state function $(g = 0)$ (Melchers, 1999). The location of the MPP is generally not known, difficult to locate, and requires a prior analysis to locate it such as a numerical maximization technique. However, once it is known the integral in Equation (3.5) can then be estimated using:

$$P_f = \frac{1}{N} \sum_{i=1}^{N} \left(I\left[g(x) \le 0\right] \frac{f_x(x)}{h_v(x)} \right)$$

(3.6)

3.3   Reliability Index Methods

3.3.1   Cornell's Reliability Index

Cornell (1967) defined the reliability index (β_C) as the ratio of the expected value of the limit state (μ_g) over its standard deviation (σ_g). For a two variable limit state (Equation(3.1)), the Cornell's reliability index assuming both variables are normally distributed can be written as:

$$\beta_C = \frac{\mu_g}{\sigma_g} = \frac{\mu_R - \mu_S}{\sqrt{\sigma_R^2 - \sigma_S^2}}$$

(3.7)

The mean and standard deviation of the variables are μ and σ respectively. The probability of failure (P_f) and the reliability index are related:

$$P_f = \Phi(-\beta_C)$$

(3.8)

where Φ is the standard normal cumulative distribution function. The reliability index is a measure of the distance from the expected value of the limit state (μ_g) to failure $(g(x)=0)$. This is illustrated in Figure 3.1.
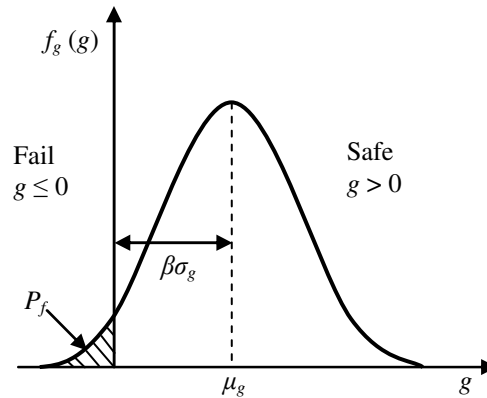

Figure 3.1: Cornell reliability index (adapted from Choi et al, 2007).

The shaded area on the diagram represents the probability of failure. The distance acts as a good representation and is written in terms of the scale parameter of the limit state function values (σ_g) (Choi et al, 2007).

This was the first analytical approximation method which could determine the probability of failure. This method was acknowledged to be inaccurate (Box, 1978). However, Lind (1973), cited by Box (1978), highlights how Cornell's model could be applied to establish safety factors for design. The work of Cornell provided a foundation for the development of further reliability index techniques.

3.3.2   First Order Second Moment Method

The work of Cornell (1969) led to the development of the First Order Second Moment (FOSM) method. This method uses a Taylor series expansion $(\breve{g})$ of the limit state function around the mean values (μ_x) of the random variables (x) so as the problem can be extended to more than two variables:

$$\breve{g} = g(\mu_x) + \sum_{i=1}^{n} \frac{\partial g}{\partial x_i}(x_i - \mu_i) \qquad (3.9)$$

The series is truncated at the linear terms in the FOSM and hence the name first order. The second moment (variance) is the highest-order statistical result used. The approximate mean value and the variance of $(\breve{g})$ can then be written as follows:

$$\mu_{\breve{g}} \approx g(\mu) \qquad (3.10)$$

$$\sigma_{\breve{g}} = \sqrt{\sum_{i=1}^{n} \left(\frac{\partial g(\mu_x)}{\partial x_i} \right)^2 \sigma_{x_i}^2} \qquad (3.11)$$

If a second order Taylor series expansion is used, the method is referred to as the Second Order Second Moment (SOSM) Method. This study does not extend to this method. As the expansion occurs at the mean point of the variables the FOSM is also referred to as the Mean Value FOSM. The FOSM reduces the complexity of the problem and forms direct links between the reliability index and the basic parameters (mean and standard deviation). Two major drawbacks with this approach are: 1) errors occur when linearising highly nonlinear limit state functions and; 2) invariance of different, yet mathematically-equivalent, formulations of the same problem is not established (Choi, 2007).

3.3.3   First Order Reliability Method

<u>Hasofer and Lind Reliability Index</u>

The invariance problem associated with the FOSM method was solved by the development of the Hasofer-Lind Reliability Index. The Hasofer-Lind Reliability Index (β_{HL}) represents the shortest distance from the origin to the limit state function in standard normal space as shown in Figure 3.2. The random variables are transformed from their original space (*X*-space) to the standard normal space (*U*-space). This type of transformation is termed the Rosenblatt

transformation (Choi et al, 2007) and is based on equating the cumulative distribution functions of the random variables throughout the transformation. For example if the variables are normally distributed they are transformed as follows:

$$U = \Phi^{-1}\left[F_x(X)\right] = \Phi^{-1}\left[\Phi\left(\frac{X-\mu}{\sigma}\right)\right] = \frac{X-\mu}{\sigma} \tag{3.12}$$

where Φ is the standard normal cumulative distribution function (CDF), Φ^{-1} is the inverse of the standard normal CDF, $F_x(X)$ is the CDF of variable X, μ_x is the mean value of X and σ_x is the standard deviation of X.
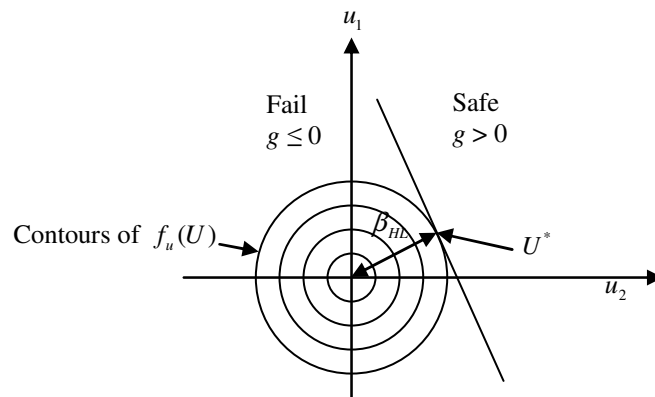

Figure 3.2: Hasofer Lind reliability index.

As β_{HL} represents the shortest distance from the origin to the failure surface, an optimization problem must formulated and solved to find this point on the limit state. This point is known as the MPP of failure (denoted U^*). An iterative process is implemented to establish this point and the reliability index can be evaluated as follows:

$$\beta_j = \frac{g(U^*) - \sum_{i=1}^{n} \frac{\partial g(U^*)}{\partial x_i} \sigma_{x_i} u_i^*}{\sqrt{\sum_{i=1}^{n}\left(\frac{\partial g(U^*)}{\partial x_i}\sigma_{x_i}\right)^2}} \tag{3.13}$$

where j is the iteration, n is the number of variables, i is the variable number and β_j is the reliability index for that iteration.

Sensitivity factors or directional cosines are found in X-space which shows the relative importance of each random variable to the probability of failure. The sensitivity factor for each variable can be found using:

$$\alpha_{jxi} = -\frac{\dfrac{\partial g(X^*)}{\partial x_i} \sigma_{x_i}}{\left[\displaystyle\sum_{i=1}^{n}\left(\dfrac{\partial g\left(X^*\right)}{\partial x_i}\sigma_{x_i}\right)^2\right]^{1/2}} \tag{3.14}$$

The relative importance of each variable to the probability of failure is given in Equation (3.14)The larger the sensitivity factor, the higher the contribution the variable has to the probability of failure, this is because:

$$\alpha_1^2 + \alpha_2^2 + ... + \alpha_n^2 = 1 \tag{3.15}$$

Also the sign of the sensitivity factor shows the relationship between the limit state value (g) and the random variables in U-space. A negative sensitivity factor means the limit state value increases as the random variable increases. Conversely, a positive sensitivity factor means the limit state value decreases when the random variable increases (Choi et al, 2007).Using this sensitivity factor a new design point can be found:

$$X = \mu_x + \beta_j \sigma_x \alpha_{jx} \tag{3.16}$$

The reliability index for another iteration (β_{j+1}) is found and the convergence is checked.

$$\varepsilon = \frac{\left|\beta_{j+1} - \beta_j\right|}{\beta_j} \tag{3.17}$$

This process is repeated until an appropriate level of convergence (ε) is achieved. Choi et al (2007) suggest a convergence tolerance of $\varepsilon \leq 0.0001$ which was used in this study.

Rackwitz-Fiessler Procedure

The Hasofer-Lind Iteration method was extended by Rackwitz and Fiessler (Rackwitz et al, 1978) to account for non Gaussian distributed variables. Each random variable with a non normal distribution is converted to an "equivalent normal" distribution. The CDF and the PDF of the actual function must be equal to the normal CDF $(\Phi(x))$ and normal PDF $(\phi(x))$ at the design point (x^*). This is achieved by equating the functions as follows:

$$F_x(x^*) = \Phi\left(\frac{x^* - \mu_X^e}{\sigma_X^e}\right) \tag{3.18}$$

$$f_x(x^*) = \frac{1}{\sigma_x^e}\phi\left(\frac{x^* - \mu_X^e}{\sigma_X^e}\right) \tag{3.19}$$

Equation (3.18) and (3.19) can be manipulated and the equivalent mean (μ_x^e) and the standard deviation (σ_x^e) at the current design point x^* can be written as:

$$\mu_X^e = x^* - \sigma_X^e\left[\Phi^{-1}\left(F_X(x^*)\right)\right] \tag{3.20}$$

$$\sigma_X^e = \frac{1}{f_X(x^*)}\phi\left(\frac{x^* - \mu_X^e}{\sigma_X^e}\right) = \frac{1}{f_X(x^*)}\phi\left[\Phi^{-1}\left(F_X(x^*)\right)\right] \tag{3.21}$$

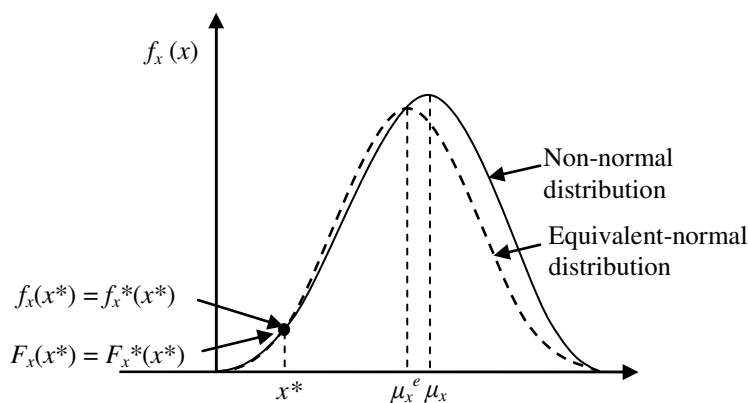The Rackwitz-Fiessler method is shown graphical in Figure 3.3.

Figure 3.3: Rackwitz-Fiessler method (adapted from Choi et al, 2007).

Reliability index methods such as FORM are very popular in structural safety research (Akgul et al, 2004; Estes et al, 2005; Frangopol et al, 2004; Marková, 2010) as it is a very computational efficient algorithm and has an acceptable level of accuracy.

3.4   FORM Model Validation

The FORM algorithm previously described is implemented in the development of a reliability analysis model. Three examples are used to validate the accuracy of the model. For all three examples failure is defined as the formation of a collapse mechanism. Limit state functions for each example are formed using principles of virtual work (Caprani, 2011). The external work done by the applied loads are equated to the internal work done in the formation of a mechanism. In each example the structure consists of a $457 \times 152 \times 74$ UB continuous beam. The model is validated against, an industry standard program, Variables Processor 1.6 (VaP). This program can conduct reliability calculations for problems with a known limit state function using both FORM and MCS.
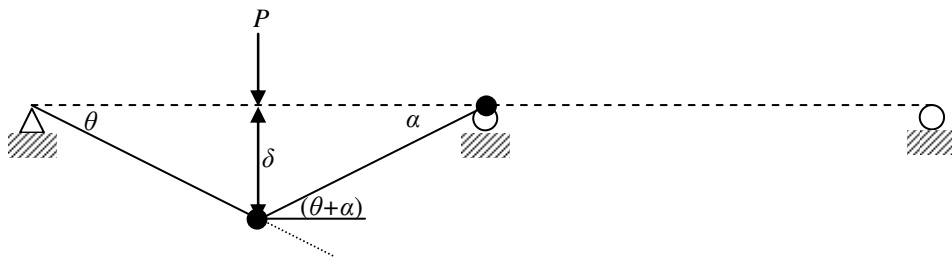
Example 1:   Single point load on a continuous beam

The first example consists of a two span continuous steel beam subjected to a single point load. This point load is positioned in the middle of the first span as shown in Figure 3.4a. An illustration of the methodology used to derive the limit state function from virtual work is given in Figure 3.4b. Two random variables were examined and include the plastic moment

capacity of the steel beam representing the resistance of the structure and the magnitude of the point load. The statistical properties are arbitrary chosen and are given in Table 3.1
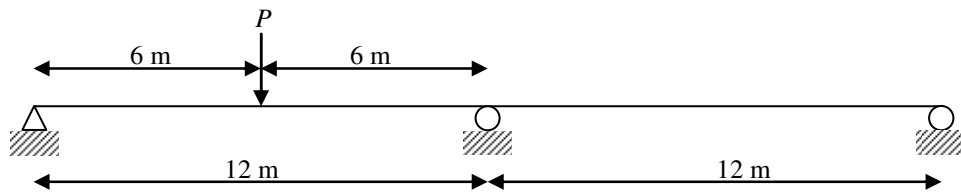
(a) Example two problem schematic;

(b) Example two limit state function derivation;

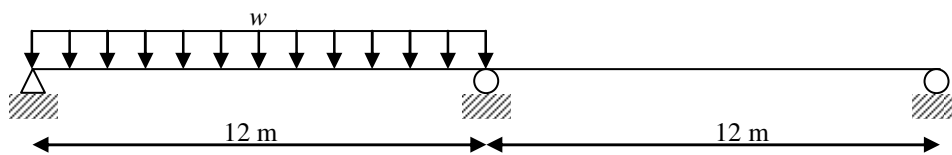Figure 3.4: Single point load on a continuous beam.

$$\theta = \alpha = \delta$$
$$\text{Internal Work} = \text{External Work}$$
$$M_P(\theta + \alpha) + M_P(\alpha) = P(\delta)$$
$$3M_P\theta = P\theta$$
$$g = 3M_P - 6P \qquad\qquad (3.22)$$
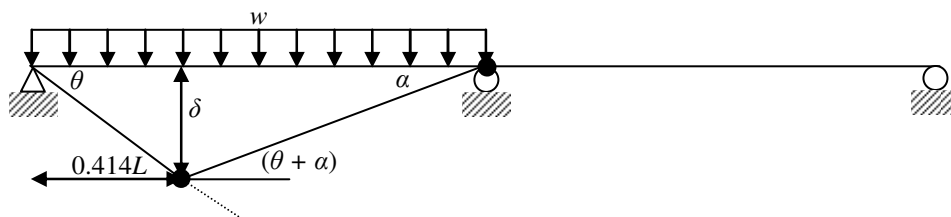
Table 3.1: Example 1 variable properties

Variable	μ	Coefficient of Variation (CoV)	Distribution
M_P	432 kNm	0.1	Log-Normal
P	100 kN	0.1	Gumbel

Example 2: UDL on a continuous beam

The load examined in this problem consists of a UDL on the first span of the same structure as shown in Figure 3.5a. Again the limit state function is derived from principles of Virtual Work and shown in Figure 3.5b. Similar to Example 1, two random variables are examined, the plastic moment capacity and the magnitude of the UDL. Table 3.2 highlights the arbitrarily chosen statistical properties of each variable.

(a) Example two problem schematic;

(b) Example two limit state function derivation;
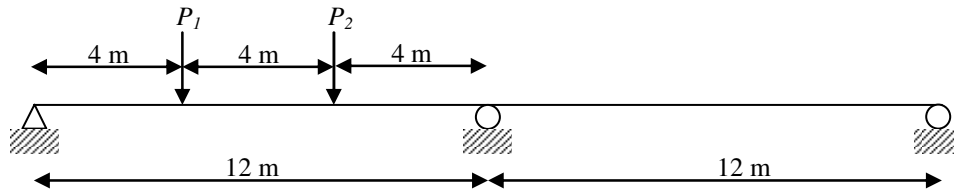
Figure 3.5: UDL on a continuous beam.

$$\delta = 7.03\alpha = 4.97\theta \Rightarrow \beta = 0.707\theta$$
$$\text{Internal Work} = \text{External Work}$$
$$M_P(\theta + \alpha) + M_P(\alpha) = (wL)(0.5)(\delta)$$
$$2.414M_P\theta = (12w)(2.485)$$
$$g = 2.414M_P - 29.82w \tag{3.23}$$
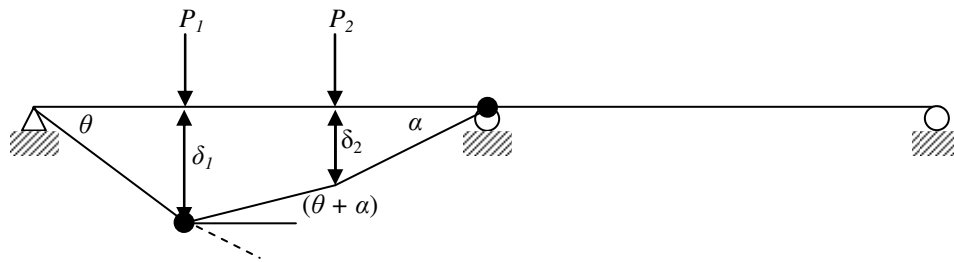
Table 3.2: Example 1 variable properties

Variable	μ	CoV	Distribution
M_P	432 kNm	0.1	Log-Normal
w	20 kN	0.2	Gumbel

Example 3:   Two point loads on a continuous beam

The final validation example looks at two point loads symmetrically positioned on the first

span as shown in Figure 3.6a. The two point loads are treated as independent uncorrelated

random variables. The plastic moment capacity of the structure is also considered random.

Table 3.3 outlines the properties of each random variable arbitrarily chosen.

(a) Example three problem schematic;

(b) Example three limit state derivation;

Figure 3.6: Continuous beam subjected to two point loads.

$$\delta_1 = 8\alpha = 4\theta \Rightarrow \alpha = 0.5\theta$$
$$\delta_2 = 4\alpha = 2\theta$$
$$\text{Internal Work} = \text{External Work}$$
$$M_P(\theta + \alpha) + M_P(\alpha) = P_1(\delta_1) + P_2(\delta_2)$$
$$2M_P\theta = P_1(4) + P_2(2)$$
$$g = 2M_P - P_1(4) + P_2(2) \qquad (3.24)$$

Table 3.3: Example 3 variable properties

Variable	μ	CoV	Distribution
M_P	432 kNm	0.1	Log-Normal
P_1	100 kN	0.1	Gumbel
P_2	75 kN	0.1	Gumbel

Reliability analysis calculations were conducting using both the developed FORM model and VaP for each of the examples. As can be seen from Table 3.4 the developed FORM code produces reliability indices very close to those found using the VaP model.

Table 3.4: Validation results

Example	FORM Model		VaP (Schneider, 1997)	
	β	P_f	β	P_f
1	4.459	4.117×10^{-6}	4.460	4.098×10^{-6}
2	3.436	2.952×10^{-4}	3.430	3.017×10^{-4}
3	3.308	4.698×10^{-4}	3.310	4.665×10^{-4}

3.5   Summary

In this chapter an introduction into reliability theory and the commonly used reliability techniques is given. A FORM model is developed. This model will be used to perform a conventional reliability assessment of existing steel composite structures subjected to realistic traffic events. Also this model will be a key component in a reliability analysis procedure which accounts for nonlinear material behaviour which is developed in this study.

Chapter 4

Nonlinear Structural Model

4.1   Introduction

A brief introduction to nonlinear finite element theory is given in this chapter. The development of a Nonlinear Finite Element Analysis (NFEA) model and accuracy validation is also described.

4.2   Finite Element Method

The Finite Element Method (FEM) is formed on the basis that it is possible to accurately describe the behaviour of a structure by dividing the structure into elements (segments). The displacement of each element subjected to the designated load is found. Continuity and equilibrium requirements between neighbouring elements and boundary conditions are enforced allowing for the overall behaviour of the structure to be determined (Becker, 2004). The FEM procedure is based on the matrix displacement method and can be found throughout literature (Chen, 1996; Becker, 2004; Ghali et al, 2009). Steps in the procedure include:

1. The structure is divided into elements connected at each end by nodes. Generally more elements increase the accuracy of the model but have a higher computational cost.

2. The process involves formulating and solving the equilibrium equation for the global displacements:

$$\{F\} = \left[K_g \right] \{u\} \qquad (4.1)$$

where F is an external force vector, K_g is the global stiffness matrix of the structure and u is the displacement vector.

3. The local stiffness matrix (k_e) for each element is compiled.

$$[k_e] = \frac{EI}{L^3} \begin{bmatrix} 12 & 6L & -12 & 6L \\ 6L & 4L^2 & -6L & 2L^2 \\ -12 & -6L & 12 & -6L \\ 6L & 2L^2 & -6L & 4L^2 \end{bmatrix} \tag{4.2}$$

where E is the Young's Modulus, I is the second moment of area and L is the length of the element.

4. The stiffness matrices of elements which share a common node are inserted into the global stiffness matrix and continuity is ensured throughout the structure.

5. Boundary conditions are enforced on the global stiffness matrix and Equation (4.1) is solved.

6. Deflections and internal forces in each element can be solved by manipulating Equation (4.1) once the displacement vector is known.

4.3   Nonlinear Finite Element Modelling

In NFEA the assumption that loads can be superimposed and reversed are invalid. The deformations beyond the elastic limit depend on the load history of the structure. This can be incorporated into the analysis by applying the load in small increments and altering the local stiffness matrices of each element accounting for non-elastic deformations. This increment loading procedure is commonly used in NFEA modelling (Chen et al, 1996).

NFEA problems are traditionally grouped as follows:

1. Material nonlinearity: Material nonlinearity is concerned with inelastic behaviour of a material. This behaviour may be described using a moment-rotation curve as shown in Figure 4.1. This figure illustrates that once material reaches its yield point, further moment will cause a rotation that moves away from elastic behaviour (Abell, 2012).
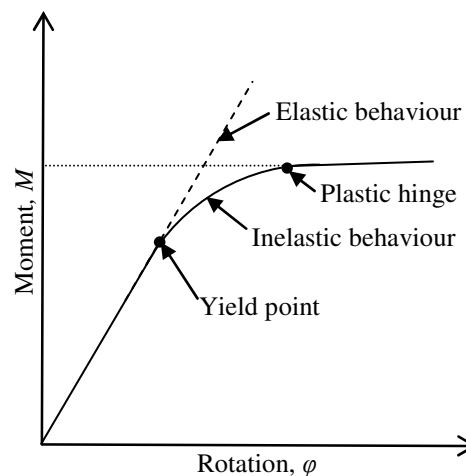

Figure 4.1: Moment rotation curve (adapted from Becker, 2004)

2. Geometric Nonlinearity: accounts for the change in geometry of the structure due to the displacements caused by the applied load.

3. Boundary Nonlinearity: This involves a situation where two surfaces come in and out of contact and the behaviour of the contacting bodies is not linearly dependent on the applied load.

4.4   Material Nonlinearity

Material Nonlinearity is the only nonlinearity consider in this study. Using plastic hinge theory local stiffness matrices are derived which account for the presence of yield and plastic hinges. A plastic hinge allows large rotation to occur at a constant moment as shown in Figure 4.1. Two common assumptions in plastic hinge theory are:

1. Plastic hinges can only form at the ends of an element (Li et al, 2007).

2. Plastic hinges have zero length (Chen, 1996).

The local stiffness matrix for an element with a hinge located at the left node is:

$$[k_1] = \frac{EI}{L^3} \begin{bmatrix} 3 & 0 & -3 & 3L \\ 0 & 0 & 0 & 0 \\ -3 & 0 & 3 & -3L \\ 3L & 0 & -3L & 3L^2 \end{bmatrix} \qquad (4.3)$$

The local stiffness matrix for an element with a hinge located at the right node is:

$$[k_2] = \frac{EI}{L^3} \begin{bmatrix} 3 & 3L & -3 & 0 \\ 3L & 3L^2 & -3L & 0 \\ -3 & -3L & 3 & 0 \\ 0 & 0 & 0 & 0 \end{bmatrix} \qquad (4.4)$$

These local stiffness matrices are the fundamentals of plastic hinge theory and are combined with a hysteric model in the development with a NFEA model. A hysteric model describes the relationship between moment and rotation due to loading. Two NFEA models were examined in this work.

4.5   Clough Model

The Clough model is a NFEA model which combines the matrix displacement method, plastic hinge theory and a simple hysteric model. The hysteric model has a bilinear moment rotation relationship. The Clough model is known as a two component model and accounts for strain hardening (q) using the summation of a) an idealised elastic-plastic component and b) an infinitely elastic component. The idealised elastic component is altered with the occurrence of plastic hinges. This is illustrated in Figure 4.2.
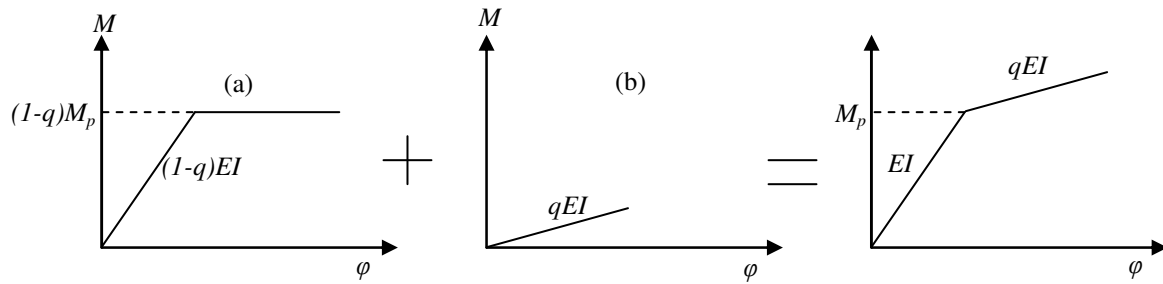
Figure 4.2: Clough model components (Li et al, 2007).

Assuming that the moment at the left node of the element (M_L) is greater than the plastic moment (M_P), the local stiffness matrix (k) can be formed from the following equation:

$$[k] = (1-q)[k_1] + q[k_e]$$ (4.5)

where k_1 is the local stiffness matrix for an element with a hinge located at the left node as given by Equation (4.3) and k_e is the elastic local stiffness matrix given in Equation (4.2).

Conversely, if the moment at the right node of the element (M_R) is greater than M_P, the stiffness matrix is given by:

$$[k] = (1-q)[k_2] + q[k_e]$$ (4.6)

where k_2 is the local stiffness matrix for an element with a hinge at the right node as given by Equation (4.4)

4.6   Generalized Clough Model

The main flaw with the Clough Model is the assumption of the bilinear moment rotation curve. The Generalized Clough model was developed in Clough et al (1990) as cited in Li et al (2007). This model uses a moment rotation curve which accounts for nonlinear material behaviour between yield and plastic moment capacity. The stiffness (K) of the structure can be written as:

$$K = REI \qquad (4.6)$$

where R is a force recovery parameter which depends on the ratio, denoted Γ, of the current moment (M) on the section its plastic moment capacity.

$$\Gamma = \frac{M}{M_p} \qquad (4.7)$$

The force recovery parameters trace the spread of plasticity through a section and represent the relative stiffness of the structure at different stages of loading. This is shown in Figure 4.3. Importantly a high force recovery parameter represents a low stiffness.
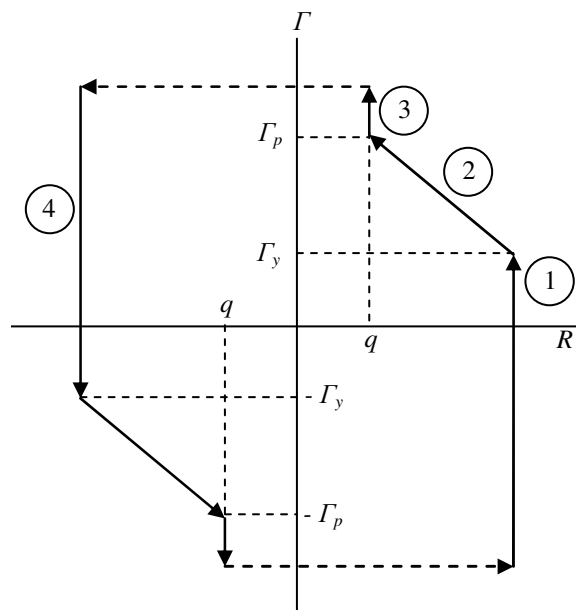
(a) Force recovery parameters under cyclic loading;
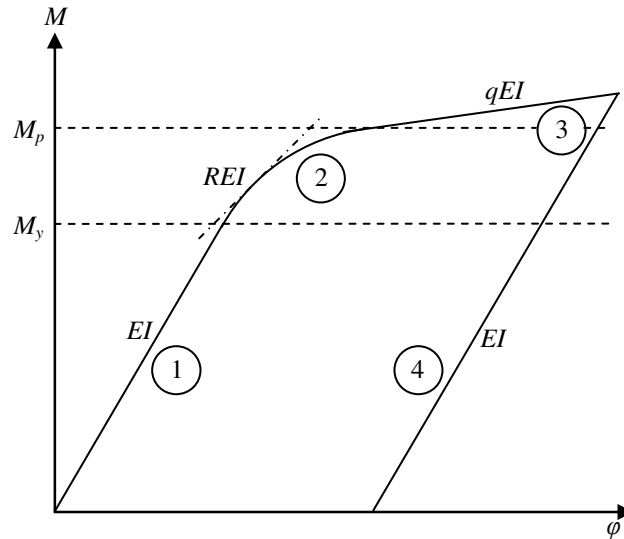
(b) Moment rotation relationship;

Figure 4.3: Stages in the behaviour of the cross section adapted from Li et al, 2007.

When the structure is subject to loading and is behaving elastically (Stage 1) the force recovery parameter is equal to one, as no reduction in stiffness has taken place:

$$\Gamma \leq \Gamma_y : \qquad R = 1 \qquad\qquad (4.8)$$

where

$$\Gamma_y = \frac{M_y}{M_p} \qquad\qquad (4.8)$$

The slope of the moment rotation curve for this stage is the equivalent of *EI*. Once the yield capacity (Stage 2) has been reached, the force recovery parameter and the stiffness of the structure reduce as follows:

$$\Gamma_y < \Gamma < \Gamma_p : \quad R = 1 - \frac{\Gamma - \Gamma_y}{\Gamma_p - \Gamma_y}(1 - q) \qquad\qquad (4.9)$$

where Γ_p is unity and q represent the strain hardening of the material.

When a plastic hinge has fully formed (Stage 3) the force recovery parameter at that location equals the value of strain hardening (q) of the critical material in the section. The slope of the moment rotation curve for this stage is qEI, obtained as follows:

$$\Gamma \geq \Gamma_p: \qquad R = q \tag{4.10}$$

During an unloading event at any point (Stage 4), the structure is assumed to behave elastically (Li et al, 2007). Hence the unloading force recovery parameter is:

$$\text{Unloading}: \quad R = 1 \tag{4.11}$$

In the Generalized Clough Model the stiffness of a beam element is obtained from two components as described in Figure 4.4.

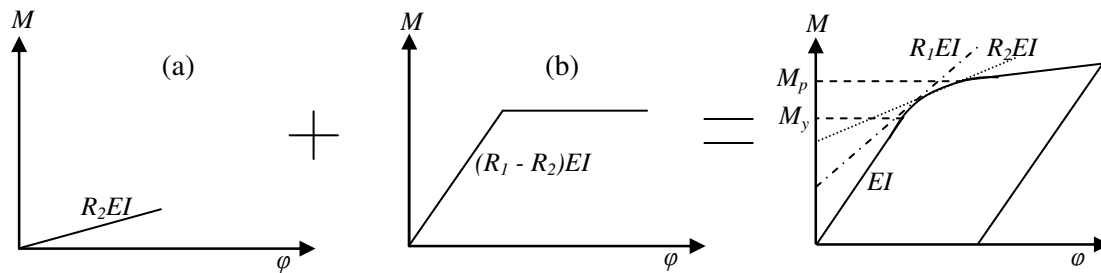

Figure 4.4: Generalized Clough model ($R_1 \geq R_2$) adapted from Li et al, 2007.

These components are a) a clamped two-end component and b) hinge-clamped end component. Thus the local stiffness matrix of the beam element can be written in either of the following formats, depending on the recovery force parameter at either end of the element (R_1, R_2):

$$[k] = R_2[k_e] + (R_1 - R_2)[k_2], \text{when } R_1 \geq R_2 \tag{4.12}$$

$$[k] = R_1[k_e] + (R_2 - R_1)[k_1], \text{when } R_1 \leq R_2 \tag{4.13}$$

When $R_1 > R_2$, the stiffness at each node is increased by multiplying the element stiffness matrix (k_e) by R_2. This is component (a) in Figure 4.4. The difference in the force recovery parameters is multiplied by the local stiffness matrix with a plastic hinge at the right node (k_2), component (b) in Figure 4.4. By adding these components together only the stiffness at the left node is reduced giving an accurate representation of stiffness at both nodes in the element.

4.7 NFEA Model Validation

The NFEA Model is validated using the same three examples outlined in Section 3.4. The limit state functions derived for each example are manipulated to find the load factors required to form a collapse mechanism and are given in Table 4.1. A mesh size of 1 m was chosen along with an increment size of 0.001.

The results validating the NFEA model are outlined in Table 4.1. The point load examples produce results equal to those found using the formulae. When examining a UDL using a FEA the mesh size is important. From the load factor derivation it is known that the one hinge occurs over the internal support and the second occurs $0.414L$ or 4.968 m from the left hand support. As it is unpractical to have a mesh fine enough to allow a hinge develop at this location (without manually placing at node at this location) meaning that only an approximate load factor can be found.

Table 4.1: NFEA Model Validation

Example	Equation	Theoretical λ	NFEA Model λ
1	$\lambda = \dfrac{3M_P}{6P}$	2.156	2.156
2	$\lambda = \dfrac{2.414M_P}{29.82w}$	1.745	1.722
3	$\lambda = \dfrac{2M_P}{P_1(4) + P_2(2)}$	1.568	1.568

4.8   Incremental Loading Procedure

The accuracy of the incremental loading procedure, described in section 4.2 depends on the size of the increments used. As the load increases, and the behaviour of the material becomes nonlinear the equilibrium path will drift away from the true path (Chen, 1996). Two solutions are known to overcome this difficulty 1) use small loading increments (as done in Section 4.7) 2) apply a convergence check after each increment has been applied to ensure convergence. For simplicity reducing the size of the increment $(\Delta\lambda)$ was chosen for this work. However, to reduce the computational expense an adaptive increment size is used as shown in Figure 4.5. Initially, the load is applied in relatively large increments of a load factor of 0.1 until the force recovery parameter at any location falls below 0.5. Then the increment size is reduced to 0.01 until a force recovery parameter below 0.25 is found anywhere in the structure. Finally the load increments are reduced further (0.001) until a collapse mechanism is formed.
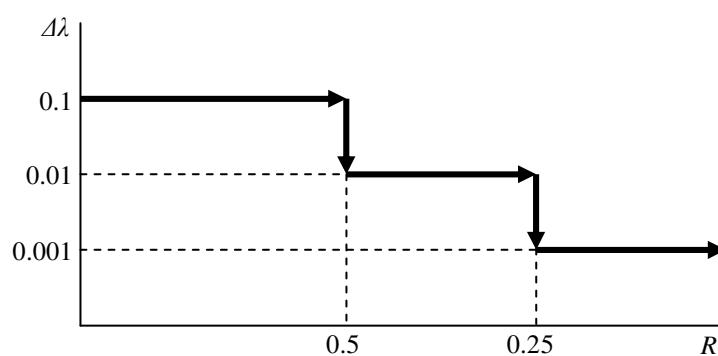
Figure 4.5: Adaptive increment size procedure.

The values for the force recovery parameter at which the increment size is to be reduced were obtained from trial and error. Example 1 from Section 4.7 is re-run to highlight the efficiency of the adaptive increment procedure and these results are shown in Table 4.2.

Table 4.2: Example 1 results using different increment sizes

$\Delta\lambda$	λ	No of increments
0.1	2.2	23
0.01	2.16	217
0.001	2.156	2157
Adaptive increment size	2.156	156

As can be seen from Table 4.2, the accuracy of NFEA model depends on the size of the increment. Using the theoretical load factor given in Table 4.1, and the results for each increment size given in Table 4.2, it can be seen the NFEA model is more accurate when a fine increment size is used. In a NFEA model the number of increments used is directly proportional to computational time. It is seen from Table 4.2 that the adaptive incremental procedure achieves the required load factor for a reduced number of increments.

4.9   Summary

The development of the one dimensional NFEA model used in this work is summarized. The model traces the spread of plasticity through a structure using the Generalized Clough model. It is validated against three benchmark examples. The model incorporates an adaptive increment procedure to ensure accuracy and reduce computation time. This NFEA model will be used in both a deterministic and a probabilistic study of a representative group of steel composite bridge structures subjected to realistic traffic events for collapse.

Chapter 5

Response Surface Modelling

5.1   Introduction

This chapter outlines the theory behind RSM. In particular, attention to the choice of response surface function, experimental design, convergence criteria and methodology is given. A RSM model is successfully developed and validated for the three benchmark examples.

The RSM is a very useful and efficient technique when explicitly-known limit state functions are unavailable. Generally when assessing existing structures subjected to various loading scenarios to collapse, advanced modelling procedures such as NFEA must be used. Simulation methods can be combined with a NFEA model easily to deal with complex problems when the probability of failure is high. However, this is not practical when dealing with low probabilities typical of structures, since a great number of iterations are required. A more efficient technique for analysing such complex problems is RSM. The main concept behind RSM is to find a polynomial approximation to the actual (unknown) limit state function. This is achieved by conducting numerical experiments at prescribed values and fitting a function to represent the surface. This function may be a first, second, or higher-order polynomial. Once an explicit approximated response function is established, a reliability analysis such as FORM (see Section 3.3.3) can be used to estimate the probability of failure of the structure under the particular loading scenario.

When using the RSM to approximate the response function, the approximated polynomial is only accurate in the area where it has been evaluated (Bucher et al, 1990). It does not represent the entire true limit state function. If the limit state surface is approximated at the most probable point (MPP) of failure (see Section 3.3.2) an accurate closed-form surface

closely representing the failure surface can be established. Since the MPP is generally unknown in nonlinear problems an iterative process involving a reliability analysis is required to identify this point.

Although the RSM method is far less computationally expensive when compared to simulation techniques it is does have limitations. Difficulties can arise when actual limit state functions are highly nonlinear, when dealing with extremely low probabilities of failure (Wisniewski et al, 2009) or when the structure is subjected to multiple loading sequences, such as dead load and live load (Wong et al, 2005).

Key aspects to the response surface method are, the choice of response function, degree of polynomial, experimental design, and convergence criteria.

5.2   Response Surface Function Selection

The response surface function is generally in the form of a polynomial due to its simplicity (Lei, 2010). The order of the polynomial is of particular importance. Higher order polynomials produce more accurate response surfaces to a certain level. However higher order polynomials may also lead to ill conditioned system of equations, and erratic behaviour in areas of valuable space not covered in the experiment design (Bucher et al, 1990). The order of the approximating function should be equal to or less than the order of the actual function (Rajashekhar et al, 1993). Commonly in the literature, first order and second order polynomials have been used and have been found to produce satisfactory levels of accuracy (Bucher, 1990; Rajashekhar, 1993; Wong, 2005). However an investigation into the use of higher- order polynomials was conducted by Gavin et al (2008) which found significant benefit to using higher-order polynomials when examining highly nonlinear limit states with multiple points of failure. Despite this, only second-order polynomials will be examined in this study due to the high computational cost associated with using higher order polynomials.

A first-order polynomial consisting n random variables can be expressed as follows:

$$\check{g} = \beta_0 + \beta_1 x_1 + \beta_2 x_2 + ... + \beta_n x_n \tag{5.1}$$

Where $\check{g}$ is a function if the random variables $x_1, x_2, ... x_n$ and the regression coefficients $\beta_0, \beta_1, ..., \beta_n$. The first-order response surface model is only appropriate when approximating the true response surface over a small region of design space where there is little curvature (Carley et al, 2004). A minimum of $n+1$ experiments are required to determine a first-order polynomial (Myers, 1995). A second order polynomial takes the following format:

$$\check{g} = \beta_0 + \sum_{j=1}^{n} \beta_j x_j + \sum_{j=1}^{n} \beta_{jj} x_j^{2} \tag{5.2}$$

A minimum of $2n+1$ experiments are needed because the quadratic terms are added to the function (Kolios, 2010). The complexity can be further increased with the addition of the mixed terms of the random variables:

$$\check{g} = \beta_0 + \sum_{j=1}^{n} \beta_j x_j + \sum_{j=1}^{n} \beta_{jj} x_j^{2} + \sum_{i<}\sum_{j=2}^{n} \beta_{ij} x_i x_j \tag{5.3}$$

The required number of samples for a second-order polynomial including mixed terms is between $\left(\dfrac{n(n-1)}{2} + 2n + 1 \right)$ and 3^n (Kolios, 2010). A better representation of the nonlinearity of the actual limit state function is achieved when the cross terms are included. A second-order polynomial including mixed terms was chosen for this work.

5.3   Experimental Design

The Experimental Design (ED) is the manner in which different combinations of the random variables are chosen. A NFEA will be performed at each combination. This will result in a set

of structural responses. From these the response surface is fitted using Least Squares regression. In the literature many suggestions for experimental designs can be found.

5.3.1 Star Experimental Design

This simple ED contains a centre point and two symmetrical combinations for each random variable (star points) as illustrated in Figure 5.1. The total number of combinations in this ED is $2n+1$, where n is the number of random variables. This design is popular for its simplicity (Bucher et al, 1990).
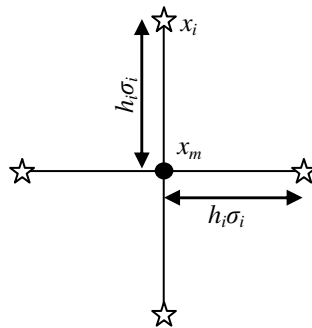

Figure 5.1: Star ED for two variable problems.

The dispersion of the star point (x_i) from the centre point (x_m) is given by:

$$x_i = x_m \pm h_i \sigma_i \qquad (5.4)$$

where σ_i is the standard deviation of the random variable and h_i is the number of standard deviation setting the size of the design space. The number of standard deviations was traditionally a user-defined input. It is important that this value is appropriate so no extreme values for any random variables are generated. For example, we assess a bridge structure subjected to dead load and live load to collapse. If an extremely low resistance and an extremely high dead load are examined, the structure may fail without any contribution from live load. Not only is this unrealistic but it will affect the approximated response surface as the live load has no influence on that experimental point. Trial and error was traditionally

used to set this value and it was only from the work of Wong et al (2005) that a link between this value and statistical properties of each random variable was made. They established that the value of h_i depends on the coefficient of variation (CoV) of the variable and proposed the value outlined in Table 5.1.

Table 5.1: Spread of design point, h_i values (Wong et al, 2005)

Range of CoV	h_i
$CoV \leq 0.05$	$0.15 / CoV$
$0.05 \leq CoV \leq 0.2$	3
$0.2 \leq CoV \leq 0.5$	2
$CoV \geq 0.05$	1

5.3.2 Full Factorial Experimental Design

Another simple ED is the Full Factorial Experimental Design. This design is called a two level factorial design if both "high" and "low" combinations of random variables are examined as shown in Figure 5.2.
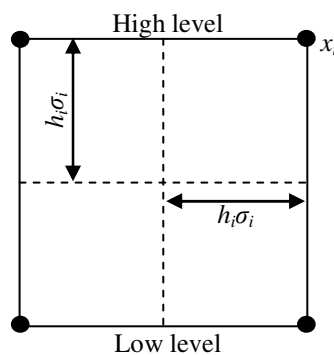
Figure 5.2: Full Factorial ED for a two variable problem.

The distance from the centre to the factorial point is $h_i\sigma_i$. A full factorial design examining two levels has 2^n experimental points, where n is the number of random variables.

The ED is described as a full factorial design if all combinations of the variables at both high and low levels are examined. Otherwise if some combinations are omitted, it is called a fractional factorial design. Fractional factorial designs may be useful when a reduced number

of experiments are required, such as when each numerical experiment is computational intensive.

5.3.3 Central Composite Design

The Star experimental design and the Full Factorial experimental design can be combined to create Central Composite Designs (CCDs) which are the most commonly used experimental designs in RSM (Deng et al, 2010). They can be combined in three ways as illustrated in Figure 5.3.
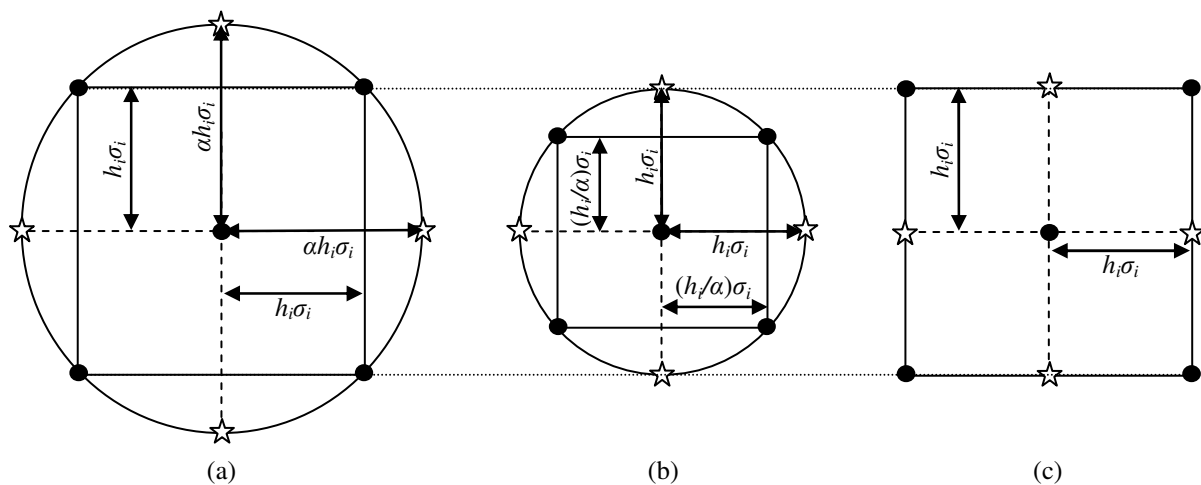
Figure 5.3: CCD for two variable problems (a)-CCC, (b)-CCI, and (c)-CCF

a) Central Composite Circumscribed Design (CCC)

These star locations represent new high and low extreme values and are a distance $\alpha h_i \sigma_i$ from the centre of the experiment design, where α is a scale parameter. The value of the scale parameter depends on the number of experiments evaluated in the factorial component of the design:

$$\alpha = [\text{number of factorial runs}]^{1/4} \tag{5.5}$$

Table 5.2 shows the value of the scale parameter corresponding to the number of factorial runs.

Table 5.2: α-values for various number of variables (NIST/SEMATECH, 2012).

Number of random variables	Factorial Runs	α scaled relative to ± 1
2	2^2	1.414
3	2^3	1.682
4	2^4	2
5	2^5	2.378
6	2^6	2.828

As the CCC design generates new extreme values, there is a requirement to assess the reasonability of the experimental points, since some points generated may be unrealistic when applied to practical problems. If the factors involved in the experiment are unlimited the CCC design type produces high quality predictions over the entire design space.

b) Central Composite Inscribed (CCI)

The Central Composite Inscribed (CCI) is a scaled-down version of the CCC design. The distance from the centre point of the ED to the star points is $h_i \sigma_i$ and the distance from the centre point to the factorial points is $(h_i / \alpha)\sigma_i$. The scale parameter (α) is calculated as before. This is used for situations when a variable has limits. The CCI design type provides a less accurate prediction over the entire spaced when compared to the CCC design type. However, it is a more feasible design in practical scenarios as no unrealistic values are examined.

c) Central Composite Face Centred (CCF)

This Central Composite Face Centred design differs as the star points are located at the centre of each factorial design. This ED provides relatively accurate predictions over the entire design space, however it is inappropriate when a high level of curvature is present (NIST/SEMATECH, 2012).

5.3.4   Box-Behnken Design (BB)

The Box-Behnken design (BB) is an ED which can only be applied to problems containing at least three variables. It examines locations at the midpoints of the edges of the design space and at the centre as shown in Figure 5.4. This experimental design is rotatable, but it contains regions of poor prediction as it ignores combined factor extremes (NIST/SEMATECH, 2012). The distance from the centre of any face in the design space to an experimental point is $h_i\sigma_i$.
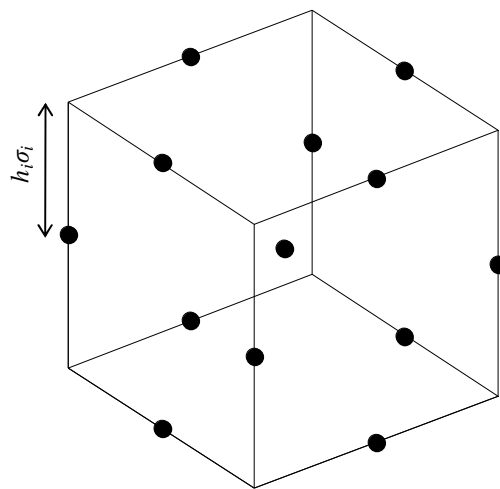
Figure 5.4: Box-Behnken design for three variables.

5.3.5   Experiment Design Working Space

The working space in which experiments are formed is an aspect of the RSM in which opinions are divided. Several researchers build the experiment design in the physical space so as non-physical/realistic experiments can be monitored (Bucher, 1990; Rajashekhar, 1993; Kim et al, 1997; Lemaire, 1996). Likewise, studies have been conducted which favour the use of building the experiment in *U*-space so as there is more control over numerical experiments (Gayton, 2003; Waarts, 2000). The experiment designs for this study were built in physical space.

5.4 Fitting of a Response Surface

A multiple regression model and the method of least squares can be used to determine the unknown regression coefficients in Equation (5.3). This is a commonly used approach in RSM (Gayton et al, 2003). The model is written in matrix notation assuming there is n variables and k experimental runs in terms of observations (Carley et al, 2004):

$$y = X\beta + \varepsilon \tag{5.6}$$

where y is an $k \times 1$ vector of observations, X is an $k \times (n+1)$ matrix of the levels of independent variables, β is a $(n+1) \times 1$ vector of the regression coefficients, and ε is an $(n+1) \times 1$ vector of random errors. The matrix of independent variables X depends on the response surface function selected. An example of the independent variable matrix for a second-order polynomial with mixed terms with two random variables is shown:

$$X = \begin{bmatrix} 1 & x_{11} & x_{12} & x_{11}^2 & x_{12}^2 & x_{11}x_{12} \\ 1 & x_{21} & x_{22} & x_{21}^2 & x_{22}^2 & x_{21}x_{22} \\ \vdots & \vdots & \vdots & \vdots & \vdots & \vdots \\ 1 & x_{k1} & x_{k2} & x_{k1}^2 & x_{k2}^2 & x_{k1}x_{k2} \end{bmatrix} \tag{5.7}$$

The regression coefficients can be obtained by using the method of least squares, as follows:

$$\beta = \left(X'X \right)^{-1} X'y \tag{5.8}$$

5.5   RSM Methodology

Various techniques for ensuring an accurate response surface approximation have been developed through the years. These techniques vary slightly with regards to ED, response surface selection and convergence criteria. The model developed in this work is based on that of Rajashekhar et al (1993). This methodology is an extension of the work of Bucher et al (1990). It involves an iterative process to ensure the ED used to approximate the polynomial is expanded around the MPP of failure. This procedure has the following steps:

1. Select only the most important random variables. A preliminary sensitivity study should be carried out and random variables of low uncertainty should be replaced by deterministic values (Melchers, 1999). The computational expense increases with every additional random variable.

2. Sample points of the variables are defined. The number of sample points depends on the Experimental Design (ED) chosen (Section 5.3). For the first iteration the centre of the ED is chosen as the mean values of each of the random variables. The design space dispersion is set by selecting a value for h_i from Table 5.1.

3. Using the "observations" obtained from the NFEAs a response surface is fitted to represent the actual (unknown) limit state function (Section 5.4).

4. Assuming the variables are uncorrelated Gaussian variables, the design point (x_d) corresponding to the MPP of failure on the approximated limit state function is found. This may be found using the FORM see Section 3.3.2 (Soares et al, 2002). From this the distance (d) from the design point to the centre of the experimental design is also measured.

5. A new experiment centre point is found using the formula below:

$$x_m = \mu + (x_d - \mu)\frac{g(\mu)}{\left[g(\mu) - g(x_d)\right]}$$

(5.9)

where $g(\mu)$ is the actual experimental observation at the mean of the variables and $g(x_d)$ is the actual experimental observation at the design point. This formula is based on linear interpolation to locate the new centre point on the straight line between the design point and the experiment centre point.

6. Another experiment design is performed around the new centre point followed by another approximation of the response surface.

7. A convergence value ε is set depending on the design space dispersion, when $h_i = 3 \Rightarrow \varepsilon = 10^{-2}$, when $h_i = 2 \Rightarrow \varepsilon = 10^{-3}$ and when $h_i = 1 \Rightarrow \varepsilon = 10^{-4}$. Typically ε is selected between 10^{-4} - 10^{-2} (Wong, 2005). This process is repeated until d is below the convergence criteria (ε).

8. This procedure is repeated with a refined design space dispersion (h_i is reduced). As outlined in Rajashekhar et al (1993) if this process is repeated indefinitely with reduced values for h_i an ill-conditioned system of equations may be achieved. For this reason once convergence has been achieved $h_i = 1$ the iteration process is stopped. This process is illustrated in Figure 5.5 and ensures that the centre of the ED is located approximately on the MPP of failure.
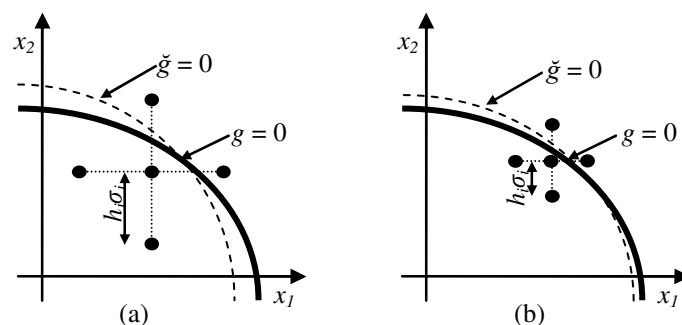
Figure 5.5: Schematic of procedure, a) $h_i = 2$, b) $h_i = 1$ (adapted from Bucher et al, 1990)

9. Once the final polynomial has been approximated, a traditional reliability calculation such as FORM (Section 3.3.2) can be conducted to find the probability of failure.

5.5.1 RSM Validation

To validate the operation of the RSM model, a recreation of an example outlined in Rajashekhar et al (1993) is performed. This example consists of a cantilever beam with a rectangular cross section subjected to a UDL. The limit state function is concerned with maximum deflection at the free end of the beam:

$$g = \frac{-(wb)l^4}{8E\left(\dfrac{bd^3}{12}\right)} + \frac{l}{325} \tag{5.10}$$

The stochastic problem consists of two random variables which are the load (w) and the depth of the beam (d). Young's Modulus (E), the width of the beam (b), and the length of the beam (l) are considered as deterministic. The statistical properties of the random variables are given in Table 5.3.

Table 5.3: Variable properties (Rajashekhar et al, 1993)

Variable	μ	σ
w	0.001 N/mm^2	0.0002 N/mm^2
d	250 mm	37.5 mm
E	2.6×10^4 MPa	---
l	6 m	---

The methodology outlined in Section 5.8 is implemented; however, the observations are obtained using Equation (5.10) rather than a NFEA. A star experiment design is used (see Section 5.3.1). It was found that this approximated response surface had two failure boundaries as shown by the blue lines in Figure 5.6.
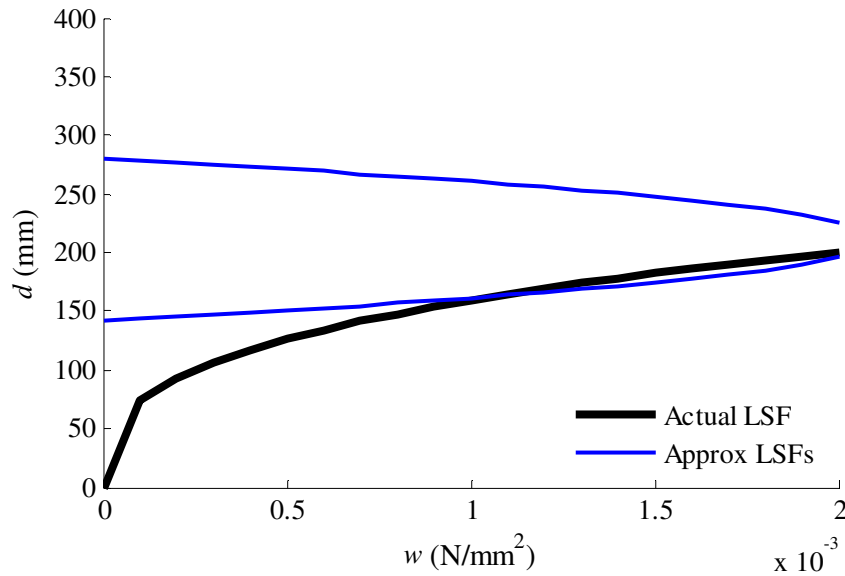
Figure 5.6: Approximated limit state functions.

The Importance Sampling (IS) technique was implemented to determine the probability of failure: 1000 samples were conducted and are plotted on Figure 5.7.
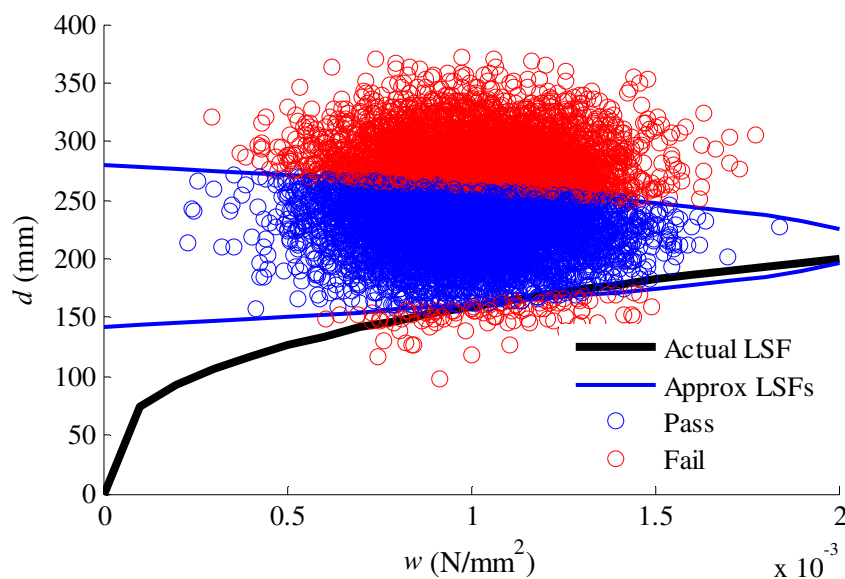
Figure 5.7: Incorrect importance sampling plot.

A sample failed if the approximated response surface $\breve{g} \leq 0$. Since, incorrectly there are two boundaries of failure, an incorrect probability of failure is determined in this case. As Wisniewski et al (2009) outlines, the RSM method is inefficient in dealing with problems containing several modes of failure. However, as can be seen from Figure 5.6 the lower limit

state function represents a good approximation of the actual limit state function around the design point as desired. The IS failure is re-defined as when a) $\check{g} \leq 0$; and b) the resistance parameter is below its mean value than an approximately correct probability of failure of 9.7×10^{-3} is established. This is shown in Figure 5.8.
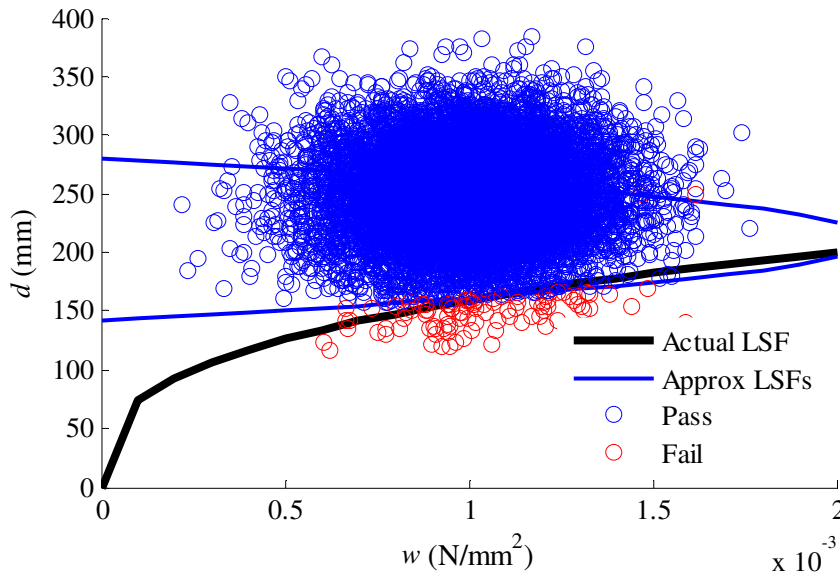
Figure 5.8: Correct importance sampling plot.

Provided that there is only one mode of failure, the RSM method is an appropriate procedure for incorporating a nonlinear structural model into a probabilistic assessment.

5.6 Reliability Analysis Considering Material Nonlinearity

The NFEA model developed in Chapter 4 is connected to the RSM to perform a reliability analysis considering material nonlinearity. The NFEA model is used as the numerical experiment in the RSM. An "observation" is taken from the NFEA model to describe how far each point in the ED is from failure. This "observation" is taken as:

$$g_{(obs)} = \lambda - 1 \tag{5.11}$$

where λ is the load factor required to cause a defined failure. A flowchart outlining the RSM methodology (Section 5.8) linked with the NFEA model is given in Figure 5.9

Inputs:
1) Structure data
2) Material properties
3) Load data

Define Failure
1) Initial Yield
2) Plastic Hinge
3) Collapse Mechanism

Select experimental design
(see Section 5.3)

Select/reduce experimental dispersion value (h_i)
(see Section 5.5)

Determine experimental design centre point (x_m)
$x_m = \mu$ for first iteration
x_m = Equation 5.9 for other iterations

Determine λ and $g_{(obs)}$ for each experiment design point (see Section 5.6)

Response Surface Approximation
(see Section 5.4)

Determine distance (d) from x_m to MPP using FORM

Check converge
Is $d < \varepsilon$

No

Yes

Convergence Criteria
If $h_i = 3$, $\varepsilon = 10^{-2}$
If $h_i = 2$, $\varepsilon = 10^{-3}$
If $h_i = 1$, $\varepsilon = 10^{-4}$

No

Is $h_i = 1$

Yes

Determine Reliability Index (β) using FORM
(see Section 3.3.2)

Figure 5.9: RSM -NFEA method flowchart

5.6.2 RSM-NFEA Model Validation

The RSM-NFEA model is validated against the three benchmark examples outlined in

Section 3.4. The Central Composite Inscribed design is used in all examples (Section 5.3.3).

The closed-form limit state functions derived in Section 3.4 are replaced by the NFEA model.

The results are validated against those obtained earlier using the FORM code and are given in

Table 5.4

Table 5.4: Example 1-RSM results

Experimental Design	No. Iterations $(h_i = 3)$	No. Iterations $(h_i = 2)$	No. Iterations $(h_i = 1)$	Total Iterations	No. FEA	Reliability Index (β)	Probability of Failure (P_f)
CCI	1	0	1	3	45	4.422	4.882×10^{-6}
	FORM Model					4.459	4.117×10^{-6}
CCI	2	1	0	3	45	3.665	1.236×10^{-4}
	FORM Model					3.436	2.952×10^{-6}
CCI	2	1	0	3	45	3.302	1.236×10^{-4}
	FORM Model					3.308	2.952×10^{-6}

All three examples converge after three iterations and the reliability indices found are close to

those found using the FORM model with the known limit state function. Figures 5.10 and

5.11 show plots of the approximated limit state function after each iteration against the actual

limit sate function. A good representation of the actual limit state function around the design

point is obtained for Example 1. However, Example 2 displays a slight divergence. It is

believed this is due to the mesh sizing problem as outlined in Section 4.7.
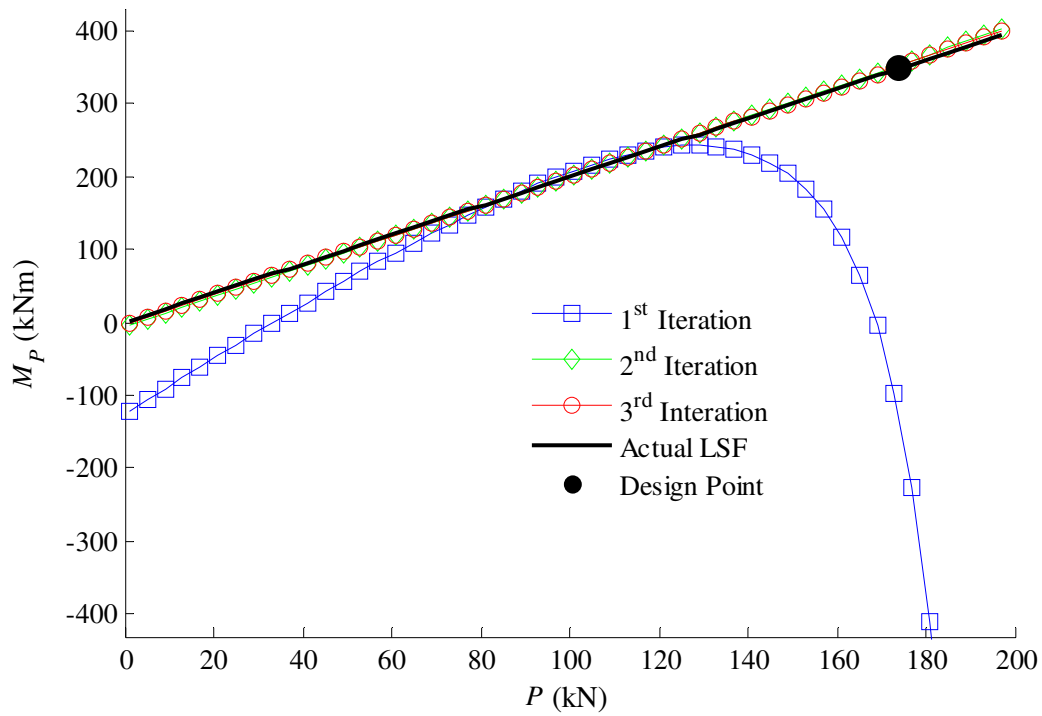
Figure 5.10: Example 1 RSM approximating functions for each iteration.
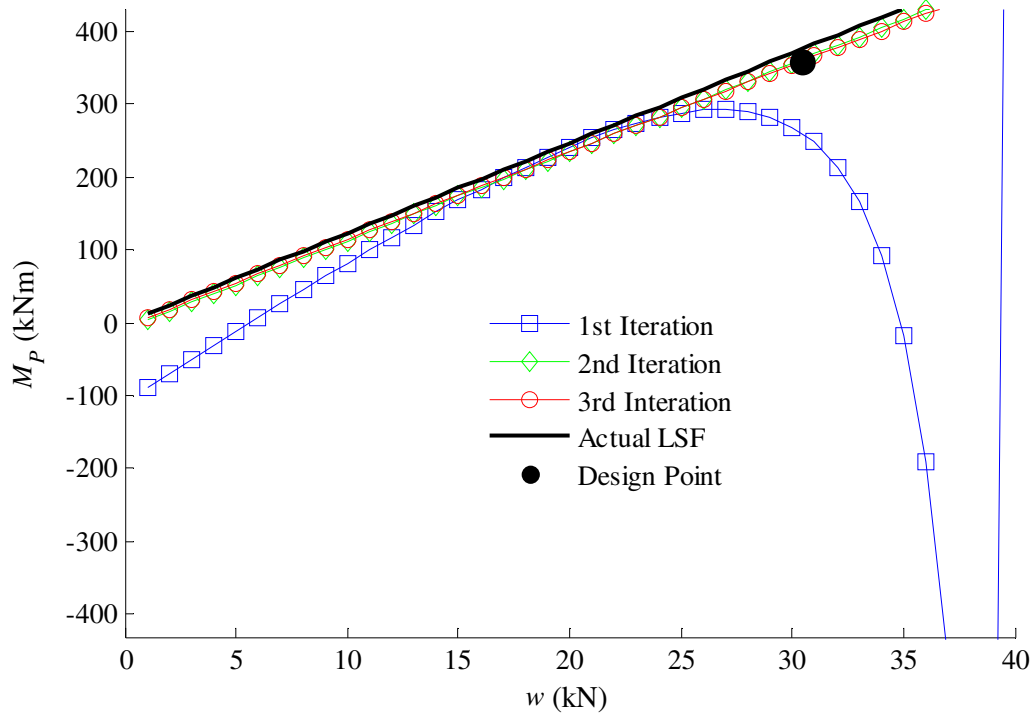
Figure 5.11: Example 2 RSM approximating functions for each iteration.

5.7   Summary

In this chapter a RSM model is developed. This model is based on the work of Rajashekhar et al (1993). This model is appropriate as it uses an iterative process to locate the ED around the MPP meaning an accurate representation of failure at that point is given. This model proves to be effective provided only one mode of failure is present. The RSM model was also linked to the NFEA model and validated using the three benchmark examples. This provides the methodology to conduct a probabilistic assessment considering nonlinear material behaviour.

Chapter 6

Bridge Models

6.1   Introduction

This chapter outlines a representative group of bridge structures used for this work. Each bridge structure differs with regard to configuration, span length, and resistance capacity. This representative group of bridge structures are used in assessing live load application in nonlinear structural models and the development of both deterministic and probabilistic assessment procedures considering material nonlinearity.

6.2   Bridge Model Geometry

The bridge configurations studied for this work are given in Figure 6.1.

a) Two-span;

b) Three-span;
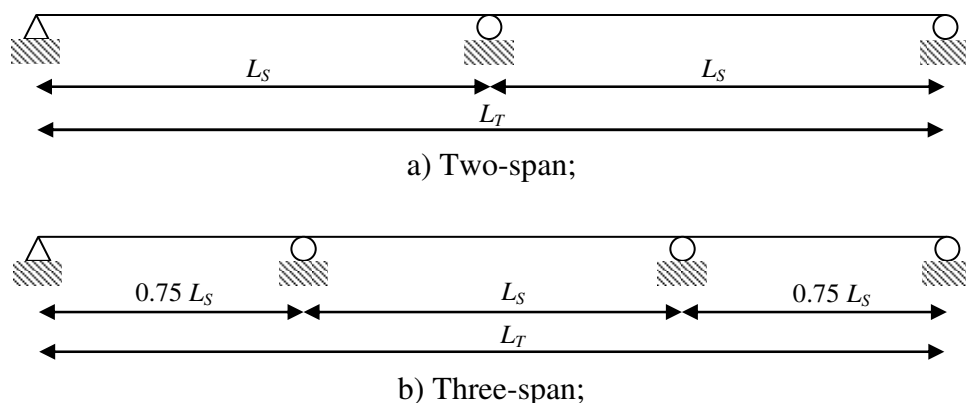
Figure 6.1: Bridge configurations.

Each bridge configuration is examined for the following total bridge lengths (L_T): 30, 40, 50, 60 m. Thus, in total, eight bridge structures are examined. Table 6.1 outlines the descriptive name given to each of the bridge structures.

Table 6.1: Bridge descriptive names

Configuration	Length (m)	Name
Two-span	30	2span-30
Two-span	40	2span-40
Two-span	50	2span-50
Two-span	60	2span-60
Three-span	30	3span-30
Three-span	40	3span-40
Three-span	50	3span-50
Three-span	60	3span-60

6.3   Lane Distribution Factors

A one-dimensional NFEA beam model is used in this work and so Lane Distribution Factors (LDF) are determined to represent transverse distribution of load. The AASHTO (AASHTO-LRFD, 2007) bridge design code outlines girder distribution factors following extensive work in the area using both in-situ tests and finite element models (Eom et al, 2001; Huo et al, 2004; Satelino et al, 2004; NCHRP report 592). For this work, similar to these studies, finite element models are developed for each bridge structure. To obtain accurate lateral distribution, LUSAS is used to develop a grillage. Common properties were assumed for each structure: Each bridge has two 3.65 m wide lanes of bi-directional traffic. Each bridge consists of a 250 mm concrete slab sitting on 4 steel plate girders spaced 2650 mm apart. The cross section used for all the bridge structures is shown in Figure 6.2.
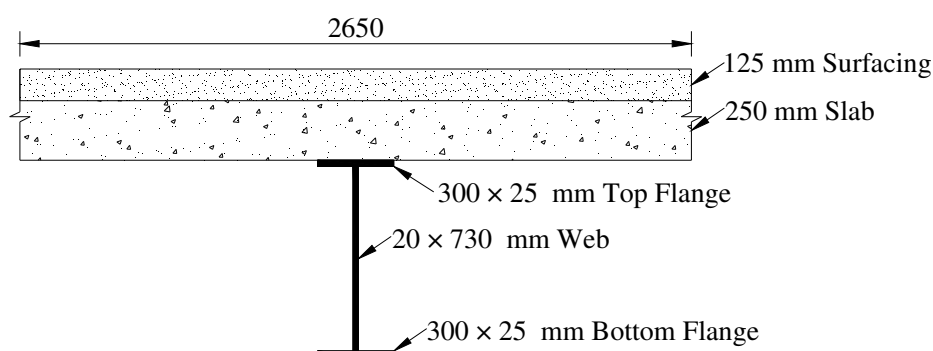
Figure 6.2: Composite cross section used for each bridge studied.

A linear elastic finite element analysis is used to determine the lateral distribution factors of the live load moment on the bridge. A grillage analysis is conducted with longitudinal

members representing the beam and slab composite section and the transverse members representing the slab section. The torsion constants of these sections were altered to allow for the overlap of members. The live load applied in this study is two 50 kN point loads 2 m apart representing a single truck axle as shown in Figure 6.3.
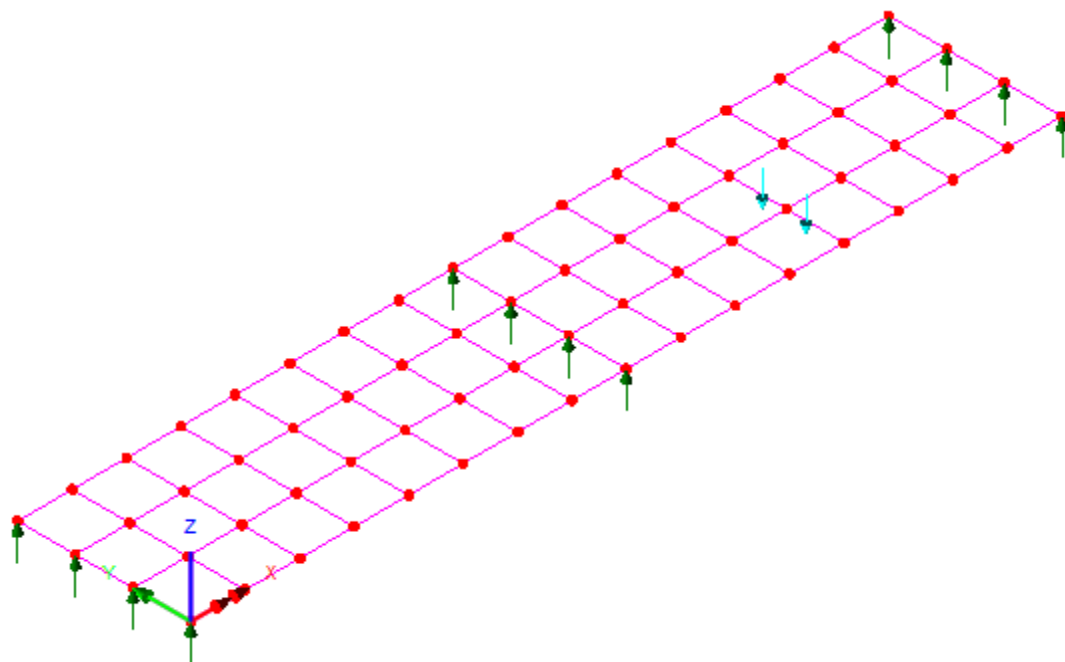
Figure 6.3: LUSAS model (2span-40 bridge)

From this analysis influence lines for each beam were drawn for predefined load effects for each bridge configuration as given in Table 6.2. An example of this is shown in Figure 6.4.

Table 6.2: Predefined load effects.

Configuration	Load Effect	Description
2	1	first span mid span bending moment
2	2	hogging moment over interior support
3	1	hogging moment over first interior support
3	2	interior span mid span bending moment
3	3	exterior span mid span bending moment
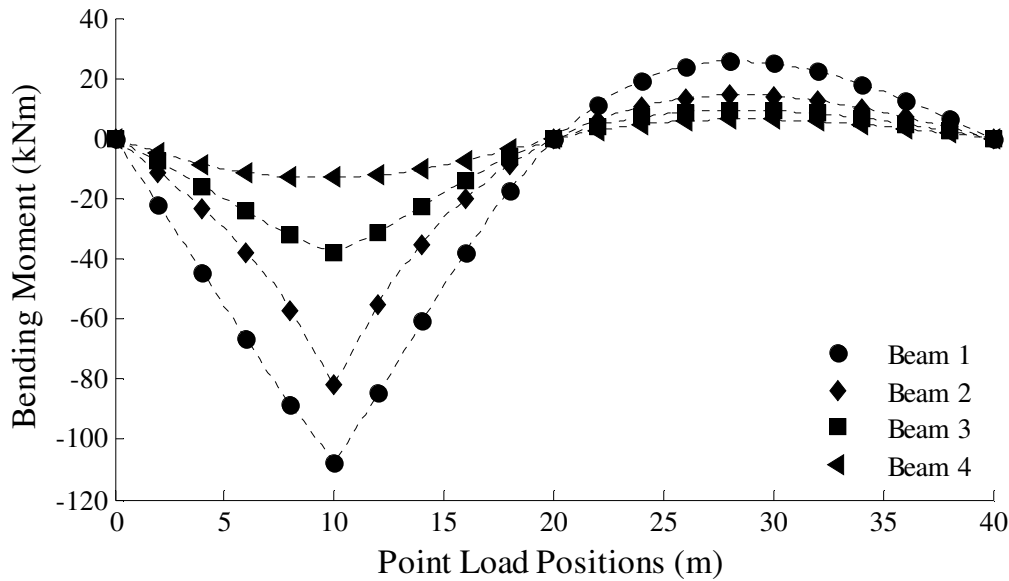
Figure 6.4: 2span-40 load effect 1 beam influence lines.

A LDF is the percentage distribution of load to each beam. This is the ratio of the bending moment (BM), at position causing maximum moment in each beam, to the total bending moment over the cross section. The LDFs are reversed for the opposite lane as each bridge is symmetrical. The critical beam for each bridge is identified as the beam carrying the highest percentage bending moment when both lanes are loaded. These beams are used for the duration of this study. A sample calculation of the LDFs of the 2span-40 bridge for load effect 1 is shown in Table 6.3. The external beams are determined critical for this example.

Table 6.3: 2span-40 load effect 1 LDF calculation.

	Beam 1	Beam 2	Beam 3	Beam 4
BM (kNm)	-107.70	-82.12	-38.20	-12.92
Total BM (kNm)	-240.94	-240.94	-240.94	-240.94
LDF-Lane 1	0.447	0.341	0.159	0.054
LDF-Lane 2	0.054	0.159	0.341	0.447
Total	0.501	0.499	0.499	0.501

The critical beam LDFs for each load effect are given in Table 6.4.

Table 6.4: Critical beams for each load effect.

Bridge	Load Effect	Critical Beam	LDF-Lane 1	LDF-Lane 2
2span-30	1	Interior	0.3722	0.1583
	2	Interior	0.3344	0.1812
2span-40	1	Exterior	0.447	0.054
	2	Exterior	0.484	0.051
2span-50	1	Exterior	0.444	0.072
	2	Exterior	0.490	0.067
2span-60	1	Exterior	0.438	0.083
	2	Exterior	0.489	0.077
3span-30	1	Interior	0.375	0.180
	2	Interior	0.416	0.154
	3	Interior	0.415	0.156
3span-40	1	Interior	0.337	0.182
	2	Interior	0.386	0.156
	3	Interior	0.389	0.158
3span-50	1	Exterior	0.480	0.046
	2	Interior	0.359	0.157
	3	Interior	0.367	0.158
3span-60	1	Exterior	0.487	0.061
	2	Exterior	0.445	0.056
	3	Exterior	0.448	0.054

6.4   Plastic moment capacity calculation

The plastic moment capacity for each critical composite beam is calculated as required for the NFEA model. Following the work of Nowak (2001), the plastic moment capacity (M_P) is chosen to represent the minimum required capacity as specified in the Eurocode:

$$M_p = \left[\alpha_D \left(D_1 + D_2 + D_3 \right) + \alpha_L \left(L \right) \left(LDF \right) \right] / \phi \qquad (6.1)$$

where α_D is dead load factor (1.35) (EC1.1, 2005), α_L is the live load factor (1.5) (EC1.1,1990), ϕ is the resistance factor (0.88) (Nowak et al, 2001), D_1 is the dead load moment due to the beam, D_2 is the dead load moment due to the slab, D_3 is the dead load moment due to the road surfacing, L is the live load moment on the structure and LDF is the maximum total LDF of the critical beam in the bridge. The live load on each structure is determined using LM1 (EC1.2, 1991). This plastic moment capacity was chosen to show the

effect of assessing existing structures to albeit a simple representation of the Eurocodes. The

plastic moment capacities for each bridge are shown in Table 6.5.

Table 6.5: Plastic moment capacity for each bridge.

Bridge	Plastic Moment Capacity (kNm)
2span-30	2694
2span-40	4279
2span-50	6295
2span-60	8592
3span-30	1422
3span-40	2015
3span-50	2963
3span-60	4055

6.5   Summary

A representative group of steel composite structures is outlined. The structures vary in regard

to structural configuration and bridge length. Each structure is designed to have the minimum

required Eurocode flexural capacity. Grillage models are developed for all structures to

determine lane distribution factors and the critical beam in each structure.

Chapter 7

Live Load Application

7.1   Introduction

This chapter examines the application of live loads in a nonlinear structural model for use in a probabilistic assessment. The live loads considered are vehicles traversing a structure. Dynamic effects are not considered. A proposed moving load approach is developed and compared to the commonly used approach of applying the live load as critically positioned static loads.

7.2   Common Approach

Commonly, in nonlinear structural models moving live loads are applied as stationary static loads (see Section 2.2.1). Commonly, the positions of these static loads are found using an elastic analysis. The live load is positioned so as to cause the maximum desired load effect. This approach is used in literature outlined in Table 7.1.

Table 7.1: Live load application literature summary

Reference	Bridge Type	No. Spans	Load	Position
Val et al (1997b)	RC Slab	1	H20	causing maximum moment
Val et al (1997b)	RC Slab	3	HS20	causing maximum moments
Ghosn et al (1998)	Steel Truss	1	HS20	causing maximum moments
Casas et al (2007)	Concrete Girder	4	Various UDLs	causing maximum moments
Casas et al (2007)	Steel Beam	2	Various UDLs	causing maximum deflection/shear
Czarnecki et al (2007)	Steel Composite	1	HS20	causing maximum moment
Wisniewski et al (2009)	Concrete Girder	4	UDL Train Model	causing maximum moment at mid-span first span
Zona et al (2010)	Steel Composite	3	Load Model 1	causing maximum moment at left intermediate support

As can be seen from Table 7.1 real traffic crossing events are not considered, only notional load models applied at positions found using an elastic analysis.

7.3   Proposed Moving Load Approach

A load must be applied incrementally when conducting a nonlinear static analysis. The proposed moving load approach is applied in increments, but also moved in increments. The load is moved in steps along the structure to represent a moving load traversing the structure.

The load is initially applied at the start of the bridge as a static load and incrementally increased in magnitude. Once fully applied, the force at this position is unloaded and concurrently incrementally applied to the next location. This procedure is illustrated in Figure 7.1 and is repeated until the load has completely traversed the structure.
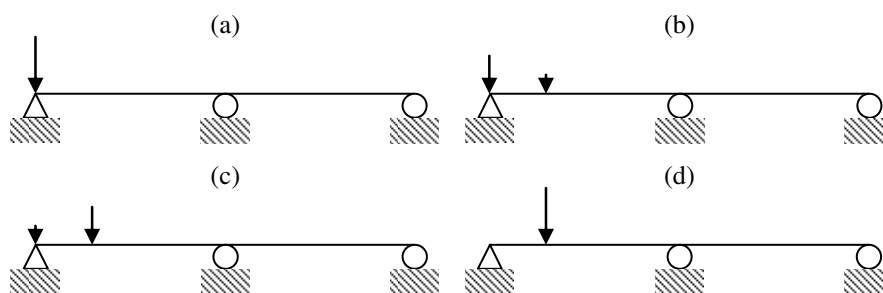
Figure 7.1: Propose moving load procedure.

Importantly, an increment is unloaded assuming that the structure behaves elastically (Li et al, 2007) .The force recovery parameters (Section 4.5) are calculated once an increment has been unloaded and before the increment is applied at its new location. This allows for the spread of plasticity through the structure. The load required to cause a defined failure is increased after each complete run across the structure.

Excluding the initial incremental loading at the first load position, and the incremental unloading at the last load position, the full load is completely applied to the structure at all times. This is shown in Figure 7.2.
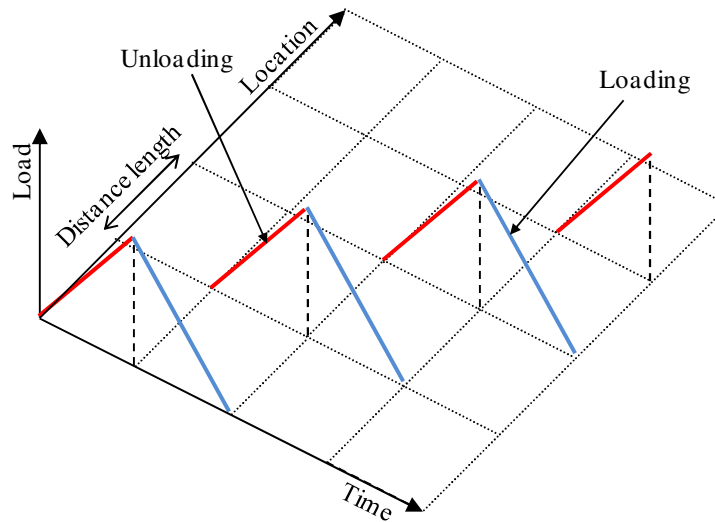
Figure 7.2: Load through time for proposed moving procedure

The methodology behind the proposed moving load approach is shown in the flowcharts given in Figure 7.3 - 7.6.
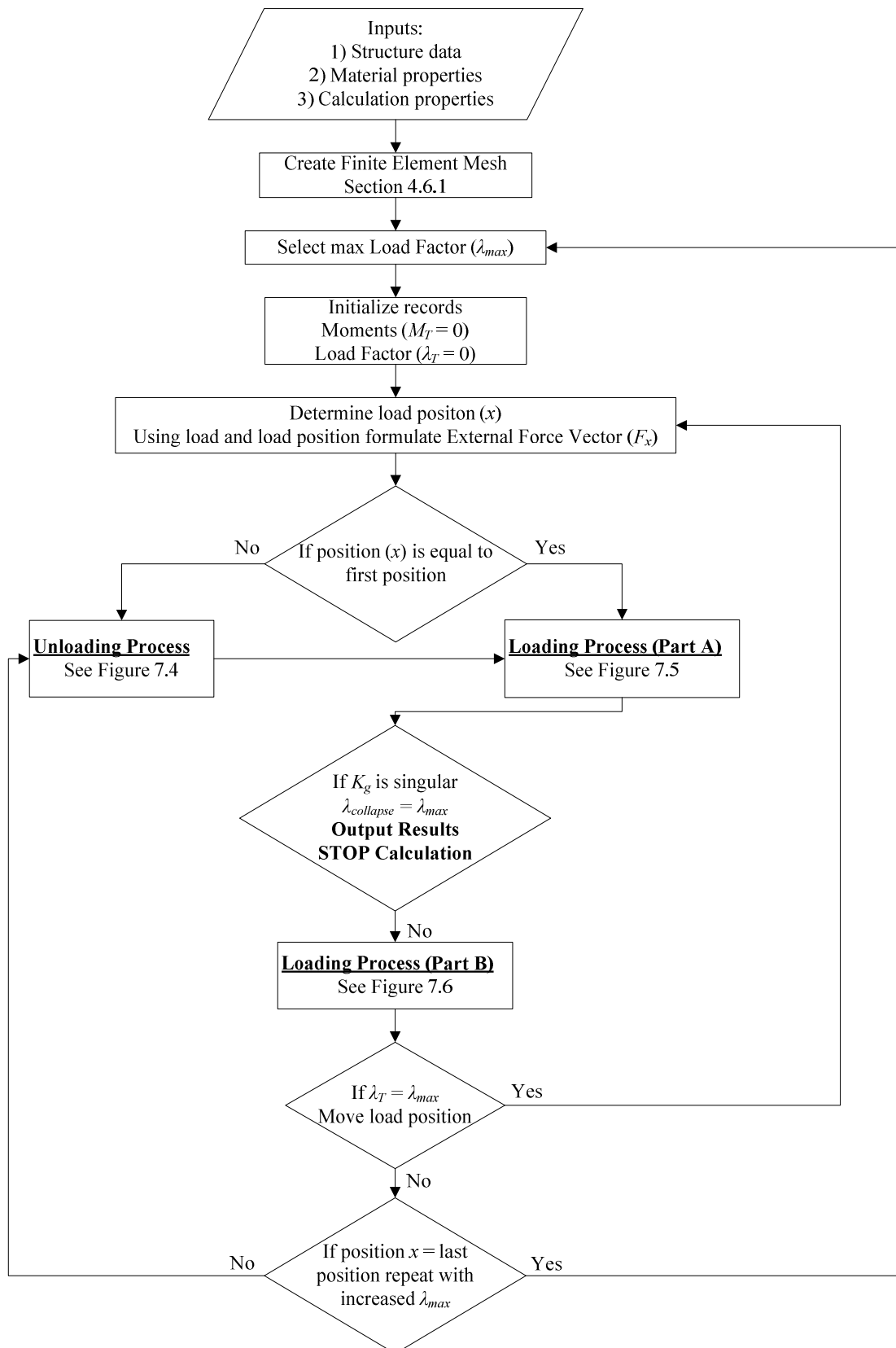
Figure 7.3: Analysis procedure of bridge subject to moving load
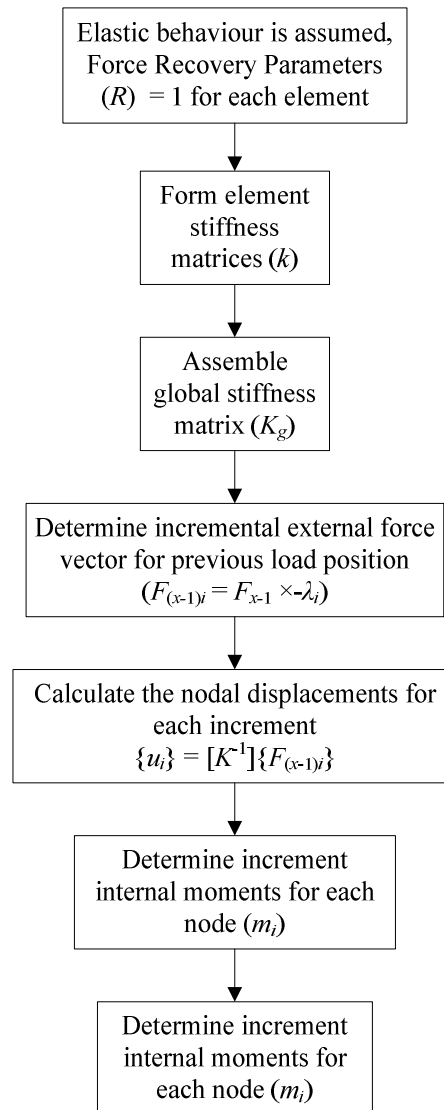
Figure 7.4: Unloading process
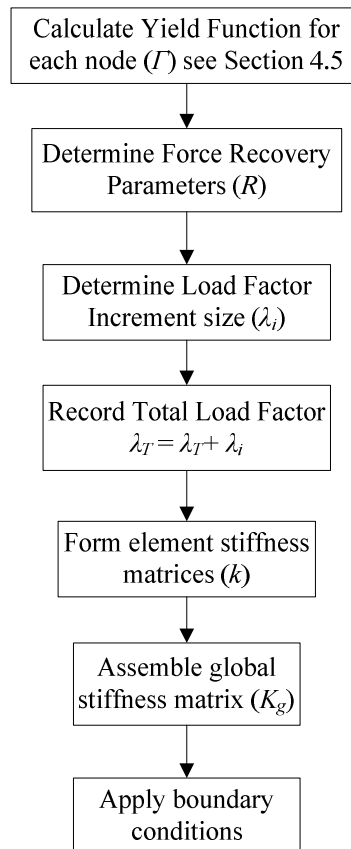
Figure 7.5: Loading process (part A)
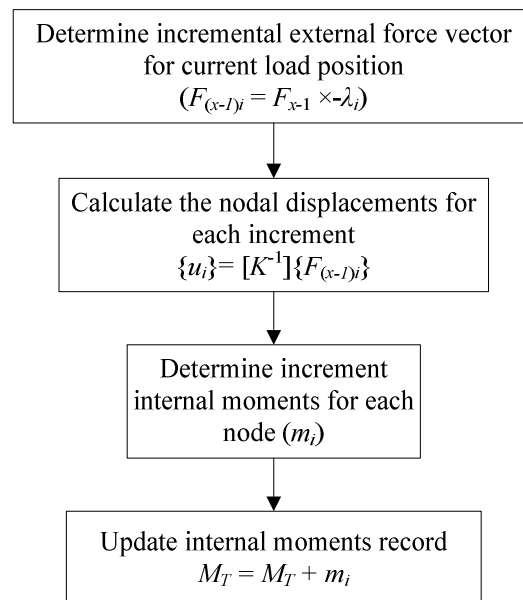
Figure 7.6: Loading process (part B)

7.3.1 Single Moving Point Load Analysis Example

To demonstrate the proposed moving load approach, the 2span-30 bridge (Section 6.1) is

subjected to a single point load of speed 1 m/s to get collapse. To establish the collapse load

factor, that is, the ratio of failure load to working load, the load is increased after each complete run across the structure, and this is continued until a collapse mechanism forms. A time step of 0.1 s corresponding to a step length of 0.1 m is used, see Figure 7.2. The yield function defined in Equation (4.7) is a ratio of bending moment to plastic moment capacity as described in Section (4.6) is used to describe the spread of plasticity though the structure as the load moves. The yield function time history is shown in Figure 7.7.
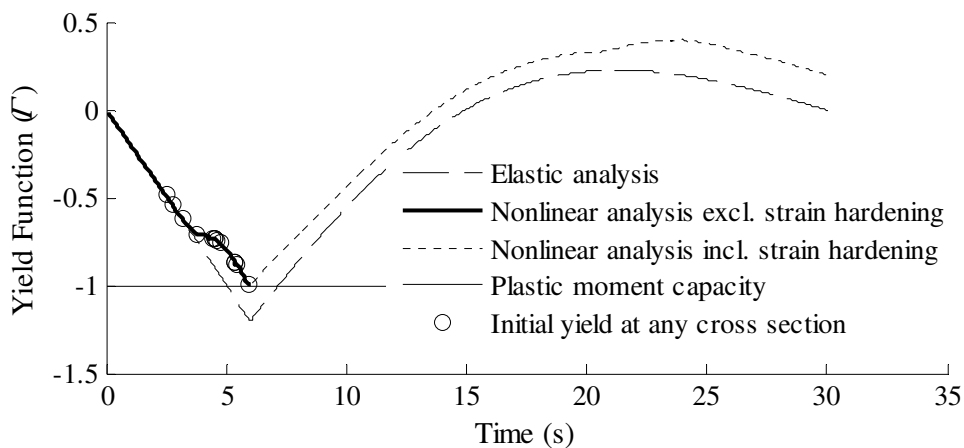
(a) Hinge formation at 6 m;
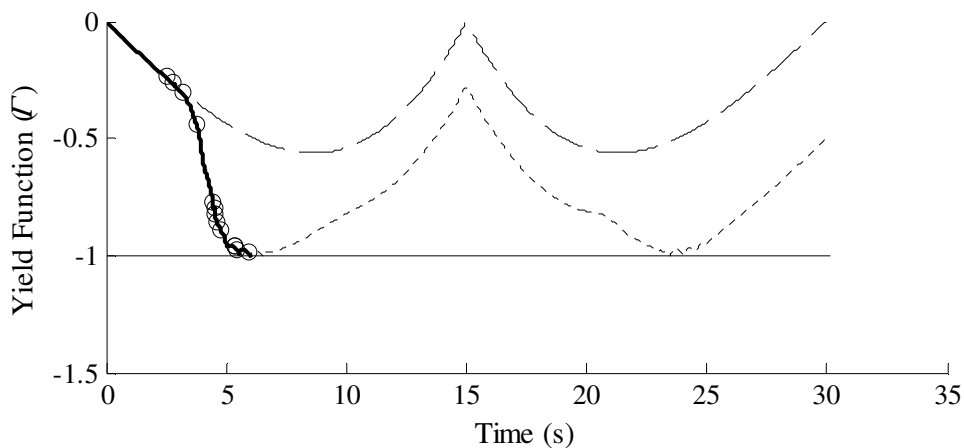
(b) Hinge formation at 15 m;

Figure 7.7: Time history of yield function.

These graphs show the difference between the proposed moving approach and an elastic analysis when strain hardening is both included and excluded. When strain hardening is included, the global stiffness matrix is prevented from turning singular meaning the analysis

will continue until the load has fully traversed the structure. When examining the nonlinear analysis excluding strain hardening it is seen that a collapse mechanism forms when the point load is approximately 6 m from the left hand side. The circles on each graph represent times at which the initial yield capacity of the structure has been exceeded at any location on the bridge. Table 7.2 gives this post-elastic behavior. Since the structure is one-degree indeterminate, a collapse mechanism occurs when two plastic hinges form at 6 m and 15 m.

Table 7.2: Post elastic behaviour activity.

Activity	Time (s)	Location
Initial Yield	2.50	2.5 m
Initial Yield	2.79	3.5 m
Initial Yield	3.16	4.5 m
Initial Yield	3.78	5.5 m
Initial Yield	4.45	15.0 m
Initial Yield	4.93	15.5 m
Initial Yield	4.54	16.0 m
Initial Yield	4.64	14.5 m
Initial Yield	4.77	17.0 m
Initial Yield	5.38	18.0 m
Initial Yield	5.38	6.5 m
Initial Yield	5.46	14.0 m
Initial Yield	5.93	7.0 m
Plastic Hinge	5.93	6.0 m
Plastic Hinge	5.93	15.0 m

7.4   NFEA mesh refinement

To obtain an accurate comparison between the common approach and the proposed moving load approach the mesh refinement must be kept consistent in the NFEA model. A finer mesh separates the structure into more elements. Generally this leads to a higher level of accuracy but is computational more expensive. In this study a non uniform mesh is used to reduce the number of elements. Points of interest are identified prior to loading such as mid span or over internal supports. A finer mesh size is used for a defined distance around these points. This non-uniform mesh is illustrated in Figure 7.8.
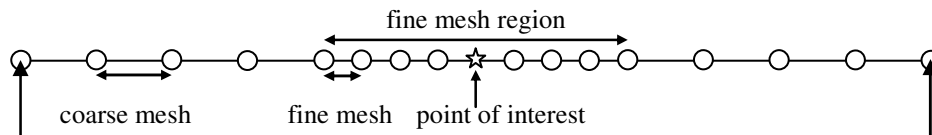
Figure 7.8: Non-uniform mesh.

The size of the coarse mesh is chosen as 0.5 m, while the size of the fine mesh was arbitrarily chosen as 0.25 m. The fine mesh covers a one metre either side of the defined point of interest. These points of interest were located on over the mid-spans and interior supports. This mesh refinement was used along with the adaptive increment process (see Section 4.7) in both the common approach and the proposed moving approach.

7.5   Live Load Combinations

A series of experiments are devised to compare the proposed approach with the commonly-used approach of placing loads at critical positions. A range of axles spacings and a number of axles are examined as given in Figure 7.9. Each experiment was applied to the eight bridge structures outlined in Chapter 6 yielding a total of 80 results for comparison.

Table 7.3: Live load combination description

Live Load Combination	Description
AS1	Single axle load
AS2-H20	Two axles, H20 design truck
AS3-HS20	Three axles, HS20 design truck
AS5-T1103	Five axles, T1103 European truck
AS2-X	Two axles, axles spacing (x) = 1.5, 3.0, 4.5, 6.0, 7.5, 9.0 m

* AS means Axle Scenario.
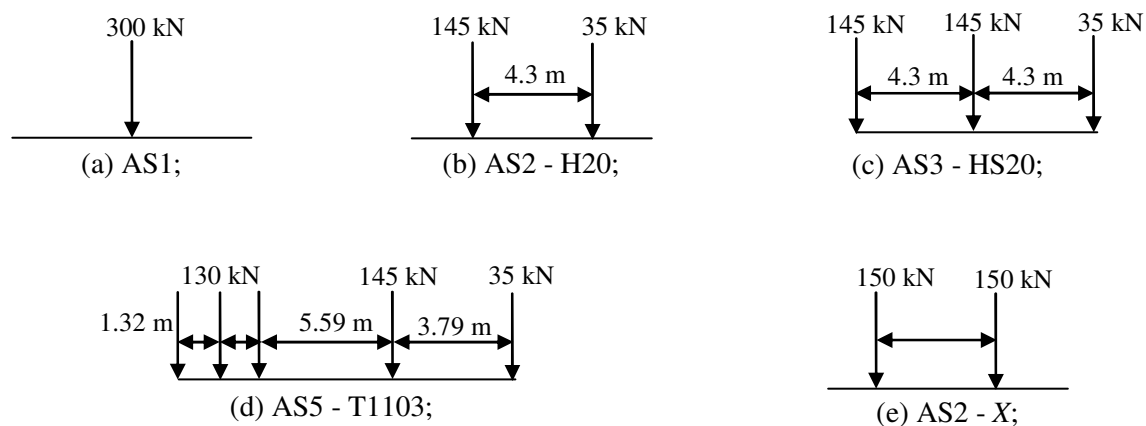
Figure 7.9 Load live combinations.

For each experiment a load factor required to cause failure is found using the common approach and the proposed moving approach. Failure is defined to occur when the global stiffness matrix becomes singular in the nonlinear analysis (Owen, 1986; Val, 1997b; Wong, 2005). This corresponds to the formation of a mechanism (Ghosn, 1998).

7.6   Common Approach Positions

For the common approach an elastic analysis is used to identify load positions, defined in Table 7.4.

Table 7.4: Static load positions

Two-span	CP 1	causing maximum bending moment at any location
	CP 2	causing maximum sagging moment at mid span of first span
	CP 3	causing maximum hogging moment over interior support
Three-span	CP 1	causing maximum bending moment at any location
	CP 2	causing maximum hogging moment over first support
	CP 3	causing maximum sagging moment at mid span of centre span
	CP 4	causing maximum sagging moment at mid span of third span

* CP refers to Common approach position.

7.7   Load Factor Ratio

The static load factors found using the common approach (λ_C) are compared to the load factor

found using the moving load approach (λ_M) in terms of a load factor ratio $(\lambda*)$:

$$\lambda* = \frac{\lambda_C}{\lambda_M} \tag{7.1}$$

If $\lambda* < 1$, the common approach under-estimates the flexural capacity of the structure;

similarly if $\lambda* > 1$ the common approach over-estimates the flexural capacity of the structure.

Load factor ratios are determined for all static positions, as per Table 7.4. Table 7.5 shows

sample results for the live load combination AS5-T1103 on the 3span-50 bridge.

Table 7.5: λ^* for AS5-T1103 on bridge 3span-50.

$\lambda*_1 = \frac{\lambda_{CP1}}{\lambda_M}$	$\lambda*_2 = \frac{\lambda_{CP2}}{\lambda_M}$	$\lambda*_3 = \frac{\lambda_{CP3}}{\lambda_M}$	$\lambda*_4 = \frac{\lambda_{CP4}}{\lambda_M}$
1.0054	1.0031	1.0424	1.2319

Table 7.5 shows the importance of applying the loads in the correct position when using the

commonly used approach. If the axle loads of the T1103 truck are applied at the position

causing maximum hogging moment over the first interior support an accurate estimation of

the structure strength capacity is found when compared to the true result (Moving load

approach). However, if the loads are positioned such as the maximum moment at mid span of

the third span is found, the strength capacity of the structure is over-estimated by

approximately 25%. The positions used in the common approach, as per Table 7.4, are shown

in Figures 7.10 - 7.13. The collapse mechanisms for each position are also shown.
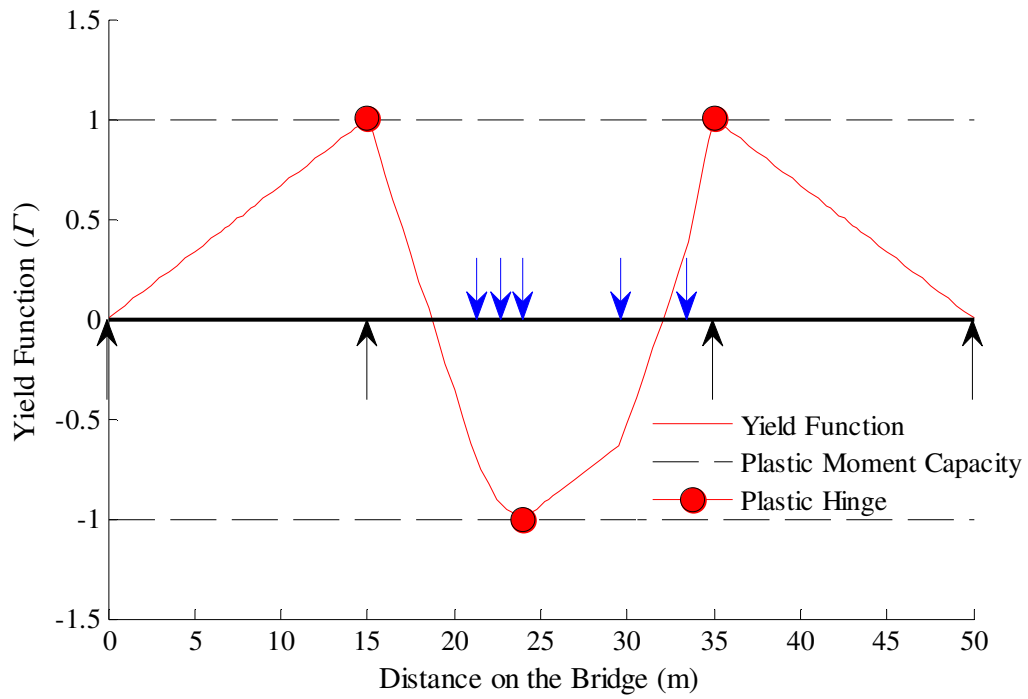
Figure 7.10: AS5-T1103, 3span-50, CP1
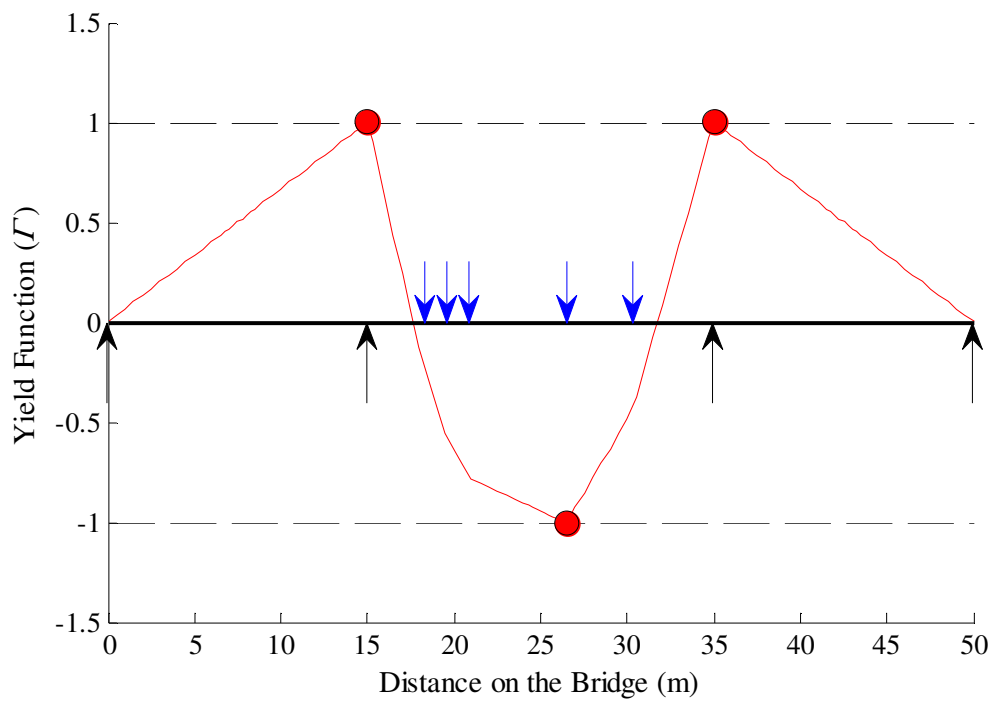
Figure 7.11: AS5-T1103, 3span-50, CP2
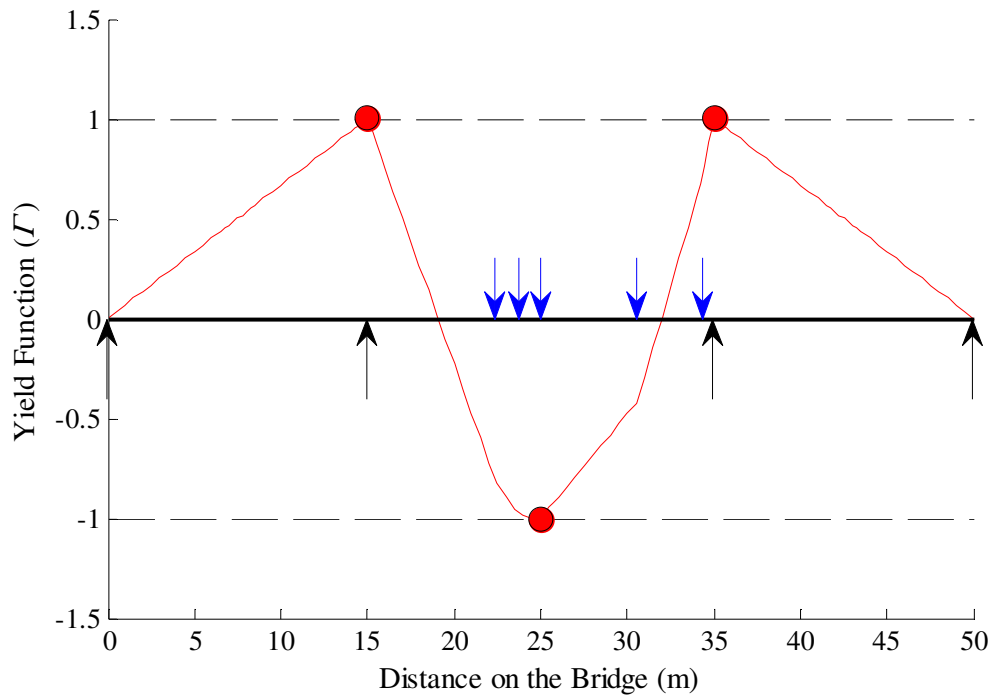
Figure 7.12: AS5-T1103, 3span-50, CP3
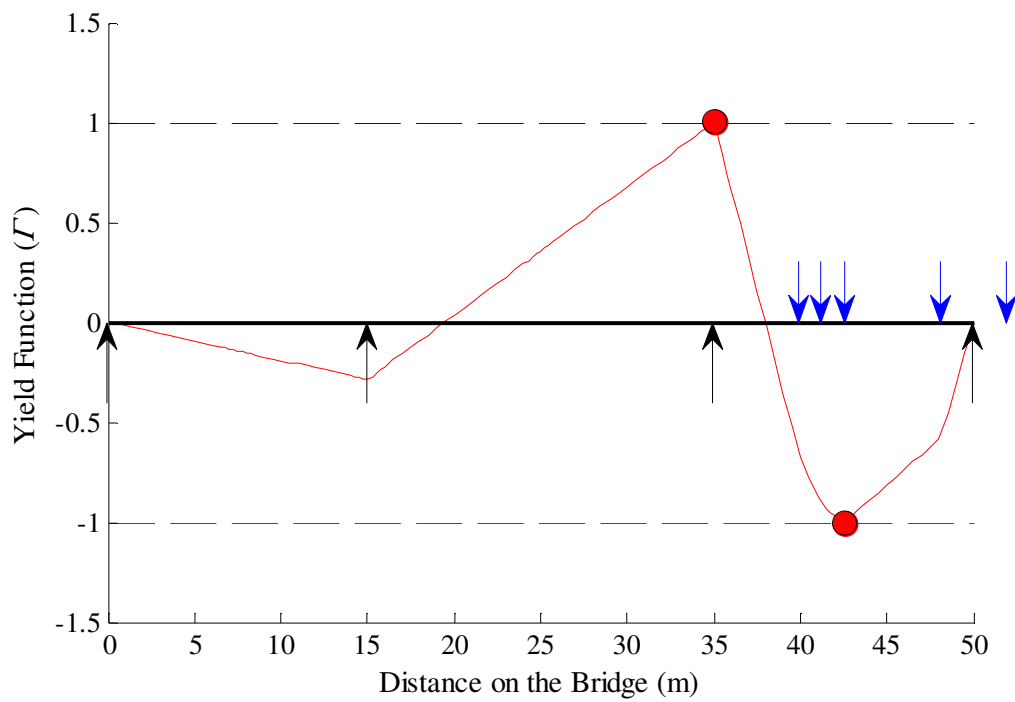
Figure 7.13: AS5-T1103, 3span-50, CP4

7.8   NFEA Modelling Issue

Due to the non-uniform mesh used in the NFEA model (Section 7.4) a modelling issue occurs which under-estimates the strength capacity for a number of static live load combinations. The global stiffness matrix turns singular without producing a true collapse mechanism. Since a fine mesh is adopted over mid-spans and internal supports (see Section 4.6) illustrated in Figure 7.14a, multiple hinges occur at closely located node points as shown in Figure 7.15a.

(a) Non-uniform mesh.

To rectify this, the problematic loading scenarios are re-run with a coarser mesh illustrated in Figure 7.14a so that non-trivial collapse mechanisms are formed as shown in Figure 7.15b.

(b) Uniform coarse mesh.

Figure 7.14: Mesh refinement
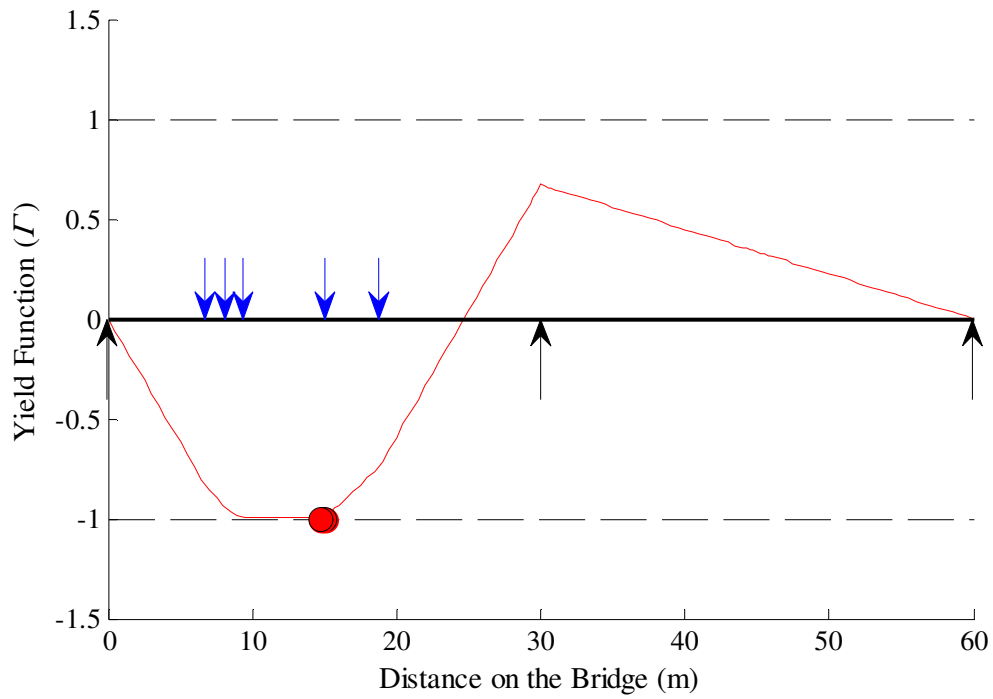
(a) Collapse mechanism with wrong mesh refinement;
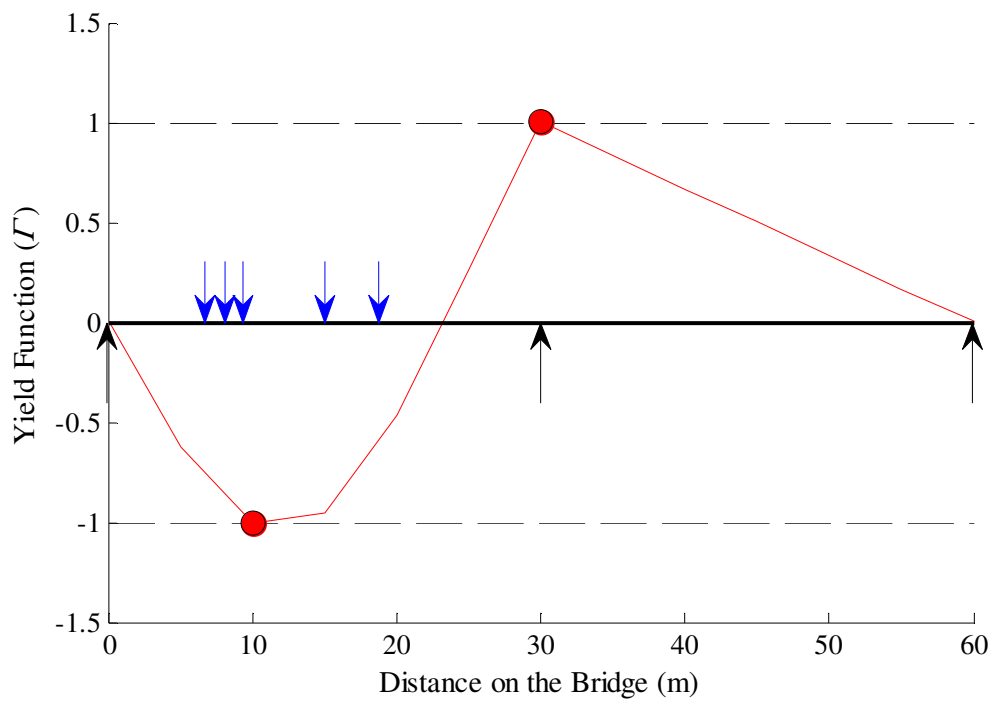
(b) Collapse mechanism with corrected mesh refinement;

Figure7.15: Bridge 2span-60 experiment AS5-T1103

7.9 Live Load Application Results

For each experiment the load factor ratio for each common approach position (see Table 7.4) is found. Figure 7.16 shows live load combination AS3-HS20, performed on bridge lengths, 30, 40, 50 and 60 m with a two equal span configuration.
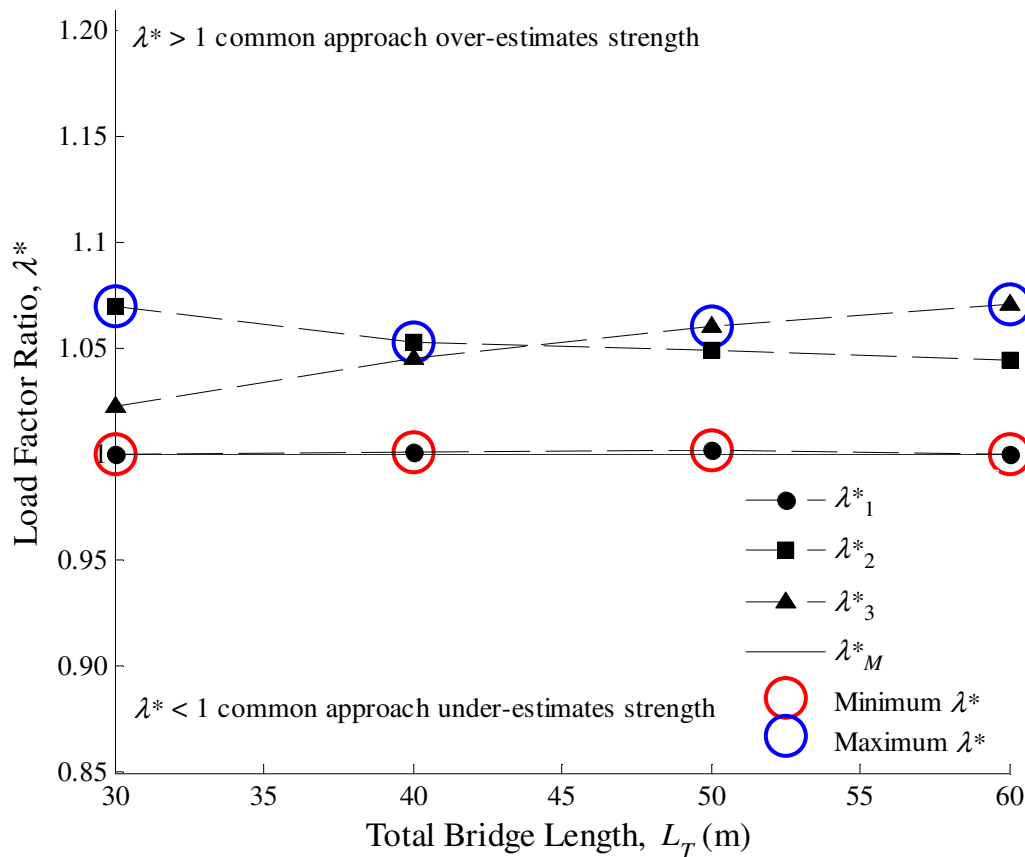
Figure 7.16: Load factor ratios versus bridge length (Configuration 1 - AS3-HS20)

Significant differences in collapse load factors are found depending on the position of load examined. The best case load position, producing a load factor similar to the moving load approach is highlighted with a red circle for each bridge length. Similarly, the worst load position is highlighted with a blue circle for each bridge length. This is done to emphasize the importance of examining several load positions using the common approach. Figure 7.16 shows that there is a difference in strength capacities of at least 5% found between the best and worst case load positions used in the common approach. The complete set of graphs for each live load combination can be found in Appendix 1.

For all live load combinations examined on the two-span structures, the best load factor ratio is found when the load is positioned to cause maximum bending moment (Table 7.4 - CP1). Numerous load positions need to be examined for three span structures because the position causing maximum bending moment does not guarantee lowest load factor ratio (lowest strength capacity estimation).

The best case load factor ratios (red) and the worst case load factor ratios (blue) for each live load combinations are shown in Figures 7.17- 7.20. If the best case load factor ratios are used to compare the common approach to the moving load approach, it is found that the strength capacities found using the two approaches are within 1% for two span structures and 3% for three span structures meaning that load redistribution as a vehicle moves across the structure has very little significance. However, if the worst case load factors are examined, the common approach overestimates the strength capacities greatly. This highlights the requirement of correctly locating the loads when using the common approach. This requirement is not present when using the proposed moving load approach as the load position is found automatically.
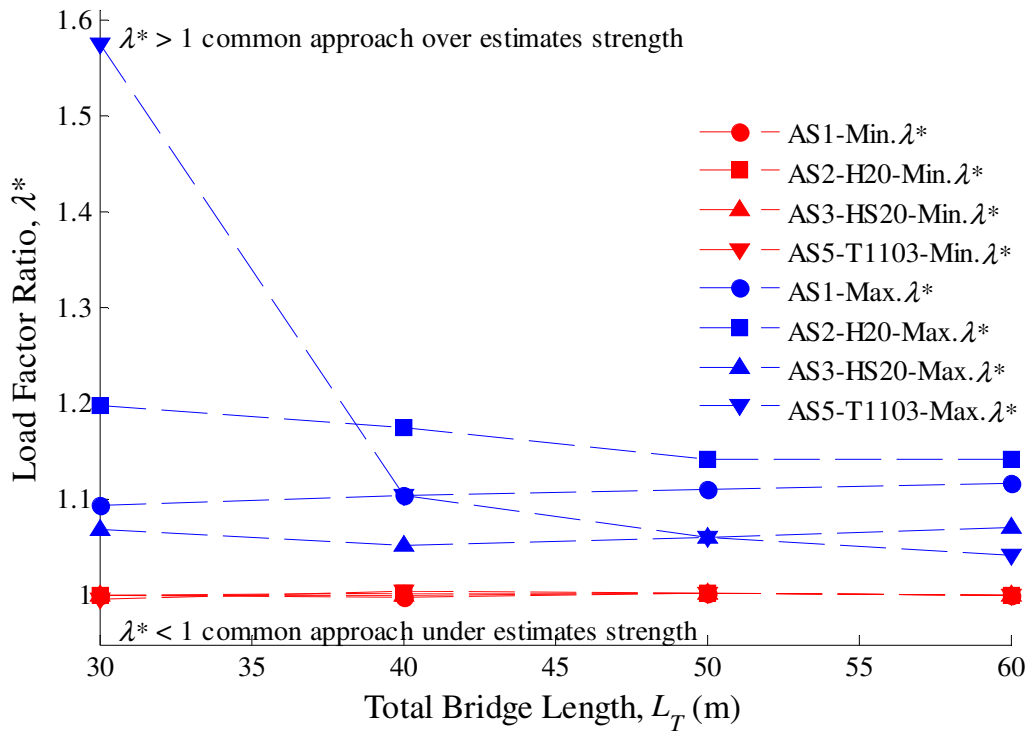
Figure 7.17: Two-span live load combinations 1-4
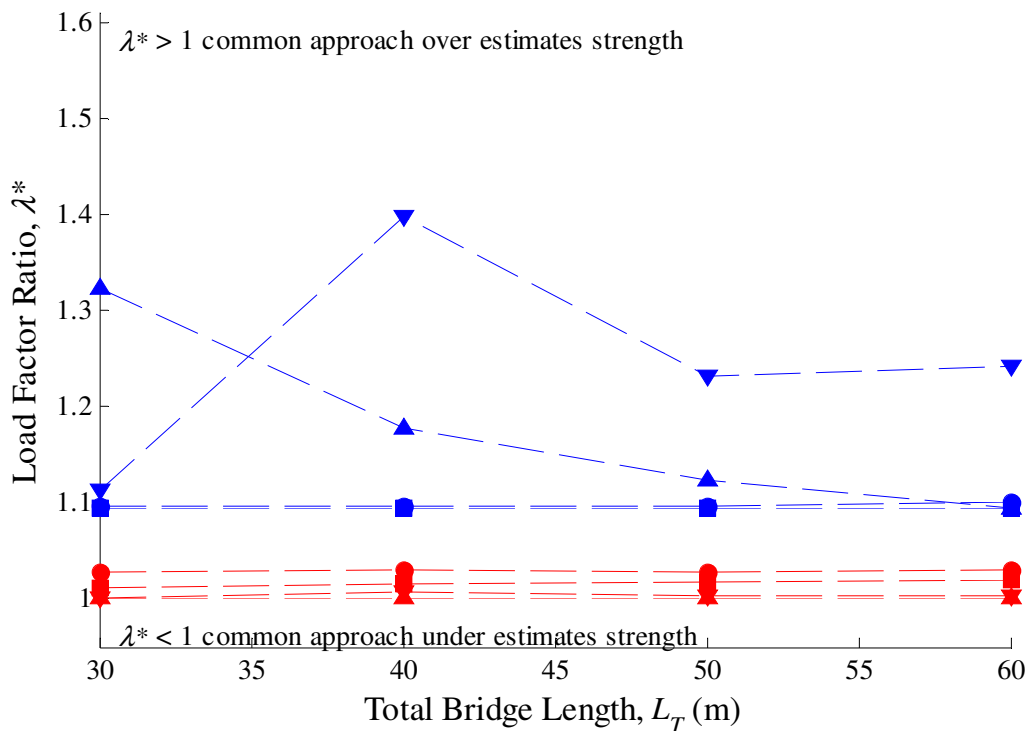
Figure 7.18: Three-span live load combinations 1-4 (see Figure 7.17 for legend).
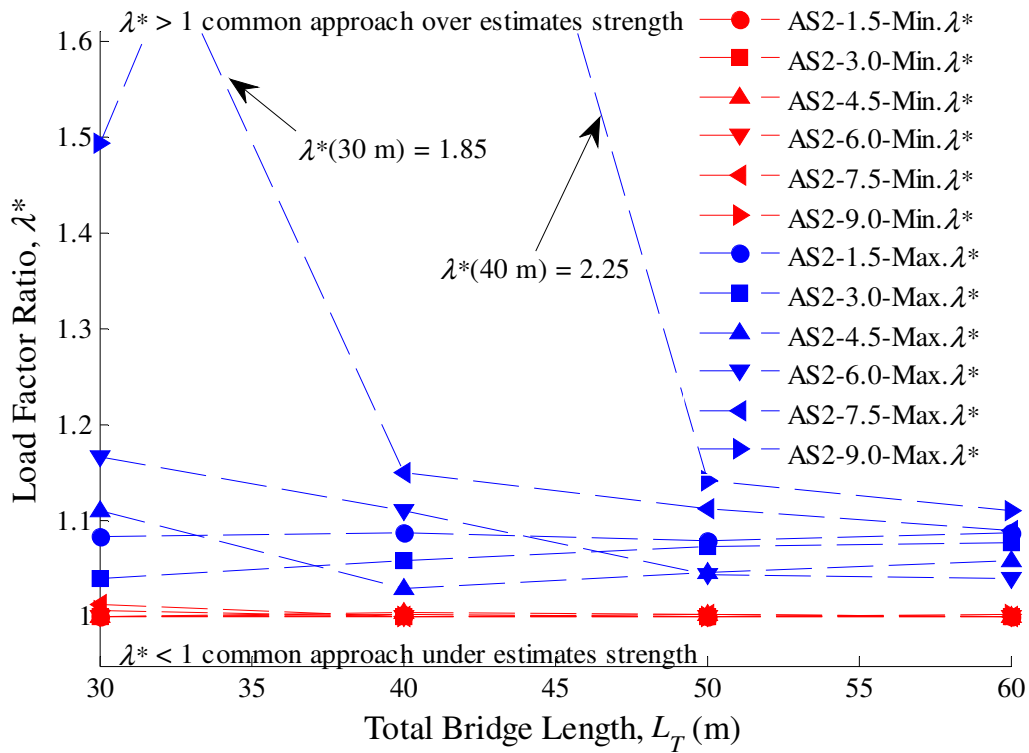
Figure 7.19: Two-span AS2-X.
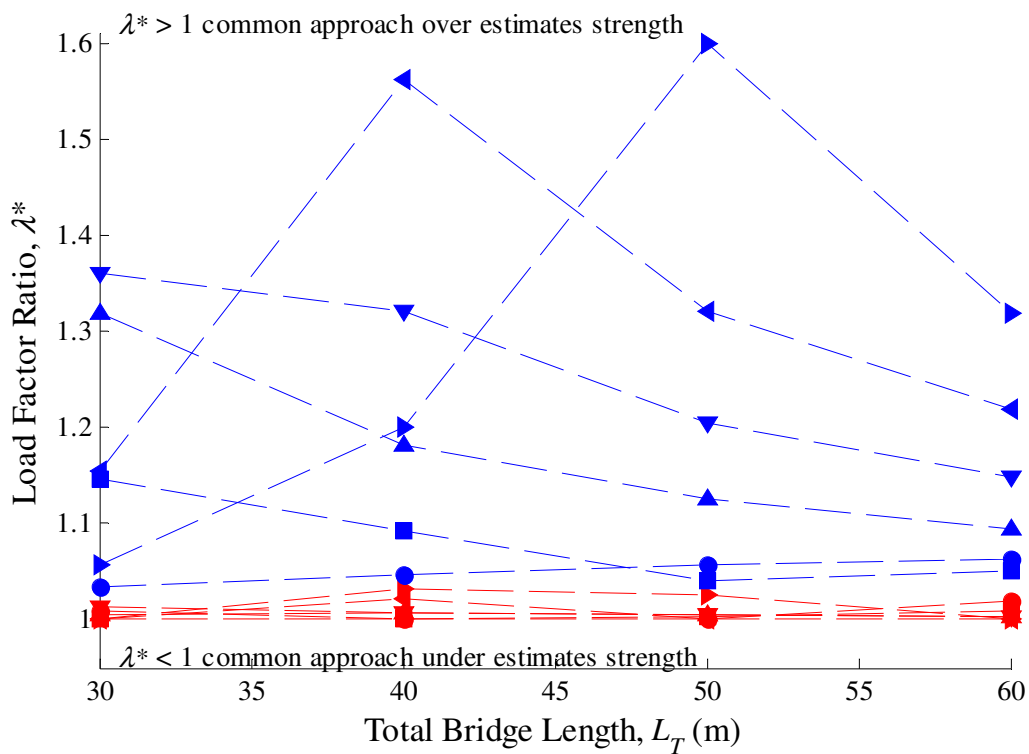
Figure 7.20: Three-span AS2-X (see Figure 7.19 for legend).

7.10   Relation to Literature

From the observations obtained, a closer examination of the work of Val et al (1997b) is conducted. In the study the authors conduct both a deterministic and a probabilistic study of a three-span continuous slab bridge. The structure is subjected to a HS20 design truck load located at various positions to cause maximum bending moment at different locations. These locations include the mid-span of the first span, the mid-span of the interior span, and at the second interior support. The truck position causing maximum bending moment at the interior support is indeed critical as it produces the lowest estimation of strength capacity. On comparison with the moving load approach, Val's critical truck position performs a good estimation of the required strength capacity of the structure is obtained.

7.11   Summary

Through the use of the proposed moving load approach it is found that some elastic means of locating the load perform well, giving accurate collapse load factors, whilst others perform poorly. For two-span structures it is concluded that locating the vehicle such that the maximum elastic bending moment anywhere is achieved gives a close estimate of the true collapse load factor found from the moving load approach. Conversely for three span structures it is important to examine numerous positions when using an elastic means to locate the load.

Chapter 8

Deterministic Safety Assessment

8.1   Introduction

In this chapter a deterministic approach is used to assess the structural safety of the representative group of steel composite structures. All resistance and load properties are treated as deterministic variables. The structural safety of the bridges considered, subjected to realistic traffic loading events, is described in terms of a load factor required to cause failure. Three definitions of failure are examined:

1. The exceedance of the initial yield capacity at any section.

2. The formation of the first plastic hinge.

3. The formation of a collapse mechanism.

Furthermore, a semi-probabilistic assessment is carried out in which resistance and dead load are assumed to be deterministic while live load is examined as a random variable.

8.2   Annual maximum traffic loading events

Monte Carlo simulation was used to generate 100 years of free flow traffic files based on measured traffic data, representing a bridge lifetime. This data was obtained using Weigh-In-Motion (WIM) data from the A6 motorway near Auxerre between Paris and Lyon, France. The model used to generate these traffic files is that of Caprani (2005). To identify severe loading events, annual maximum load effects are obtained using linear elastic analysis for considered load effects. The load effects for each bridge configuration are outlined in Table 8.1.

Table 8.1: Considered load effects.

Configuration	Load Effect	Description
2	1	first span mid span bending moment
2	2	hogging moment over interior support
3	1	hogging moment over first interior support
3	2	interior span mid span bending moment
3	3	exterior span mid span bending moment

The influence lines corresponding to each of these load effects are given in Figure 8.1.
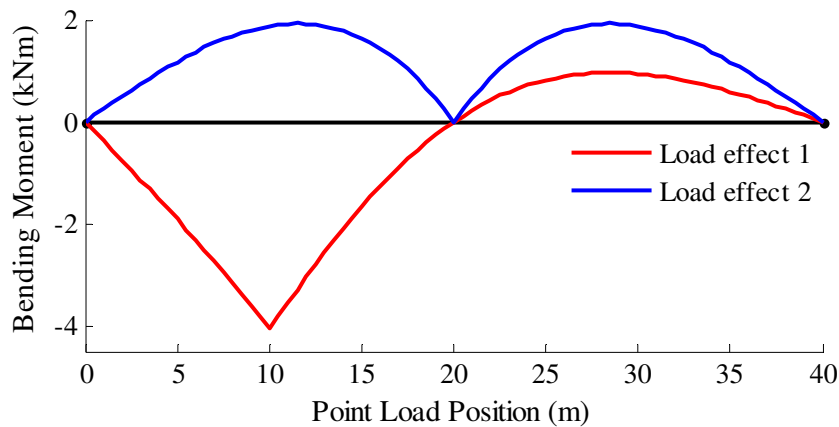
(a) Two-span structures;
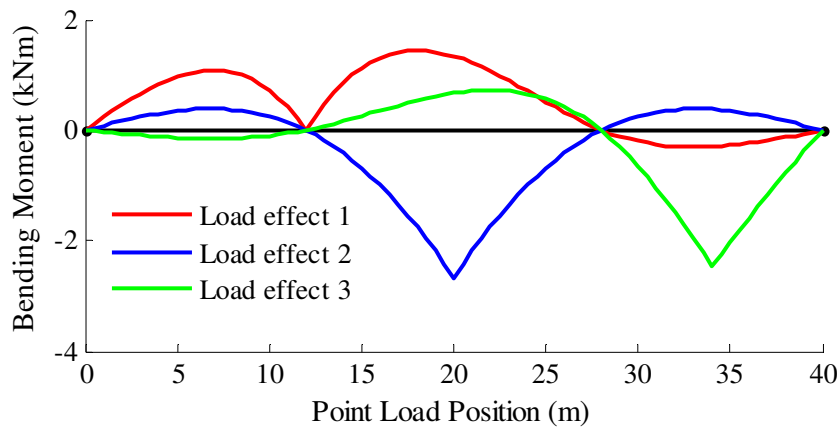
(b) Three-span structures;

Figure 8.1: Influence lines for each structural configuration.

Each annual maximum loading event consists of a unique traffic scenario typically comprised of a number of heavy trucks. Consequently the random variables describing the annual maximum loading event include the number of trucks, speed, truck positions, number of axles of each truck, axle spacing, Gross Vehicle Weight (GVW) and axle load distribution. Only

trucks were considered in each loading event but the influence of cars is allowed for in the spatial arrangement of these trucks. For this study, an event begins with the arrival of a truck and ends with the departure of a truck. Sample annual maximum loading events are shown for bridge 2span-50 in Figure 8.2.
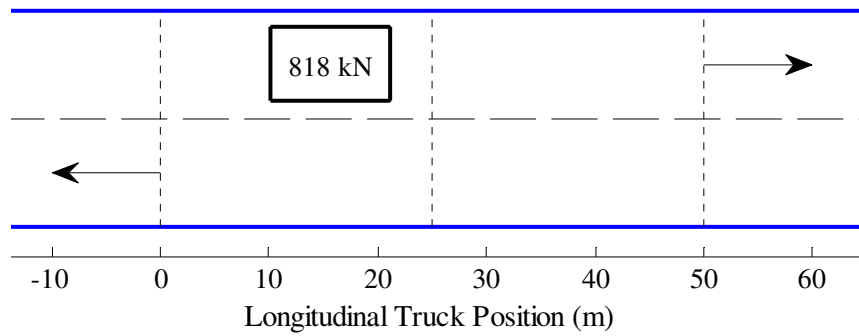
(a) 2span-50 m bridge; load effect 1; first span mid-span bending moment;
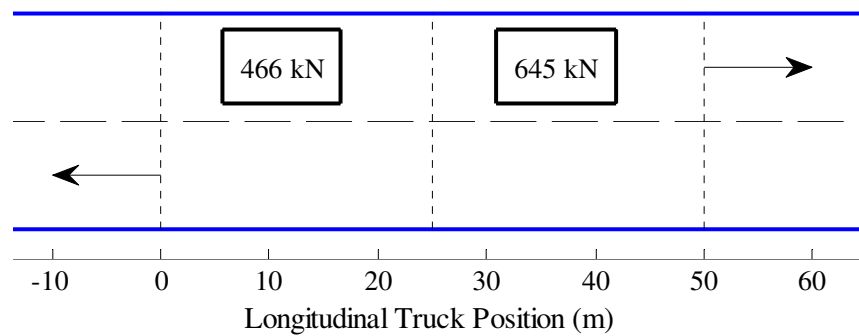
(b) 2span-50 m bridge; load effect 2; hogging moment over interior support.;

Figure 8.2: Sample annual maximum load events.

Notably, different load effects identify different traffic arrangements by virtue of the shape of the influence lines as shown in Figure 8.2.

8.3   Load application

The NFEA model described in Chapter 4 is used for this deterministic assessment. Both dead and live load is considered, while any dynamic effects are ignored. The dead load is divided into three components: dead load due to the slab, beam and surfacing. Each bridge is subjected to the dead load prior to the application of any live load. The moment induced is subtracted from the plastic moment capacity of the bridge.

8.3.1   Extension to Live Load Application Study

The study in Chapter 7 concludes that moving live loads may be applied as non-moving static loads in the NFEA model provided appropriate positions are examined. These positions may be found using an elastic analysis. However, the study in Chapter 7 was limited to one-truck loading events. To extend this study, a comparison is made between the commonly used approach and the proposed moving load approach for a two-truck loading event for collapse shown in Figure 8.3.
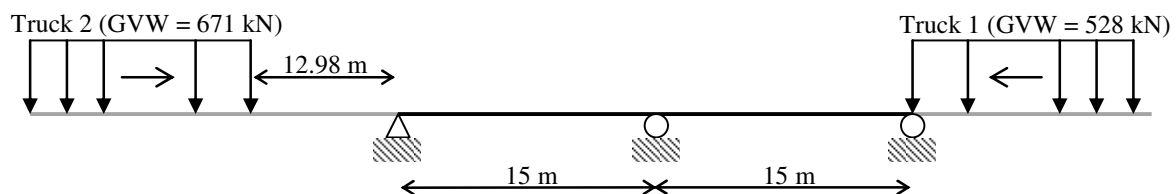
Figure 8.3: Two-truck loading event.

Truck 1 as shown in Figure 8.3 moves from right to left at a constant velocity of 22.3 m/s. Truck 2 is 12.98 m away from the bridge when the event begins and moves from left to right at a velocity of 23.6 m/s. A time step of 0.05 s is used. The non-uniform mesh in the NFEA model (see Section 4.6.1) consists of a fine mesh (0.25 m) at mid-span and over the interior support and a coarse mesh (0.5 m) everywhere else. The stationary static positions are those outlined in Table 7.4 and shown in Figure 8.4.
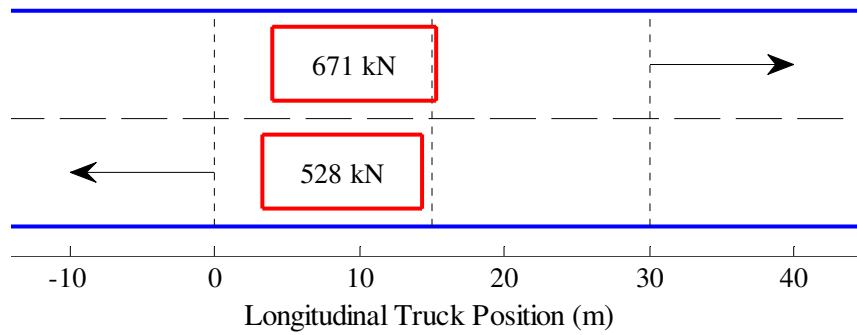
(a) position causing maximum bending moment anywhere (CP 1);
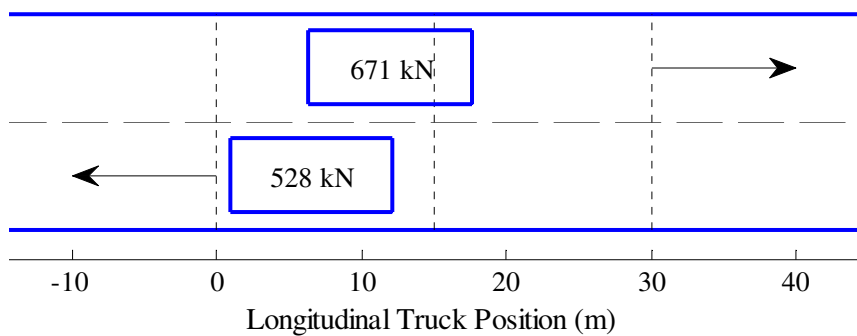
(b) position causing maximum sagging moment at mid-span of first span (CP 2);
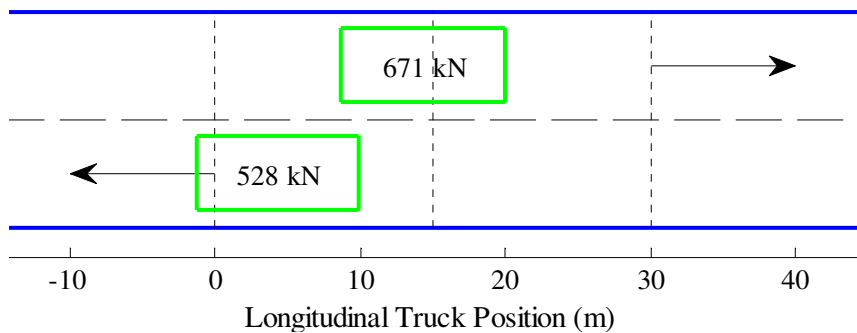
(c) position causing maximum hogging moment over interior support (CP 3);

Figure 8.4: Truck positions causing maximum desired load effects.

These positions were found using an elastic analysis and the elastic bending moment diagrams for each is given in Figure 8.5.
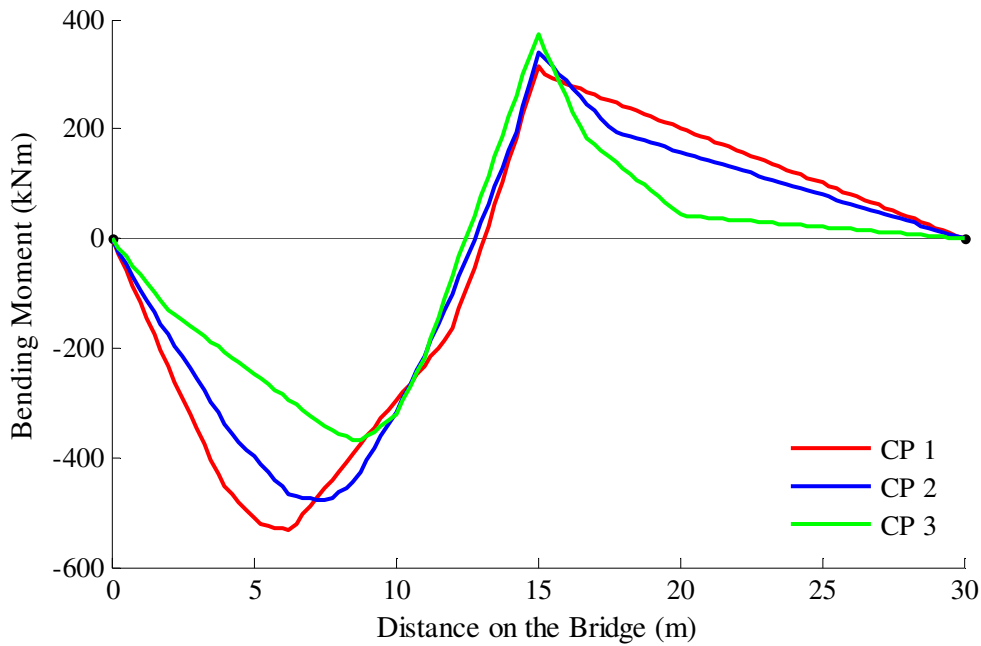
Figure 8.5: Elastic bending moment diagram for each position.

The same event is analysed using the proposed moving load procedure (see Section 7.3). The first truck is 3.24 m from the left-hand support when failure occurs as shown in Figure 8.6. This position is the same position found that causes maximum bending moment anywhere in the structure (see Figure 8.4(a)).
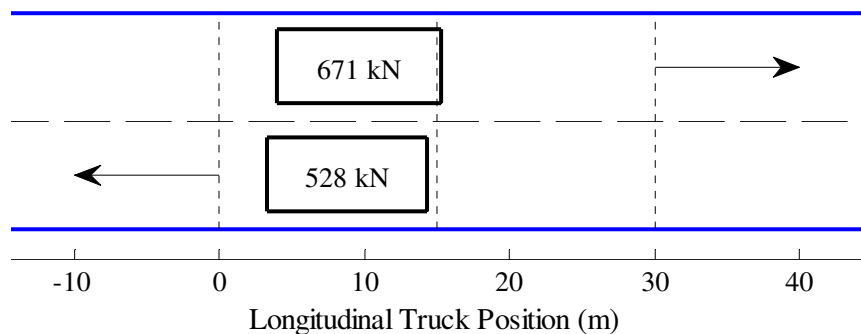
Figure 8.6: Failure position found using proposed moving load procedure.

The comparison between the common approach and the proposed moving approach is described in terms of a load factor ratio (see Section 7.6). These are given in Table 8.2

Table 8.2: λ^* for two truck event on bridge 2span-30.

$\lambda *_1 = \dfrac{\lambda_{CP1}}{\lambda_M}$	$\lambda *_2 = \dfrac{\lambda_{CP2}}{\lambda_M}$	$\lambda *_3 = \dfrac{\lambda_{CP3}}{\lambda_M}$
1.0047	1.0844	1.2712

The stationary position causing maximum moment bending moment at any location (CP1) compares the best to the proposed moving load approach as concluded in Chapter 7. Not only are the vehicle positions at failure the same but the load factors found are approximately equal.

8.3.2   Deterministic Study Live Load Application

Despite the findings of Chapter 7 and the extended live load application study, the traffic events used for this deterministic study are applied as stationary loads positioned according to the considered load effects given in Table 8.1. This may result in an over-estimation of the structures strength capacity. However, it allows a comparison on the suitability of each load effect (Table 8.1) for generating extreme traffic events for collapse to be made.

8.4   Deterministic Study Results

The 100 pre-selected annual maximum loading events were analysed for each load effect using the NFEA model to determine the load factor for each definition of failure. These load factors are calculated by increasing the axle weights proportionally. Table 8.3 outlines the notation used for each load factor.

Table 8.3: Load factor symbols for each failure definition.

Symbol	Failure Definition
λ_1	exceedance of the initial yield capacity
λ_2	formation of the first plastic hinge
λ_3	formation of a collapse mechanism

A sample of the results obtained are given in Figure 8.7. As may be expected, less conservative definitions of failure yield higher the load factors. Notably, all load factors found are above one which would indicate failure. Thus for the structures and traffic examined no flexural failures are found to occur. This indicates that the minimum flexural resistance outlined in the Eurocode is adequate (see Section 6.3). The results shown in Figure 8.7 are typical of all the results found which are given in Appendix 2
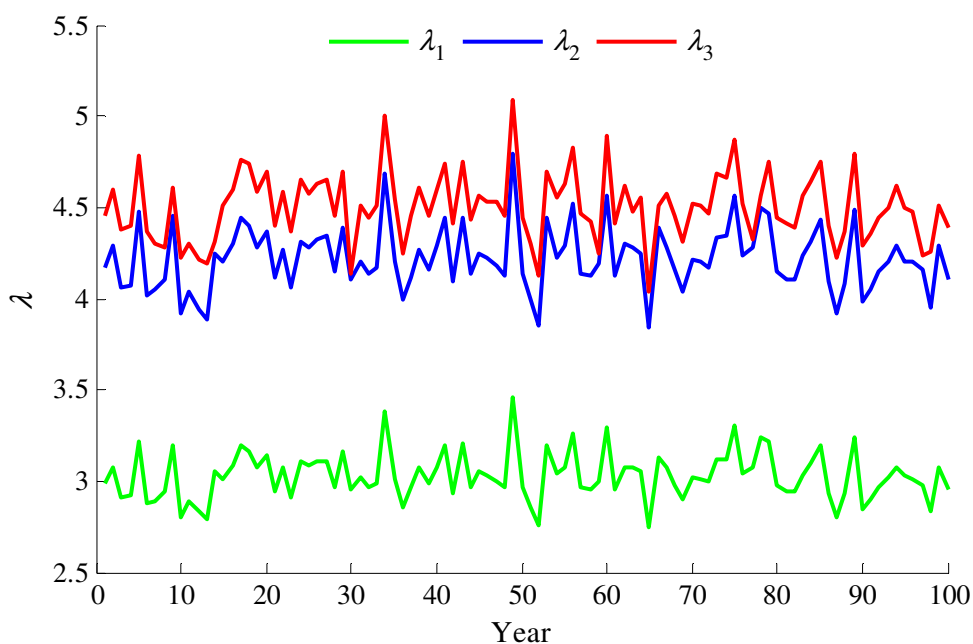
Figure 8.7: 2span-50 bridge; load factors found for the events identified using load effect 1.

8.5   Semi-probabilistic study

The deterministic analysis of each annual maximum event does not describe the lifetime safety level of the bridge. A statistical analysis is therefore required to estimate this lifetime load factor. This can be seen as a semi-probabilistic study since only live load is considered as random. Extreme value statistical theory is implemented to arrive at such an estimate. It is assumed that individual loading events are independent and identically distributed. Traditionally, an extreme value distribution is fitted to maximum values recorded in a reference period (day, week, month, or year). However, the load factor values obtained

represent the minimum load factor for each year. This minimum problem is rescaled to a maximum problem so that typical extrapolation techniques can be employed as follows:

$$g = 1 - \lambda \tag{8.1}$$

where g is the limit state, failure is deemed to occur when the $g > 1$ (i.e. when $\lambda < 1$). The limit state values found using Equation (8.1) for each annual load factor are then used to fit a Generalized Extreme Value (GEV) distribution, given by:

$$G(s) = \exp\left\{-\left[1 - \xi\left(\frac{s - \mu}{\sigma}\right)\right]_+^{1/\xi}\right\} \tag{8.2}$$

where $[h]_+ = \max(h, 0)$ and μ, σ, ξ are the location, scale and shape parameters respectively (Coles, 2001). The lifetime limit state value (g_{LT}) is estimated for a return period of 1000 years. This return period is chosen as it approximates a 5 % probability of exceedance in 50 years given in Eurocode 1 Part 2 (EN 1991-2). A sample extrapolation plot on Gumbel probability paper (Ang & Tang, 1975) is shown in Figure 8.8.
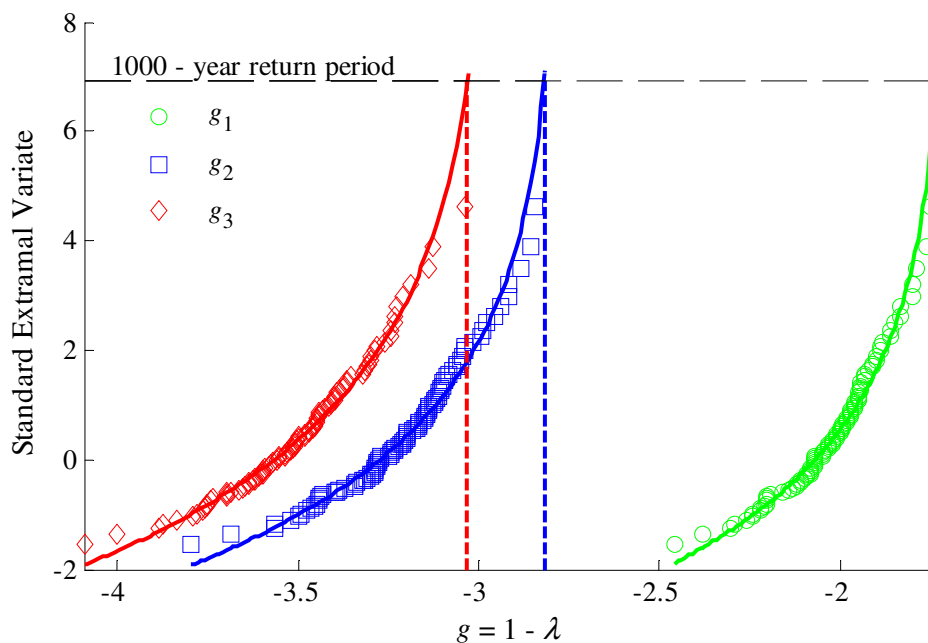
Figure 8.8: Bridge 2span-50 load effect 1: extrapolation for lifetime safety level.

The life-time load factor (λ_{LT}) can then be estimated as follows:

$$\lambda_{LT} = 1 - g_{LT} \qquad (8.3)$$

8.6   Semi-Probabilistic Study Inaccuracy

Generally, it is found that the less conservative definitions of failure result in higher lifetime load factors as expected. However an interesting result occurs when the 3span-40 bridge is examined with regard to maximum hogging moment over the first interior span as highlighted in Figure 8.9. In this case, the lifetime load factor for the collapse limit state is lower than the lifetime load factor for the plastic hinge formation limit state. This result occurs due to the significant variability in the distribution for λ_3 (as may be seen by the difference between the 'shapes' of the data points in Figure 8.9).
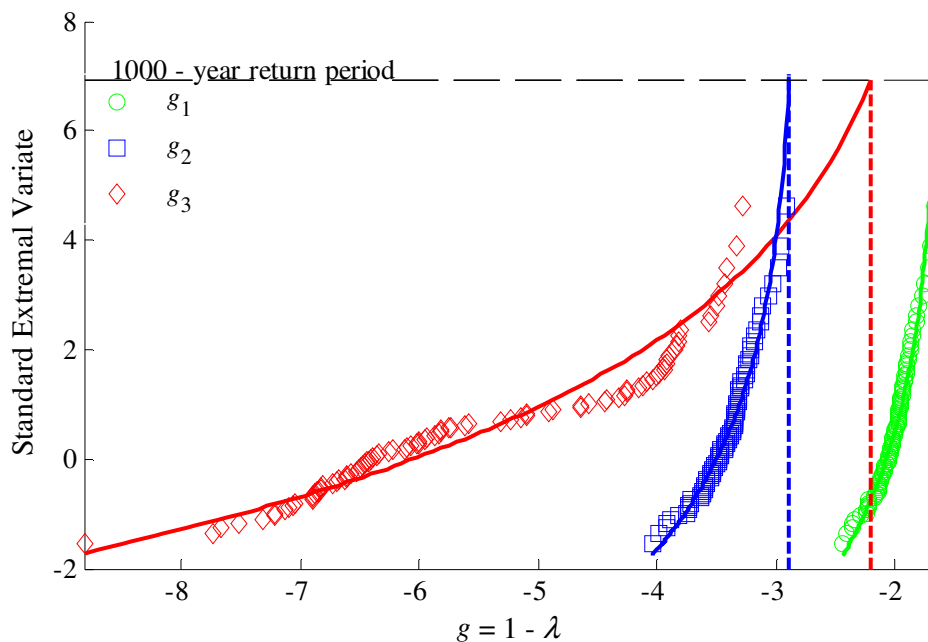
Figure 8.9: Bridge 3span-40 load effect 1 extrapolation results.

On further examination of this structure and traffic, it is found that the load factors found causing collapse failure display a high level of variability as shown in Figure 8.10.
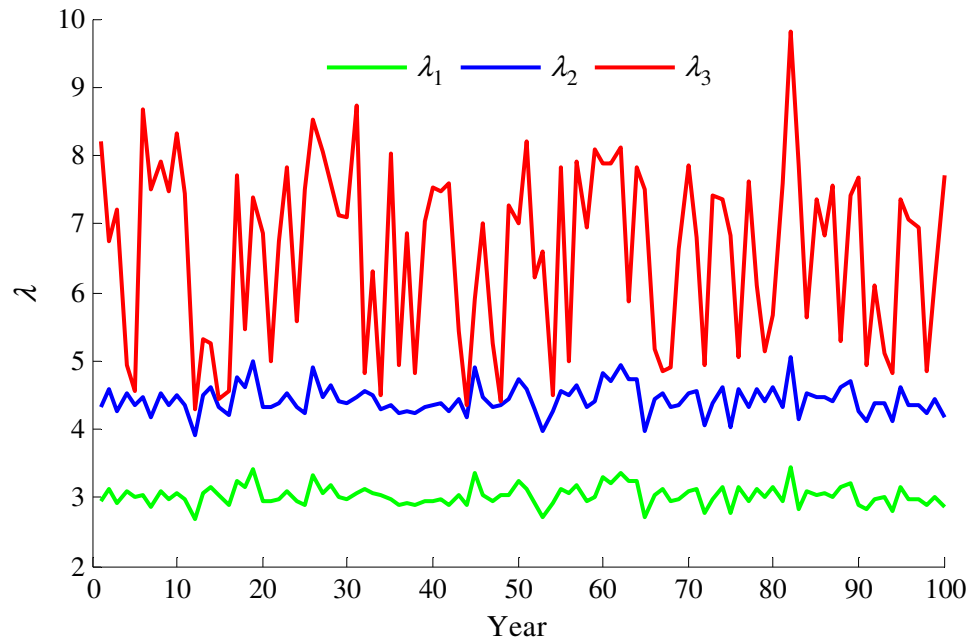
Figure 8.10: Bridge 3span-40 load factor results for load effect 1.

The reason for the high variability of the load factors is mainly due to the positioning and number of the trucks. Figure 8.11 shows the truck positions for the annual maximum event with the highest collapse load factor.
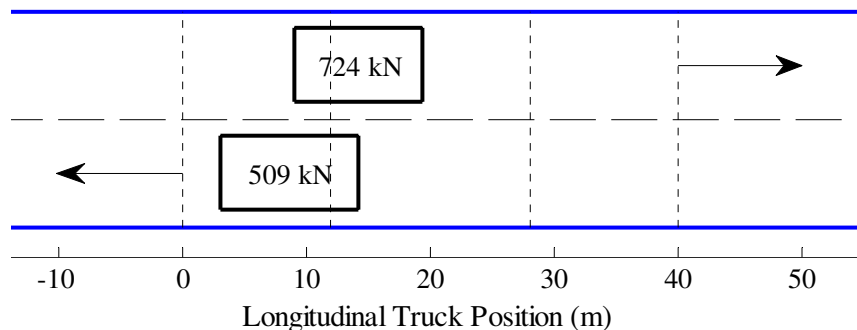
Figure 8.11: Bridge 3span-40-load effect 1-year 82- truck positions.

As can be seen, the truck locations produce a maximum bending moment over the first interior support. Since for a collapse mechanism to occur, two plastic hinges are required in the exterior spans or three are required in the interior span. Therefore a relatively high load factor is required for either of these mechanisms to occur due to the truck positions. Figure 8.12 shows a bending moment diagram for each of the limit states at failure. As can be seen, a significant increase in moment is required, once a plastic hinge has formed, for the

formation of a mechanism. This loading event does not represent an extreme traffic event for the formation of a collapse mechanism.
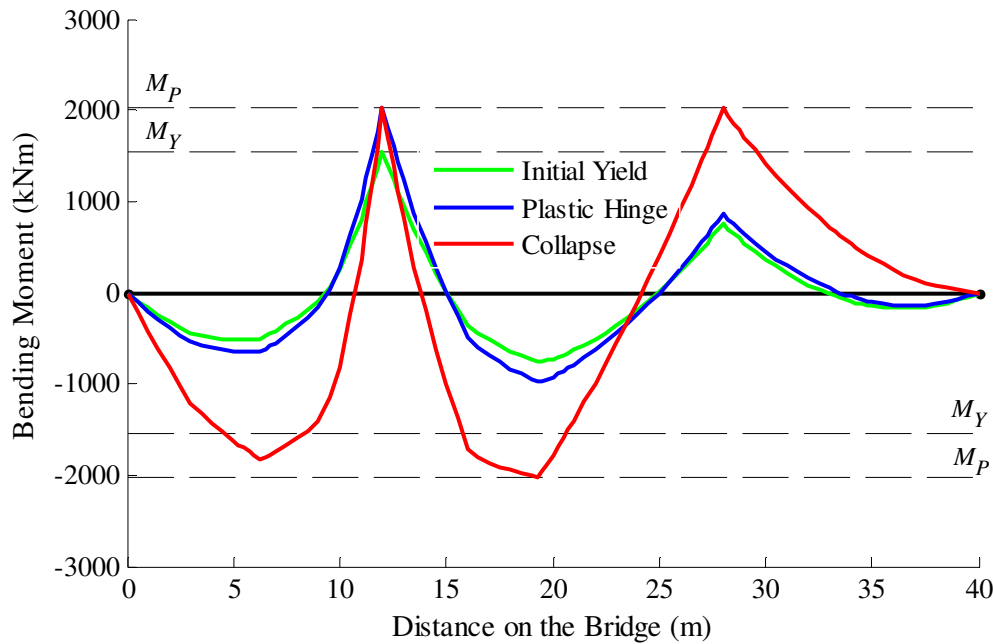
Figure 8.12: Bending moment diagrams at failure for three limit states.

As high load factors are required, events such as shown in Figure 8.11 may not be described as extremes. In cases where non-extreme data may be included, Castillo (1988) recommends extrapolating only the top $2\sqrt{n}$ data points as shown in Figure 8.13.
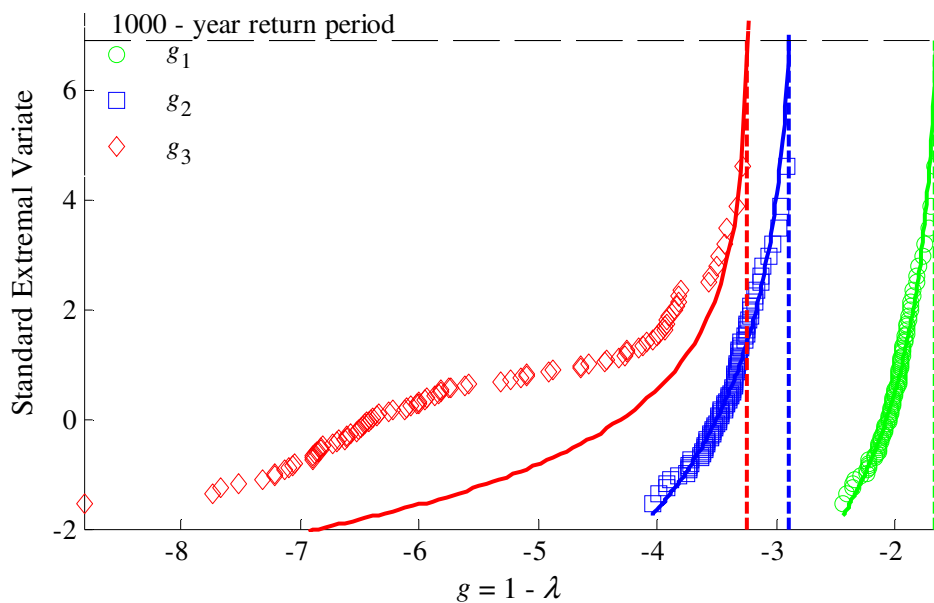
Figure 8.13: Bridge 3span-40 load effect 1 modified extrapolation results.

8.7   Semi-Probabilistic Study Results

The semi-probabilistic study explained in Section 8.5 is completed for all representative

bridge structures. The lifetime load factor results are given in Table 8.4 -8.5.

Table 8.4: Two-span bridges lifetime load factors.

Bridge Length (m)	Load Effect 1 Traffic			Load Effect 2 Traffic		
	λ_{1LT}	λ_{2LT}	λ_{3LT}	λ_{1LT}	λ_{2LT}	λ_{3LT}
30	2.614	3.600	3.859	3.235	4.763	4.898
40	2.482	3.449	3.700	2.002	3.016	3.948
50	2.735	3.819	4.031	2.144	3.278	3.915
60	2.801	3.934	4.112	2.219	3.439	4.242

Table 8.5: Three-span bridges lifetime load factors.

Bridge Length (m)	Load Effect 1 Traffic			Load Effect 2 Traffic			Load Effect 3 Traffic		
	λ_{1LT}	λ_{2LT}	λ_{3LT}	λ_{1LT}	λ_{2LT}	λ_{3LT}	λ_{1LT}	λ_{2LT}	λ_{3LT}
30	2.669	3.795	5.120	2.575	3.515	3.817	3.082	4.155	4.508
40	2.664	3.897	4.245	2.490	3.458	3.681	2.933	3.982	4.317
50	2.157	3.245	3.600	2.685	3.745	4.015	3.113	4.239	4.723
60	1.966	2.932	3.716	2.394	3.383	3.717	3.017	4.128	4.172

The results for the two-span structures subjected to traffic generated using load effect 1(see

Table 8.1) are shown in Figure 8.14. It can be seen that all lifetime load factors are above a

load factor of one, indicating that the bridge is safe against failure by any definition for the

traffic considered. All extrapolation graphs are shown in Appendix 2.
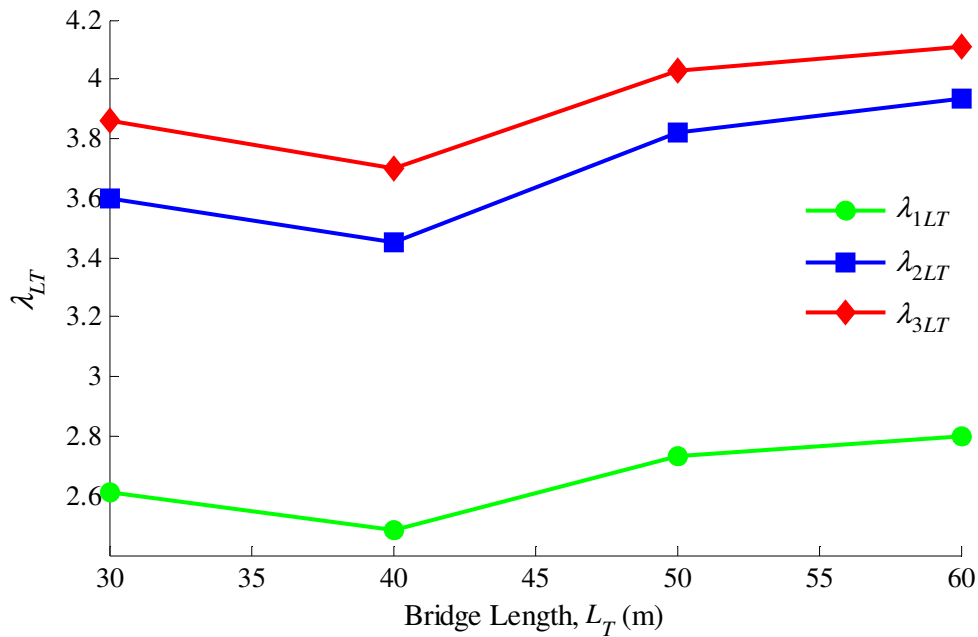
Figure 8.14: Two-span life-time load factors for load effect 1 events.

From the results given in Table 8.4 a comparison of the load effects used to generate extreme traffic loading events is made and is given in Figure 8.15. For the majority of bridge lengths examined with a two span configuration, the traffic events generated using load effect 1 produce lower lifetime load factors than load effect 2 (see Table 8.1). This means that identifying traffic events causing maximum sagging moment at mid-span of the first span is more critical than maximum hogging moment over the interior support because there is a higher possibility of structural collapse in the structures lifetime.
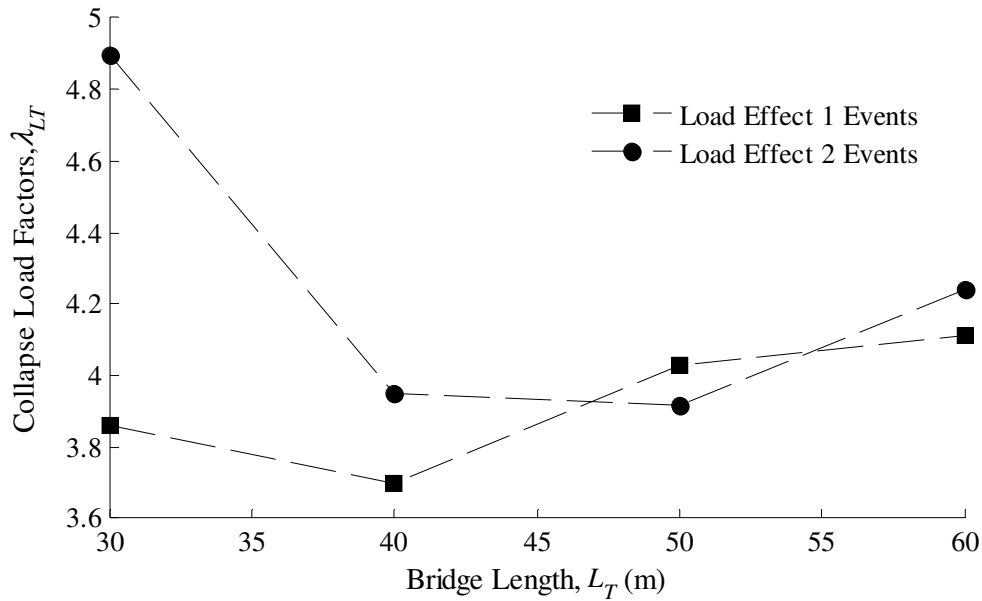
Figure 8.15: Two-span structures life-time collapse load factors for all events.

The comparison of load effects used to generate traffic is also made for three span structures and is given in Figure 8.16. It is found that for bridge lengths below 45 m, the governing load effect for generating extreme load effects for collapse is maximum sagging moment at mid-span of interior span. For the total bridge length over 45 m extreme traffic events for collapse should be generated causing maximum hogging moment over the first interior support.
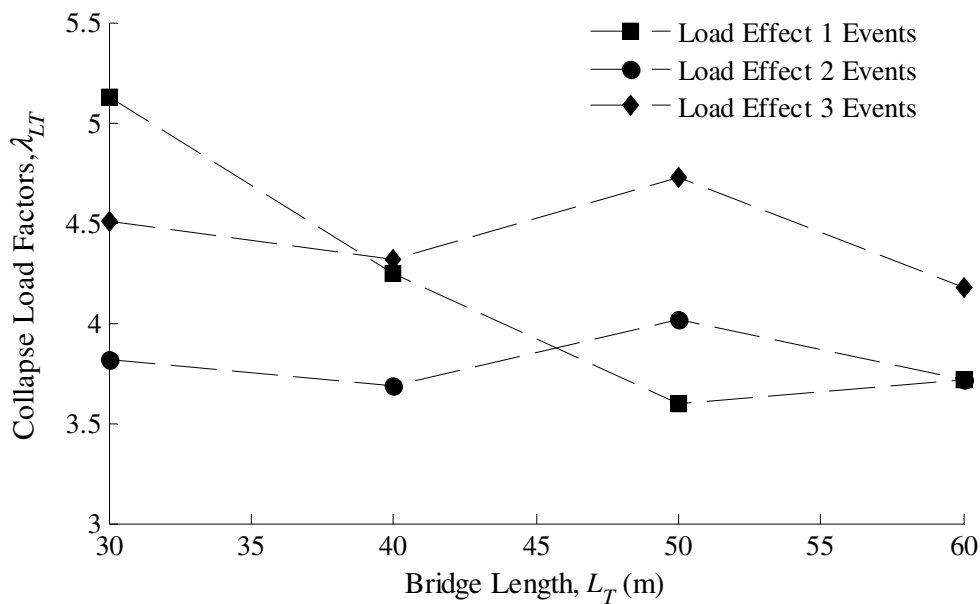
Figure 8.16: Three-span structures life-time collapse load factors for all events.

8.8   Discussion/Summary

Simulated annual maximum traffic loading events based on real traffic data are identified. The safety of each event is described in terms of an axle load multiplier needed to cause failure. Three definitions of flexural failure are used. Each load factor is dependent on the numerous variables involved in the traffic loading event. It is found that all load factors are above one, and so, at the defined resistance, failure does not occur. Notably, the resistance used is the minimum flexural capacity prescribed by the Eurocode. The deterministic study is progressed to a semi-probabilistic study to determine the lifetime load factor. Live load is only described as a random variable. The lifetime load factor corresponds to the 1000-year return period. Again each lifetime load factor is far in excess of unity, and meaning that failure is unlikely to occur for the defined resistance and traffic.

Notable conclusions can be drawn from examining the lifetime load factors found using the initial yield limit state. Twice the average annual maximum loading event is required to cause exceedance of the initial yield capacity. Importantly, the same traffic was used in this study as in the calibration of Eurocode LM1 (EN 1991-2). This highlights the significant reserve capacity the Eurocode prescribes with regard to flexure because of the safety factors applied (see Section 6.3). A further study comparing the minimum Eurocode flexure capacity with the minimum AASHTO flexure capacity is given in Appendix 3.

Critical load effects are identified as those generating events giving the lowest lifetime load factor. For two-span structures, traffic events causing maximum bending moment at mid-span is critical for collapse. For three-span structures with bridge lengths less than 45 m, traffic events should be generated causing maximum sagging moment at mid-span of the first span when assessing collapse. While for bridge lengths between 45-60 m, traffic events causing maximum hogging moment over the first interior span are more important for collapse.

At a return period of 1000 years, the structures examined behave elastically as no yield is present. This then can confirms that it is appropriate to use an elastic structural model for a reliability assessment. However, an increase in the structural safety level may be found if material nonlinearity is accounted for in a reliability assessment. A reliability procedure accounting for material nonlinearity is presented in Chapter 9.

Chapter 9

Reliability Analysis Considering Nonlinear Material Behaviour

9.1   Introduction

In this chapter a procedure for conducting a reliability analysis accounting for nonlinear material behaviour is developed. This procedure is applied to the representative steel bridges of Chapter 6, and compared to a traditional reliability analysis calculation. The traffic generated as part of the deterministic study described in Chapter 8 is used in both the traditional and proposed reliability calculations.

9.2   Conventional Reliability Analysis

The FORM model described in Chapter 3 is used here as the traditional reliability analysis approach (referred to in this work as the FORM approach). This approach is commonly used in practice as it is believed to provide a reasonably adequate measure of safety for very little computational expense. The limit state functions examined are:

$$g_1 = M_Y - D_1 - D_2 - D_3 - L \qquad (9.1)$$

$$g_2 = M_P - D_1 - D_2 - D_3 - L \qquad (9.2)$$

where M_Y is the initial yield capacity of the cross section, M_P is the plastic moment capacity of the cross section, D_1 is the dead load moment due to the self weight of the beam, D_2 is the dead load moment due to the self weight of the slab, D_3 is the super-imposed dead load moment due to the road surfacing and L is the live load moment on the structure. Equation (9.1) is the limit state function representing failure by exceedance of the initial yield

capacity. Equation (9.2) represents failure by the formation of the first plastic hinge. No nonlinear material behaviour is accounted for in these limit state functions. The bias factor and coefficient of variation chosen for the resistance capacity are 1.12 and 0.1 respectively, following Czarnecki & Nowak (2007). The bias factor for each of the three components of dead load is taken as 1.03, 1.05 and 1 respectively. The coefficients of variation for each dead load component are chosen as 0.08, 0.1, and 0.3 respectively (Nowak, 1993). The statistical properties of the live load are found by fitting a normal distribution to the load effect values found using an elastic analysis of the annual maximum truck events. This is similar to the approach used by Park et al (1998) and Nowak et al (2001). All variables are written in terms of moments with units of kNm and assumed to be normally distributed. As a sample, the input parameters for bridge 2span-50 are given in Table 9.1:

Table 9.1: Sample FORM inputs for bridge 2span-50

Variable	Bias factor	CoV	Characteristic value (kNm)	μ (kNm)	σ (kNm)
M_Y	1.12	0.1	4842	5423	542
M_P	1.12	0.1	6295	7050	705
D_1	1.03	0.08	178	173	14
D_2	1.05	0.1	1294	1232	123
D_3	1	0.3	570	570	171
L (LE1)	1	---	---	1215	30
L (LE2)	1	---	---	1158	46

The sensitivity factors for each variable given in Table in 9.1 are shown in Table 9.2 (see Section 3.3.2). These sensitivity factors highlight the contribution of each variable towards the probability of failure for the limit state function given in Equation 9.1 and 9.2. It is seen that the resistance (M_Y, M_P) is of vital importance and as expected has the highest contribution towards failure.

Table 9.2: Sensitivity factors (α) for bridge 2span-50 load effect 1 events

	M_Y	M_P	D_1	D_2	D_3	L (LE1)
β_1	-0.9307	---	0.0237	0.2155	0.2931	0.0512
β_2	---	-0.9572	0.0188	0.1673	0.2319	0.0405

The lifetime reliability indices are found for each set of traffic generated for each bridge structure using FORM as described in Section 3.3. These results are shown in Table 9.3-9.4

Table 9.3: Two-span bridges, FORM lifetime reliability indices.

Bridge Length (m)	Load Effect 1 Traffic		Load Effect 2 Traffic	
	β_{1LT}	β_{2LT}	β_{1LT}	β_{2LT}
30	4.481	5.755	5.002	6.166
40	3.911	5.304	4.105	5.457
50	3.834	5.242	3.924	5.313
60	3.755	5.178	3.799	5.208

Table 9.4: Three-span bridges, FORM lifetime reliability indices.

Bridge Length (m)	Load Effect 1 Traffic		Load Effect 2 Traffic		Load Effect 3 Traffic	
	β_{1LT}	β_{2LT}	β_{1LT}	β_{2LT}	β_{1LT}	β_{2LT}
30	5.186	6.305	5.037	6.189	5.010	6.168
40	5.019	6.176	4.454	5.734	4.163	5.468
50	4.358	5.658	4.244	5.569	4.545	5.805
60	4.120	5.469	3.895	5.293	3.910	5.305

9.3   Reliability Analysis Considering Nonlinear Material Behaviour

To develop a reliability analysis procedure which accounts for material nonlinearity, the NFEA model is linked to a FORM analysis using the RSM (see Section 5.8). This proposed reliability procedure is referred to in this work as the RSM reliability approach. This allows a reliability analysis to be conducted without explicitly defining a limit state function. This is useful because closed-form limit state functions describing collapse failure are generally unavailable. The RSM replace the NFEA model with an approximated polynomial function by conducting a series of nonlinear experiments.

9.3.1 Experimental Design

The iterative process of Rajashekhar et al (1993) (see Section 5.8) is used along with the Box-Behnken ED (see Section 5.3.4). A performance study for each of the EDs given in Section 5.3 is given in Appendix 3. This study concludes that convergence criteria are met with the least number of NFEAs using the BB design. This design also performs to the highest level of accuracy when compared to a MCS. Each experimental design was built in the physical working space of the variables.

9.3.2 Selection of Random Variables

To simplify the reliability calculation using the RSM, selected variables in each loading event are assumed to be deterministic. The number of trucks, the axle spacing of each truck, the axle load distribution, the speed of each truck and the longitudinal position of each truck are treated in this way as they are not highly variable and are not considered to influence the result greatly. This is done because the RSM is highly impractical when dealing with a large number of random variables (Melcher, 1999).

Similar to the traditional reliability analysis, the resistance capacity of the section, the dead load due to slab, the dead load due to the beam and the dead load due to surface are all considered to be random variables. Also the GVW of each truck in the loading event is considered random. The CoV for the GVW of each truck was taken as 0.1 and assumed to be normally distributed (Wong, 2005). For example, with the above considerations, a one-truck loading event has 5 random variables. The number of random variables increases in the presence of more trucks. Notably, the resistance capacity is expressed in terms of moment (kNm) while the random loading variables are expressed as load (kN). The statistical properties (Bias Factor and CoV) assumed for the FORM analysis are again adopted (Table 9.1). As an example Table 9.5 outlines the inputs required for the 2span-50 bridge.

Table: 9.5 Sample RSM inputs for the 2span-50 bridge

Variable	Bias factor	CoV	Characteristic value	μ	σ
M_Y (kNm)	1.12	0.1	4842	5423	542
M_P (kNm)	1.12	0.1	6295	7050	705
D_1 (kN)	1.03	0.08	2.279	2.212	0.177
D_2 (kN)	1.05	0.1	16.56	15.774	1.577
D_3 (kN)	1	0.3	7.288	7.288	2.186
GVW LE1 (kN)	1	0.1	818	818	81.8
GVW_1 LE2 (kN)	1	0.1	466	466	46.6
GVW_2 LE2 (kN)	1	0.1	645	645	64.5

9.3.3   Nonlinear Reliability Indices for Each Annual Maximum Event

Three approximate polynomial functions representing each definition of failure are found for each loading event. Each polynomial is a second order function including mixed terms (see Section 5.2). Examples of the coefficients of these functions are given in Table 9.6.

Table: 9.6 Example polynomial functions (2span-50, Load Effect 1 Events)

Variables	Initial yield coefficients	Plastic hinge coefficients	Collapse coefficients
	1.496	2.247×10-1	1.780×10-1
M_P	8.181×10-4	1.207×10-3	1.132×10-3
D_1	-4.4314×10-1	-9.092×10-2	-2.566×10-1
D_2	-7.283×10-2	-5.405×10-2	3.960×10-3
D_3	-4.024×10-2	-3.343×10-2	3.594×10-2
GVW_1	-1.689×10-3	-5.791×10-4	-1.201×10-3
GVW_2	-3.443×10-3	-2.724×10-3	-2.746×10-3
M_P^2	9.003×10-8	1.419×10-7	1.071×10-7
D_1^2	6.894×10-2	4.321×10-3	4.023×10-2
D_2^2	-6.202×10-5	-4.480×10-4	-9.800×10-4
D_3^2	-8.072×10-4	-1.090×10-5	-1.990×10-3
GVW_1^2	6.051×10-7	1.797×10-7	1.043×10-6
GVW_2^2	1.796×10-6	1.310×10-6	9.685×10-7
$M_P \cdot D_1$	-1.113×10-5	-1.903×10-5	-1.068×10-5
$M_P \cdot D_2$	-8.742×10-6	-1.130×10-5	-1.144×10-5
$M_P \cdot D_3$	-7.659×10-6	-1.215×10-5	-1.069×10-5
$M_P \cdot GVW_1$	-1.103×10-7	-1.452×10-7	-1.131×10-7
$M_P \cdot GVW_2$	-7.827×10-7	-1.031×10-6	-8.319×10-7
$D_1 \cdot D_2$	-4.51×10-16	-6.715×10-4	1.144×10-3
$D_1 \cdot D_3$	-3.589×10-3	-2.745×10-3	-4.431×10-16
$D_1 \cdot GVW_1$	1.099×10-4	1.730×10-5	5.493×10-6
$D_1 \cdot GVW_2$	1.075×10-4	1.088×10-4	5.805×10-5
$D_2 \cdot D_3$	-1.611×10-3	-1.894×10-3	-4.193×10-3
$D_2 \cdot GVW_1$	4.932×10-5	1.664×10-5	7.151×10-6
$D_2 \cdot GVW_2$	5.429×10-5	6.202×10-5	5.857×10-5
$D_3 \cdot GVW_1$	-5.117×10-19	1.201×10-6	3.736×10-6
$D_3 \cdot GVW_2$	1.044×10-4	1.079×10-4	8.017×10-5
$GVW_1 \cdot GVW_2$	5.329×10-7	4.436×10-7	4.690×10-7

Table 9.7 shows the sensitivity factors for each variable for the event given in Table 9.6. Similar to the conventional reliability analysis the resistance capacity has the highest impact on the probability of failure.

Table 9.7: Sensitivity factors (α) for bridge 2span-50 load effect 1 events 1

	M_Y	M_P	D_1	D_2	D_3	GVW_1	GVW_2
β_1	-0.9370	---	0.0281	0.2132	0.1757	0.0126	0.2114
β_2	---	-0.9610	0.0210	0.1722	0.1524	0.0114	0.1519
β_3	---	-0.9548	0.0133	0.1506	0.1578	0.0145	0.2010

9.4 Reliability Indices Considering Material Nonlinear Behaviour

The reliability indices are found using FORM with approximated polynomials representing the limit state functions. Table 9.8 gives the symbols for each calculated reliability index.

Table 9.8: Reliability Index symbols for each failure definition

Symbol	Failure Definition
β_1	exceedance of initial yield capacity
β_2	formation of a plastic hinge
β_3	formation of a collapse mechanism

The reliability indices for each year for the 2span-50 bridge examining the traffic found using load effect 1 are shown in Figure 9.1. A consistent difference can be found between the initial yield capacity exceedance and the plastic capacity exceedance limit states, as may be expected. This difference relies solely on the shape factor of the considered beam.
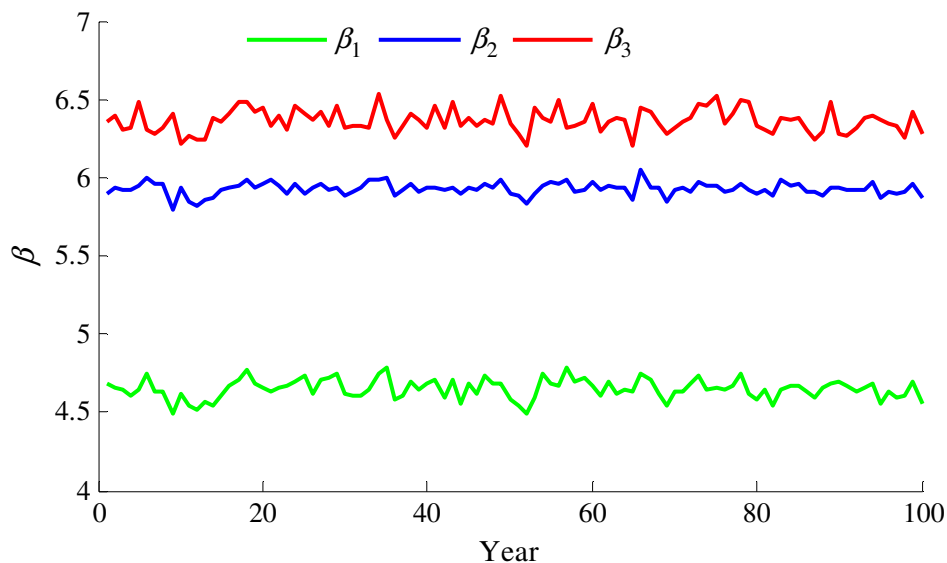
Figure 9.1: Bridge 2span-50 RSM reliability indices for each traffic event

9.5   Cumulative Reliability Indices Considering Material Nonlinear Behaviour

To compare the nonlinear reliability analysis with a traditional reliability analysis, the bridge lifetime reliability index is determined by combining the reliability indices from each annual maximum event. It is assumed that the annual maximum loading events are independent of each other and represent the annual reliability index (though it is acknowledged that this is not strictly true). The probability (P_{fn}) of bridge failure during (n) events can be found from (Melchers, 1999):

$$P_{fn} = 1 - \prod_{i=1}^{n}[1 - \Phi(-\beta_i)] \tag{9.3}$$

Then the reliability index (β_n) describing the probability of failure through (n) years is:

$$\beta_n = -\Phi^{-1}(P_{fn}) \tag{9.4}$$

where $-\Phi^{-1}$ is the inverse standard normal distribution. The results are shown in Figure 9.2. It can be seen that the reliability index for each limit state reduces through time. The lifetime reliability index (β_{LT}) is taken as the cumulative reliability index (β_n) at 100 years.
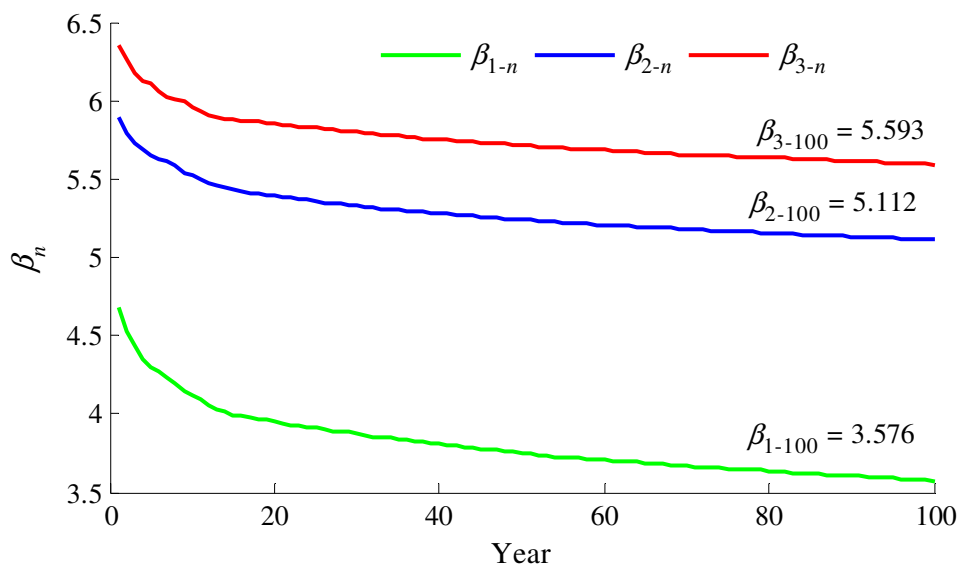
Figure 9.2: Bridge 2span-50 RSM cumulative reliability indices for each traffic event

The graphs for this procedure are given in Appendix 5.The results following this procedure are given in Table 9.9-9.10.

Table 9.9: Two-span bridges; lifetime reliability indices considering nonlinear material behaviour (RSM).

Bridge Length (m)	Load Effect 1 Traffic			Load Effect 2 Traffic		
	β_{1LT}	β_{2LT}	β_{3LT}	β_{1LT}	β_{2LT}	β_{3LT}
30	4.328	5.620	5.953	4.148	5.467	6.350
40	3.718	5.213	5.556	2.894	4.562	5.820
50	3.576	5.112	5.593	2.654	4.395	5.675
60	3.460	5.024	5.583	2.596	4.357	5.656

Table 9.10: Three-span bridges; lifetime reliability indices considering nonlinear material behaviour (RSM).

Bridge Length (m)	Load Effect 1 Traffic			Load Effect 2 Traffic			Load Effect 3 Traffic		
	β_{1LT}	β_{2LT}	β_{3LT}	β_{1LT}	β_{2LT}	β_{3LT}	β_{1LT}	β_{2LT}	β_{3LT}
30	4.313	5.572	6.803	4.593	5.740	6.080	4.494	5.689	6.037
40	3.877	5.253	6.059	3.865	5.266	5.585	4.298	5.589	5.853
50	3.340	4.857	5.435	3.888	5.269	5.614	4.584	5.828	6.397
60	2.921	4.578	5.577	3.497	5.003	5.355	3.516	5.024	5.333

The cumulative reliability index graphs for each bridge structure are in the Appendix 4.

9.6   Comparison to Conventional Reliability Analysis

The traditional reliability analysis is compared to the proposed reliability analysis accounting for nonlinear material behaviour. This comparison will assess the influence of nonlinear material behaviour on bridge safety. A direct comparison can be made when examining the exceedance of initial yield capacity and formation of a plastic hinge limit states as closed-form limit states are available. This allows for the assessment of the performance of a traditional FORM analysis. A sample of the results are shown in Figure 9.3. The lifetime reliability indices found using each method for each definition of failure are shown plotted against total bridge length. These sample results are for bridges with a two-span configuration, subjected to traffic loading events found using load effect 1.
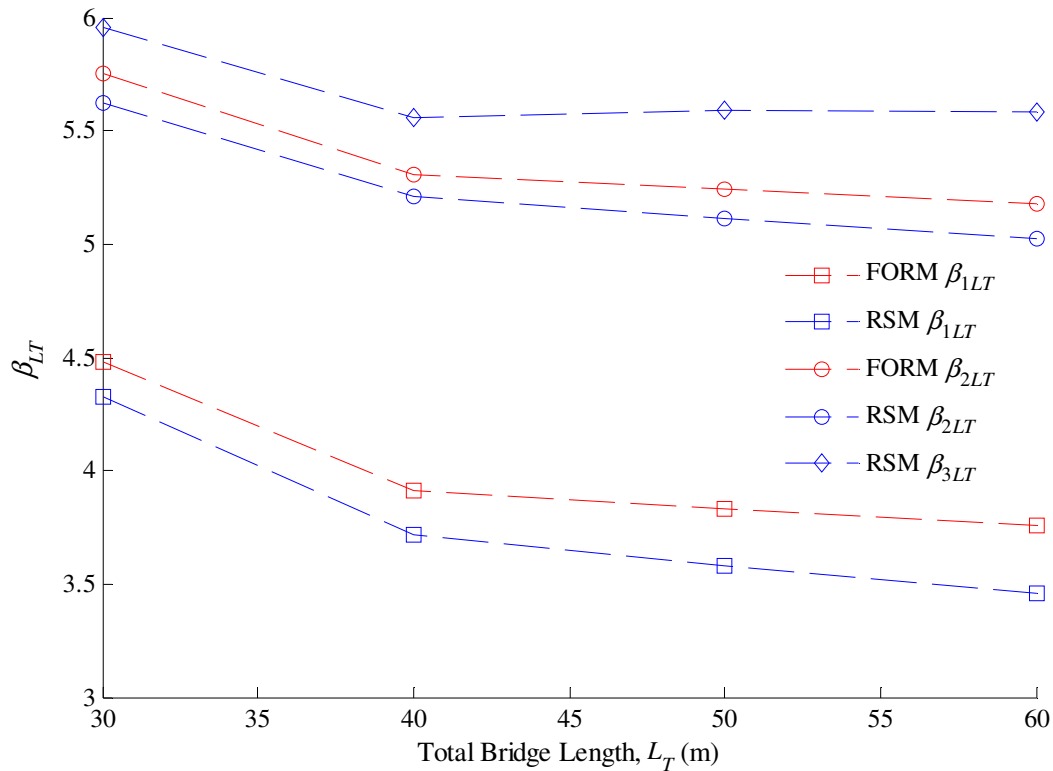
Figure 9.3: Configuration 1 life-time reliability indices for load effect 1 events.

For the results shown in Figure 9.3, the two reliability approaches have a similar trend when examining the exceedance of initial yield capacity and the formation of a plastic hinge limit states. However, the traditional FORM calculation produces higher reliability indices. Figure 9.4 summarizes the comparison between the conventional FORM reliability analysis procedure and the proposed RSM procedure for all definitions of failure.

Structural safety of the collapse limit state found using the nonlinear method can only be compared to the structural safety found using the FORM method for the plastic hinge formation limit state function as this is the least conservative limit sate available using the FORM approach. It is seen from Figure 9.4, that typically a higher reliability indices are found using a nonlinear analysis regarding a collapse limit state.
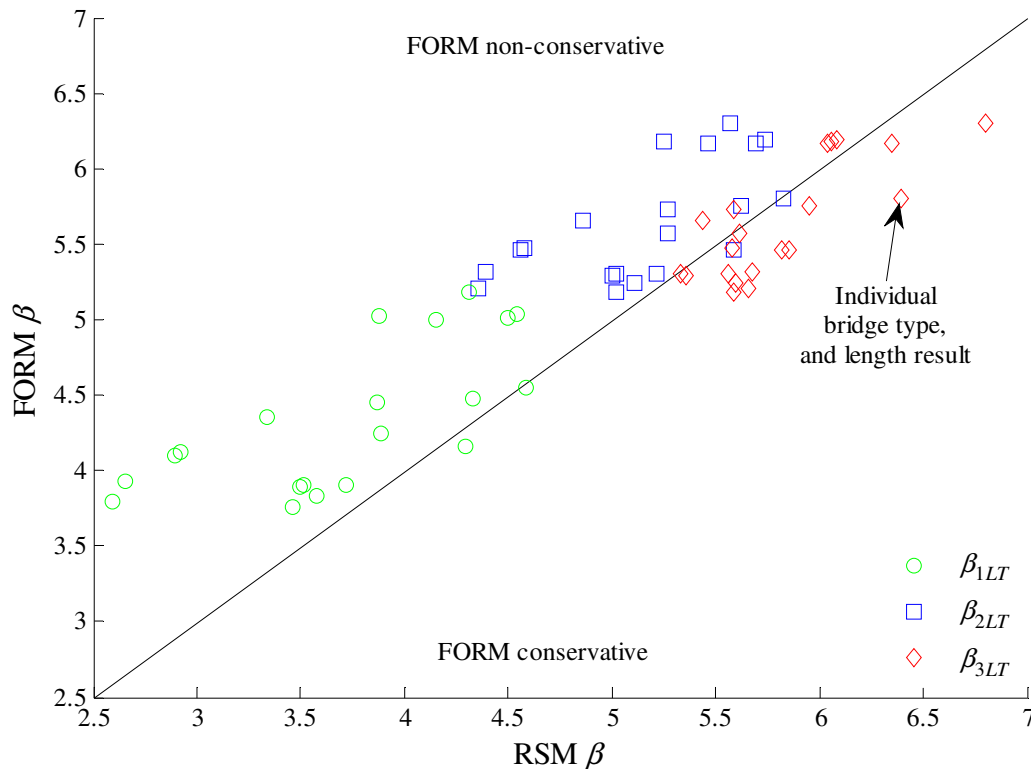
Figure 9.4: Life-time reliability indices comparison.

9.7 Discussion

In this study a comparison is made between traditional reliability analysis and the proposed reliability analysis considering material nonlinearity which uses the RSM. Lower reliability indices are found using the proposed approach for the initial yield and plastic hinge formation limit states. This indicates that a conventional reliability analysis may indeed behave non-conservatively and give a false estimation of the true level structural safety.

In total eight bridge structures are examined, four with a two-span configuration and four with a three-span configuration. Traffic events identified using two influence lines are examined for the two-span configuration and events found using three influence lines are examined for the three-span structural configuration. In total, 20 separate scenarios are examined to obtain an accurate comparison. For the majority of scenarios examined it is found that the RSM approach considering nonlinear material behaviour produces higher reliability indices for collapse than those using the conventional FORM reliability analysis.

This highlights the benefits of accounting for material nonlinear behaviour in a reliability assessment.

The difference between the reliability indexes found using the conventional approach (which is based on the formation of the first plastic hinge) and the proposed approach (which allows for actual collapse) may be seen as a measure of the beam redundancy: differences of up to 7% are found.

The target reliability indices for serviceability and ultimate limit states for 1 year are given in the Eurocode (EC1.1 1990) to be 2.9 and 4.7 respectively. All annual reliability indices found using the proposed reliability procedure are well-above these target levels. The target reliability indices for serviceability and ultimate limit states after 50 years are also given in the Eurocode as 1.5 and 3.8 (EC1.1 1990). Even though the life-time reliability indices found using the proposed method considering material nonlinearity represent a 100 years, they are still far greater than these targets. This indicates the conservatism associated with the prescribed minimum Eurocode flexural capacity for the traffic and bridges considered.

Parson Brickenhoff (2003) conducted an examination into why bridges failed assessments throughout the UK and concluded that the main contributing factor for these failures was conservative assessment methods. This study outlines a more rational assessment procedure accounting for the load redistribution associated with ductile material behaviour.

9.8   Summary

This chapter compares the proposed reliability analysis accounting for nonlinear material behaviour to a traditional reliability analysis. This comparison is performed on the representative group of steel composite bridges subjected to annual maximum loading events. The results indicate that a higher level of structural safety may be found when material

nonlinearity is accounted for. Accounting for nonlinear material behaviour in a probabilistic

assessment is found to be beneficial.

Chapter 10

Conclusions

10.1   Objective Conclusions

This study combines three main subject areas: structural reliability, nonlinear finite element modelling and the RSM to address the objectives in Chapter 1. The following conclusions are found for these objectives:

10.1.1 Objective 1: Live Load Application in a Nonlinear Assessment

Commonly live loads are applied as static loads positioned according to an elastic analysis in a nonlinear assessment positioned according to an elastic analysis. Two difficulties associated with this approach are: 1) where should the static loads be applied? and 2) does this accurately represent failure under a moving load? A series of experiments are conducted on a representative group of steel composite bridges. Initially the live loads are applied as static loads at several positions. These positions include those causing maximum bending at any location, at mid spans and at the internal supports. A load factor required to cause collapse is found for each of these positions. Further, it is found, that for a two-span bridge, it is sufficient to locate the live loads where it causes overall maximum moment anywhere. However, this is not the case for a three-span structure and various possible load positions should be examined to ensure the critical load factor is found.

A proposed moving load procedure is developed to assess the performance of this commonly used technique. The moving load approach involves an incremental unloading/loading procedure which allows for the spread of plasticity to be traced throughout the structure while accurately representing a moving load. The lowest load factor found using the common approach is compared to that found using the proposed moving load approach, again for a

series of experiments. For the majority of scenarios examined it is found that the common approach slightly over-estimates the strength capacity of the structure. However, only marginal differences between the two approaches are found, the maximum being 3 % for a single point load on a three span structure. It is concluded that it is sufficient to apply live loads as static loads positioned according to an elastic analysis once multiple positions are examined and a critical position is determined.

10.1.2 Objective 2: Deterministic Safety Assessment

A one dimensional NFEA model is used to assess a representative group of steel composite bridges. These bridges are subjected to annual maximum traffic loading events determined from MCS based upon WIM traffic data. Three definitions of failure are examined: exceedance of initial yield capacity; the formation of a plastic hinge; and the formation of a collapse mechanism. Failure is described using a load factor, which is a multiple of the axle loads required to cause failure. The strength capacity of each bridge is defined as the minimum flexural requirement prescribed by the Eurocode. Load factors are found for each annual maximum event and are combined to determine a lifetime load factor using an extrapolation process based on extreme value statistical theory. As may be expected, the less conservative the definitions of failure give higher load factors. All lifetime load factors found are above a load factor of 1; there is adequate flexural capacity of each bridge structure.

Using the lifetime load factors the suitability of each load effect for generating extreme traffic loading events is assessed. Critical load effects were determined as producing minimum lifetime load factors. It is found that for two span structures the maximum sagging moment in the spans is the critical load effect. For three span structures of a total length between 30-45 m maximum sagging moment at mid-span of the interior span is critical while for total lengths between 45-60 m the hogging moment at first interior support is critical.

10.1.3 Objective 3: Probabilistic Safety Assessment

While a deterministic assessment may provide some knowledge of structural safety, it is now common to assess structural safety using a reliability analysis. Since statistical properties are used in a reliability analysis, a more rational representation of safety is found.

Traditionally an elastic structural model is used in a reliability assessment. The extra strength capacity available if material nonlinearity is accounted for is therefore ignored. This study examines a simplified probabilistic assessment which incorporates a nonlinear structural model and so allows for load redistribution. A comparison between this method and a traditional reliability analysis is made. The difference between the traditional reliability index and the proposed method may be considered as a measure of the beam load sharing/redundancy capabilities. The difference between the two approaches is found to be as high as 7%.

The nonlinear reliability procedure may act as a foundation in the development of an evaluation procedure for existing bridge structures. Thus for a more accurate assessment of the rehabilitation measures required may be found.

10.2   Further Work

There is no doubt that the increase in computer power has made reliability calculations more feasible to perform. However, a reliability analysis is only as accurate as the variables inputted. A limitation of this research and an area for further work is the definition of the resistance capacity of the structure. The resistance of each bridge used in this study is modelled as a single variable representing the minimum required design resistance. The reliance of the probabilistic assessments on this variable is highlighted by the large sensitivity factor found in Chapter 9. Not only should the resistance be extended to more variables but also should corporate a deterioration model to accurately represent an existing structure.

The reliability analysis procedure developed accounting for nonlinear material behaviour, although effective, still contains numerous limitations. The first limitation is the number of random variables which the RSM can be use effectively. The number of random variables effects the computation time greatly. For this reason it is common to assume deterministic properties for variables of low uncertainty. While this does make the problem more manageable, it does narrow the scope of the practical problem. Further work is required to identify important variables before a nonlinear reliability analysis can be performed i.e. a sensitivity analysis.

References

AASHTO LRFD (1998), Bridge Design Specification, American Association of State Highway and Transportation Officials, Washington, DC.

Abell, M. (2012). Material Nonlinearity, *CSI Knowledge base* [online].Available at wiki.csiberkeley.com/display/kb/Material+nonlinearity .Accessed on 15/08/12.

Akgul, F. & Frangopol, D.M. (2004). Time-dependent interaction between load rating and reliability of deteriorating bridges. Journal of Structural Engineering, 130(12):1875-1888.

Ang, A. H-S. and W. H. Tang (1975), *Probability Concepts in Engineering Planning and Design*, Volume1, John Wiley & Sons, pp. 198-199.

Becker, A. (2004). *An Introductory Guide to Finite Element Analysis*. Suffolk: Professional Engineering Publishing.

Biodini, F., Bontempi, Frangopol, D.M & Malerba, P.G. (2004). Reliability of material and geometrically nonlinear reinforced and prestressed concrete structures, *Computers and Structures*, 82:102 -1031.

Box, G.E.P., Hunter, W.G. & Hunter, J.S. (1978). *Statistics for Experimenters- An Introduction to Design, Data Analysis, and Model Building*, John Wiley & Sons, Canada

Bucher, C. & Most, T. (2008). A comparison of approximate response functions in structural reliability analysis, *Probabilistic Engineering Mechanics*, 23:154-163.

Bucher, C.G. & Bourgund, U. (1990). A fast and efficient response surface approach for structural reliability problems. *Journal of Structural Safety* 7:57-66.

Caprani , C. (2005). *Probabilistic Analysis of Highway Bridge Traffic Loading*. Phd Thesis University College Dublin.

Caprani, C. (2011). *Virtual Work*. Dublin Institute of Technology. Lecture Notes

Carley, K.M., Kamneva, N.Y. & Reminga, J. (2004) *Response Surface Methodology*, CASOS Technical Report, Centre for Computational Analysis of Social and Organizational Systems.

Casas, J. R., Wisniewski, D.F. & Cervenka, J.(2007).Safety formats and required safety levels- Backgrounfddocument, SB4.4.3, Sustainable Bridges - VI Framework program, Brussels.

Castillo, E. (1988). *Extreme Value Theory in Engineering*, Academic Press, New York.

Chen, W., Goto, Y. & Richard Liew, J. (1996). *Stability Design of Semi-Rigid Frames*. New York: John Wiley & Son.

Choi, S.K., Grandhi, R.V. & Canfield, R.A. (2007). *Reliability - based structural design.* London: Springer.

Choudhury, D. (1986). Analysis of curved nonprismatic reinforced and prestressed concrete box girder bridges, *Structural Engineering Mechanics and Materials*, UCB/SEMM-86/13.

Coles, S.G. (2001). *An Introduction to Statistical Modelling of Extreme Values*. London: Springer-Verlag.

Collings, D. (2005). *Steel-Composite Bridges*, Thomas Telford, London.

Cooper, D.I. (1997). Development of short span bridge - specific assessment live loading, *Safety of Bridges*, Thomas Telford, London, 64-89.

Cost 345. (2004). *Procedures Required for Assessing Highway Structures*. Available from http://cost345.zag.si/: Cordis.

Czarnecki, A.A & Nowak,A.S.(2007). Reliability-based evaluation of steel girder bridges, *Proceedings of the Institution of Civil Engineers* - Bridge Engineering, 1-7.

Deng, L. & Cai, C.S.(2010). Bridge Model Updating Using Response Surface Method and Genetic Algoritim. *Journal of Bridge Engineering*, September/October, 2010.

Du, J.S. & Au, F.T.K. (2005).Deterministic and reliability analysis of prestressed concrete bridge girders: comparison of the Chinese, Hong Kong and AASHTO LRFD Codes, *Journal of Structural Safety*, 27:230-45.

EC1. 1(2005), *Eurocode 1: Basis of Structural Design*, European Standard EN 1990-1. Brussels: European Committee for Standardisation.

EC1.3. (2003), *Eurocode 1: Actions on Structures*, Part 2: Traffic loads on bridges, European Standard EN 1991-2. Brussels: European Committee for Standardisation.

Eom, J. & Nowak, A.S. (2001). Live Load Distribution for Steel Girder Bridges. *Journal of Bridge Engineering,* ASCE 489 -497.

Estes, A. & Frangopol, D.M. (1999). Repair optimization of highway bridges using system reliability approach. *Journal of Structural Engineering*, ASCE, 125(7):766-775.

Estes, A.C. & Frangopol, D.M. (2005). Load Rating versus Reliability Analysis, *Journal of Structural Engineering*, 131:843-847.

Ferreira, L.M, Nowak, A.S., & El Debs, M.K. (2008). Development of truck weight limits for concrete bridges using reliability theory, *Ibracon Structures and Materials Journal* 1(4):421-450.

Frangopol, D.M, Kallen, M.J. & Van Noortwijk, J.M. (2004). Probabilistic models for life cycle performance of deteriorating structures: review and future directions. *Proceedings of Structural Engineering Materials*, 6:197 - 212.

Gavin, H.P & Yau, S.C. (2008). High-order limit state function in the response surface method for structural reliability analysis. *Journal of Structural Safety* 30:162-179.

Gayton, N., Bourinet, J.M. & Lemaire, M. (2003). CQ2RS: A new statistical approach to the response surface method for reliability analysis. *Journal of Structural Safety* 25:99-121.

Ghali, A. Neville, A & Brown, T. (2009). *Structural Analysis-A unified classical and matrix approach*. London: Spon Press.

Ghosn, M. & Moses, F. (1986). Reliability calibration of a bridge design code, *Journal of Structural Engineering*. 112 (4):745-763.

Ghosn, M. & Moses, F. (1998). *Redundancy in Highway Bridge Superstructures*. Transportation Research Board, Washington, DC, NCHRP Report 406.

Haldar, A. & Mahadevan, S. (2000). *Reliability assessment using stochastic finite element analysis*. John Wiley & Sons, 2000.

Hendy, C.R. & Johnson, R.P. (2006). *Designer's Guide to EN 1994-2 Eurocode 4: Design of composite steel an concrete structures*. Part 2: General rules and rules for bridges. Thomas Telford. Bristol.

Huo, X.S., Wassermann, E.P & Zhu, P.(2004). Simplified Method of Lateral Distribution of Live Load Moment. *Journal of Bridge Engineering*. ASCE 382 - 390.

Hwang, E.S., Paik, I.R., & Nguyen, S., H. (2010). Reliability Analysis of Stresses in Prestressed Concrete Girder Under Service Load, *Proceedings of 11th International Conference on Applications of Statistics and Probability in Civil Engineering*, 1-4 August 2011, Zurich, Switzerland.

Iles, D.C. (2001). *Design Guide for Composite Highway Bridges*. The Steel Construction Institute. Spon Press. London.

Imhof, D. (2004). *Risk Assessment of Existing Bridge Structures*. PhD Thesis University of Cambridge

Jeong, S.M., Kim, S.J., Kim, Y.B., & Park, K.T. (2003). Reliability Analysis on Flexural Behaviour of FRP Bridge Decks, *Proceedings from the Conference on Advanced Materials for Construction of Bridges, Buildings and Other Structures III*, Davos Switzerland.

Khaleel, M.A. & Itani, R.Y. (1993). Safety Evaluation of Existing Partially Prestressed Concrete Girder Bridge, *Journal of Computers & Structures* 48(5):763-771.

Kim, S.H. & Na, S.W. (1997). Response surface method using vector projected sampling points. *Journal of Structural Safety* 19(1):3-19.

Kolios, A.I. (2010). *A multi-configuration approach to reliability based structural integrity assessment for ultimate strength*. PhD Thesis Cranfield University.

Lei, Y. (2010). *Fatigue Reliability of ship structure*. PhD Thesis, University of Glasgow.

Lemaire, M. (1998). Finite element and reliability: combined methods by response surface. In: Frantziskonis GN. editor, PROBAMAT-21st century: probabilities and materials. Tests, models and applications for the 21st century, vol. NATO ASI series 3. High technology, vol. 46. Kluwer Academic; 1998:317–31.

Li, G.Q. & Li, J.J. (2007). *Advanced Analysis and Design of Steel Frames*. Sussex: John Wiley & Sons.

Liu,Y. & Moses, F. (2001). Bridge design with reserve and residual reliability constrains. *Journal of Structural Safety*,11(1), 29-42.

Marková, J. (2010). Reliability Assessment of Existing Concrete Bridges, *Journal of KONBiN*, (14, 15).

Melchers, R.E. (1999). *Structural Reliability Analysis and Prediction*. Sussex: John Wiley and Sons.

Myers, R.H. (1995). *Response surface methodology: process and product optimization using designed experiments*,Wiley, New York.

NCHRP report 592(2007). *Simplified Live Load Distribution Factor Equations*, Transportation Research Board.

Neves, R.A., Chateauneuf, A., Venturini, W.S. & Lemaire, M. (2005). Reliability analysis of reinforced concrete grids with nonlinear material behavior, *Journal of Reliability Engineering and System Safety* 91:735-744.

Nicholson, B.A. (1997). *Simple Bridge Design using prestressed Beams*. Leicester: Uniskill Ltd.

NIST/SEMATECH e-Handbook of Statistical,Methods,http://www.itl.nist.gov/div898/handbook/,11/05/2012.

Nowak, A.S. & Park, C.H. (2001). Reliability analysis of prestressed concrete bridge girders: comparison of Eurocode, Spanish Norma IAP and AASHTO. *Journal of Structural Safety* 23:331-344.

Nowak, A.S. (1993).Live Load model for highway bridges, *Journal of Structural Safety*, 13:53-66.

Nowak, A.S. (1999). *Calibration of LRFD Bridge Design Code NCHRP Report 368*, Washington D.C., Transportation Research Board, 1999.

of Technology, Delft University Press, Delft

Owen, D.R.J. & Hinton, E.(1986). *Finite Elements in Plasticity Theory and Practice*. Swansea: Pineridge Press Limited.

Park, C.H., Nowak, A.S., Das, P.C. & Flint, A.R. (1998). Time-varying reliability model of steel girder bridges. *Proceedings of the institution of Civil Engineers - Structures and Buildings*, 128:359-367.

Parsons & Brickenhoff (2003). *A review of bridge assessment failures on the motorway and trunk road network*. Final Project Report prepared for the Highways Agency. Parsons Brinckerhoff Ltd.

Rackwits, R. (1982). *Response surfaces in structural reliability*. Berichte zur Zuverlassigkeitstheorie der Bauwerke, Heft 67 Munchen.

Rackwitz, R. & Fiessler, B. (1978). Structural Reliability under Combined Random Load Sequences, *Journal of Computer and Structures* 9:489-494.

Rajashekhar, M.R. & Ellingwood, B.R. (1993). A new look at the response surface approach for relaibiltiy analuysis. *Journal of Strucutral Safety* 12:205-220.

Schneider, J. (2006). *Introduction to Safety and Reliability of Structures*. International Association for Bridge and Structural Engineering.IABSE-AIPC-IVBH, Zurich, Switzerland.

Soares, R.C., Mohamed, A., Venturing, W.S. & Lemaitre, M. (2001). Reliability analysis of non-linear reinforced concrete frames using the response surface method. *Journal of Reliability Engineering and System Safety* 75:1-16.

Sotelino, E.D., Liu, J., Chung, W. & Phuvoravan, K. (2004) *Simplified Load Distribution Factor for use in LRFD Design*, Indiana Department of Transportation and Federal Highway Administration.

Spanish Norma IAP-98, Actions in highway bridges. Road Directorate, Spanish Ministry of Public Works, Madrid 1998.

Stewart, M.G., Rosowsky, D.V. & Val, D.V. (2001). Reliability - based bridge assessment using risk-ranking decision analysis, *Journal of Structural Safety* 23:397-405.

Tabsh, S.W. & Nowak, A.S. (1991). Reliability of highway girder bridges. *Journal of Structural Engineering*, ASCE, 117:23772 - 2388.

Tonias, D.E. & Zhao, J.J. (2007). *Bridge Engineering-Design, Rehabilitation and Maintenance of Modern Highway Bridges*, 2nd Edition, McGraw-Hill, New York

Torrii, A.J. & Machado, D.A. (2010). Reliability analysis of nonlinear reinforced concrete beams. *Proceedings for Asociacón Argentina de Mecánica Computacional Conference*, 15 - 18 November 2010, Buenos Aires, Argentina.

Val, D & Melchers, R.E. (1997). Reliability of Deteriorating RC Slab Bridges, *Journal of Structural Engineering*,123(12), 1638-1644.

Val, D., Bluger, F. & Yankelevsky D. (1997) Reliability evaluation in nonlinear analysis of reinforced concrete structures. *Journal of Structural Safety* 19(2):203-17.

Vu, K.A.T. & Stewart, M.G. (2000). Structural reliability of concrete bridges including improved chloride - induced corrosion models, *Journal of Structural Safety* 22:313-333.

Waarts, P.H., (2000), Structural reliability using finite element methods, Ph.D. thesis, Delft University.

Wisniewski, D.F., Casas, J.R. & Ghosn, M. (2009). Simplified probabilistic non-linear assessment of existing railway bridges. *Structural and Infrastructure Engineering: Maintenance, Management, Life - Cycle Design and Performance*, 5(6):439-453.

Wong, S.M., Hobbs, R.E. & Onof, C. (2005). An adaptive response surface method for reliability analysis of structures with multiple loading sequences, *Journal of Structural Safety*, 27:287-308.

Xu, L., Liu, Y. & Grierson, D.E.(2005). Nonlinear analysis of steel frameworks through direct modification of member stiffness properties, *Advances in Engineering Software*, 36:312-324.

Zona, A., Barbato, M., Dall'Asta, A. & Dezi, L. (2010). Probabilistic analysis for design assessment of continous steel-concrete composite girders. *Journal of Constructional Steel Research* 66:897-905.

Appendix 1

Live Load Application Graphs

Appendix 1   Live Load Application Graphs

A1.1   Introduction

This appendix contains the results graph form Chapter 7. The common approach of applying moving live loads as stationary loads is assessed against the proposed moving load procedure in terms of a load factor ratio (see Section 7.7). The stationary loads are positioned according to Table 7.4. The positions causing the maximum load factor ratio are highlighted in blue while the positions causing the minimum load factor ratio are highlighted in red. The common approach of applying the live loads as static loads positioned according to an elastic analysis is found to behave quite similar to the proposed moving load approach, when appropriate positions are examined.

A1.2   Two-Span Structures
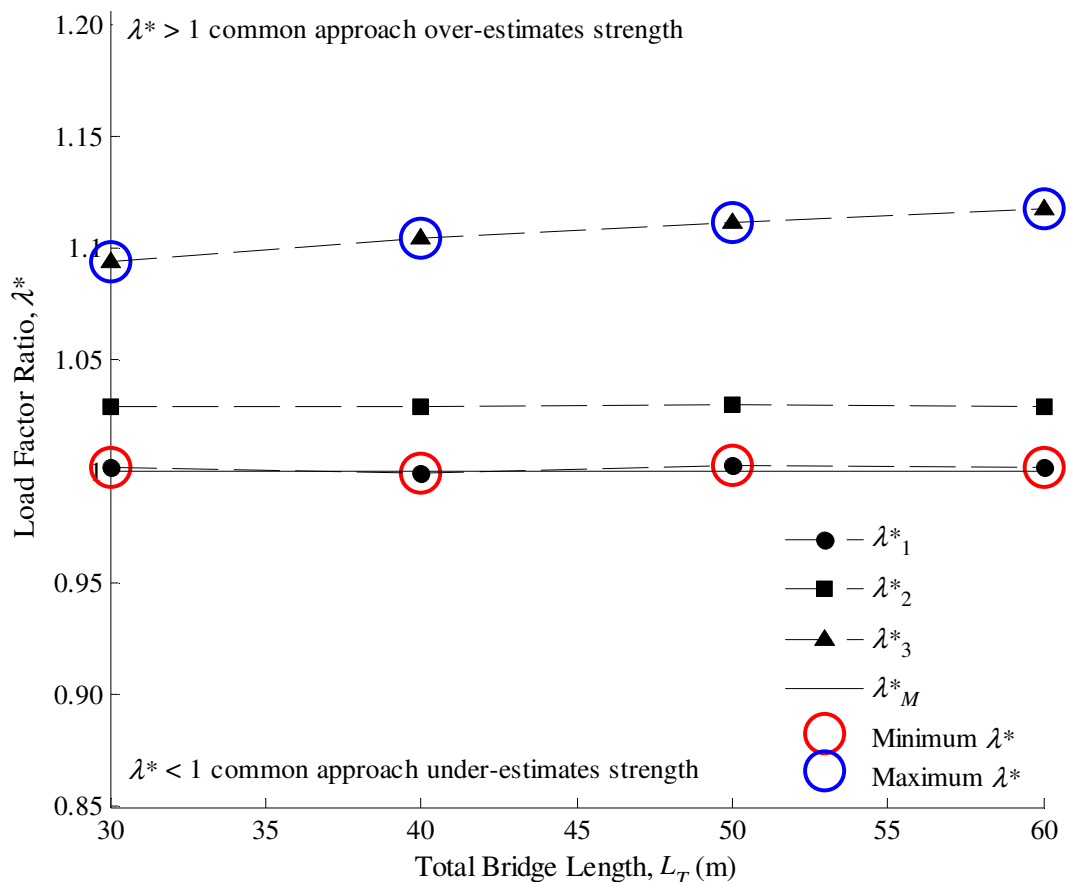
Figure A1.1: AS1 (one axle)
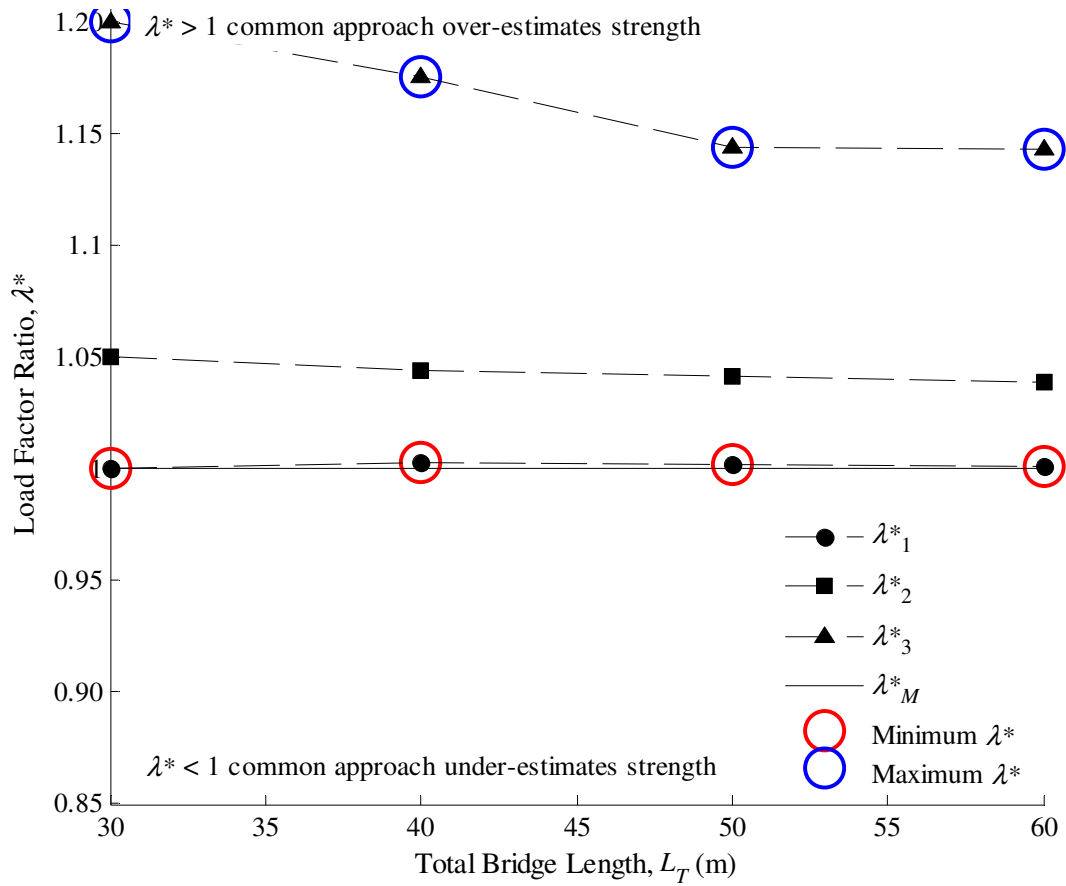
Figure A1.2:AS2-H20 (two axles)
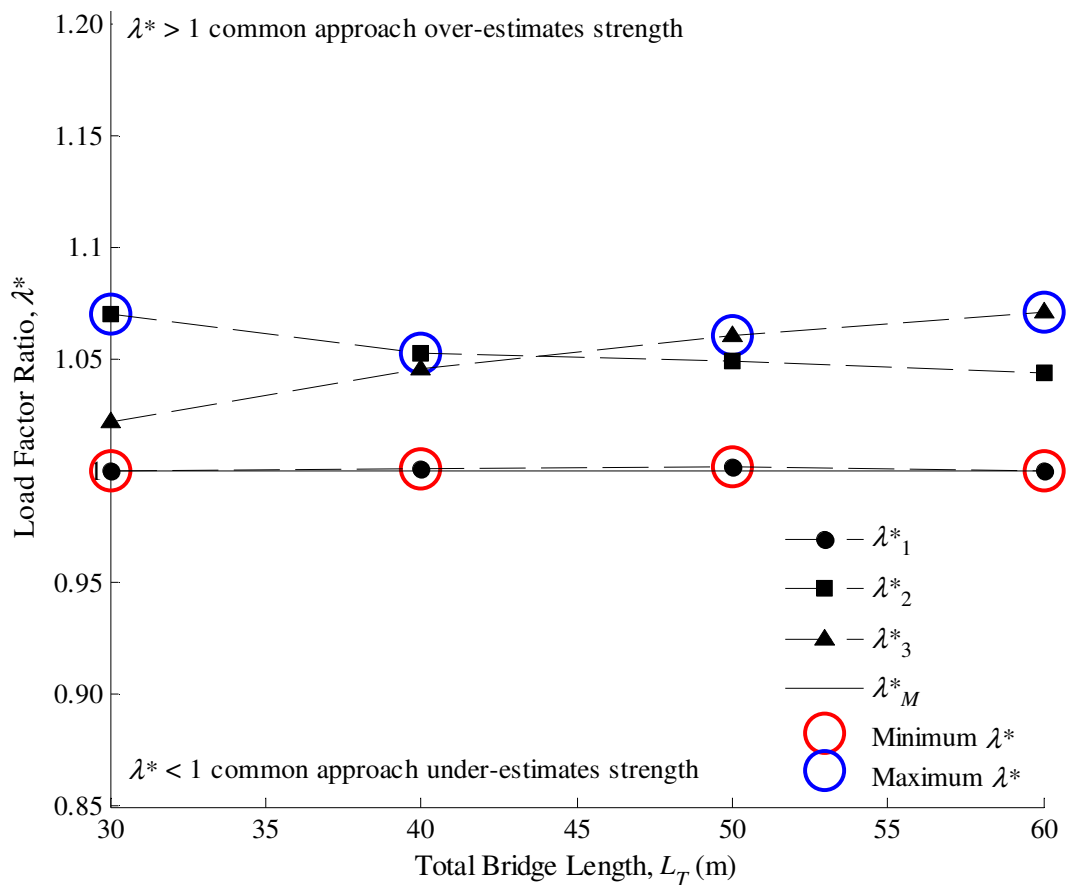
Figure A1.3: AS3-HS20 (three axles)
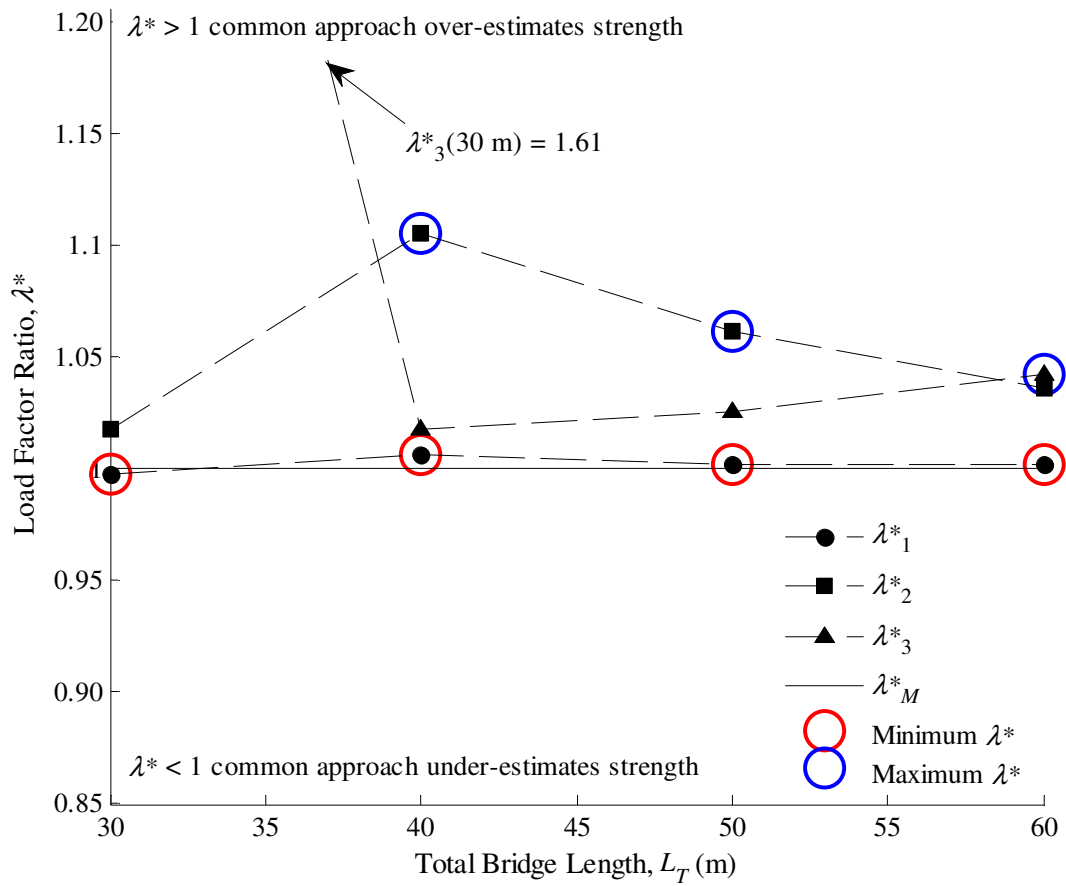
Figure A1.4: AS5-T1103 (five axles)
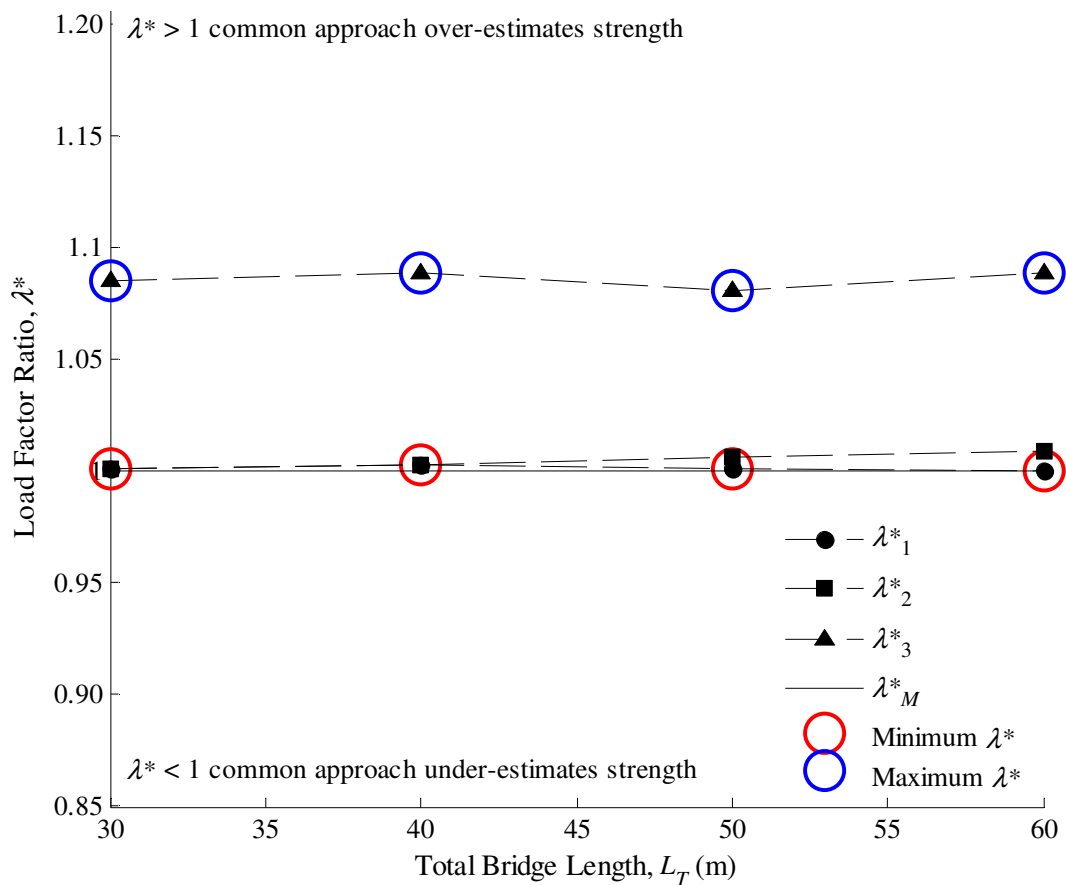
Figure A1.5: AS2-1.5 (two axles 1.5 m apart)
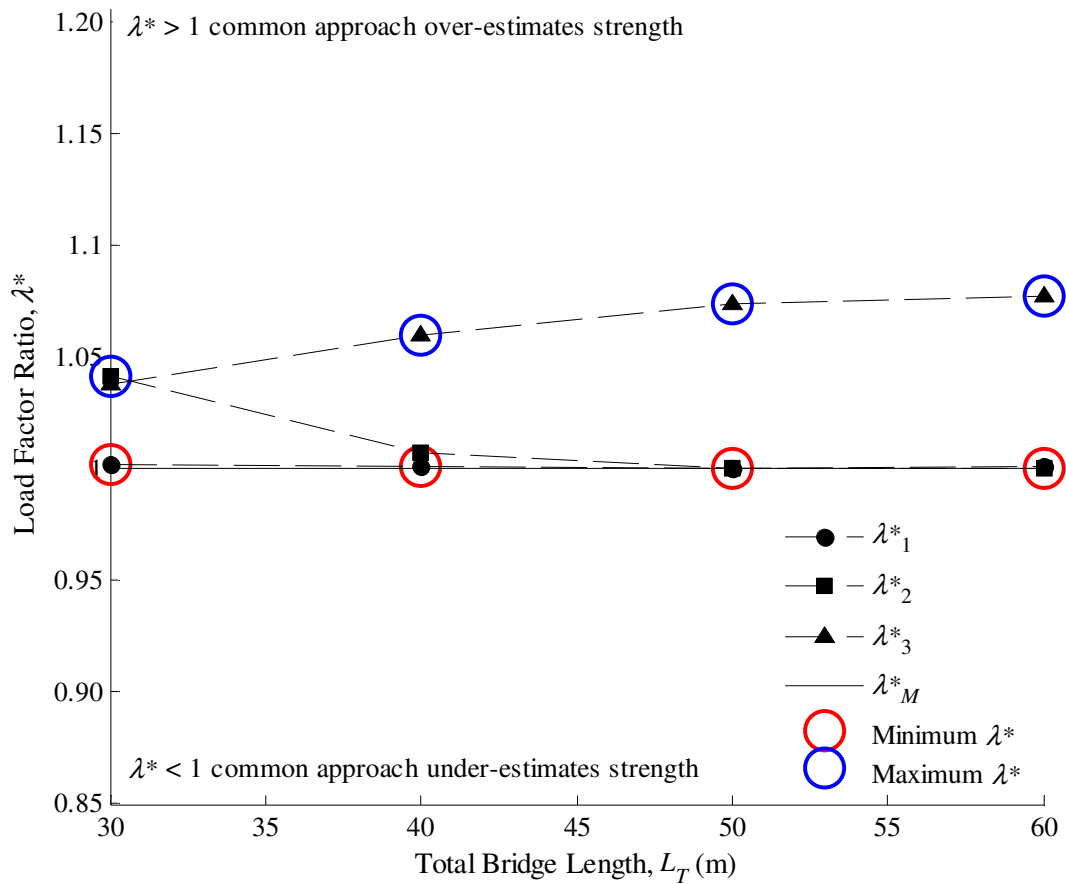
Figure A1.6: AS2-3.0 (two axles 3.0 m apart)
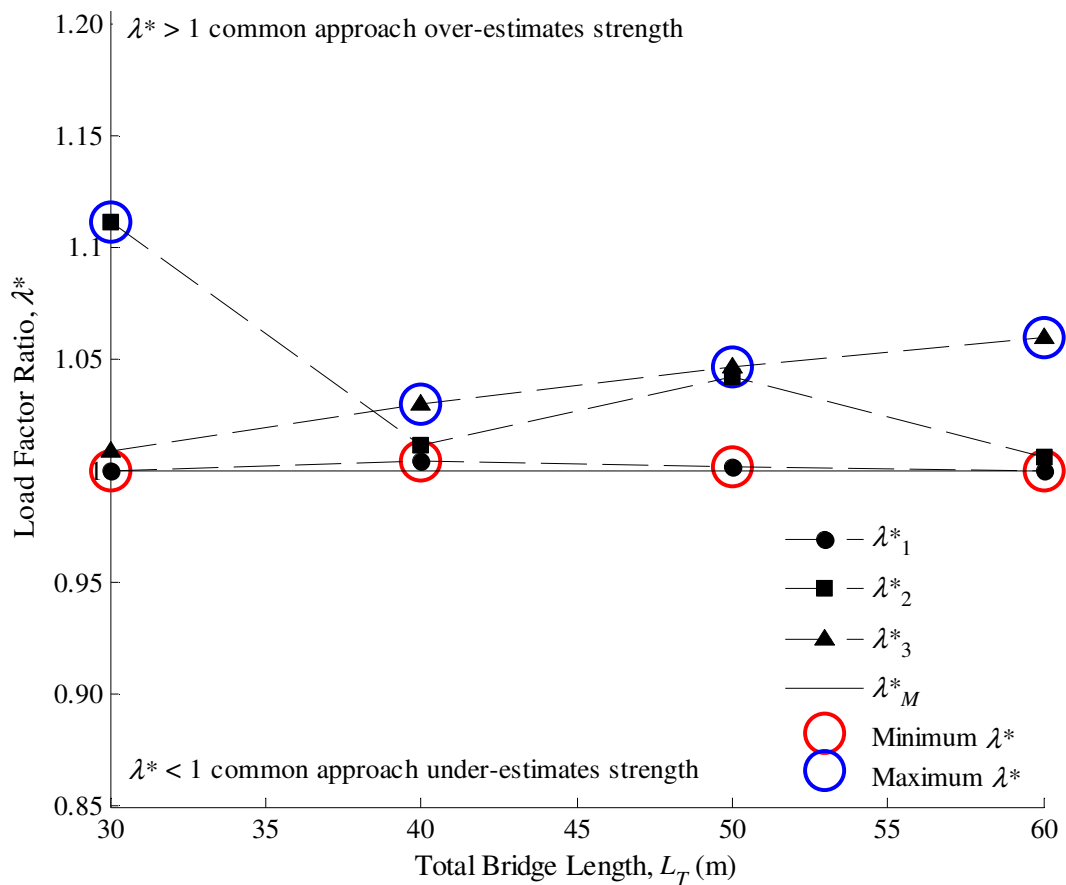
Figure A1.7:AS2-4.5 (two axles 4.5 m apart)
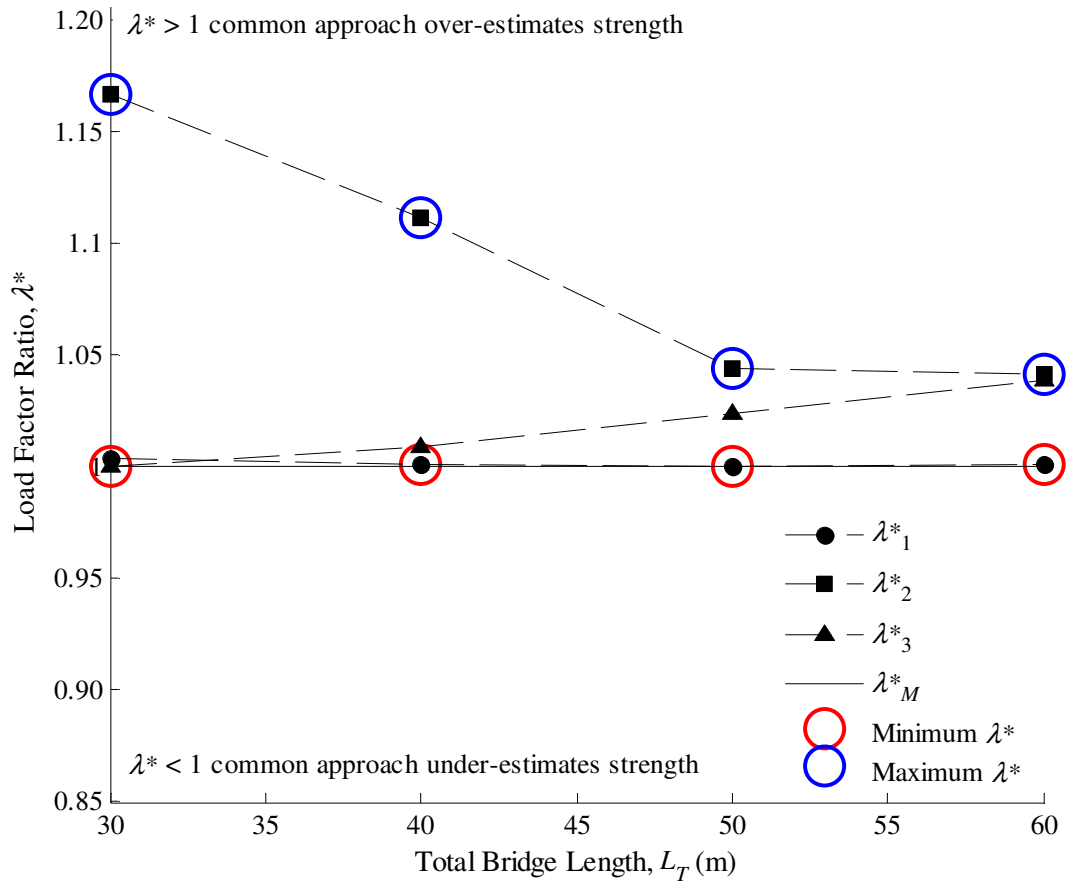
Figure A1.8: AS2-6.0 (two axles 6.0 m apart)
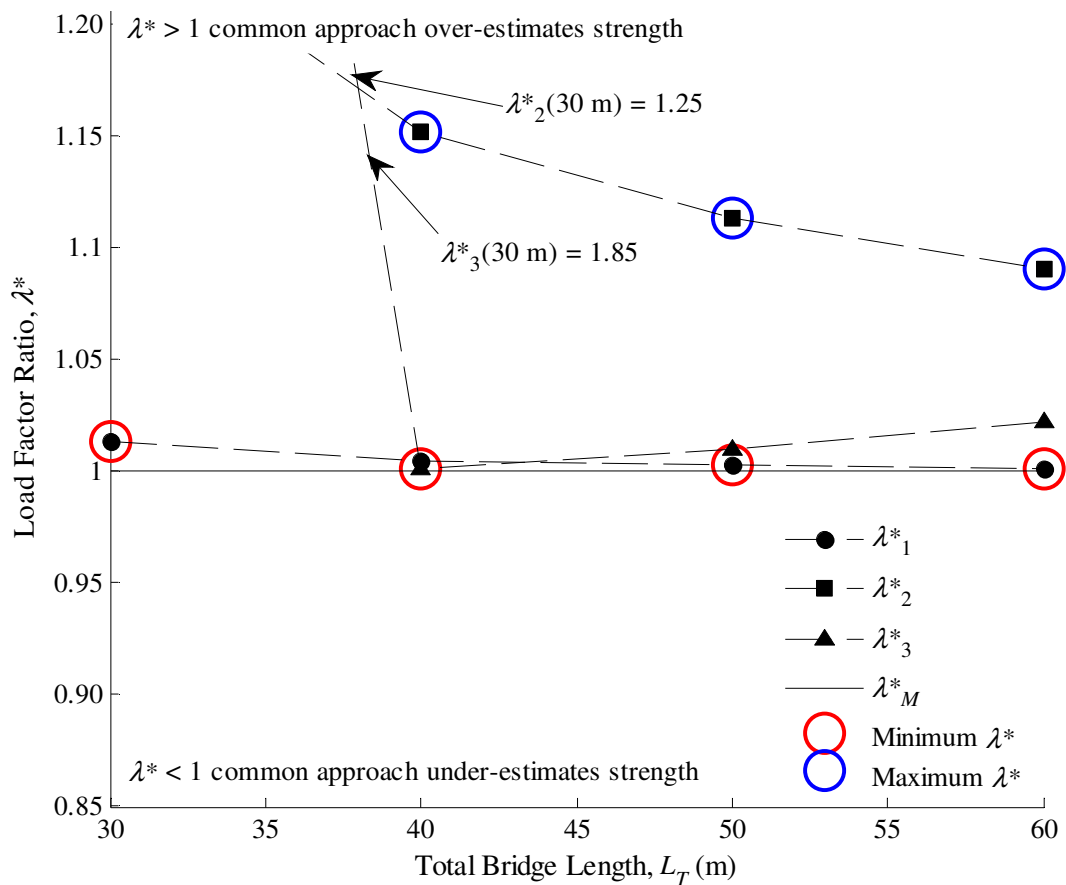
Figure A1.9: AS2-7.5 (two axles 7.5 m apart)
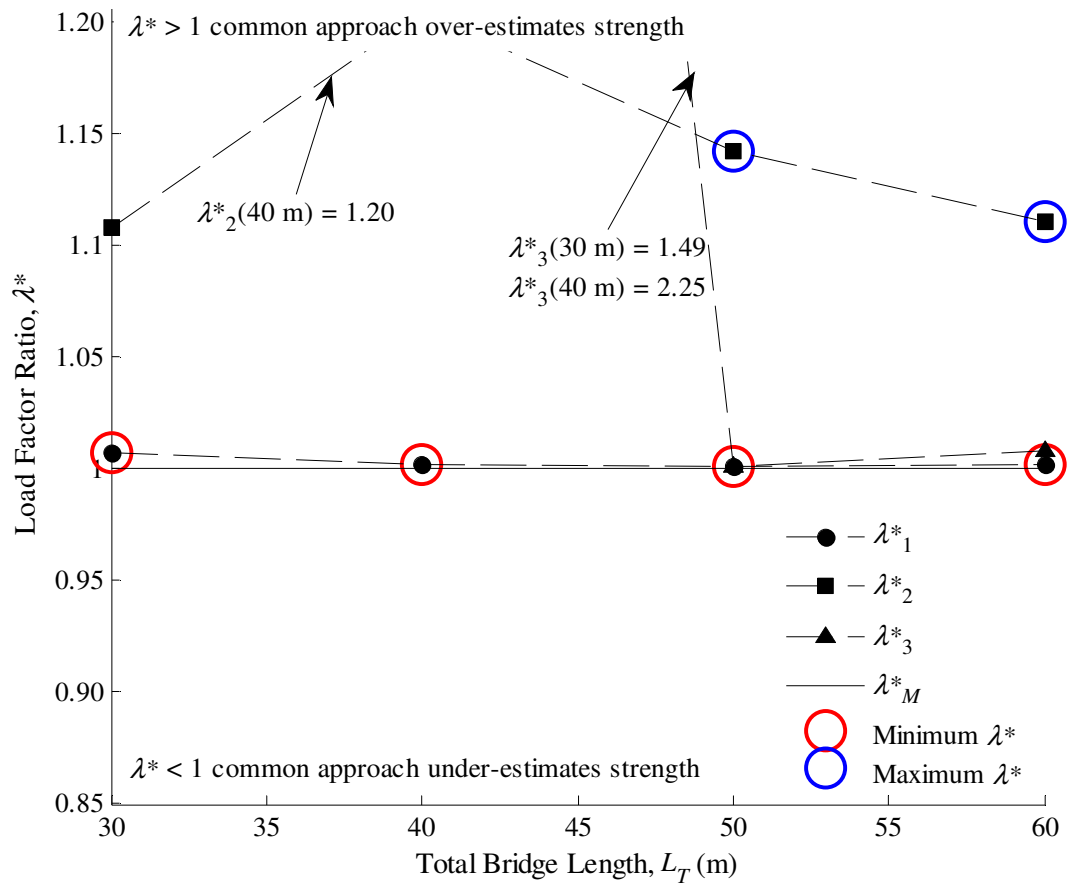
Figure A1.10: AS2-9.0 (two axles 9.0 m apart)

A1.3 Three-Span Structures
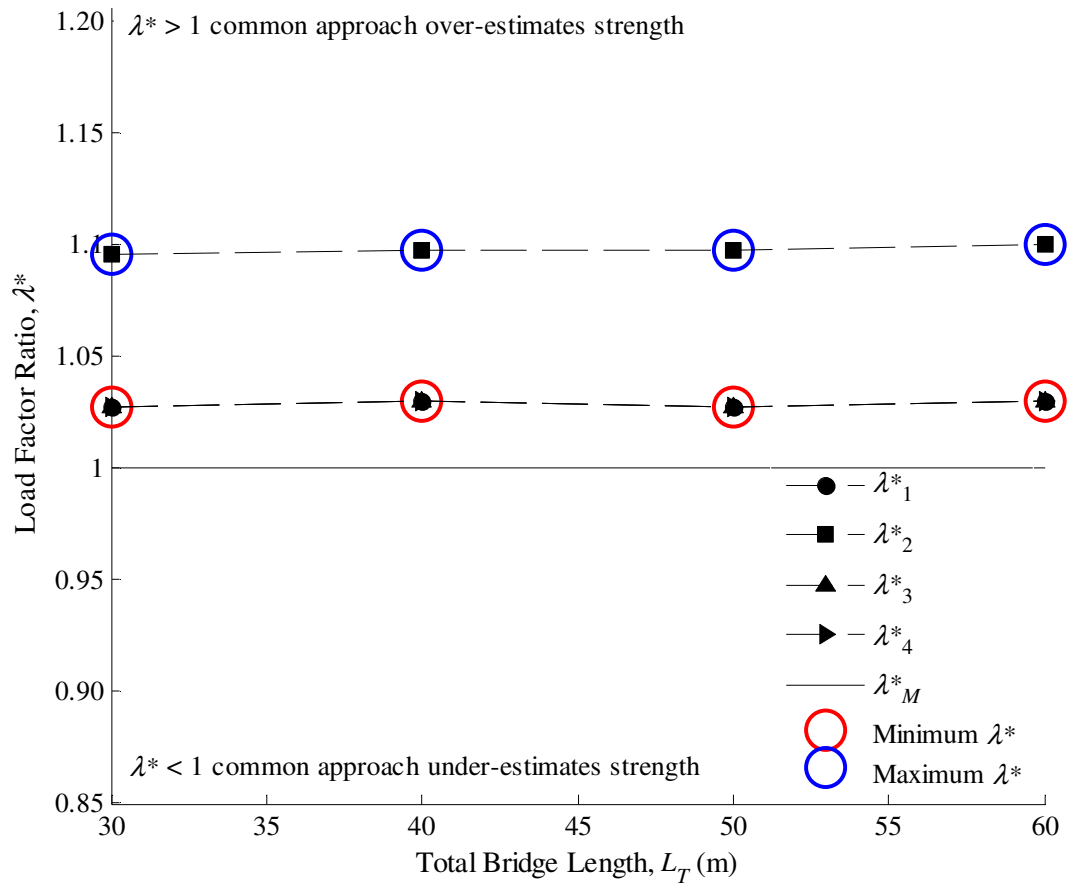
Figure A1.11: AS1 (one axle)
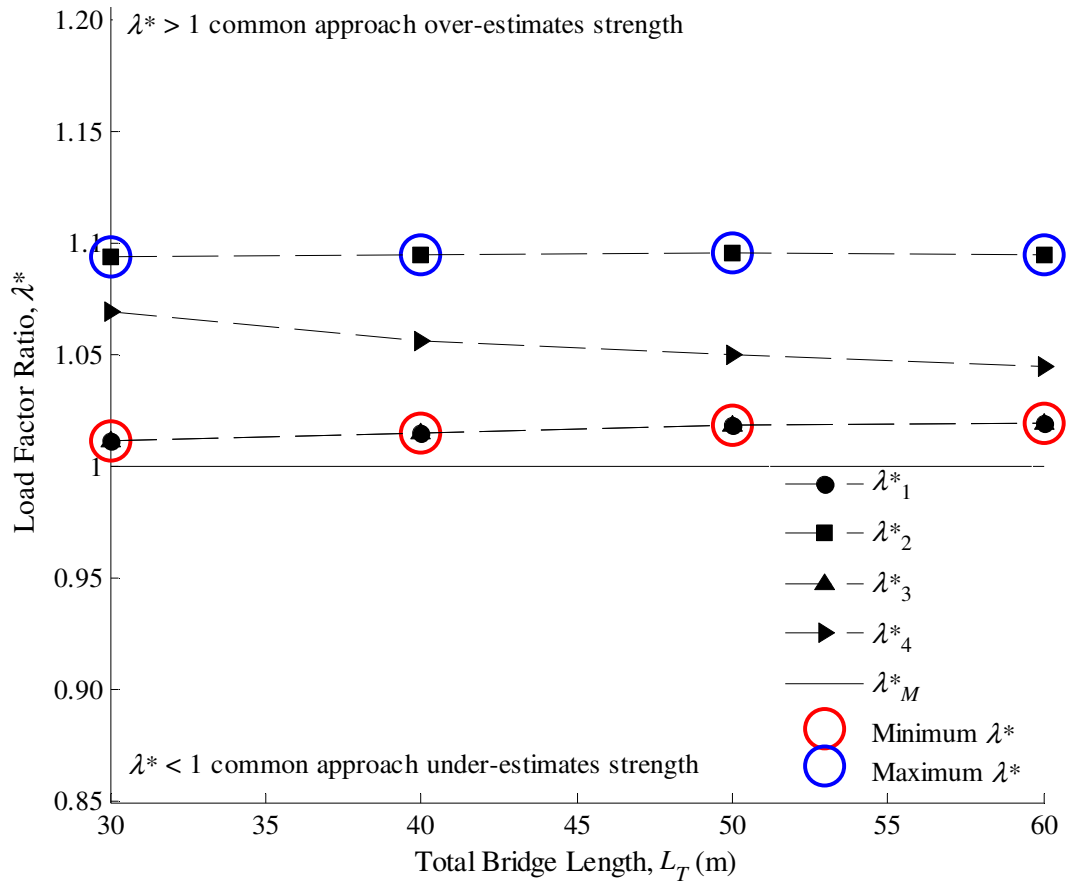
Figure A1.12: AS2-H20 (two axles)
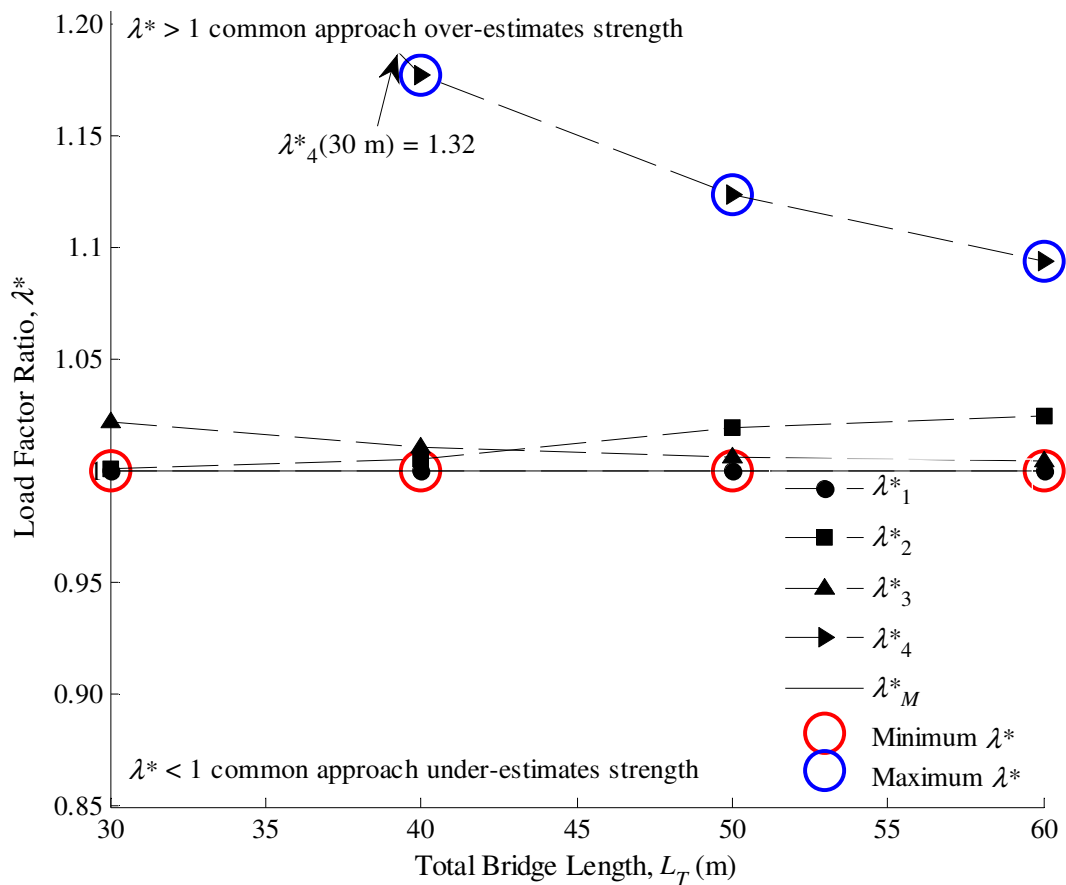
Figure A1.13: AS3-HS20 (three axles)
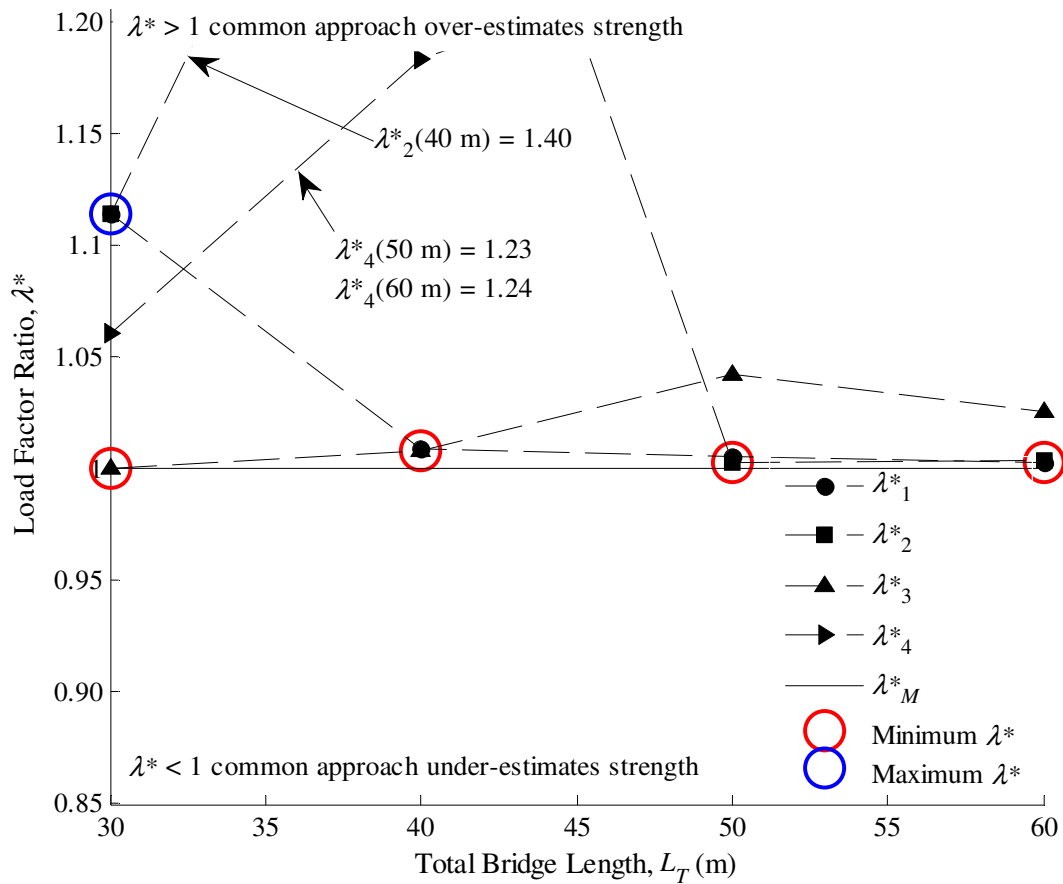
Figure A1.14: AS5-T1103 (five axles)
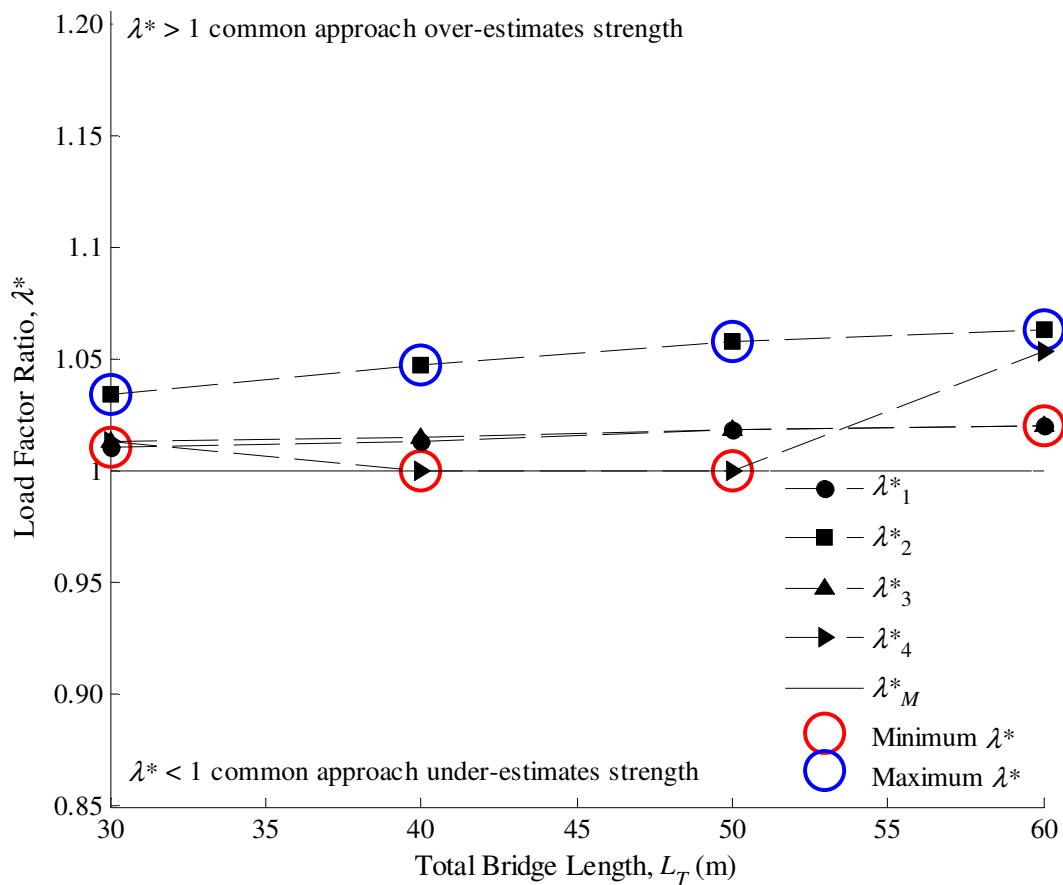
Figure A1.15:AS2-1.5 (two axles 1.5 m apart)
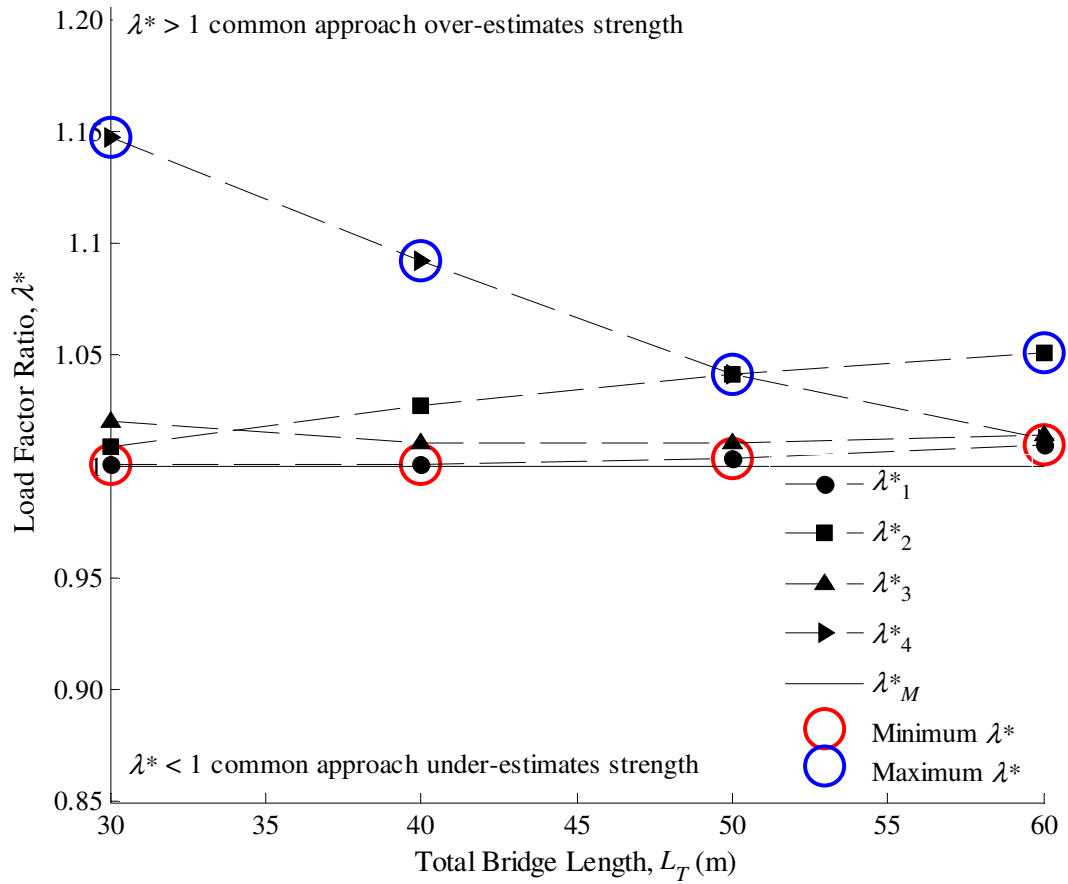
Figure A1.16:AS2-3.0 (two axles 3.0 m apart)
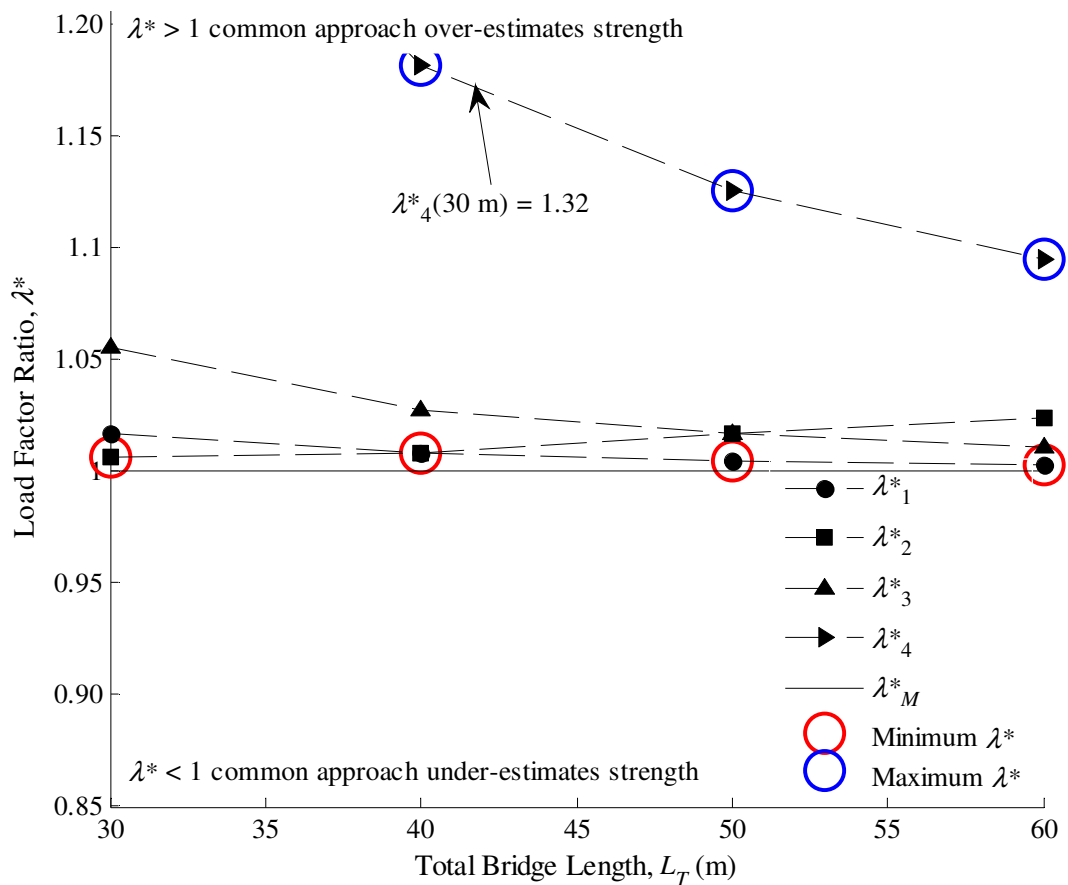
Figure A1.17:AS2-4.5 (two axles 4.5 m apart)
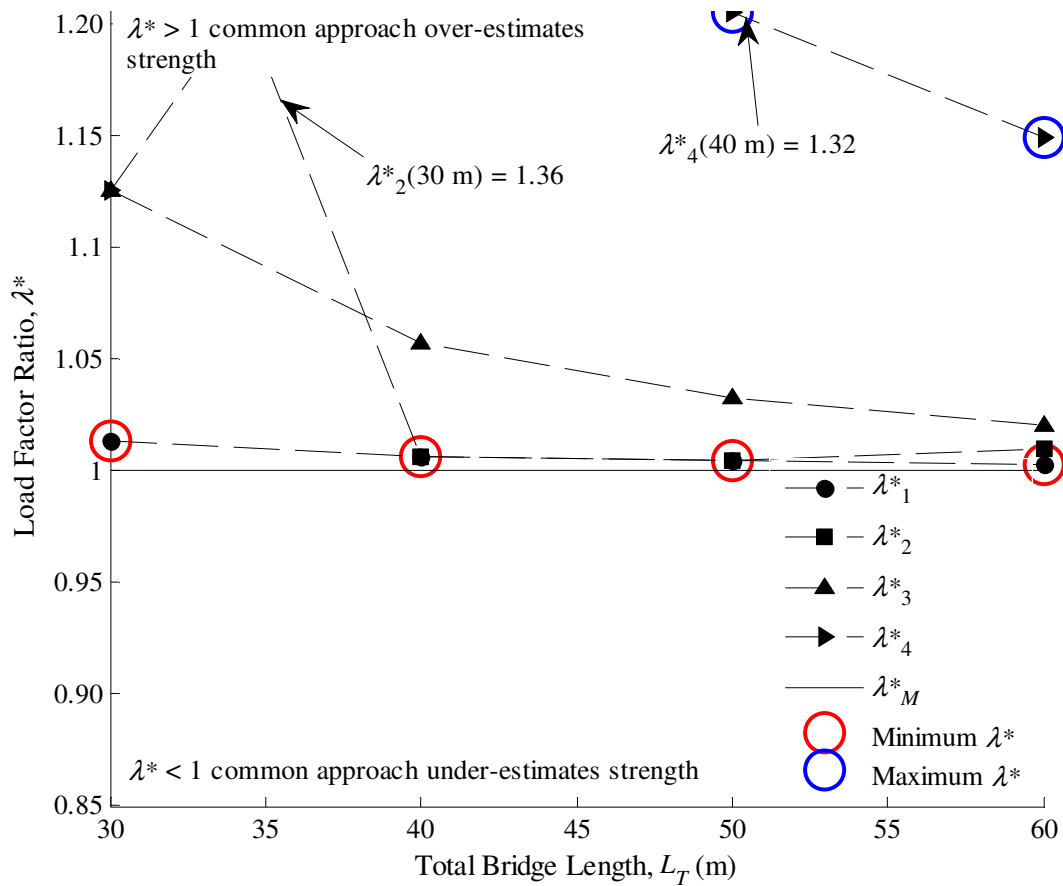
Figure A1.18:AS2-6.0 (two axles 6.0 m apart)
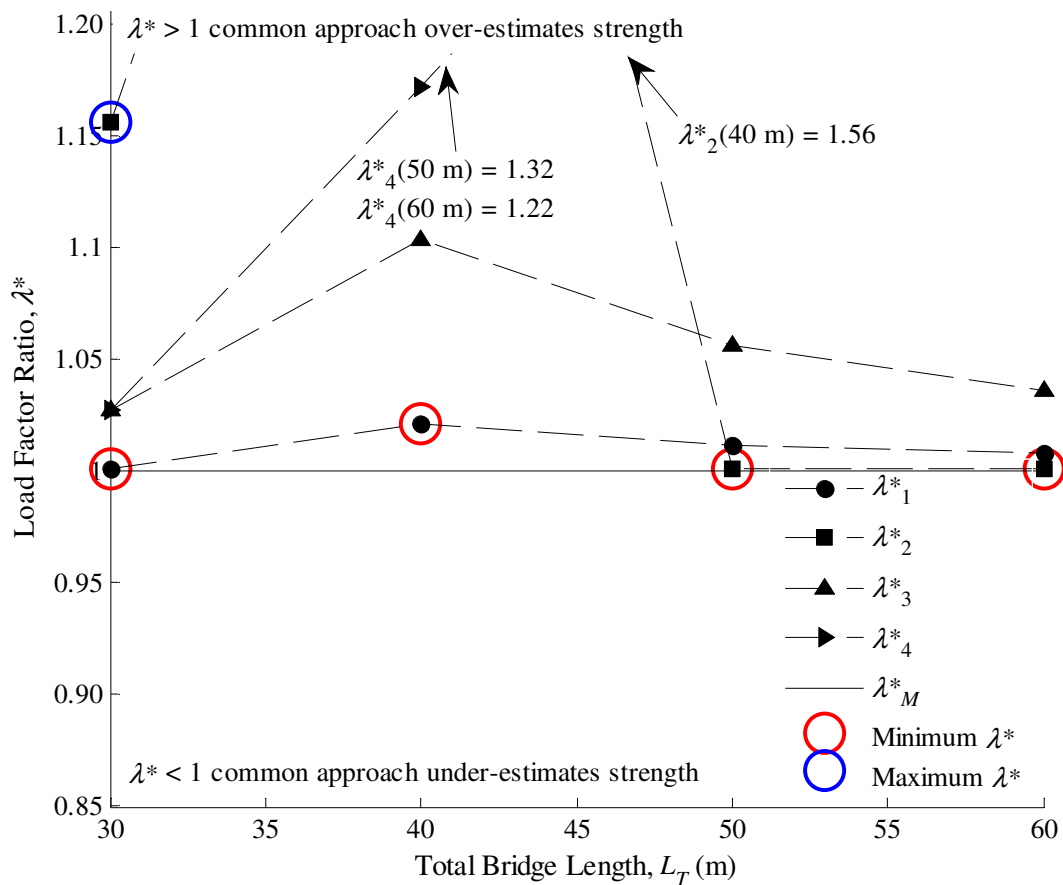
Figure A1.19:AS2-7.5 (two axles 7.5 apart)

Figure A1.20: AS2-9.0 (two axles 9.0 apart)

Appendix 2

Deterministic Study

Appendix 2   Deterministic Study

A2.1   Introduction

The results of the deterministic study carried out in Chapter 8 are contained in this Appendix. Graphs of the failure load factors are shown for each annual maximum loading event. The limit state extrapolation graphs for the semi-probabilistic study are also given.

A2.2   Two-Span Structures
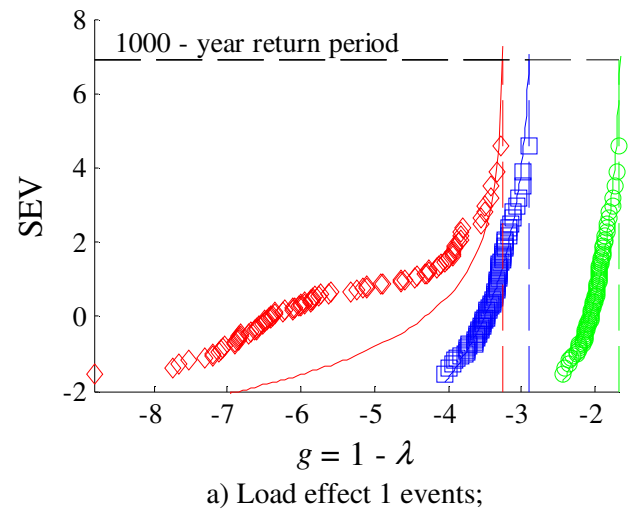

a) Load effect 1 events;

a) Load effect 1 events;

b) Load effect 2 events;
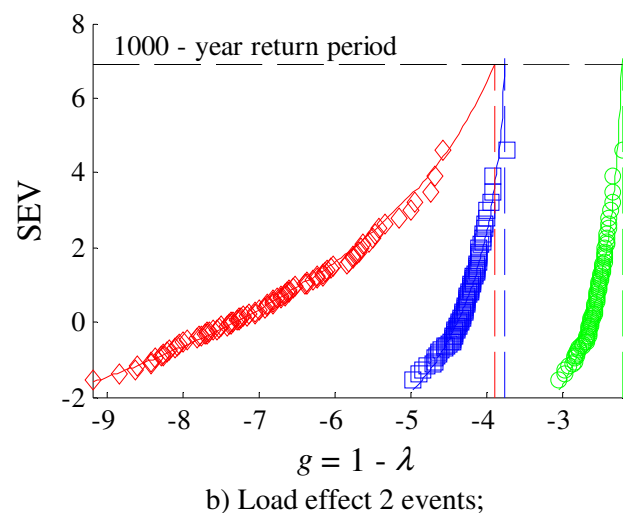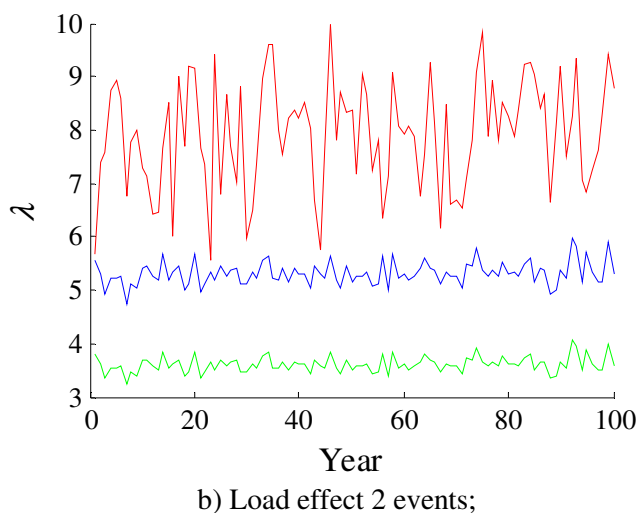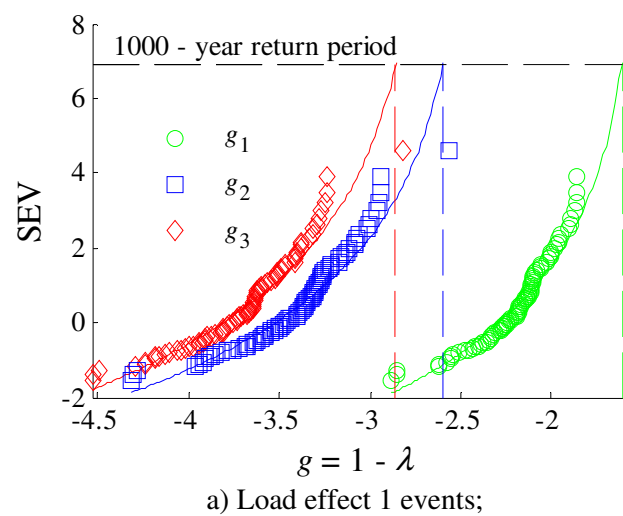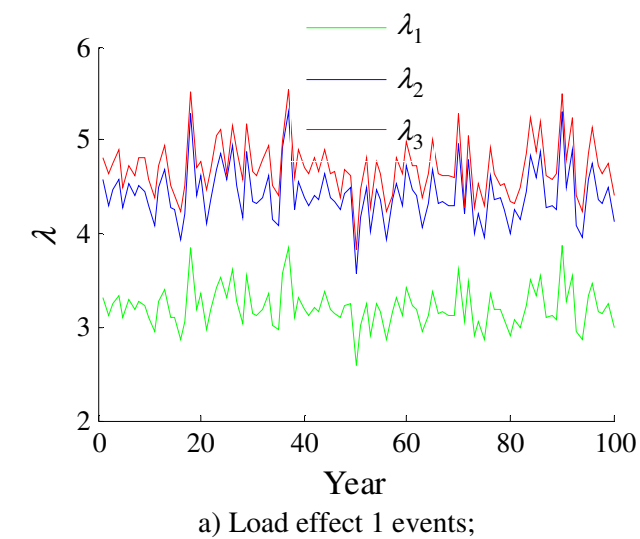
Figure A2.1: Two-span 30 bridge load factors.

b) Load effect 2 events;

Figure A2.2: Two-span 30 bridge limit state extrapolation.

a) Load effect 1 events;

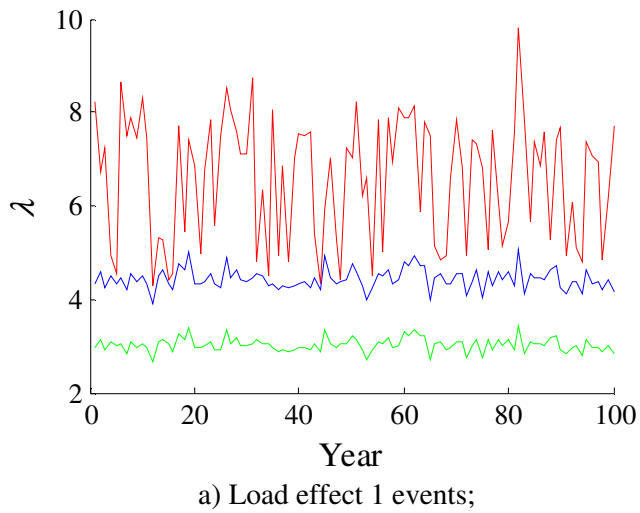a) Load effect 1 events;
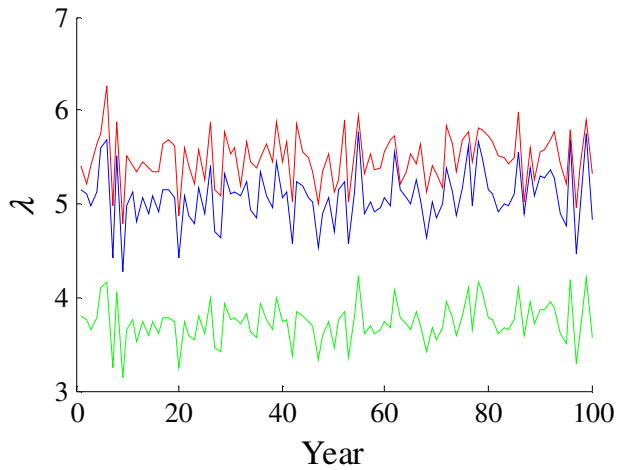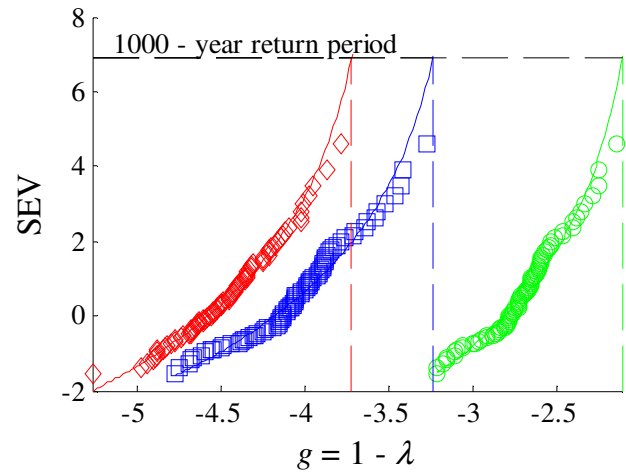

b) Load effect 2 events;

b) Load effect 2 events;
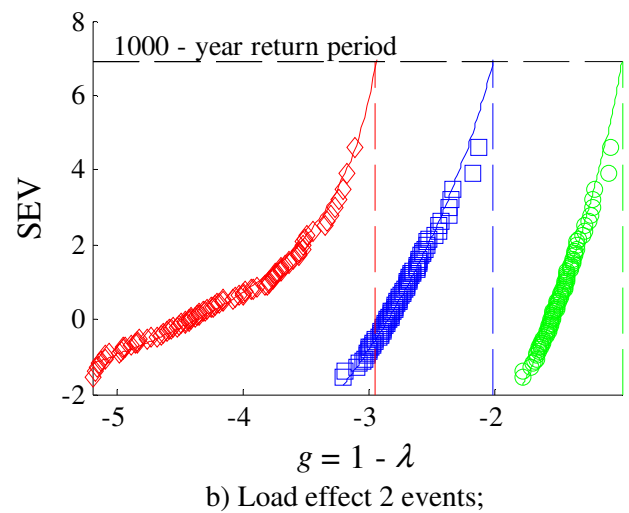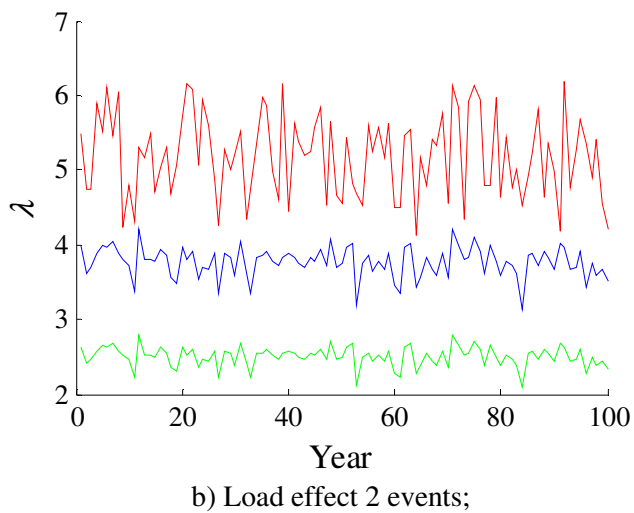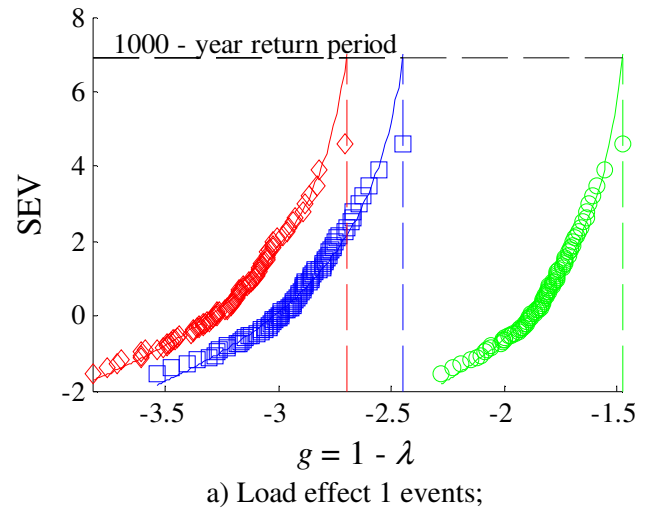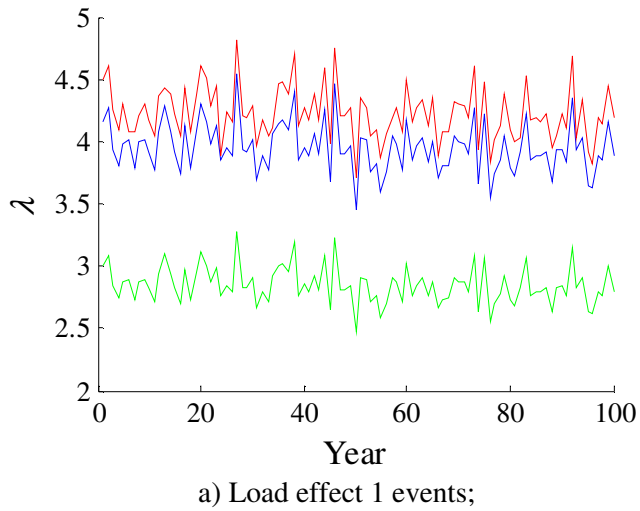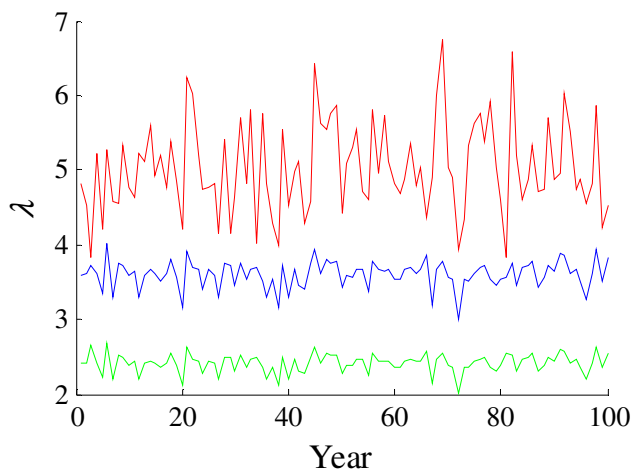
Figure A2.3: Two-span 40 bridge load factors.

Figure A2.4: Two-span 40 bridge limit state extrapolation.

a) Load effect 1 events;

b) Load effect 2 events;
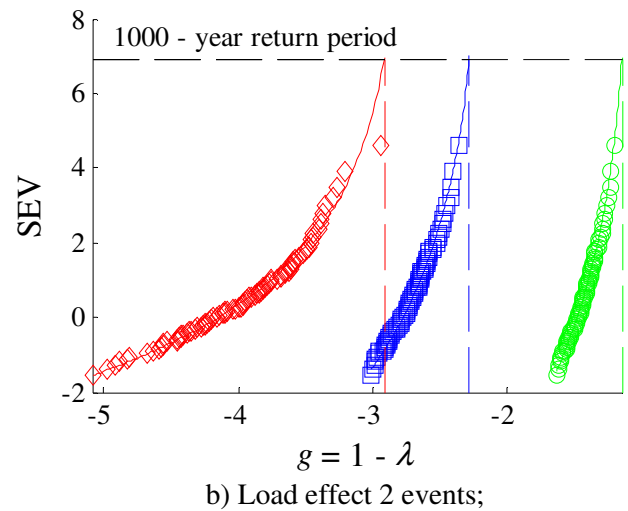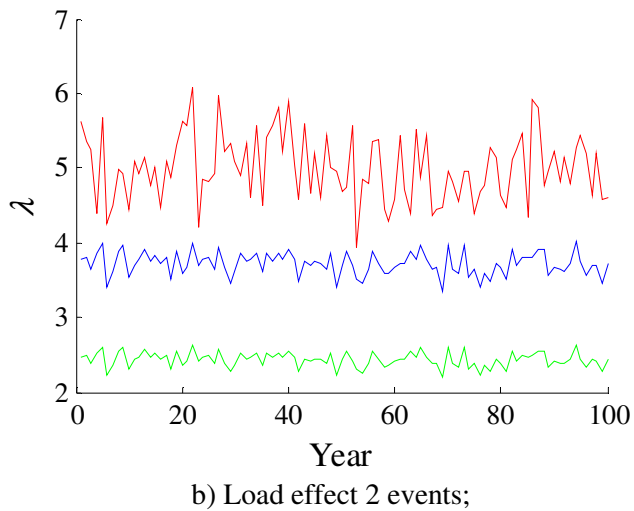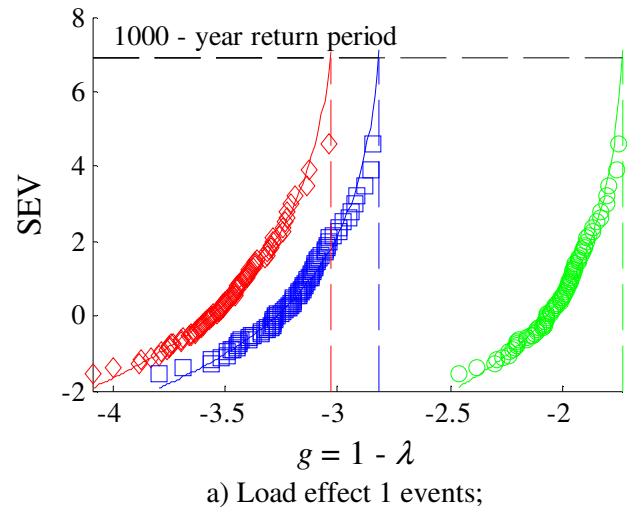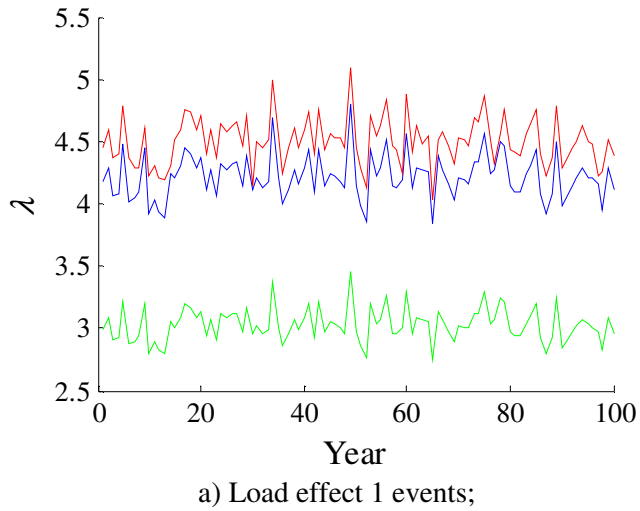
Figure A2.5: Two-span 50 bridge load factors.

a) Load effect 1 events;

b) Load effect 2 events;

Figure A2.6: Two-span 50 bridge limit state extrapolation.

a) Load effect 1 events;

a) Load effect 1 events;

b) Load effect 2 events;

b) Load effect 2 events;
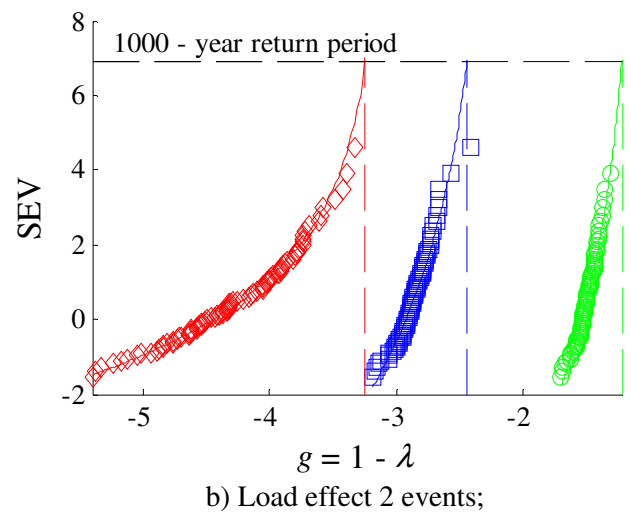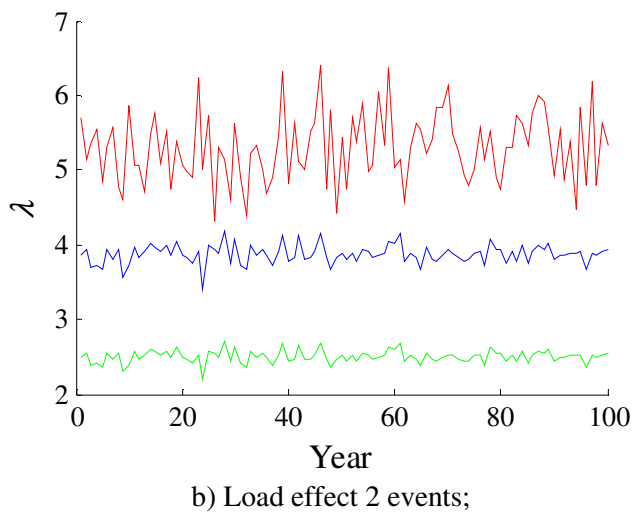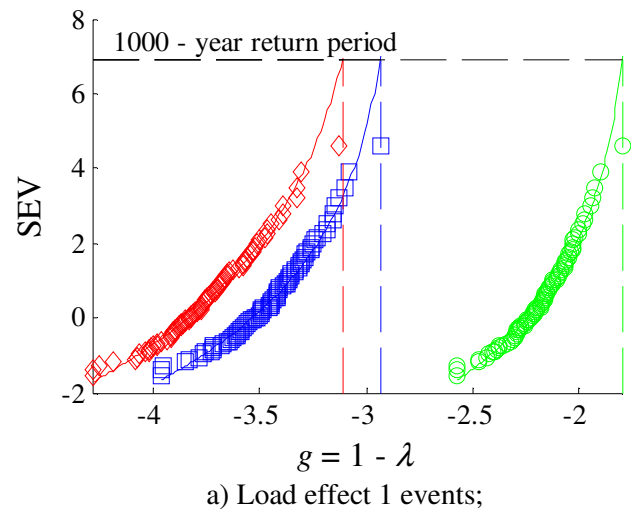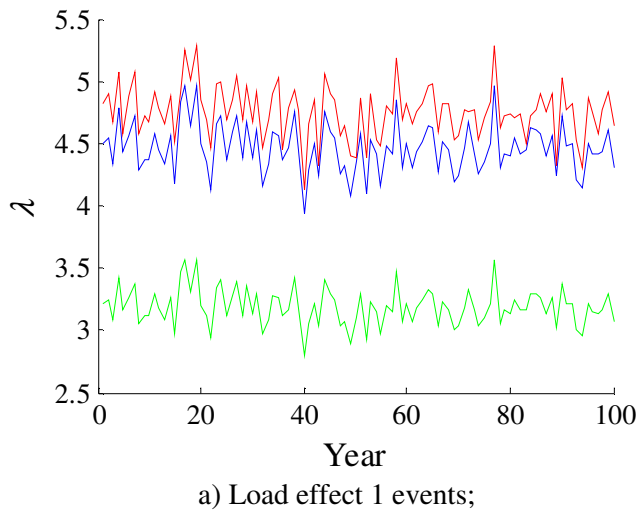
Figure A2.7: Two-span 60 bridge load factors.

Figure A2.8: Two-span 60 bridge limit state extrapolation.

Table A2.1: Two-span bridges lifetime load factors

Bridge Length (m)	Load Effect 1 Traffic			Load Effect 2 Traffic		
	λ_{1LT}	λ_{2LT}	λ_{3LT}	λ_{1LT}	λ_{2LT}	λ_{3LT}
30	2.614	3.600	3.859	3.235	4.763	4.898
40	2.482	3.449	3.700	2.002	3.016	3.948
50	2.735	3.819	4.031	2.144	3.278	3.915
60	2.801	3.934	4.112	2.219	3.439	4.242

Figure A2.9: Two-span structures life-time load factors for load effect 1 events.
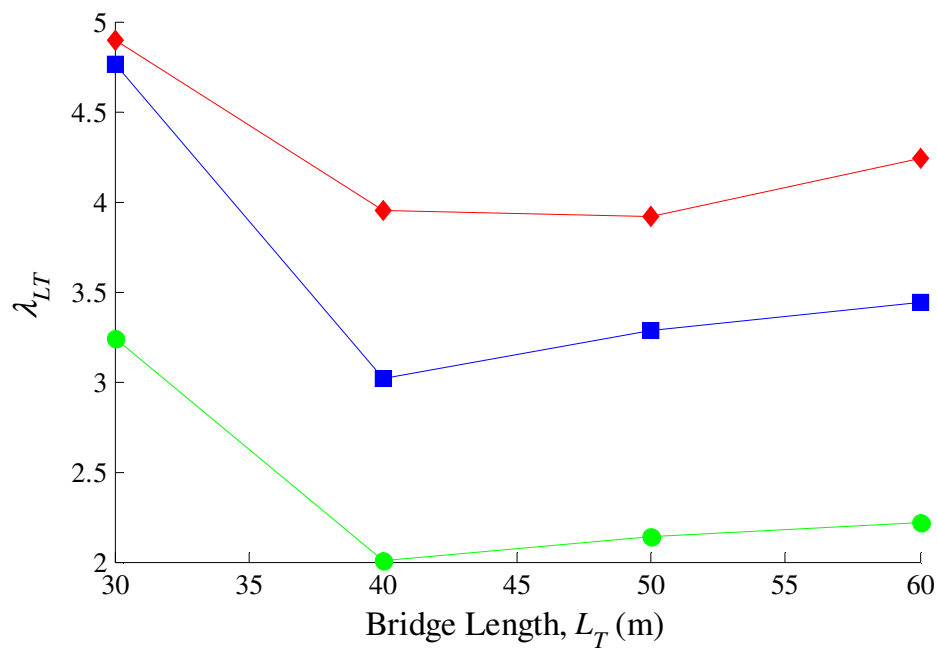
Figure A2.10: Two-span structures life-time load factors for load effect 2 events.

## A2.2 Three-Span Structures
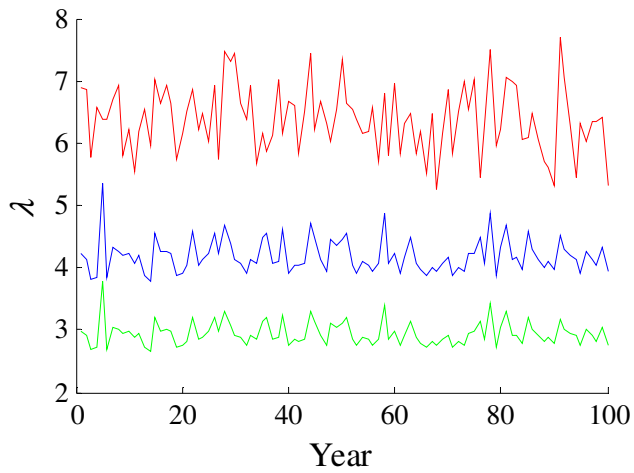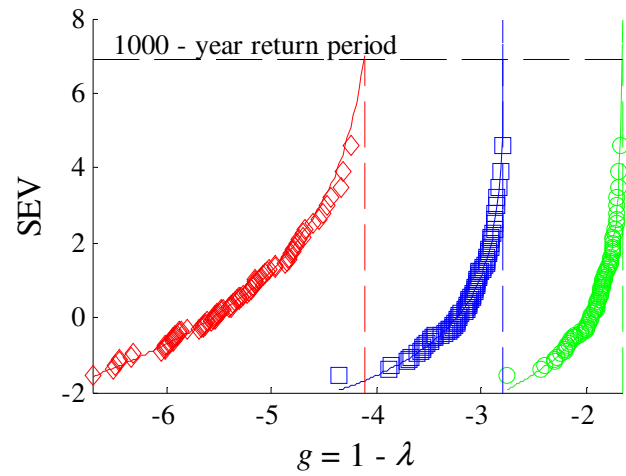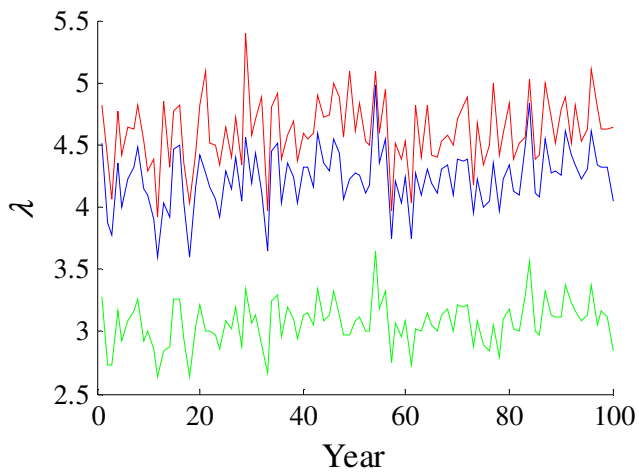
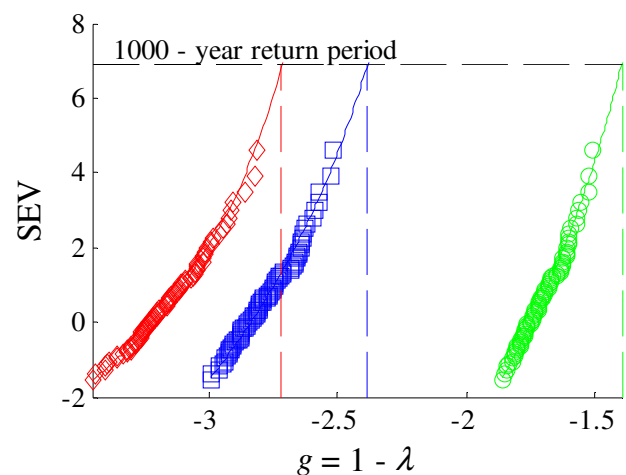a) Load effect 1 events;

a) Load effect 1 events;

b) Load effect 2 events;
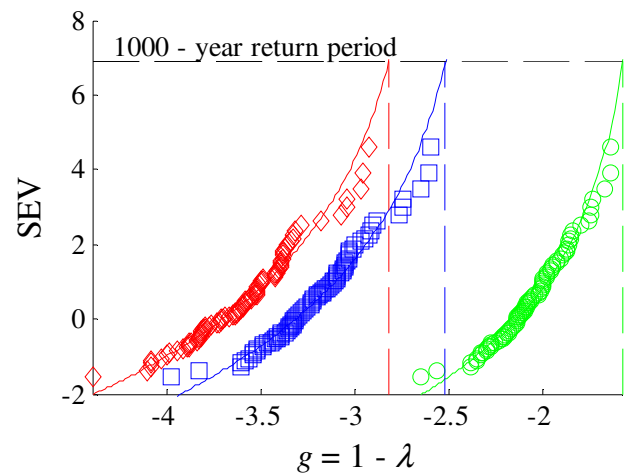
b) Load effect 2 events;
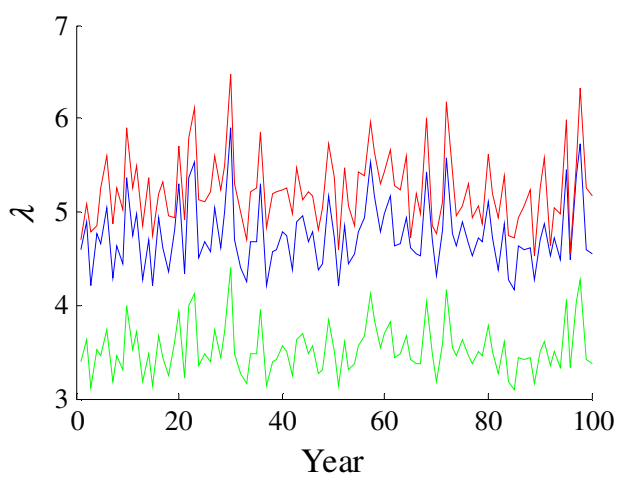
c) Load effect 3 events;
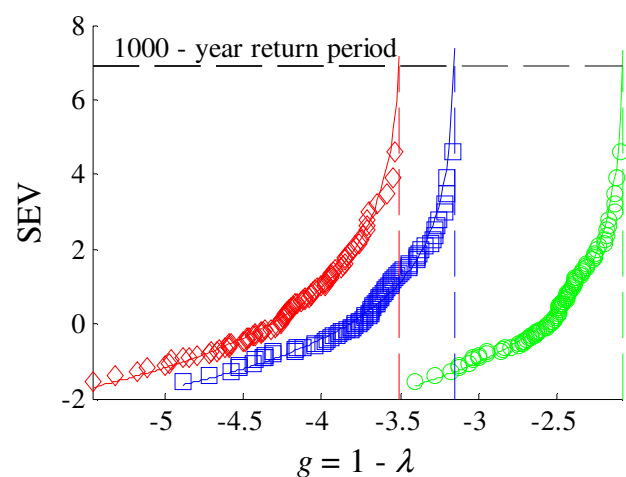
c) Load effect 3 events;

Figure A2.11: Three-span 30 bridge load factors.

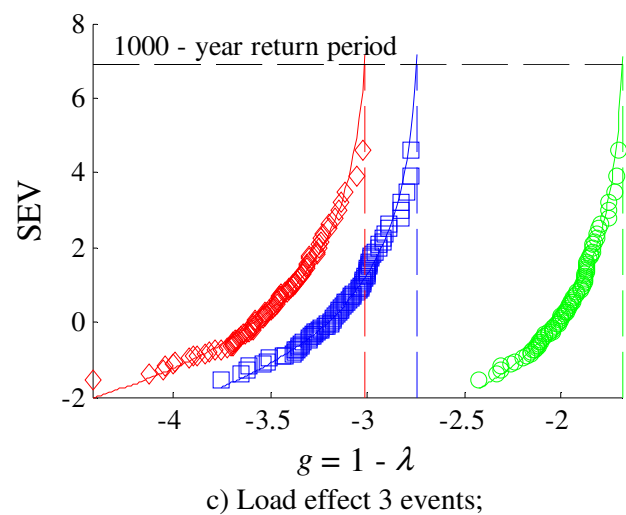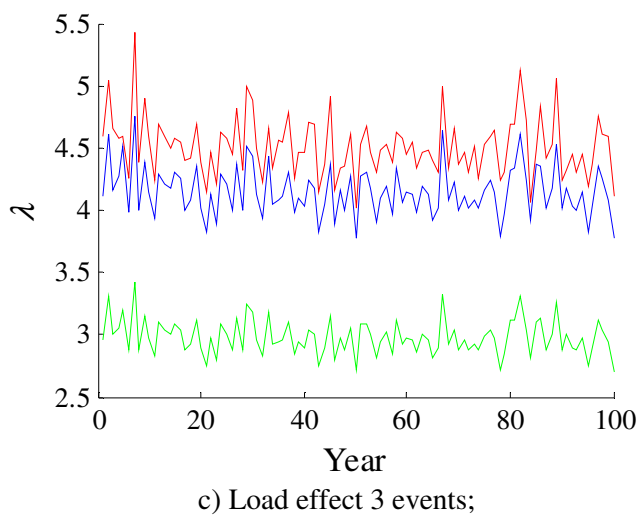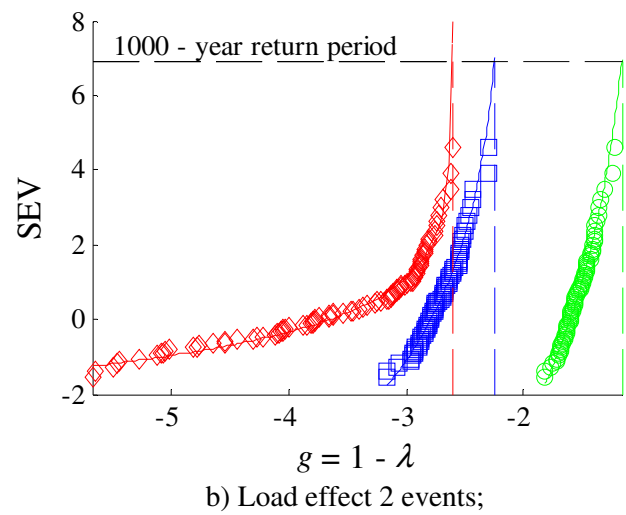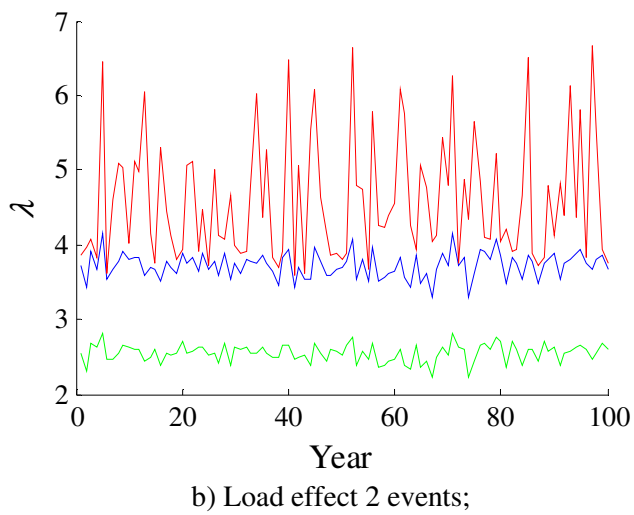Figure A2.12: Three-span 30 bridge limit state extrapolation.

a) Load effect 1 events;

b) Load effect 2 events;

c) Load effect 3 events;
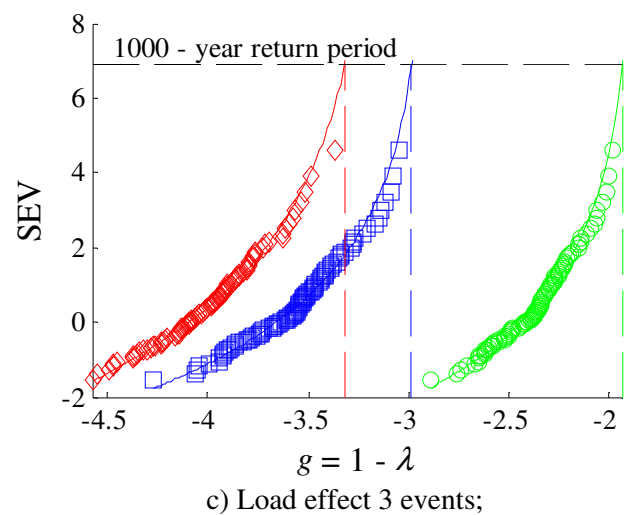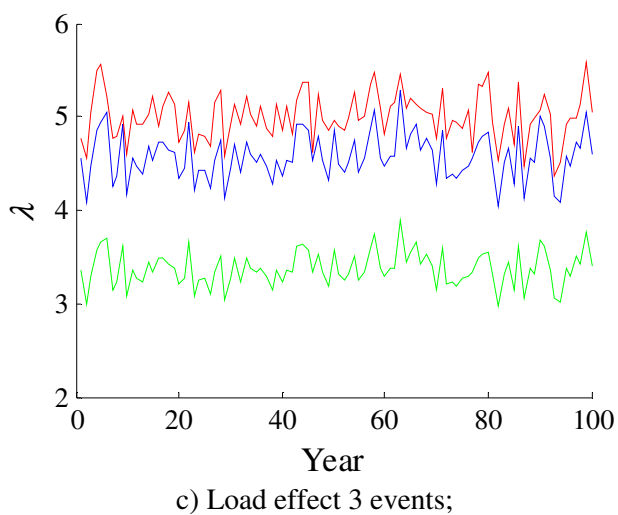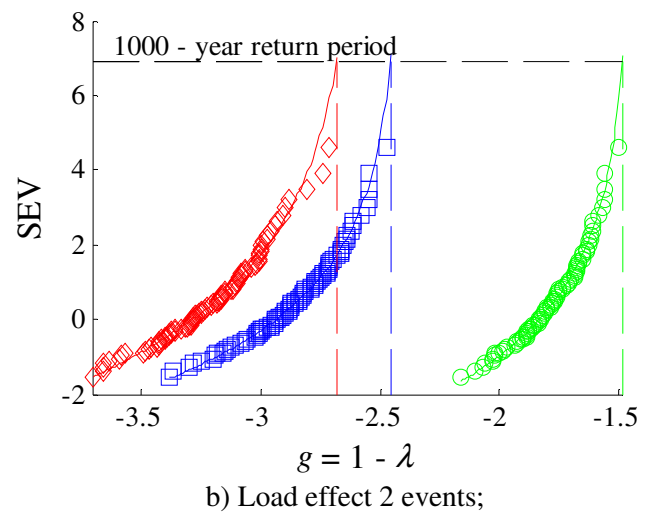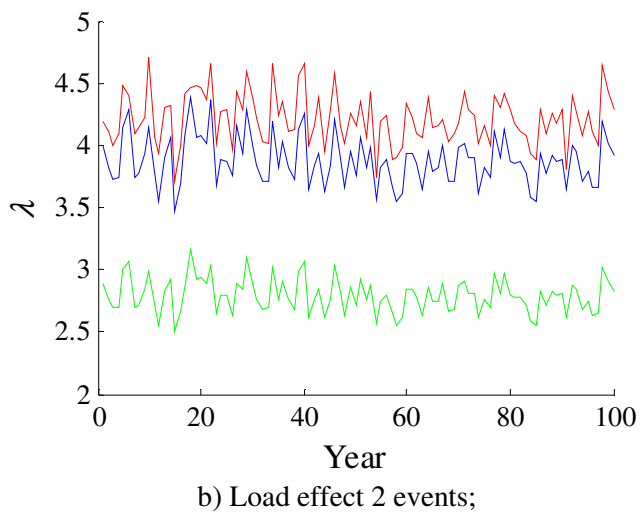
Figure A2.13: Three-span 40 bridge load factors.

a) Load effect 1 events;

b) Load effect 2 events;

c) Load effect 3 events;

Figure A2.14: Three-span 40 bridge limit state extrapolation.

a) Load effect 1 events;

a) Load effect 1 events;

b) Load effect 2 events;
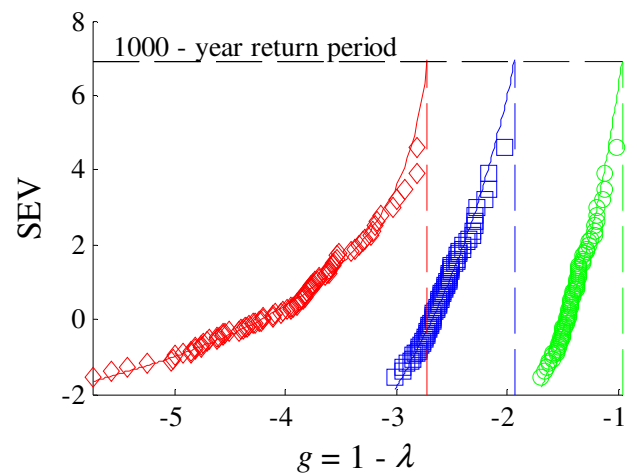
b) Load effect 2 events;
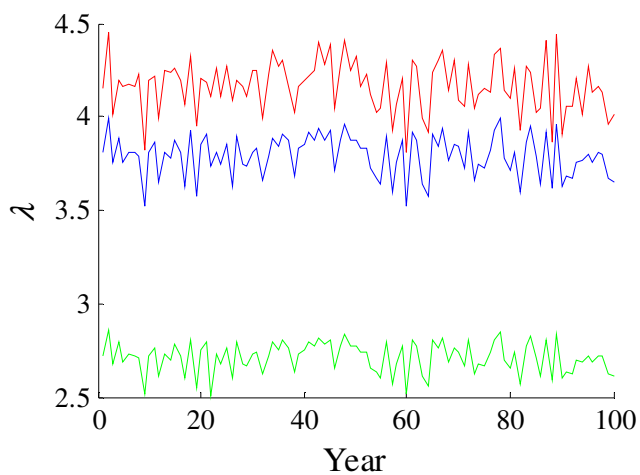
c) Load effect 3 events;

c) Load effect 3 events;

Figure A2.15: Three-span 50 bridge load factors.

Figure A2.16: Three-span 50 bridge limit state extrapolation.

a) Load effect 1 events;

a) Load effect 1 events;

b) Load effect 2 events;

b) Load effect 2 events;

c) Load effect 3 events;

c) Load effect 3 events;
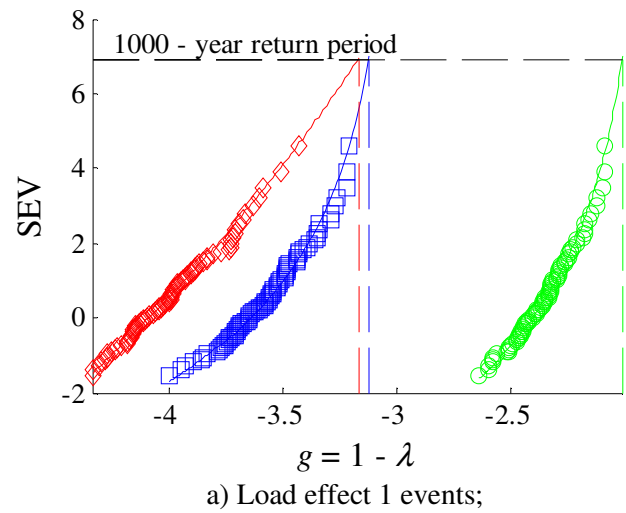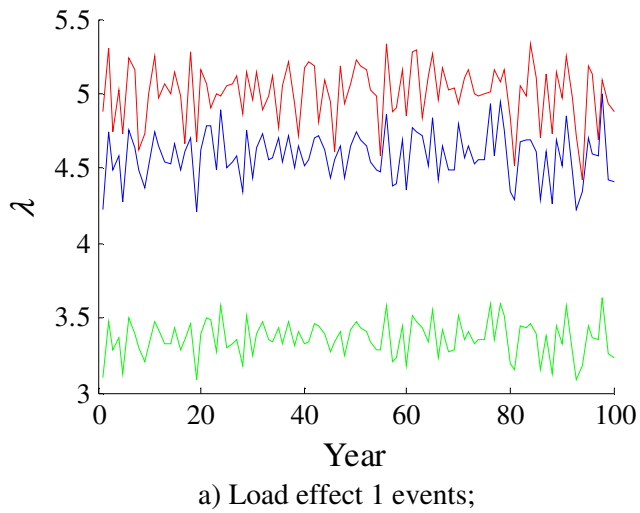
Figure A2.17: Three-span 60 bridge load factors.

Figure A2.18: Three-span 60 bridge limit state extrapolation.

Table A2.2: Three-span bridges lifetime load factors.

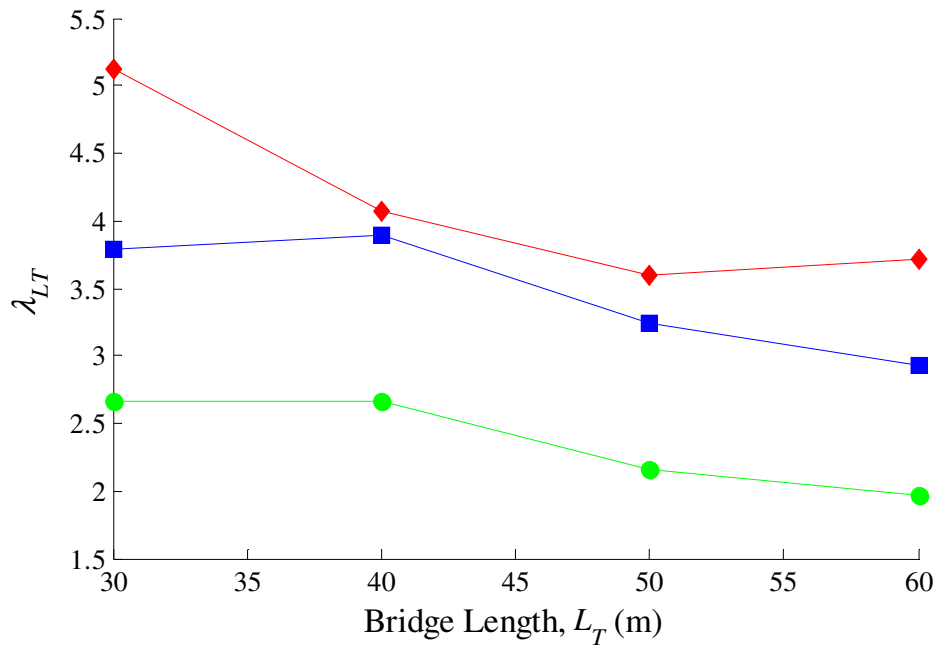| Bridge Length (m)	Load Effect 1 Traffic			Load Effect 2 Traffic			Load Effect 3 Traffic		
	λ_{1LT}	λ_{2LT}	λ_{3LT}	λ_{1LT}	λ_{2LT}	λ_{3LT}	λ_{1LT}	λ_{2LT}	λ_{3LT}
30	2.669	3.795	5.120	2.575	3.515	3.817	3.082	4.155	4.508
40	2.664	3.897	4.245	2.490	3.458	3.681	2.933	3.982	4.317
50	2.157	3.245	3.600	2.685	3.745	4.015	3.113	4.239	4.723
60	1.966	2.932	3.717	2.394	3.383	3.717	3.017	4.128	4.172

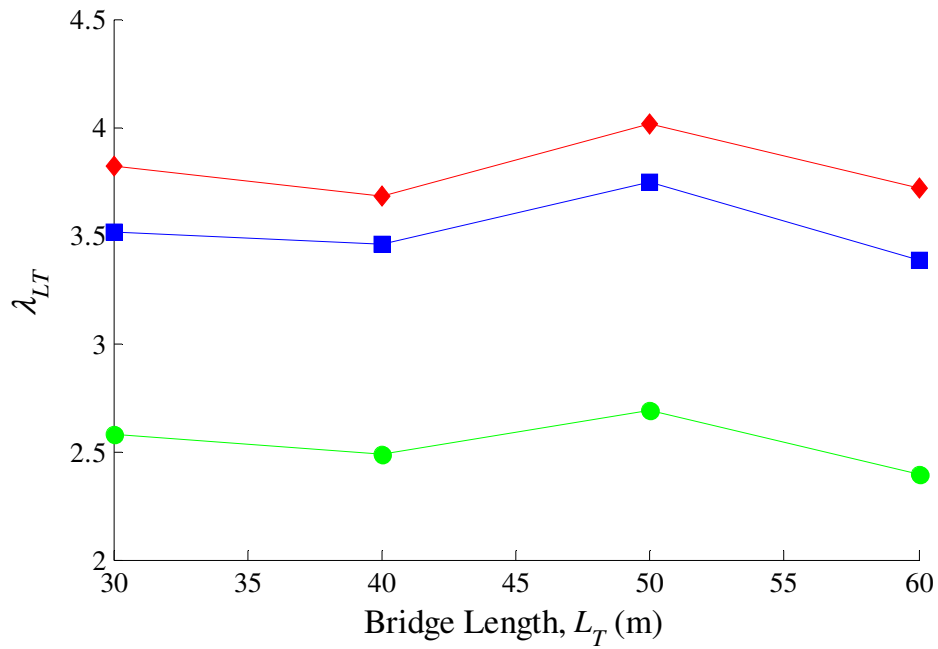Figure A2.19: Three-span life-time load factors for load effect 1 events.

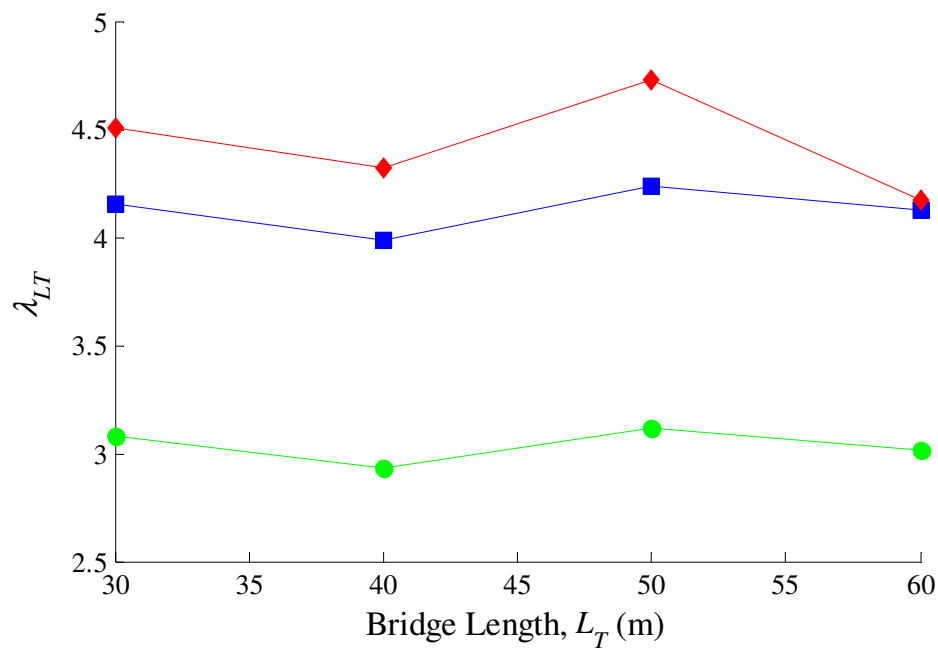Figure A2.20: Three-span life-time load factors for load effect 2 events.

Figure A2.21: Three-span life-time load factors for load effect 3 events.

Appendix 3

Lifetime Load Factor Comparison

Appendix 3   Lifetime Load Factor Comparison

A3.1 Introduction

In this Appendix a further study into the lifetime load factors (see Section 8.5) for the 2span-40 bridge (Figure A3.1) is performed.
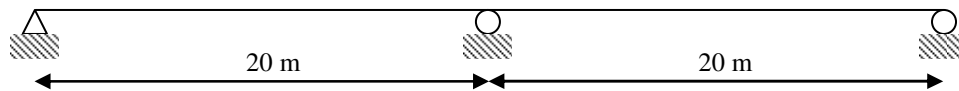

Figure A3.1: Two-span 40 bridge

The lifetime load factors for a range of plastic moment capacities are found (see Section 8.5). The plastic moment capacities examined include:

1. Minimum Eurocode flexure capacity (as before) (EC1.2, 2005).

2. Minimum Eurocode flexure capacity excluding safety factors.

3. Minimum AASHTO flexure capacity (AASHTO-LRFD, 2007).

4. Minimum AASHTO flexure capacity excluding the safety factors.

5. Actual plastic moment capacity of the steel composite section (see Figure 6.2)

The structure is subjected to 100 annual maximum traffic loading events (see Section 8.2). These loading events are identified as causing maximum sagging moment at mid-span of the first interior span. This was deemed a critical load effect in Section 8.7.

Load factors are found for each annual maximum event for three definitions of failure which are 1) Exceedance of initial yield capacity (λ_1), 2) formation of the plastic hinge (λ_2) and 3) formation of a collapse mechanism (λ_3). These are then combined using the methodology given in Section 8.5 to determine the lifetime load factors (λ_{LT}).

A3.2 Flexure Resistance Design

The plastic moment capacities (1-4) are calculated following the work of Nowak et al (2001):

$$M_p = \left[\alpha_{D_1}(D_1) + \alpha_{D_2}(D_2) + \alpha_{D_3}(D_3) + \alpha_L(L)(LDF) \right] / \phi \tag{A3.1}$$

where D_1 is the dead load moment due to the beam, D_2 is the dead load moment due to the slab, D_3 is the dead load moment due to the road surfacing given in Table A3.1, L is the live load moment on the structure and LDF is the maximum total LDF of the critical beam in the bridge. The safety factors $\alpha_{D_{1-3}}$ and α_L are given in Table A3.2.

Table A3.1: Dead load calculation

Type	Density (kN/m^3)	Thickness (m)	Width (m)	Area (m^2)	Load (kN/m)	Moment (kNm)
D_1	77*	---	---	0.0296	2.28	114
D_2	25*	0.25	2.65	0.6625	16.56	828
D_3	22*	0.13	2.65	0.3313	7.29	364
		Total			26.13	1306

* Values taken from Iles (2010)

Table A3.2: Safety factors

Variable	Eurocode	AASHTO
D_1	1.35	1.25
D_2	1.35	1.25
D_3	1.35	1.5
L	1.5	1.75
ϕ	0.88	1

The live load model as specified in the Eurocode and AASHTO design codes are used to calculate the live load subjected to each girder. These live load models are given in Figure A3.2. The live loads corresponding to each load model is given in Table A3.3
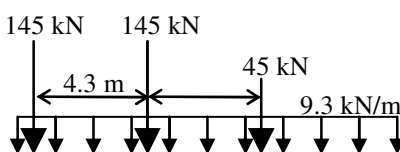
Table A3.3: Live load calculation.

	Eurocode	AASHTO
Lane Live Load	2494.9 (kNm)	2284.2 (kNm)
Lane Distribution Factor*	0.535	0.535
Girder Live Load	1334.7 (kNm)	1221.97 (kNm)

*see Section 6.3
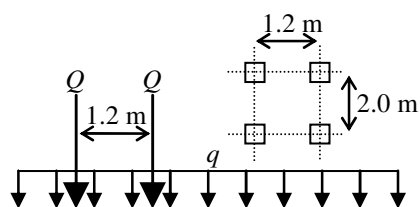
Lane 1: Q = 300 kN q = 9.0 kN/m^3

Lane 2: Q = 200 kN q = 2.5 kN/m^3

Lane 3: Q = 100 kN q = 2.5 kN/m^3

(a) Eurocode LM1 (EC1.2, 2005);

(b) AASHTO live load model (AASHTO-LRFD, 2007);

Figure A3.2: Live load models

The plastic moment capacities examined are given in Table A3.4.

Table A3.4: Flexure resistance capacities.

Resistance	M_P
Eurocode	4279.33 kNm
Eurocode (excluding safety)	2641.19 kNm
AASHTO	3862.68 kNm
AASHTO (excluding safety factors)	2528.47 kNm
Actual Moment Capacity (Iles, 2001)	5211.29 kNm

A3.3   Lifetime Load Factor Comparison Results

The load factors for each loading events for each definition of failure are given in Figure A3.3-A3.5. The actual moment capacity of the structure displays the highest level of conservatism, followed by the Eurocode, then the AASHTO. A significant number of failures were found when examining the load factors required for exceedance of initial yield ($\lambda_1 < 1$) when the AASHTO minimum moment capacity excluding safety factors is used.
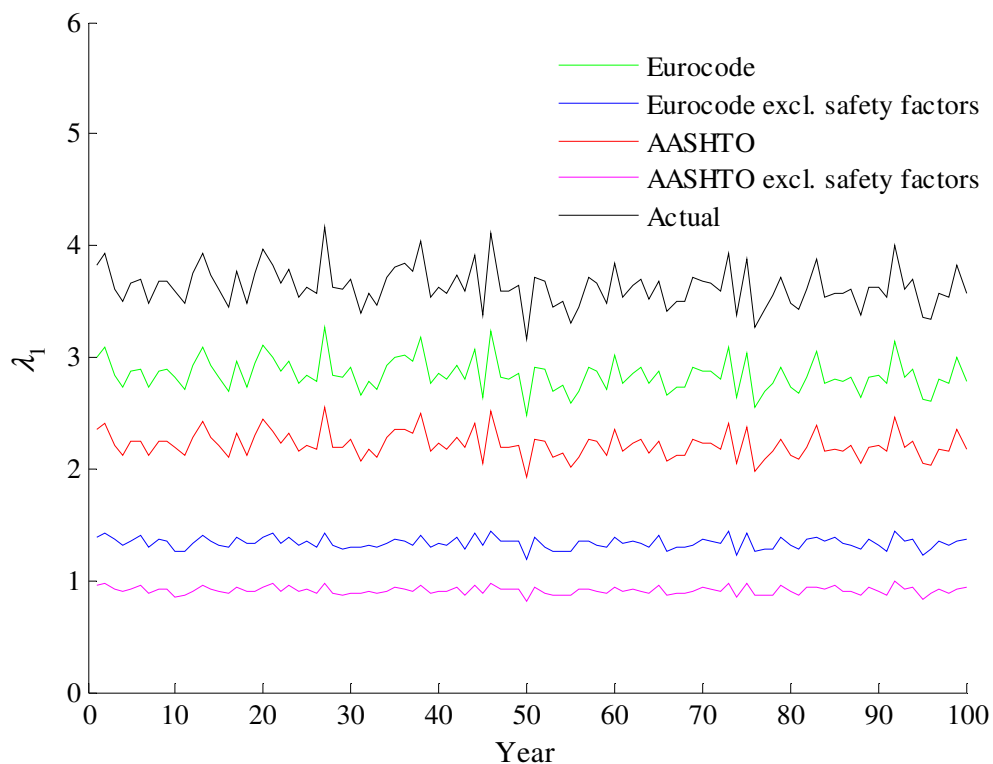

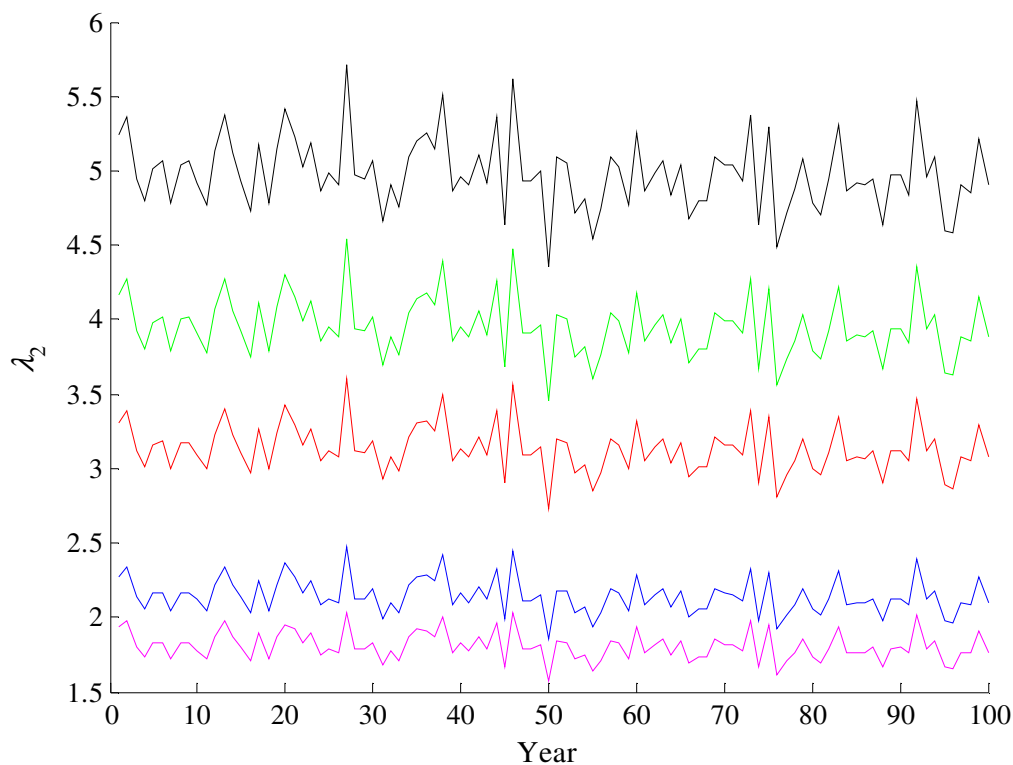Figure A3.3: Load factors causing initial yield.

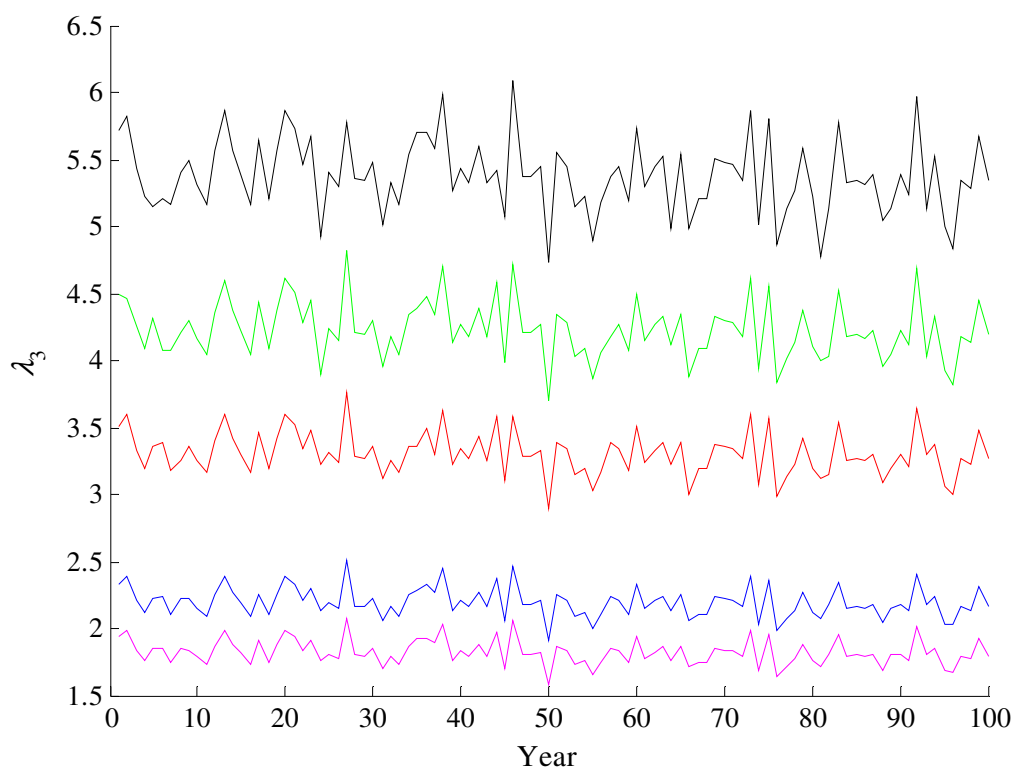Figure A3.4: Load factors causing plastic hinge formation.

Figure A3.5: Load factors causing collapse mechanism formation.

The lifetime load factors corresponding to a 1000 year return period are given in Table A3.4

The results shown highlight the conservatism associated with the Eurocode. Even when the

safety factors are excluded from the minimum flexure capacity as defined by the Eurocode, the structure will not reach the initial yield capacity. However if the moment capacities are removed from the AASHTO resistance calculation, the initial yield capacity of the structure will be exceeded in its lifetime ($\lambda_{1LT} < 1$). All plastic moment capacities are safe against plastic hinge and collapse mechanism failures for the traffic examined.

Table A3.4: Lifetime load factors.

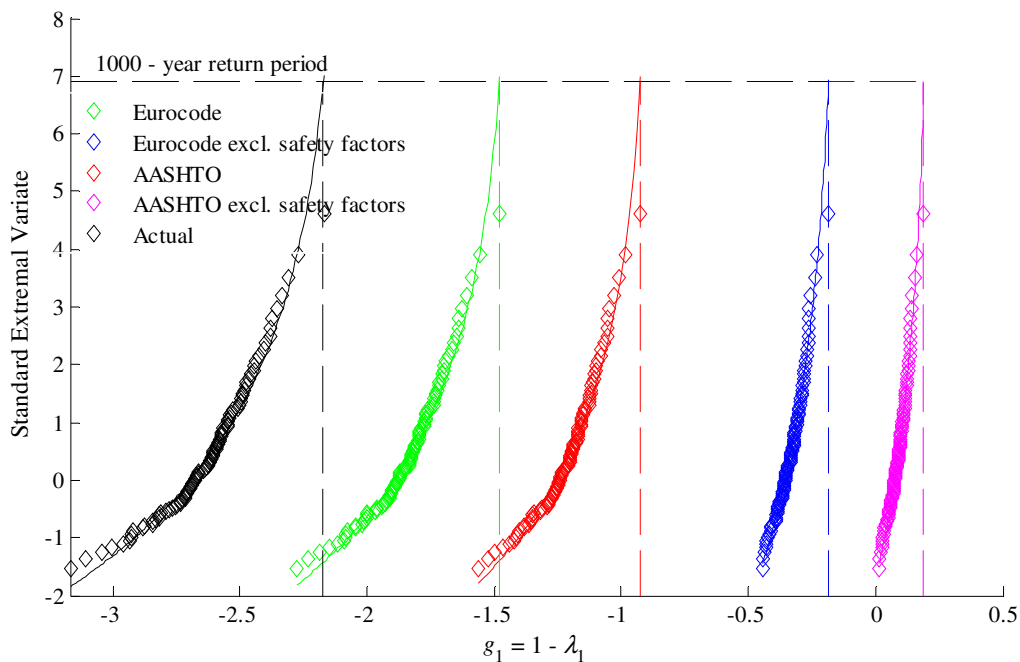| Resistance	λ_{1LT}	λ_{2LT}	λ_{3LT}
Eurocode	2.482	3.449	3.700
Eurocode (excluding safety factors)	1.185	1.861	1.916
AASHTO	1.926	2.730	2.888
AASHTO (excluding safety factors)	0.809	1.567	1.588
Actual Moment Capacity	3.172	4.357	4.675

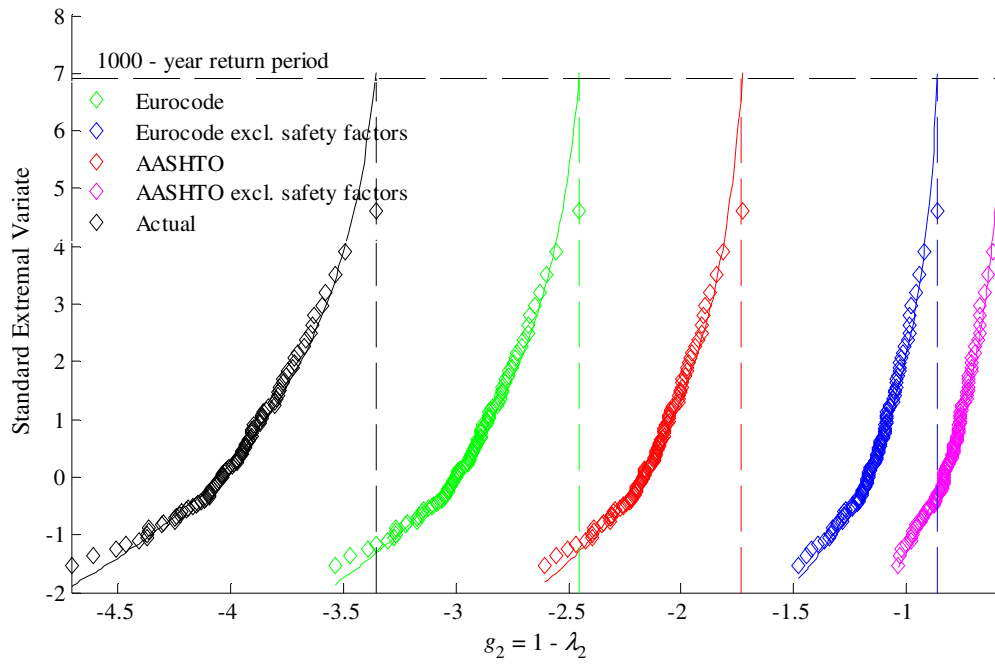Figure A3.6: Initial yield lifetime load factor extrapolation results.

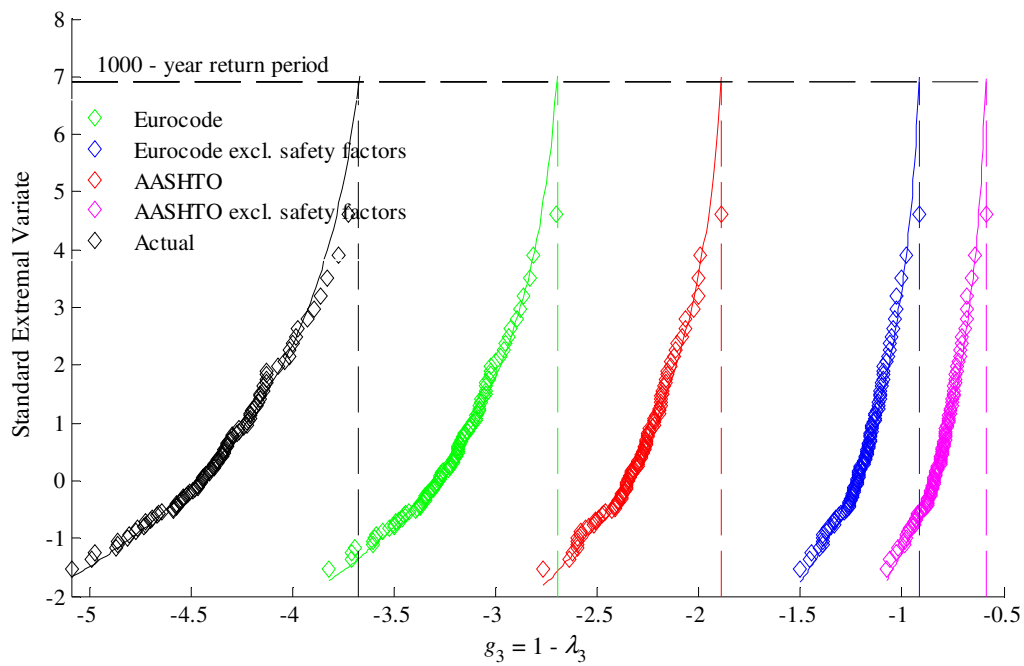Figure A3.7: Plastic hinge lifetime load factor extrapolation results.

Figure A3.8: Collapse lifetime load factor extrapolation results.

Appendix 4

Experimental Design Comparison

Appendix 4   Experimental Design Study

A4.1   Introduction

The performance of the EDs outlined in Section 5.3 are examined. A series of loading events are examined on the two-span bridge shown in Figure A4.1.
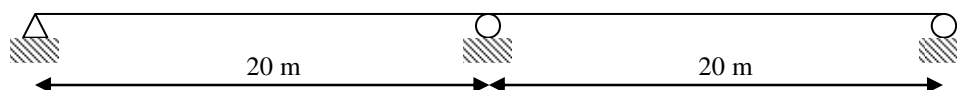

Figure A4.1: Two-span 40 bridge.

The reliability index is found using the RSM methodology described in Section 5.8 for each ED. These results are then compared to those found using MCS (see Section 3.2.1). The limit state function is the formation of a collapse mechanism.

The loading events are randomly generated (see Section 8.2). The random properties for each loading event are the plastic moment capacity (M_P) of the structure and the GVW of each truck. The coefficient of variation of the plastic moment capacity was taken as 0.1 (Czarnecki et al, 2007) and the coefficient of variation of the GVW for each truck was taken as 0.18 (Nowak et al, 2001). The structure is only subjected to live load. Importantly, the plastic moment capacity of each structure is chosen so as reliability index of approximately zero is found. This is to ensure a high probability of failure is found meaning a reduced number of Monte Carlo simulations are required.

The accuracy of each ED is found by normalizing the reliability indices found using RSM with those found using MCS:

$$accuracy = \frac{\beta}{\beta_{MC}} \tag{A4.1}$$

The closer this ratio is to unity the more accurate the ED design is. The number of NFEAs required for each ED to converge is also assessed.

For each loading event a figure showing the position of each truck is given. A table presenting the random variable inputs and a table giving the performance of each ED are also given.
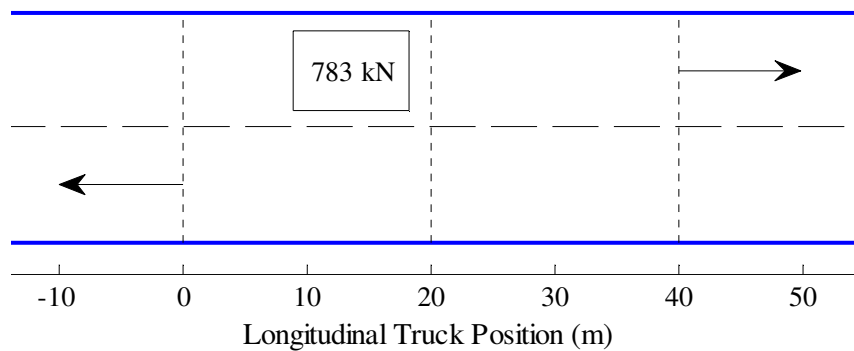
A4.2   One Truck Loading Event

Figure A4.2: One truck event truck position.

Table A4.1: One truck event random variables.

Variable	μ	CoV	Distribution
M_P (kNm)	726	0.1	Normal
GVW (kN)	783	0.18	Normal

Table A4.2: One truck event RSM results.

Experimental Design	No. Iterations (h=3)	No. Iterations (h=2)	No. Iterations (h=1)	Total Iterations	No. NFEAs	β	β / β_{MC}
CCC	1	1	1	3	45	0.086	1.139
CCI	1	1	1	3	45	0.085	1.123
CCF	1		1	3	45	0.083	1.093
BB	Not applicable for problems with two random variables						
Monte Carlo					10000	0.076	1

A4.3 Two Truck Loading Event
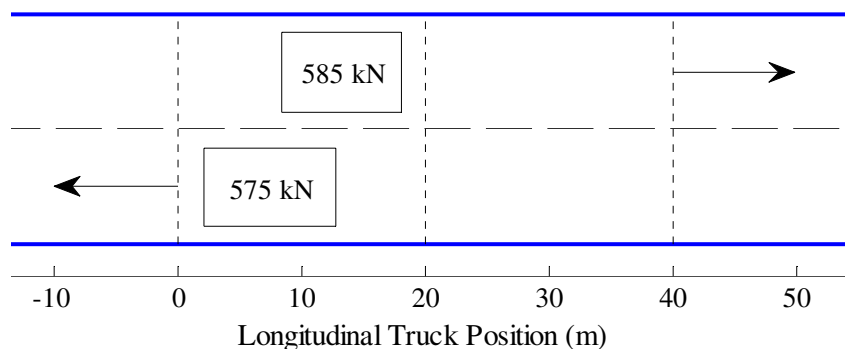
Figure A4.3: Two truck event.

Table A4.3: Two truck event random variables.

Variable	μ	CoV	Distribution
M_P (kNm)	834	0.1	Normal
GVW (kN)	585	0.18	Normal
GVW (kN)	575	0.18	Normal

Table A4.4: Two truck event RSM results.

Experimental Design	No. Iterations (h=3)	No. Iterations (h=2)	No. Iterations (h=1)	Total Iterations	No. NFEAs	β	β / β_{MC}
CCC	3	1	1	5	110	-0.207	0.989
CCI	2	0	1	3	66	-0.208	0.994
CCF			Did not converge after 10 iterations.				
BB	1	0	1	2	34	-0.210	1.004
Monte Carlo					10000	-0.2091	1

A4.4 Three Truck Loading Event
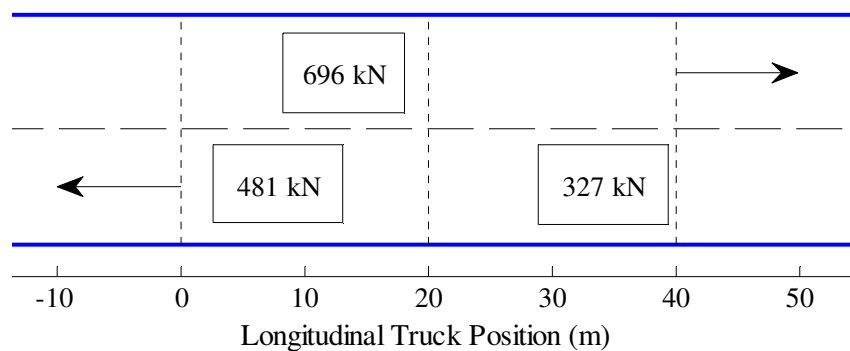
Figure A4.4: Three truck event.

Table A4.5: Three truck event random variables.

Variable	μ	CoV	Distribution
M_P (kNm)	834	0.1	Normal
GVW (kN)	696	0.18	Normal
GVW (kN)	481	0.18	Normal
GVW (kN)	327	0.18	Normal

Table A4.6: Three truck event RSM results.

Experimental Design	No. Iterations (h=3)	No. Iterations (h=2)	No. Iterations (h=1)	Total Iterations	No. NFEAs	β	β / β_{MC}
CCC	1	2	1	4	132	-0.209	0.963
CCI	1	0	1	2	66	-0.208	0.958
CCF	Did not converge after 10 iterations.						
BB	1	0	1	2	58	-0.210	0.968
Monte Carlo					10000	-0.217	1

A4.5 Four Truck Loading Event
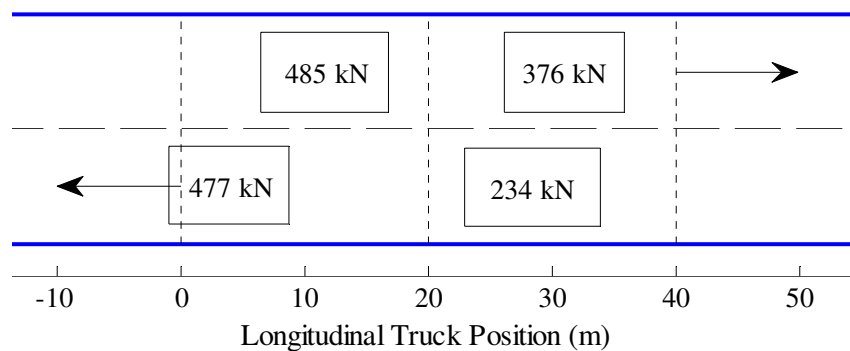
Figure A4.5: Four truck event.

Table A4.7: Four truck event random variables.

Variable	μ	CoV	Distribution
M_P (kNm)	645	0.1	Normal
GVW (kN)	477	0.18	Normal
GVW (kN)	485	0.18	Normal
GVW (kN)	376	0.18	Normal
GVW (kN)	234	0.18	Normal

Table A4.8: Four truck event RSM results.

Experimental Design	No. Iterations (h=3)	No. Iterations (h=2)	No. Iterations (h=1)	Total Iterations	No. NFEAs	β	β / β_{MC}
CCC	Did not converge after 10 iterations.						
CCI	3	0	1	4	136	0.381	1.041
CCF	Did not converge after 10 iterations.						
BB	1	0	1	2	96	0.378	1.033
Monte Carlo					10000	0.366	1

A4.6   Experimental Design Comparison Results

The accuracy of ED is compared using Equation (A4.1). The results are shown in Figure A4.6. The Box-Behnken design is not applicable for the one truck loading event as a minimum of three random variables are required. The CCF design did not converge after ten iterations for the two, three, and four truck loading events. When convergence is achieved all EDs produce a high level of accuracy. However, it is found that the BB design has the highest level of accuracy when compared to MCS for each of these loading events.
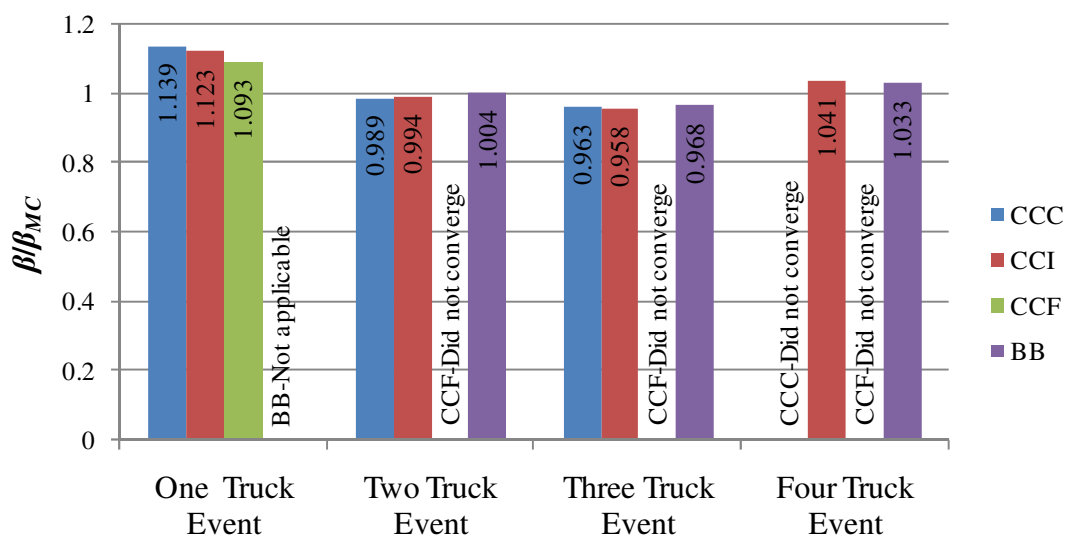

Figure A4.6: Experimental design accuracy comparison.

The number of NFEAs required for each experimental design to reach convergence is also important. These results for each ED are shown in Figure A4.7.
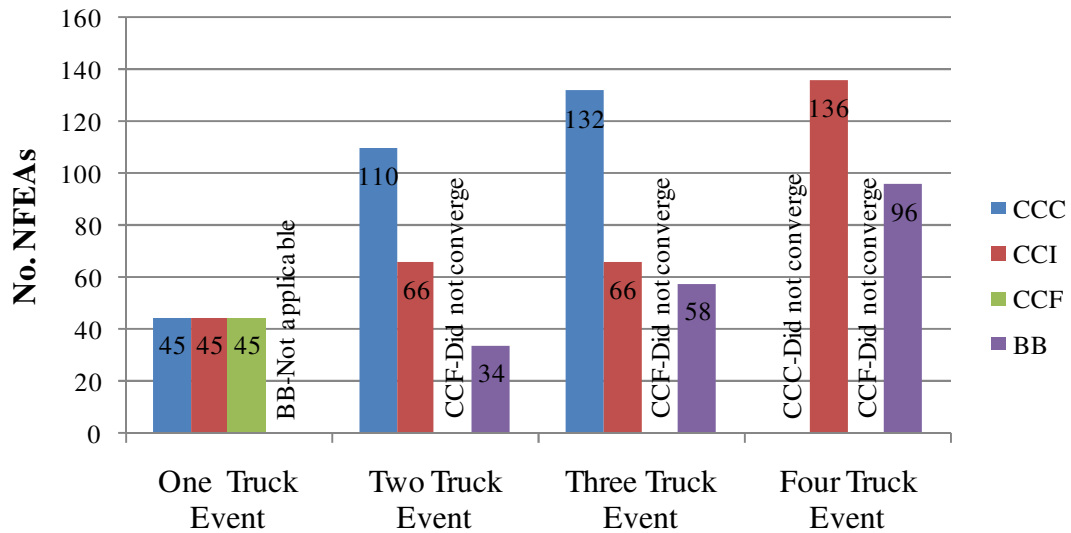
Figure A4.7: No. NFEAs required for convergence with each experiment design.

It is found that the BB design requires the least number of NFEAs to reach convergence for each of these loading events. From this study is recommended that the BB design be used in the reliability analysis procedure considering nonlinear material behaviour.

Appendix 5

Probabilistic Study

Appendix 5   Probabilistic Study

A5.1   Introduction

This appendix contains the graphs for the probabilistic study as part of Chapter 9 carried out on the representative set of steel composite structures. The reliability indices found using the probabilistic assessment methodology given in Section 5.5. The reliability indices for each annual maximum loading event are given along with the cumulative reliability indices.
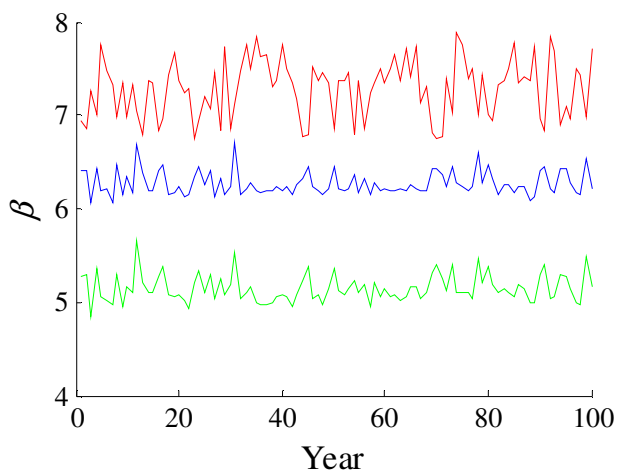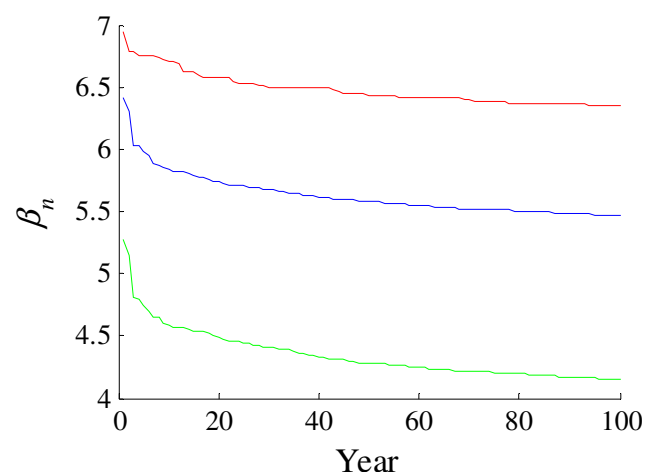
A5.2   Two-Span Structures
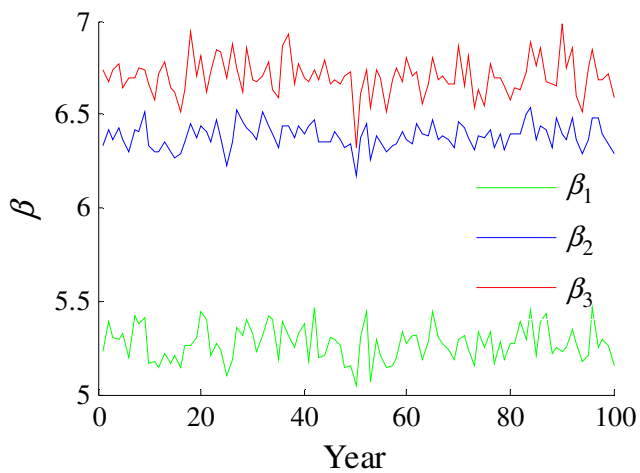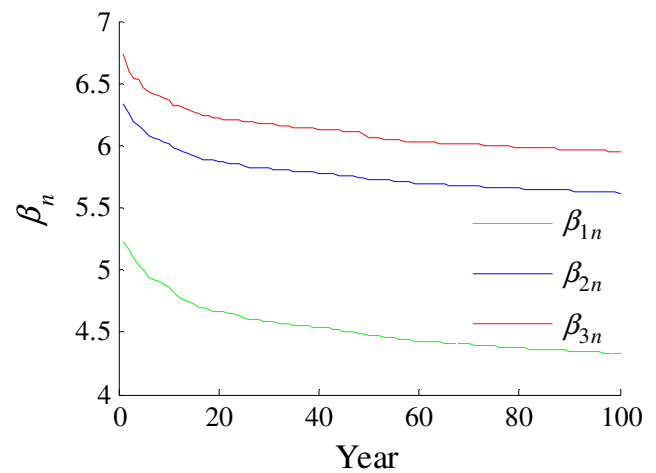
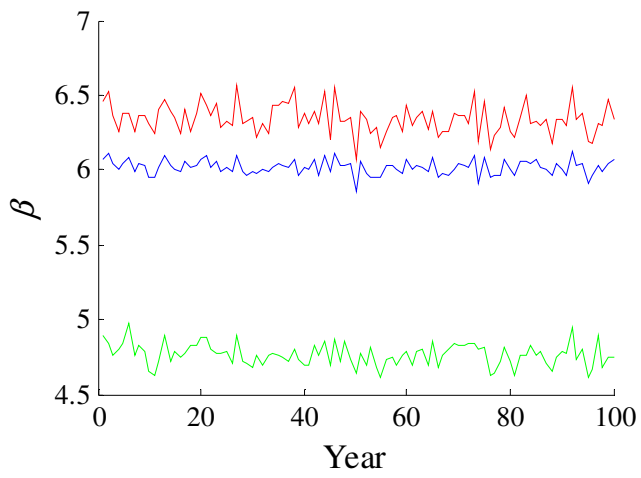a) Load effect 1 events;

b) Load effect 2 events;

Figure A5.1: Two-span 30 bridge reliability indices.

a) Load effect 1 events;

b) Load effect 2 events;

Figure A5.2: Two-span 30 bridge reliability indices cumulative reliability indices.

a) Load effect 1 events;

a) Load effect 1 events;

b) Load effect 2 events;

b) Load effect 2 events;

Figure A5.3: Two-span 40 bridge reliability indices.

Figure A5.4: Two-span 40 bridge reliability indices cumulative reliability indices.

a) Load effect 1 events;

b) Load effect 2 events;

Figure A5.5: Two-span 50 bridge reliability indices.

a) Load effect 1 events;

b) Load effect 2 events;

Figure A5.6: Two-span 50 bridge reliability indices cumulative reliability indices.

a) Load effect 1 events;

a) Load effect 1 events;
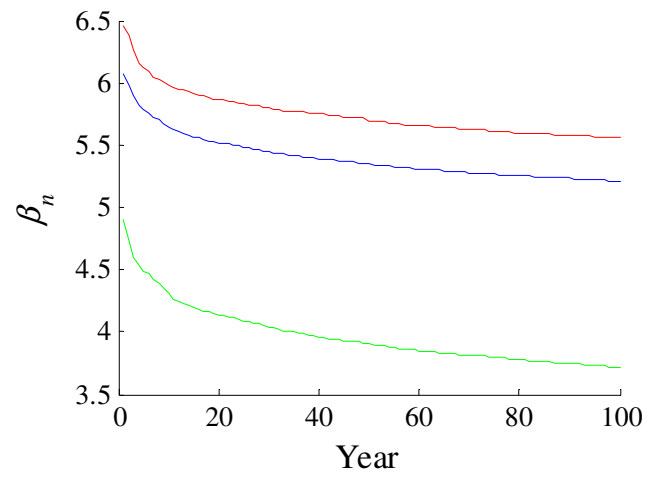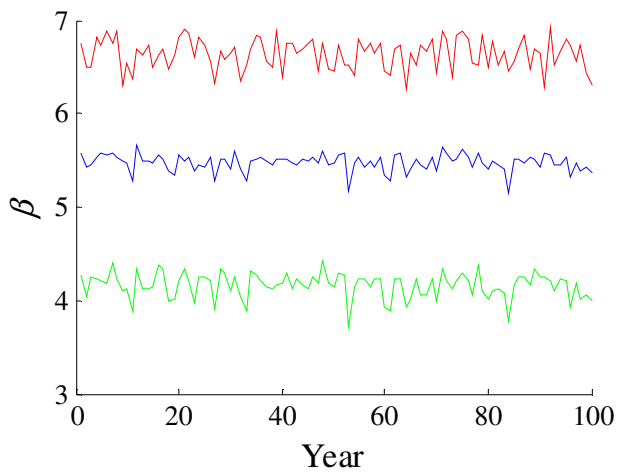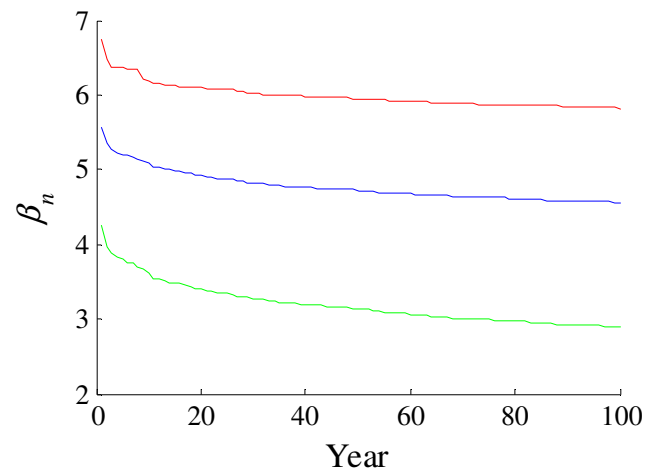

b) Load effect 2 events;

b) Load effect 2 events;

Figure A5.7: Two-span 60 bridge reliability indices.

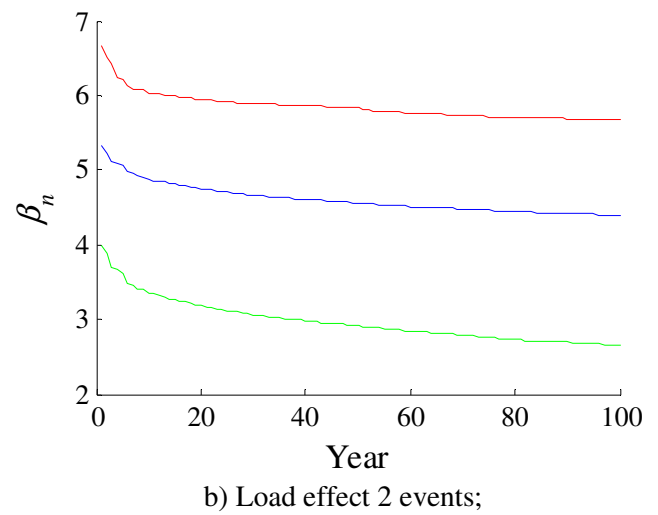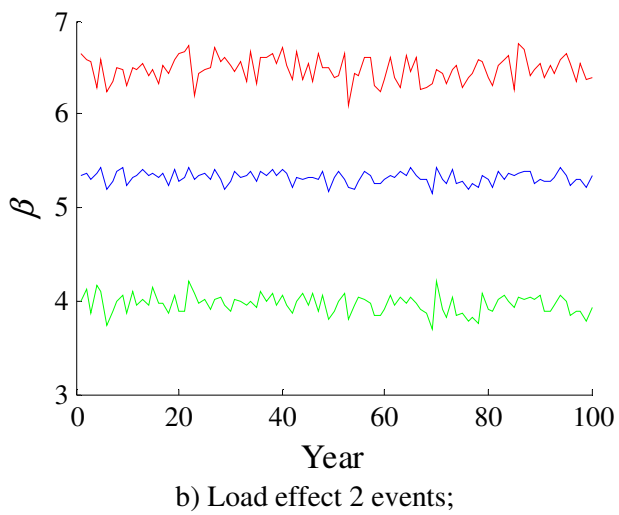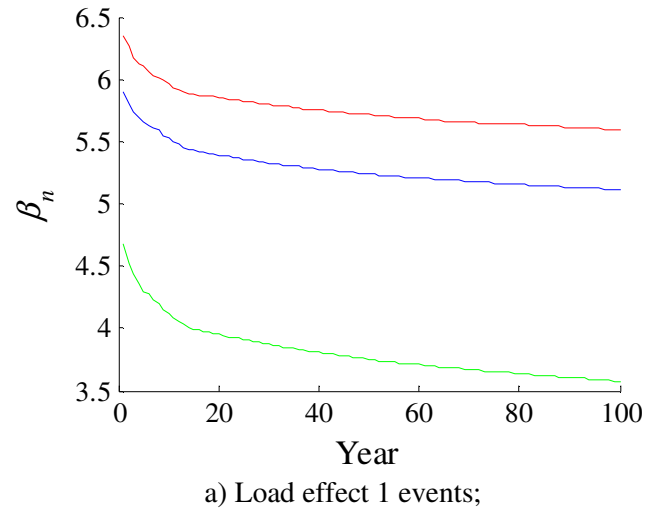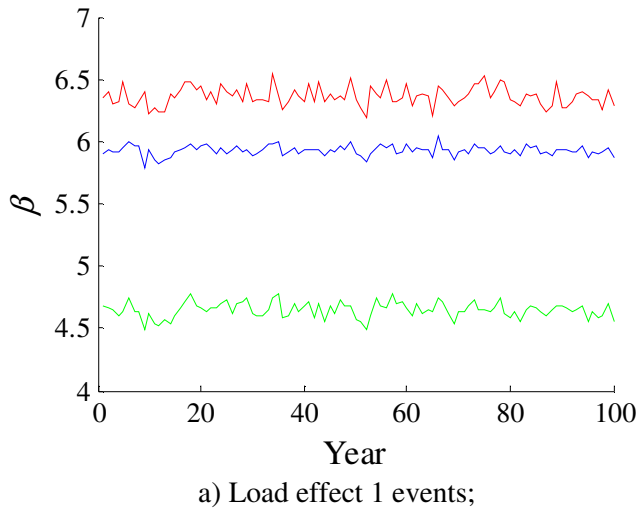Figure A5.8: Two-span 60 bridge reliability indices cumulative reliability indices.

Table A5.1: Two-span bridges; lifetime reliability indices considering nonlinear material behaviour (RSM).

Bridge Length (m)	Load Effect 1 Traffic			Load Effect 2 Traffic		
	β_{1LT}	β_{2LT}	β_{3LT}	β_{1LT}	β_{2LT}	β_{3LT}
30	4.328	5.620	5.953	4.148	5.467	6.350
40	3.718	5.213	5.556	2.894	4.562	5.820
50	3.576	5.112	5.593	2.654	4.395	5.675
60	3.460	5.024	5.583	2.596	4.357	5.656

Table A5.2: Two-span bridges; lifetime reliability indices (FORM).

Bridge Length (m)	Load Effect 1 Traffic		Load Effect 2 Traffic	
	β_{1LT}	β_{2LT}	β_{1LT}	β_{2LT}
30	4.481	5.755	5.002	6.166
40	3.911	5.304	4.105	5.457
50	3.834	5.242	3.924	5.313
60	3.755	5.178	3.799	5.208

Figure A5.9: Two-span structures life-time reliability indices for load effect 1 events.

Figure A5.10: Two-span structures life-time reliability indices for load effect 2 events.

A5.3   Three-Span Structures
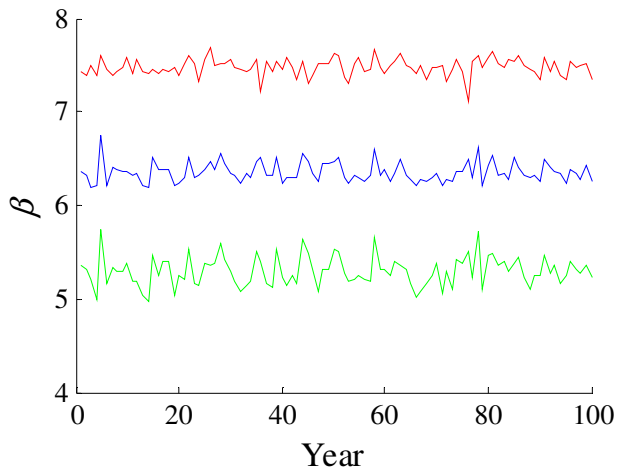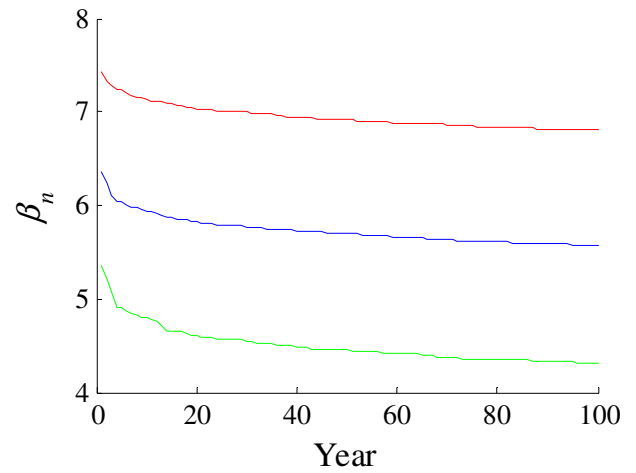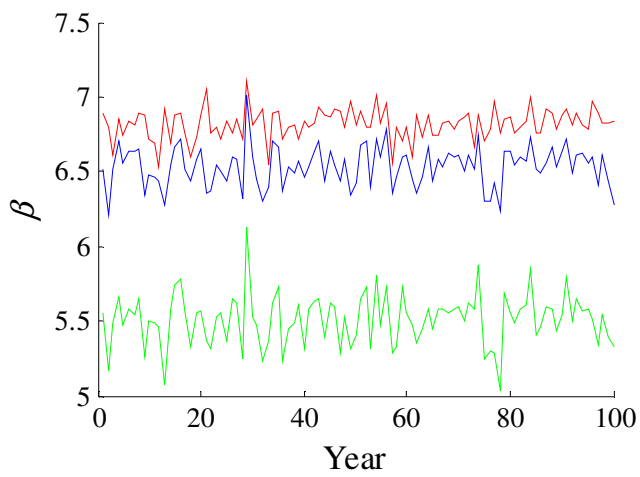
a) Load effect 1 events;

a) Load effect 1 events;

b) Load effect 2 events;
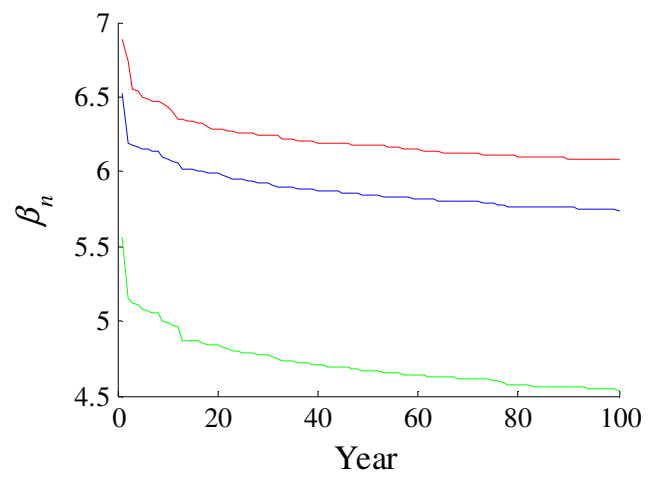
b) Load effect 2 events;
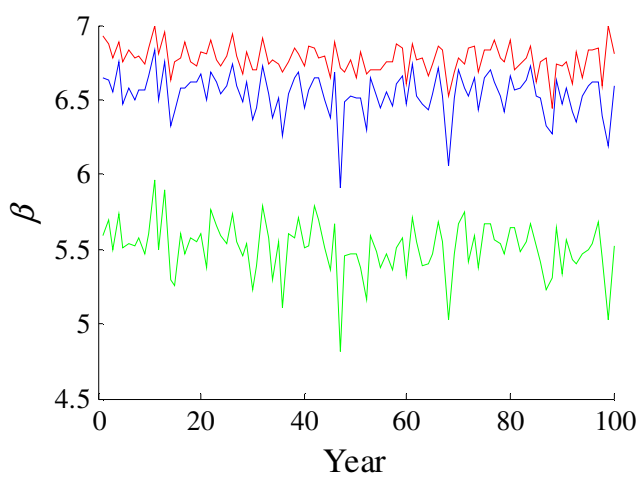
c) Load effect 3 events;
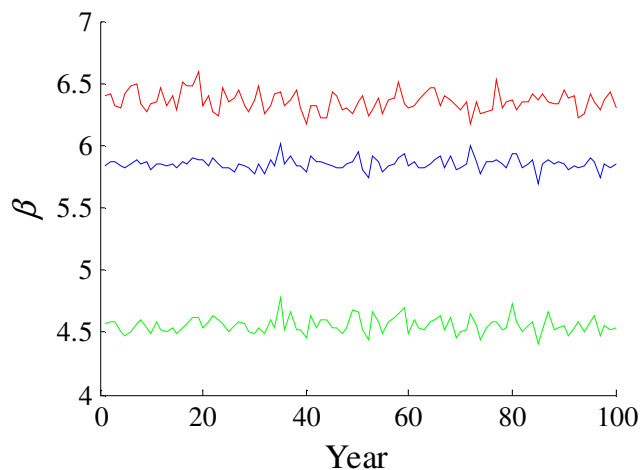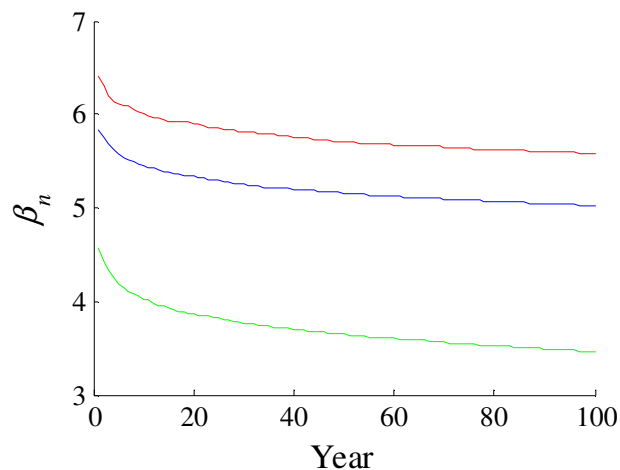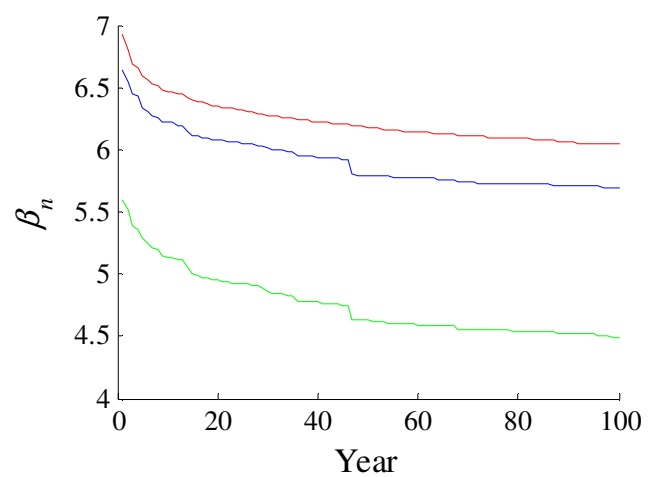

c) Load effect 3 events;

Figure A5.11: Three-span 30 bridge reliability indices.
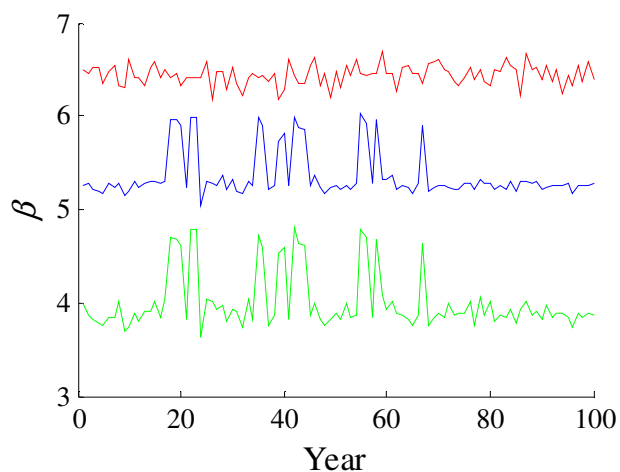
Figure A5.12: Three-span 30 bridge reliability indices cumulative reliability indices.

a) Load effect 1 events;

b) Load effect 2 events;

c) Load effect 3 events;
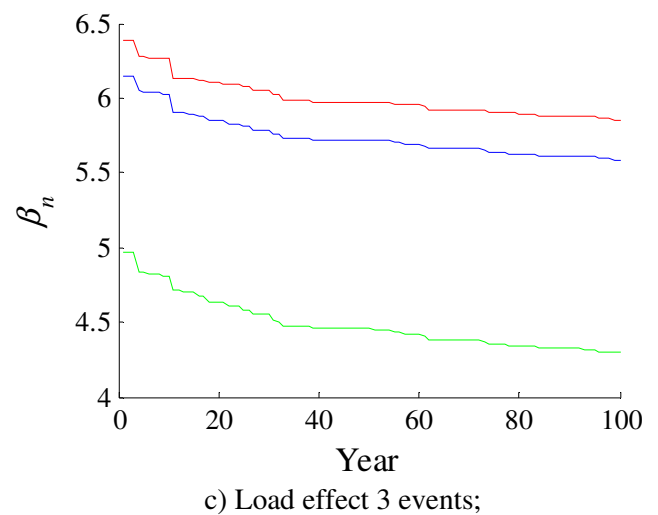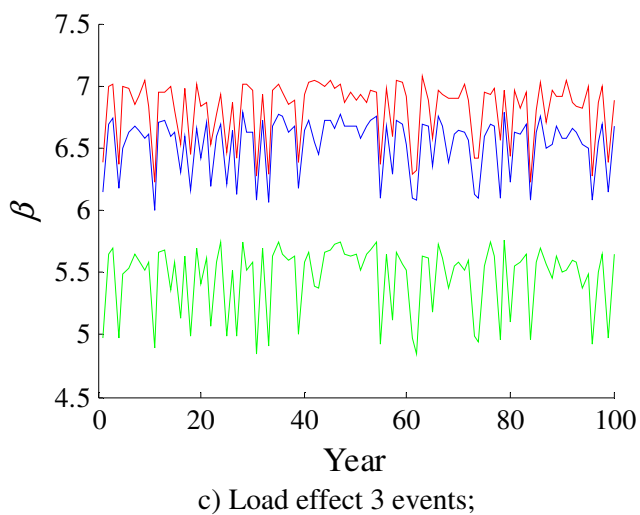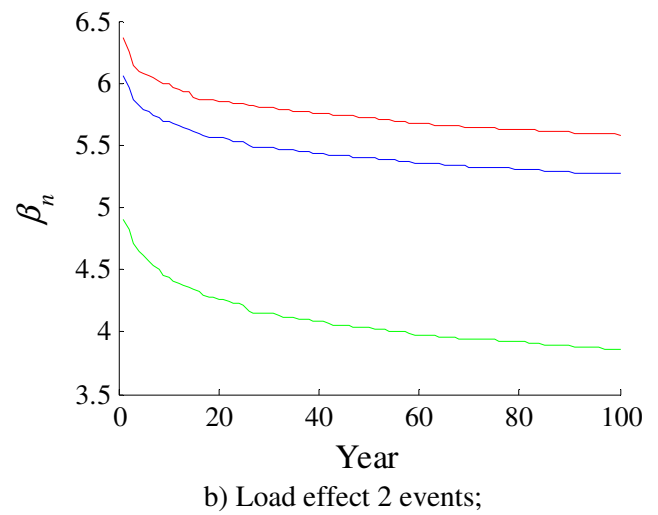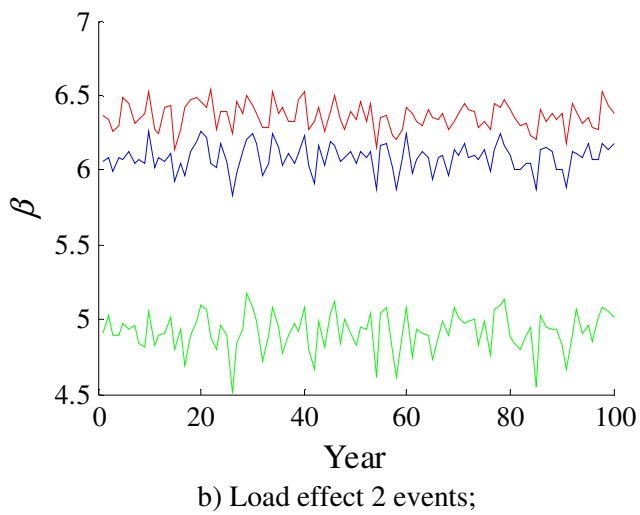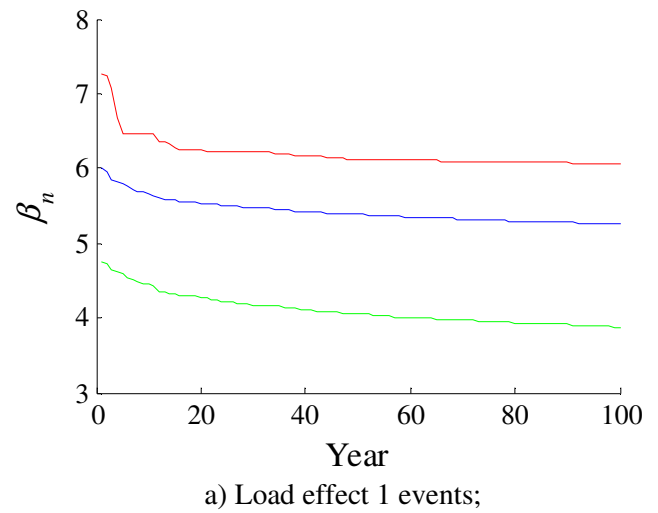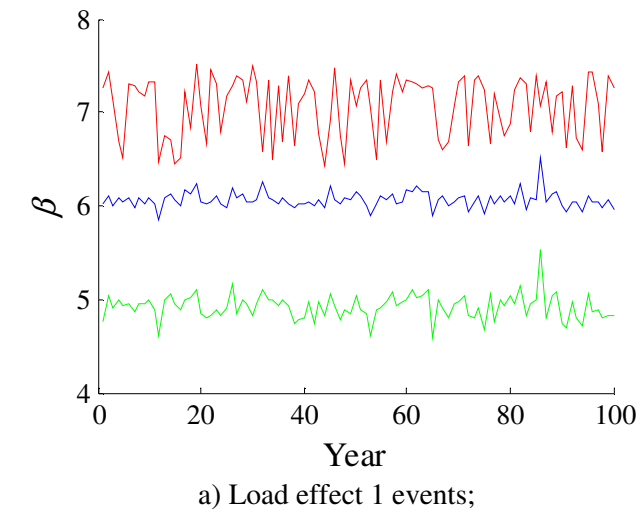
Figure A5.13: Three-span 40 bridge reliability indices.

a) Load effect 1 events;

b) Load effect 2 events;

c) Load effect 3 events;

Figure A5.14: Three-span 40 bridge reliability indices cumulative reliability indices.

a) Load effect 1 events;

a) Load effect 1 events;

b) Load effect 2 events;

b) Load effect 2 events;

c) Load effect 3 events;

c) Load effect 3 events;
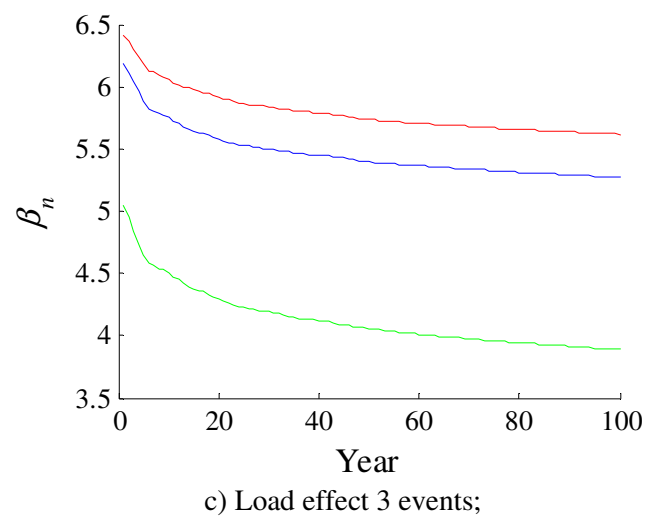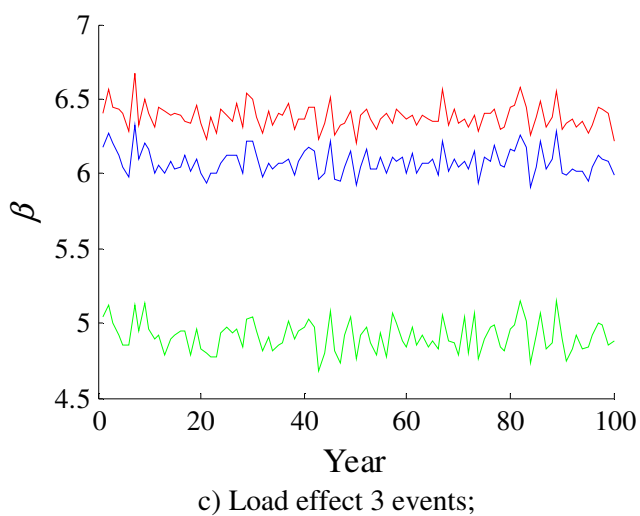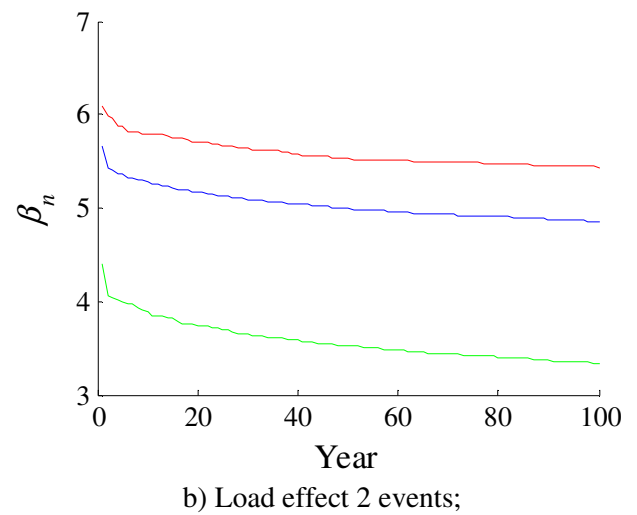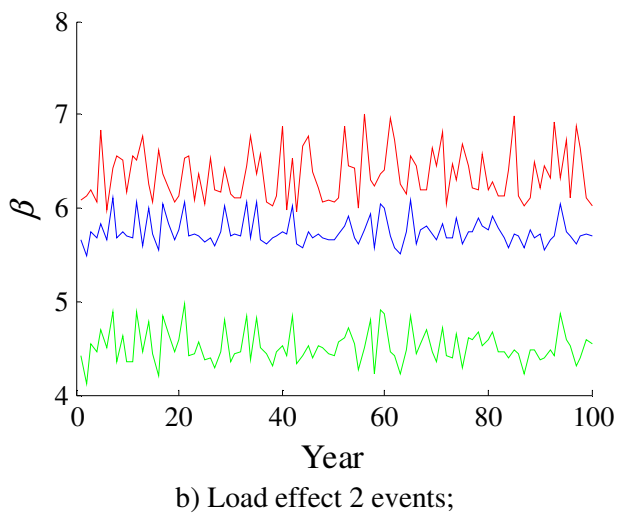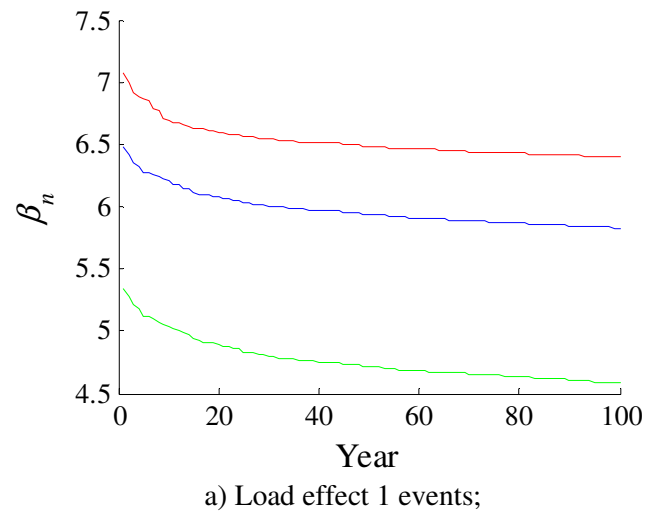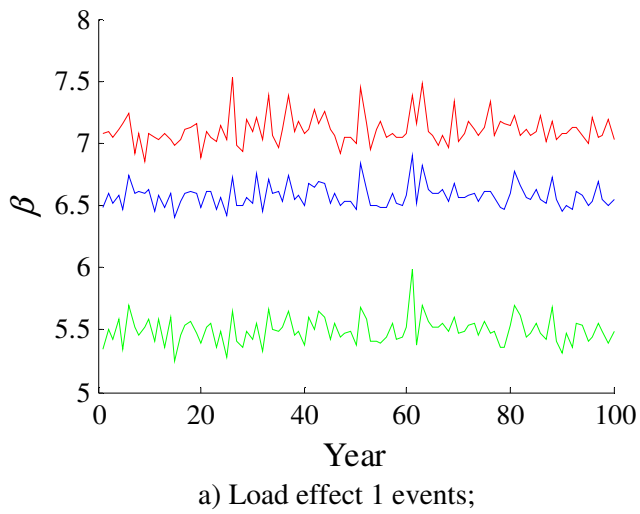
Figure A5.15: Three-span 50 bridge reliability indices.

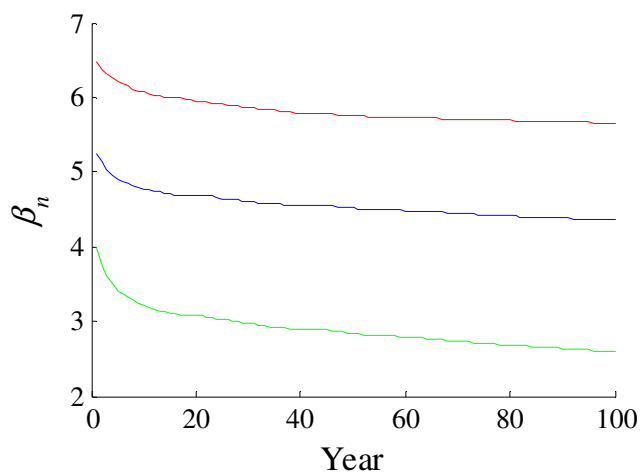Figure A5.16: Three-span 50 bridge reliability indices cumulative reliability indices.

a) Load effect 1 events;

a) Load effect 1 events;

b) Load effect 2 events;

b) Load effect 2 events;

c) Load effect 3 events;

c) Load effect 3 events;
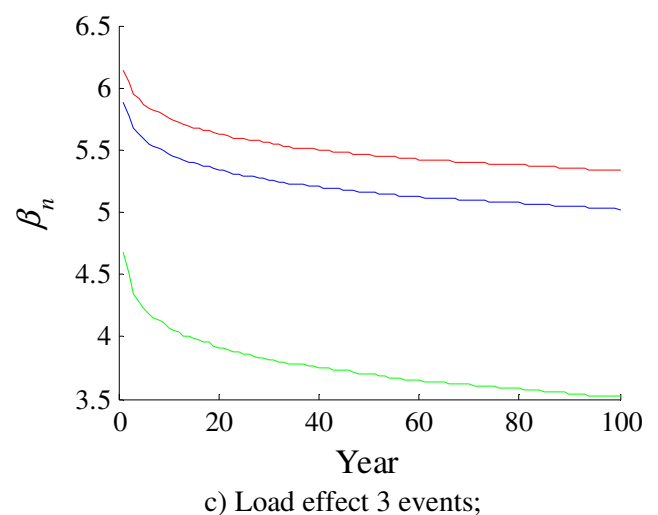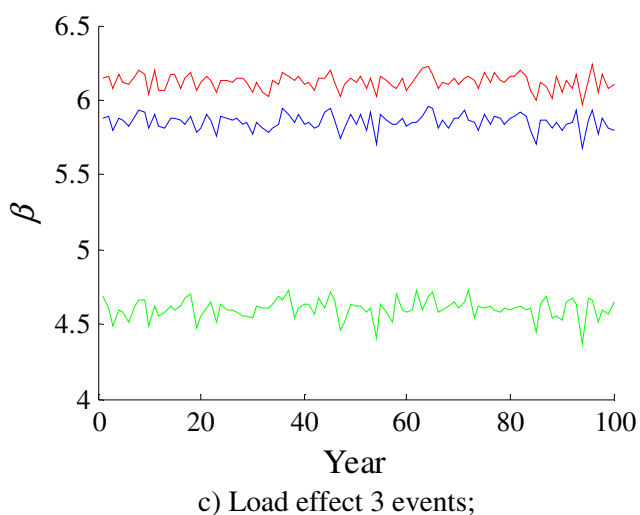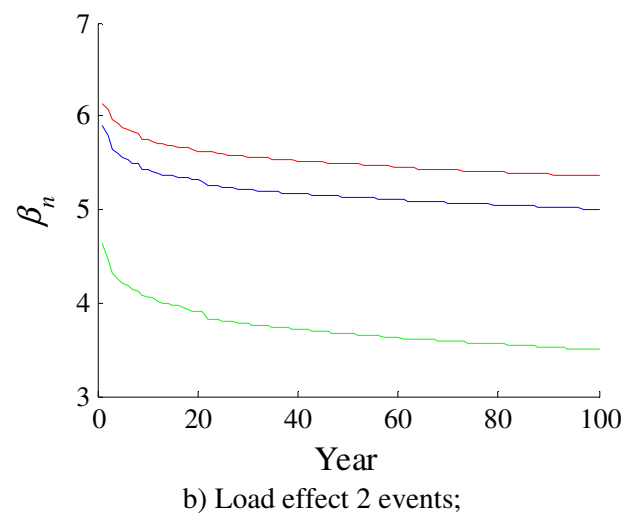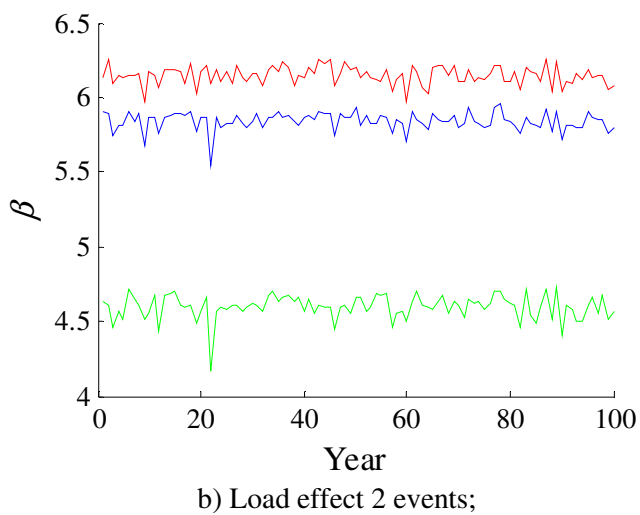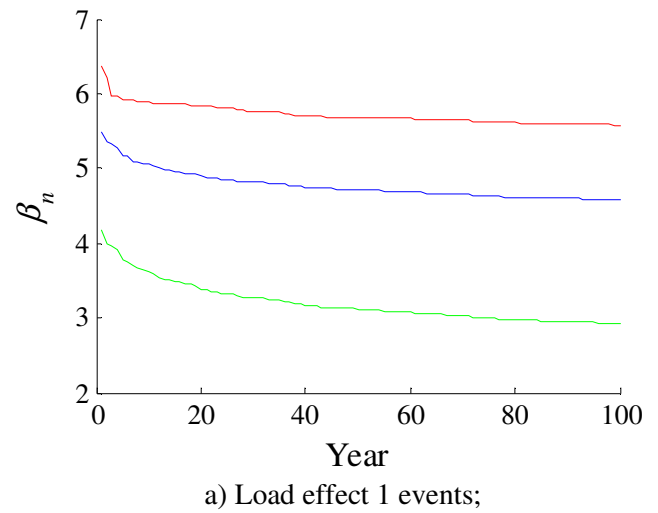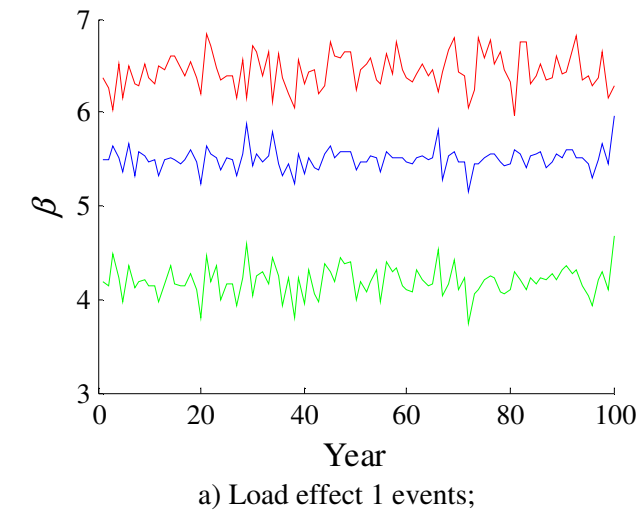
Figure A5.17: Three-span 60 bridge reliability indices.

Figure A5.18: Three-span 60 bridge reliability indices cumulative reliability indices.

Table A5.3: Three-span bridges; lifetime reliability indices considering nonlinear material behaviour (RSM).

Bridge Length (m)	Load Effect 1 Traffic			Load Effect 2 Traffic			Load Effect 3 Traffic		
	β_{1LT}	β_{2LT}	β_{3LT}	β_{1LT}	β_{2LT}	β_{3LT}	β_{1LT}	β_{2LT}	β_{3LT}
30	4.313	5.572	6.803	4.593	5.740	6.080	4.494	5.689	6.037
40	3.877	5.253	6.059	3.865	5.266	5.585	4.298	5.589	5.853
50	3.340	4.857	5.435	3.888	5.269	5.614	4.584	5.828	6.397
60	2.921	4.578	5.577	3.497	5.003	5.355	3.516	5.024	5.333

Table A5.4: Three-span bridges; lifetime reliability indices (FORM).

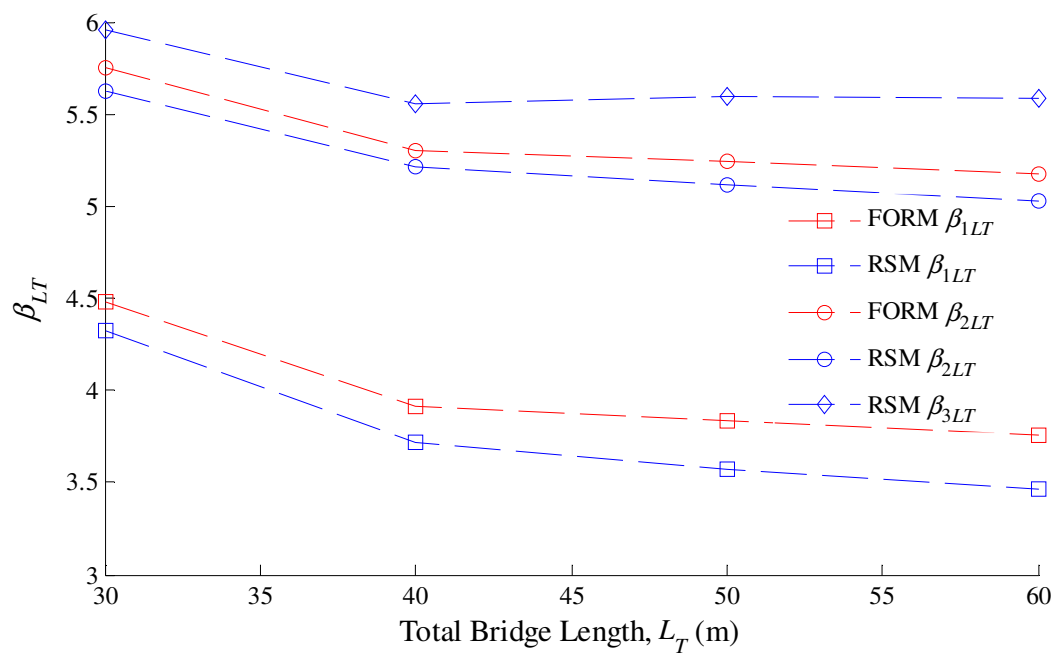| Bridge Length (m)	Load Effect 1 Traffic		Load Effect 2 Traffic		Load Effect 3 Traffic	
	β_{1LT}	β_{2LT}	β_{1LT}	β_{2LT}	β_{1LT}	β_{2LT}
30	5.186	6.305	5.037	6.189	5.010	6.168
40	5.019	6.176	4.454	5.734	4.163	5.468
50	4.358	5.658	4.244	5.569	4.545	5.805
60	4.120	5.469	3.895	5.293	3.910	5.305

Figure A5.19: Three-span life-time reliability indices for load effect 1 events.
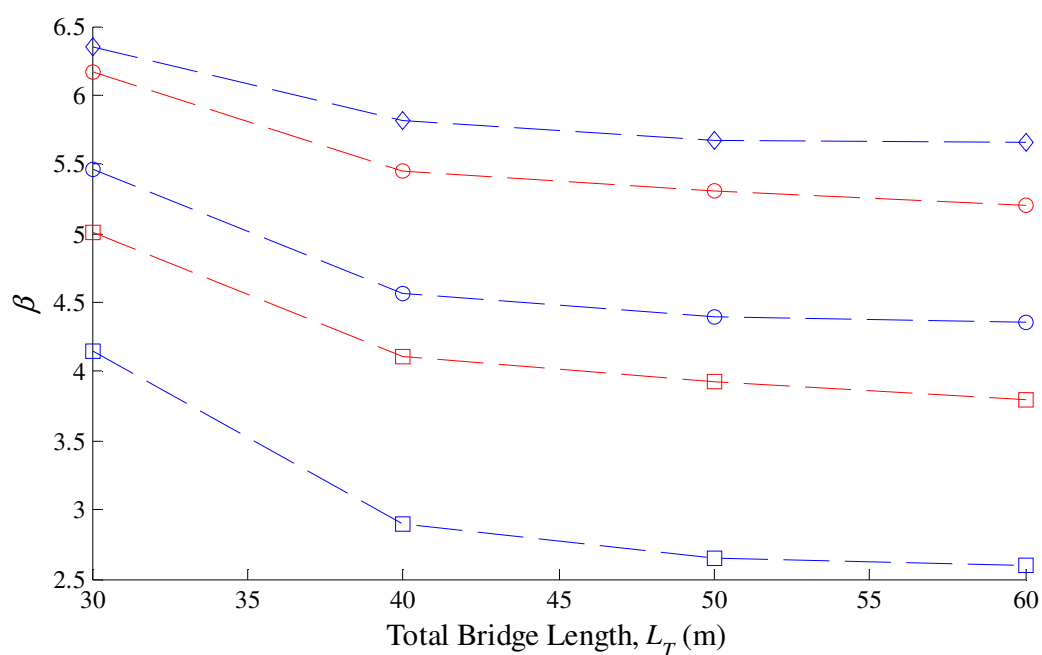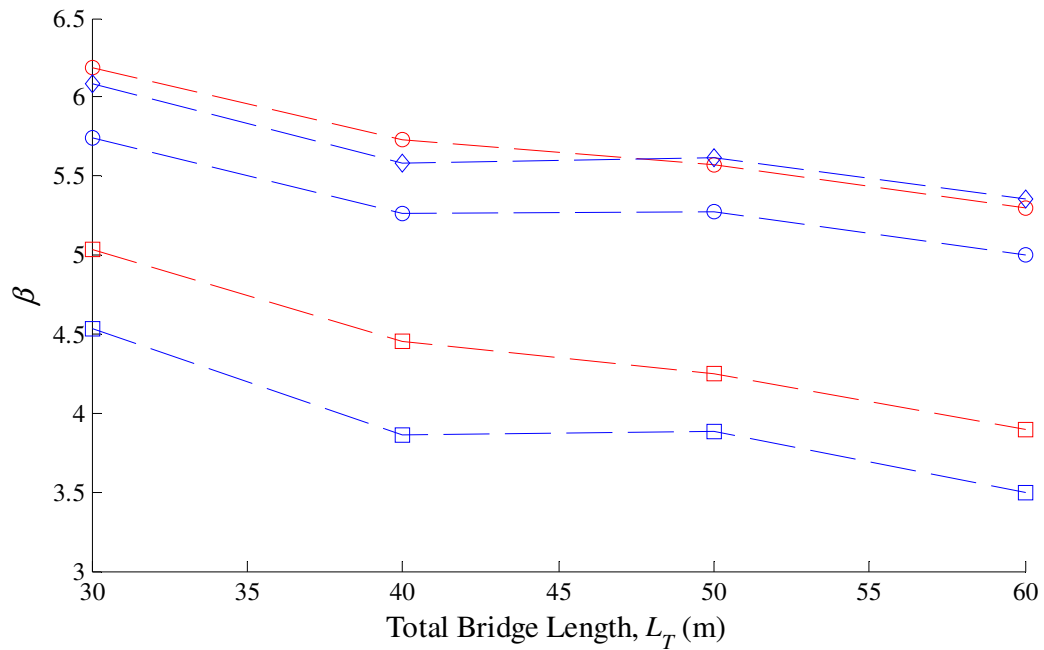
Figure A5.20: Three-span life-time reliability indices for load effect 2 events.
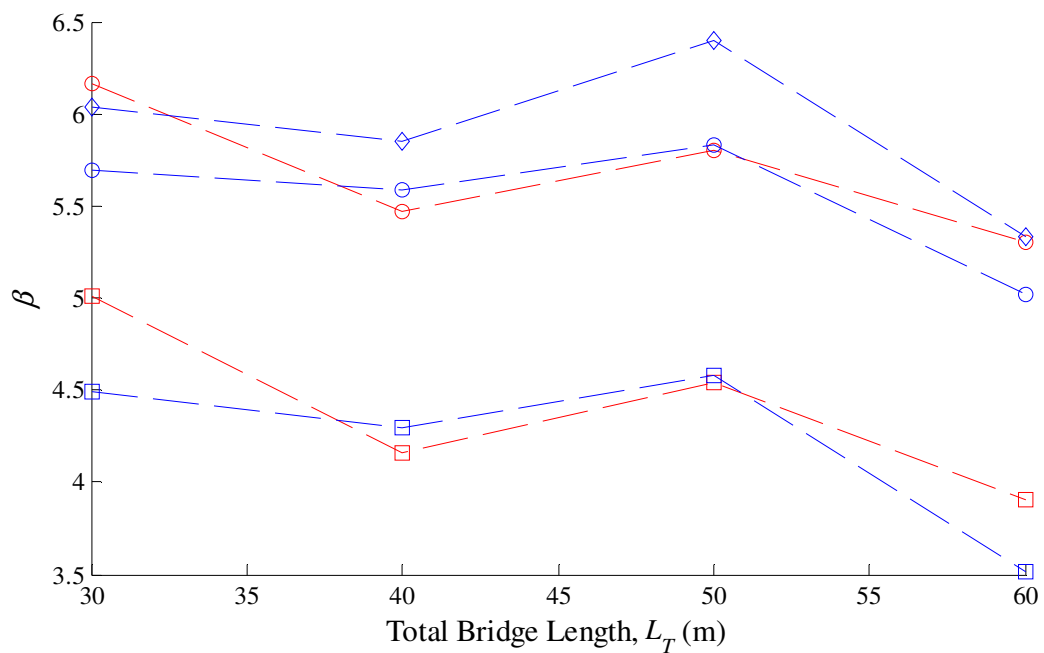
Figure A5.21: Three-span life-time reliability indices for load effect 3 events.

Appendix 6

Conference Papers

1. *Reliability Analysis of Highway Bridge Structures considering Ultimate Traffic Load Effects*, 6th International Conference on Bridge Maintenance, Safety and Management, Lake Stresa, Italy, July 8 -12th 2012.

2. *Probabilistic Analysis of an Indeterminate Beam Subjected to Moving Loads Considering Material Nonlinearity*, Bridge & Concrete Research in Ireland, Dublin Institute of Technology & Trinity College Dublin, September 6-7th 2012.

Reliability analysis of highway bridge structures considering ultimate load effects

L.A. McCarthy & C.C. Caprani
Department of Civil & Structural Engineering, Dublin Institute of Technology, Ireland

ABSTRACT: In the reliability analysis of bridge structures, it is often assumed that the bridge responds elastically to the highway loads it is subjected to. In this work a nonlinear material response of a three span beam and slab bridge structure is assessed using a nonlinear finite element model. The bridge is subjected to a lifetime of simulated traffic: 100 years annual maximum truck traffic loads determined from Monte Carlo Simulation of Weigh in Motion (WIM) data are used. A load factor for bending failure for each annual maximum event is established. Extrapolations are carried out to determine the load factor at the level of characteristic loading using a 1000-year return period, in order to determine if linear elastic response is appropriate at this level. Furthermore the reliability index for this indeterminate structure is also established using the First Order Reliability Method.

1 INTRODUCTION

1.1 *Bridge assessment*

Better assessment of existing highway structures can prolong the life of such structures with consequent savings to rehabilitation and replacement budgets. At present, there are over one million bridge structures in Europe with a total replacement cost of €400 billion (Cost 345). Appropriate procedures and techniques are vital for an accurate assessment of a bridge structures. It is no longer feasible to assess bridge stock in accordance to design rules for new structures as this may be overly conservative and unrealistic in many cases. The European Cost 345 project identified five levels of assessment ranging from a simple conservative method to an accurate probabilistic assessment. This study is concerned with a probabilistic method of calculating the reliability of a bridge structure.

Presently the reliability of bridge structures is generally based on an elastic analysis, or a static collapse analysis based on an idealized moment–rotation curve. Whilst this is a safe approach by virtue of the Lower Bound Theorem, it may give unacceptably conservative results in many cases. By modeling real structural behavior better, it is possible to obtain more accurate assessment of safety levels.

Traffic loading is a highly variable loading phenomenon and so bridge safety is sensitive to the model assumed for it. Extreme bridge traffic loading events may lead to elastic-plastic deformation of a bridge beam, or even failure. However, it is common to model such events in a reliability framework using elastic analysis. At the ultimate limit state, an elastic-plastic analysis may be more appropriate to estimate the actual strength of the structure.

1.2 *Nonlinear modeling in reliability analysis*

Several researchers have investigated reliability analysis incorporating a nonlinear structural behavior models. The main difficulty associated with a First Order Reliability Method (FORM) is that the gradient of the failure function needs to be established (Torii et al 2010). This proves very complex when incorporating a nonlinear structural model. Val et al (1997) proposed a method directly combining a finite element model with FORM, taking geometric and material nonlinearities into account. Torii et al (2010) linked a nonlinear finite element model to FORM using sensitivity analysis. Soares et al (2001) and Neves et al (2005) both successfully implemented a reliability analysis with a nonlinear structural model using the response surface method. All of the studies outlined examine concrete structures subjected to static loading. However, Khaleel et al (1992) determine bridge capacity using a nonlinear finite element model and investigated the reliability analysis for a moving load. However they limit their study to single vehicle cases.

2 NONLINEAR FINITE ELEMENT MODEL

2.1 Introduction

Nonlinear elastic-plastic analysis of structures is suitable when the actual strength of a structure is required when subjected to a certain form of loading (Chen et al, 1996). Only material nonlinearity is considered in this study.

Using the matrix displacement method, the formation of plastic hinges can be found based on incremental loading of the structure. At each increment the stiffness equations for the elements are found on the basis of forces and displacement induced on the structure in the previous increment (Li & Li, 2007). This analysis updates the stiffness equations so as to allow for the formation of plastic hinges. Plastic hinge formation is based on the assumption that plasticity is concentrated at the element ends only (Chen et al, 1996).

This work uses 1-dimensional beam elements to represent the bridge. As a result, the Generalized Clough Model, described in Li & Li (2007) is suitable, and used for this work. This model is also well-suited to this problem as it does not require integration of the constitutive equations over the element cross section at each increment. With this simpler computational approach, the analyses can perform more quickly. This is required for this study given the large number of separate analyses involved in analyzing bridges subjected to moving truck loads. Further, cyclic loading histories are accounted for. This is necessary for proper consideration of bridge traffic loading events, when vehicles traversing the bridge can cause sagging and hogging moments at a given cross section depending on the bridge configuration (for example two-span bridge).

2.2 Formulation

Clough et al (1990) proposed a moment rotation curve that traces the spread of plasticity through a section by the use of force recovery parameters (R). This approach is described in detail by Li & Li (2007). The force recovery parameters are calculated based on a yield function, given by:

$$\Gamma = \frac{M}{M_p} \qquad (1)$$

where M = the moment currently on the cross section, and M_p = the plastic moment capacity of the section. The values of the force recovery parameters are based on the yield function, as shown in Figure 1, in which Γ_y is the yield function at the yield moment of the cross section, M_y, and Γ_p is the yield function at M_p.

When the structure behaves elastically (Stage 1) the force recovery parameters are unity:

$$\Gamma \leq \Gamma_y: \qquad R = 1 \qquad (2)$$

Beyond yield (Stage 2), the stiffness reduces due to the formation of plasticity in the cross section, identified through the yield function:

$$\Gamma_y \leq \Gamma \leq \Gamma_p: \quad R = 1 - \frac{\Gamma - \Gamma_y}{\Gamma_p - \Gamma_y} \qquad (3)$$

Once the section is fully plastic (Stage 3), the force recovery parameter takes the value of strain hardening of the material, q:

$$\Gamma \geq \Gamma_p: \qquad R = q \qquad (4)$$

During an unloading event at any point (Stage 4), the structure is assumed to have its elastic stiffness:

$$\text{Unloading}: \qquad R = 1 \qquad (5)$$
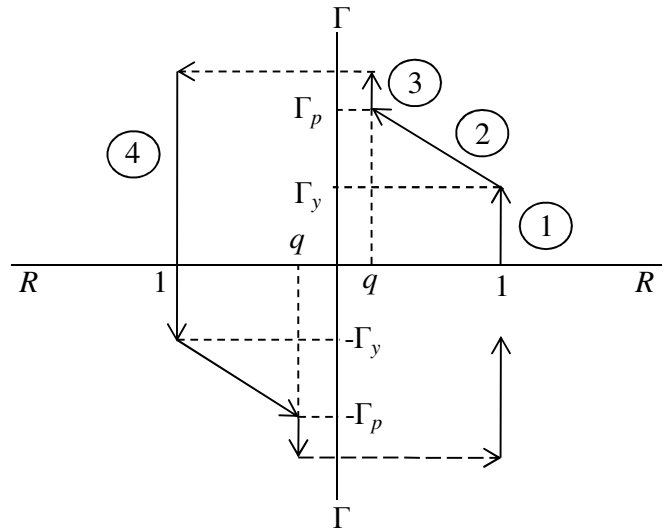
(a) Force recovery parameters under cyclic loading;
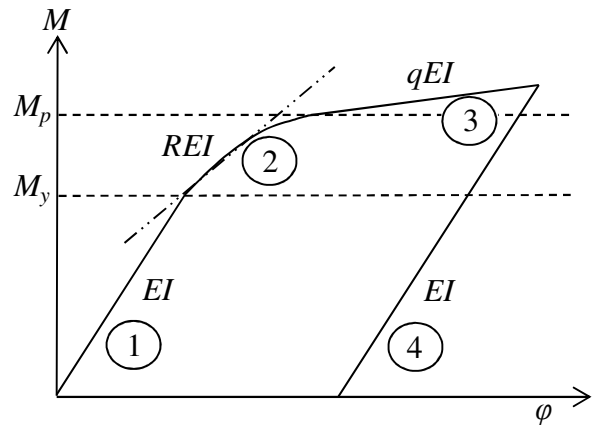
(b) Moment rotation relationship;

Figure 1. Stages in the behavior of the cross section.

Unloading states are identified through the yield function at successive increments i, as:

$$\Gamma_i \geq \Gamma_{i-1} : \qquad \text{loading} \tag{6}$$

$$\Gamma_i < \Gamma_{i-1} : \qquad \text{unloading} \tag{7}$$

The force recovery parameters are determined at each end of the beam element, and are denoted R_1 and R_2 for ends 1 and 2 respectively. The force recovery parameters alter the element local stiffness matrices as follows:

$$R_1 \geq R_2 : \qquad [k_g] = R_2[k_e] + (R_1 - R_2)[k_2] \tag{8}$$

$$R_2 \geq R_1 : \qquad [k_g] = R_1[k_e] + (R_2 - R_1)[k_1] \tag{9}$$

in which k_g is element tangent stiffness matrix at the current loading state. The elastic element stiffness matrix, k_e, is given by:

$$[k_e] = \frac{EI}{L^3}\begin{bmatrix} 12 & 6L & -12 & 6L \\ 6L & 4L^2 & -6L & 2L^2 \\ -12 & -6L & 12 & -6L \\ 6L & 2L^2 & -6L & 4L^2 \end{bmatrix} \tag{10}$$

The stiffness matrix with an element with a hinge at end 1, k_1, is given by:

$$[k_1] = \frac{EI}{L^3}\begin{bmatrix} 3 & 0 & -3 & 3L \\ 0 & 0 & 0 & 0 \\ -3 & 0 & 3 & -3L \\ 3L & 0 & -3L & 3L^2 \end{bmatrix} \tag{11}$$

The stiffness matrix with an element with a hinge at end 2, k_2, is given by:

$$[k_2] = \frac{EI}{L^3}\begin{bmatrix} 3 & 3L & -3 & 0 \\ 3L & 3L^2 & -3L & 0 \\ -3 & -3L & 3 & 0 \\ 0 & 0 & 0 & 0 \end{bmatrix} \tag{12}$$

where EI is the flexural rigidity of the cross section and L is the element length.

2.3 Incremental approach for bridge traffic loading events

The incremental procedure outlined in Ghali et al (2009), Becker (2004), and Chen et al (1996) is used as the vehicle(s), represented by point loads, move across the bridge structure. At each increment of loading, the equilibrium equation is formulated and solved:

$$\lambda\{F\} = [K_g]\{u\} \tag{13}$$

where λ = load factor, F = external force vector, K_g = global stiffness matrix and u = displacement vector.

To represent the moving loads that the bridge is subjected to, a loading -unloading procedure is used. Loading and unloading are both done simultaneously to signify a moving load across a bridge structure, as shown in Figure 2. Node locations are subject to mesh refinement. Node 1 unloads as node 2 loads. In this way, the effects of a plastic hinge forming from loads positioned at a previous location can be accounted for when the load moves position.
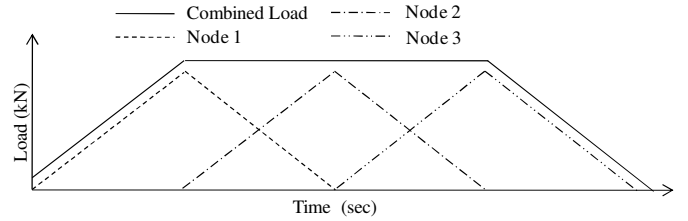
Figure 2. Incremental Loading/Unloading Procedure.

The accuracy of the incremental procedure depends on the size of the increments used, since at the onset of nonlinearity the equilibrium path will drift away from the actual path (Chen et al, 1996). A convergence study was used to determine the maximum acceptable increment step for minimum computational effort.

3 RELIABILITY ANALYSIS

3.1 Background

In recent years reliability analysis has become a vital tool in the safety assessment of structures. The probability of failure of a structure is evaluated based on a limit state function. Limit sate functions can be described as ultimate limit states, in which the structure is assessed against actual collapse, and serviceability limit states, in which the structure is assessed for the acceptability of its in-service functionality (Choi et al, 2007).

The probability of failure for a given limit state function can be defined as follows:

$$p_f = \int \cdots \int_{g(x) \leq 0} f_x(x)\, dx \tag{14}$$

where $g(x)$, is a limit state function of basic random variables x, and $f_x(x)$ is the joint probability density function of those variables. The probability of failure is approximated by the Hasofer-Lind reliability index, β (Melchers, 1999), given by:

$$\beta \approx -\Phi^{-1}(p_f) \tag{15}$$

where Φ^{-1} is the inverse standard normal distribution function.

177

3.2 Limit State Function

For structural safety at the ultimate limit state, failure is often deemed to occur when the applied load effect (S) is greater than the structural resistance (R) giving a limit state equation of:

$$g = R - S \qquad (16)$$

For which the probability of failure, Equation (14), is then given by:

$$p_f = P[g < 0] \qquad (17)$$

where $g < 0$ is the failure region, $g = 0$ is the failure surface, and $g > 0$ is the safe region, and it is assumed that R and S are statistically independent.

Typically failure is deemed to occur when the load effect, found using linear elastic methods, reaches M_p at a single cross section. This ignores the extra strength of a structure in resisting collapse due to plastic redistribution of loads. When considering a nonlinear analysis, it is preferable to consider failure as total collapse of the structure, or a similar catastrophic condition of the structure. Failure at the onset of collapse occurs when the global stiffness matrix becomes singular (Owen & Hinton, 1986):

$$g = \det\left(K_g\right) \qquad (18)$$

However, because strain hardening is considered as part of this study, singularity of the global stiffness matrix does not occur. As a result, Failure was defined for this analysis when the bending moment at any section reaches a maximum allowable post-yield bending moment. For this work, this value was taken as $1.1M_p$, which reflects an allowance for the ductility ratio of the cross section:

$$g = 1.1M_p - M \qquad (19)$$

In this manner, the extra strength of a structure in resisting collapse due to plastic redistribution of loads is allowed for.

3.3 Structure loading

The moments caused on the structure are a combination of those due to the dead load of the structure, and the live load due to the traffic.

$$S = D_1 + D_2 + D_3 + L \qquad (20)$$
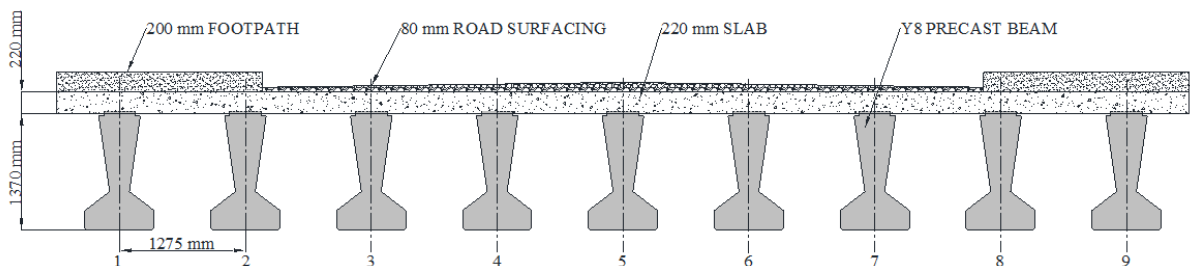
where D_1 is the dead load moment due to the beam, D_2 is the dead load moment due to the slab, D_3 is the dead load moment due to the road surfacing, and L is the live load moment on the structure. The limit state function, Equation (19), therefore becomes:

$$g = 1.1M_p - (D_1 + D_2 + D_3 + L) \qquad (21)$$

at any cross section in the structure.

4 BRIDGE & TRAFFIC MODEL

4.1 Bridge model

A three span slab and beam bridge was chosen for this investigation. The bridge caters for two lanes of traffic and consists of a 220 mm slab sitting on nine Y8 prestressed concrete girders spaced 1.275 m apart, as shown in Figure 3. The two outer spans are 20 m in length and the middle span is 28 m in length. The modulus of elasticity is taken as 31 GPa for the slab and 34 GPa for the beam. The modulus of strain hardening was taken to be 1.5 % of the modulus of elasticity of the prestressed concrete beam. (Li et al, 2007). The load effects considered in this study are shown in Table 1.

Table 1. Load effects considered in this study.

Load Effect 1	hogging moment over first interior support
Load Effect 2	interior span mid span bending moment
Load Effect 3	exterior span mid span bending moment

4.2 Lane distribution factors

A linear elastic finite element analysis was used to determine the lane distribution factors of the live load moment on the bridge. A grillage analysis was conducted with longitudinal members representing the beam and slab composite section and the transverse members representing the slab section. The torsion constants of these sections were altered to allow for the overlap of members. The slab and beam were both assumed to have identical material properties of grade C50 concrete. The live load considered was two 50 kN point loads 2 m apart representing a single truck axle.

Figure 3. Bridge cross section.

Influence lines for each beam were drawn for three specified load effects and are shown in Figure 4. The percentage distribution of the lane load was found by calculating the ratio of the bending moment of each beam to the total bending moment at the cross section. The lane distribution factors are reversed for the opposite lane as the bridge is symmetrical.
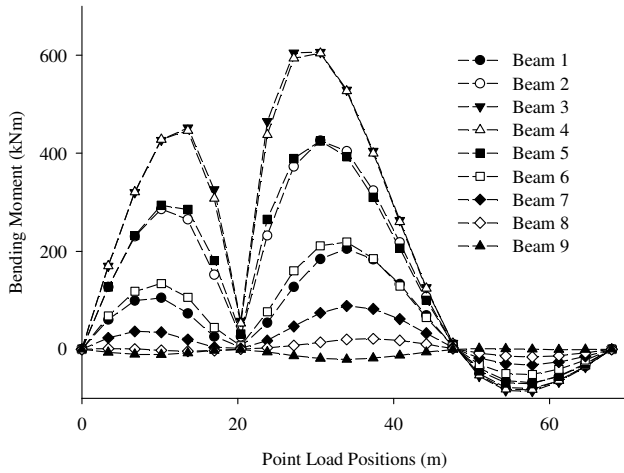
(a) Load Effect 1;
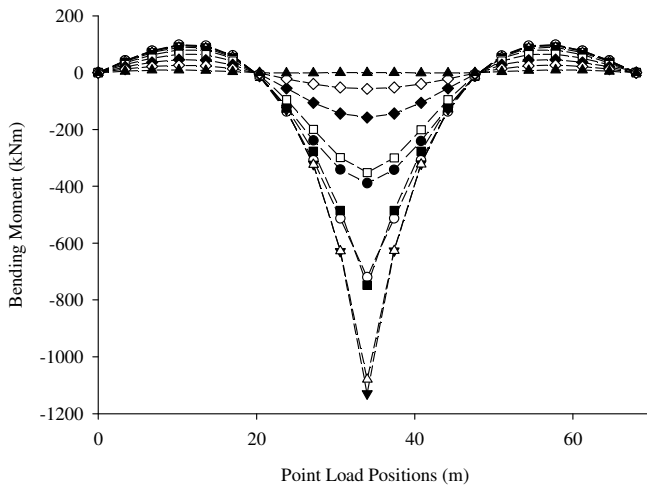
(b) Load Effect 2;
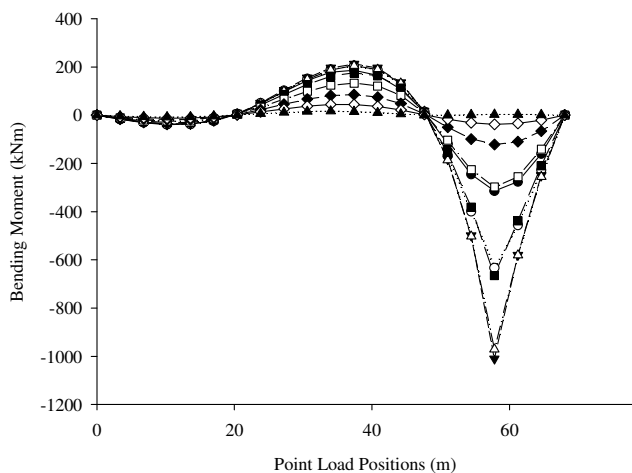
(c) Load Effect 3;

Figure 4. Influence lines for the longitudinal beams.

When only the left lane was loaded, beam 3 (see Figure 3) was determined to be critical. However, since the critical loading events typically involve trucks in both lanes, beam 5 is critical. Beam 5 carries approximately 16 % of the load when one lane is loaded and 32 % when the bridge has two lanes loaded. This value varies slightly depending on the load effect under analysis.

4.3 Traffic simulation

Monte Carlo simulation was used to generate 100 years of free flow traffic files based on measured traffic data obtained using Weigh-In-Motion from the A6 motorway near Auxerre between Paris and Lyon, France. As a form of pre-selection of critical loading events, annual maximum load effects were obtained using linear elastic analysis for the considered load effects. The lane distribution factors and influence lines described were used for this pre-selection. Typical annual maximum loading events are shown in Figure 5.

(a) Load Effect 1;

(a) Load Effect 2;

(a) Load Effect 3;
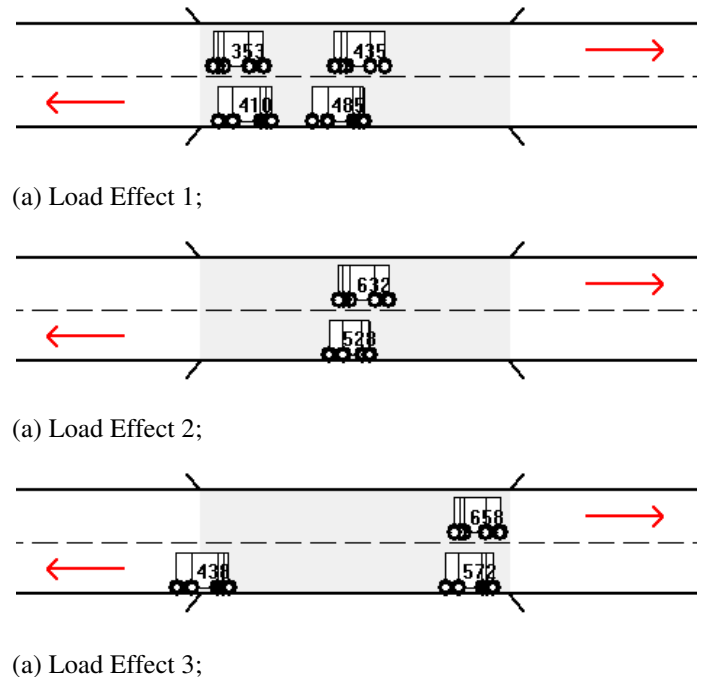
Figure 5. Sample annual maximum loading events (the truck weight is shown in deci-tonnes on each vehicle).

4.4 Resistance Model

The initial yield and plastic moment capacities of the prestressed beams are required for the nonlinear analysis. The plastic moment capacity was chosen to represent a minimum required resistance defined in the Eurocode, following the work of Nowak et al (2001):

$$M_p = \left[\alpha_D \left(D_1 + D_2 + D_3 \right) + \alpha_L \left(L \right) \left(LF \right) \right] / \phi \qquad (22)$$

where α_D is dead load factor (1.35), α_L is live load factor (1.5) and ϕ is the resistance factor (0.88). D_1,

179

D_2 and D_3 were calculated as 847 kNm, 423 kNm and 176 kNm. *LF* is the lane factor (0.16) calculated as described previously. The live load, *L* was calculated using Load Model 1 from Eurocode 1 Part 2 (EN 1991-2) to be 5757 kNm. An allowance of 10 % over-design was accounted for resulting in a plastic moment capacity of 4167 kNm using Equation (22). The initial yield moment capacity was then determined on the basis of a shape factor of 1.79 (Nicholson, 1997) to be 2328 kNm.

5 BRIDGE SAFETY RESULTS

5.1 *Calculation of load factor at failure*

The 100 pre-selected annual maximum loading events were analyzed for each load effect using the described non-linear finite element model to determine the load factor at failure. Each such loading event was unique and consists of a large number of variables such as number of trucks, number of axles, axles spacing, vehicle spacing, speed of trucks and axle weights. The failure load factor was calculated by increasing the axle weights proportionally, Equation (13), and repeating the non-linear analysis until failure occurred, as defined by Equation (19).

For each loading event, the elastic analysis result is plotted against the load factor: an example is shown in Figure 6 where strong linear correlation is evident. However, this was not found to be the case in general, as will be seen in later results.
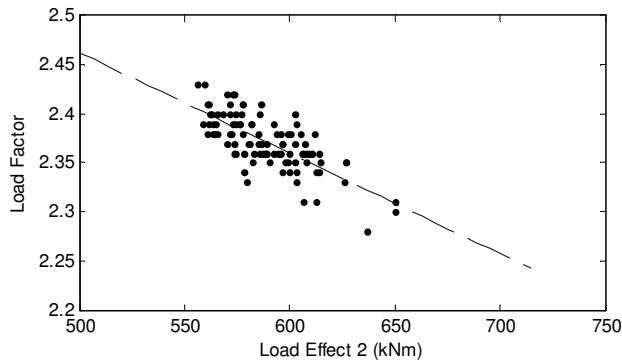
Figure 6. Load factor and elastic analysis load effect relationship for Load Effect 2.

5.2 *Characteristic load effect*

Based on the elastic analysis results, the annual maximum data is fitted using the Generalized Extreme Value (GEV) distribution, given by:

$$G(s) = \exp\left\{-\left[1 - \xi\left(\frac{s - \mu}{\sigma}\right)\right]_+^{1/\xi}\right\} \qquad (23)$$

where $[h]_+ = \max(h, 0)$ and μ, σ, ξ, are the location, scale and shape parameters respectively. The 1000-year return period load effect value is then esti-

mated, as shown in the Gumbel paper plot of Figure 7. See Coles (2001) for further details on the fitting and extrapolation procedure used.
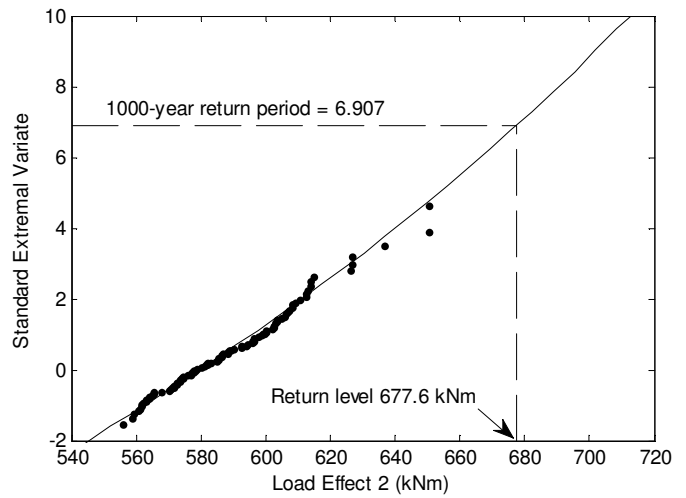
Figure 7. Sample extrapolation to 1000-year return period for Load Effect 2.

5.3 *Combined set of results*

Given the (albeit approximate) linear relationship between the load factor and elastic analysis results, and knowledge of the elastic analysis characteristic load effect, it is possible to infer the load factor that could be observed in the 1000-year return period. To this end, Figures 6 and 7 are overlaid, and the load factor at 1000-years predicted as shown in Figure 8 for each of the load effects considered.

Table 2 gives the numerical results corresponding to the predictions of Figure 8. It is clear that the means of arriving at a 1000-year load factor should include an allowance for variation from the simple linear regression of load factor against elastic load effect. Consequently the method used here is only an approximate estimation of return period safety.

The results of Table 2 also demonstrate that the prestressed concrete bridge design examined is probably not governed by ultimate load effect considerations, but by the more usual in-service stress limits.

Table 2. Results from extrapolations.

Variable	1000-year load effect (elastic analysis) kNm	1000-year load factor (non-linear analysis)
Load Effect 1	585.3	2.43
Load Effect 2	677.6	2.28
Load Effect 3	554.8	2.64

180
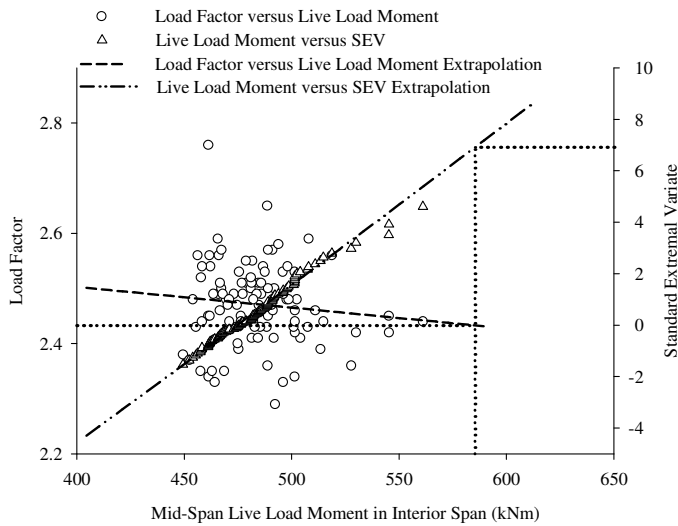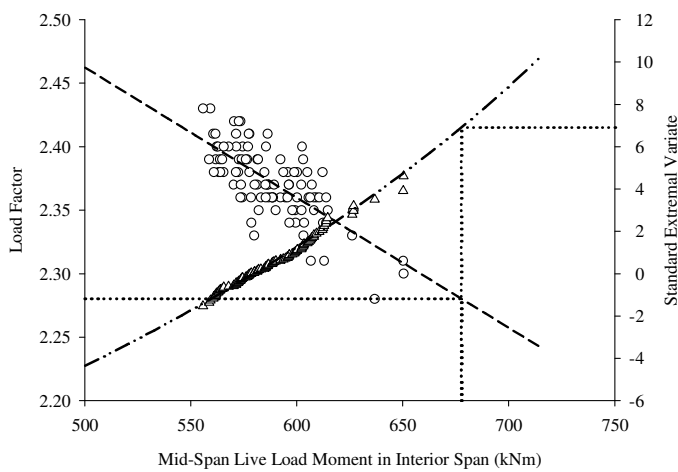
(a) Load Effect 1;
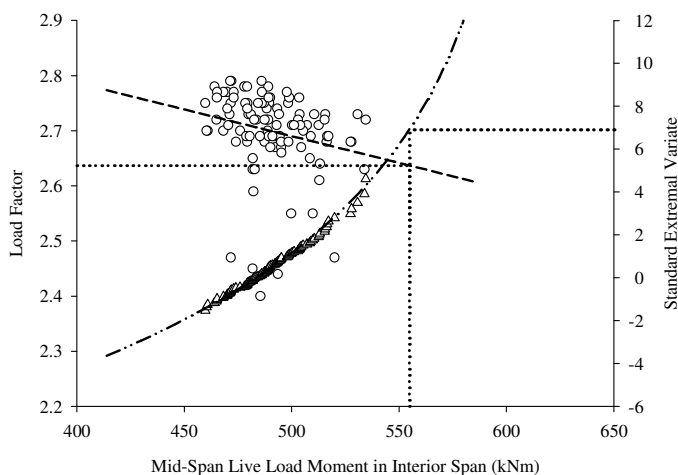
(b) Load Effect 2;

(c) Load Effect 3

Figure 8. Elastic extrapolations and determination of lifetime load factor.

5.4 *FORM analysis*

To complement the results presented, the more common FORM is applied to the bridge for compar-ison. The statistical descriptions of the variables needed to perform the reliability analysis are shown in Table 3. The coefficients of variation and distribu-tions are similar to those outlined in previous studies (Nowak et al, 2001 and Hwang et al, 2010). The live loads were taken as the extrapolated characteristic load effects. Similar to the nonlinear analysis Equa-tion (21) was taken as the limit state function.

The Rackwitz-Fiesler (1978) algorithm was used to determine the lifetime reliability index corres-ponding to each load effect. This describes the life-time probability of failure for each load effect. This method consists of an iterative process which searches for a point on the limit state surface where the probability of failure is greatest. It is of interest to compare the load effect values at this point, with those estimated both from the elastic prediction, and from the non-linear results.

Table 3. FORM reliability analysis variables

Variable	Distribution	Location (kNm)	Scale (kNm)	CoV*
D_1	Normal	847	67.8	0.08
D_2	Normal	423	42.3	0.10
D_3	Normal	177	53.1	0.30
M_p	Log- normal	3724	279.3	0.075
LE1	Gumbel	585.3	117.1	0.20
LE2	Gumbel	677.6	135.5	0.20
LE3	Gumbel	554.8	111	0.20

* CoV – Coefficient of Variation.

Table 4 gives the results of the FORM analysis. For comparison, the target reliability indices are also given (EC 1). The design point live load effect val-ues are also given, and it can be seen that they are considerably higher than the characteristic load ef-fects previously found. This confirms that there is a low probability of failure. When the design point live load effects are compared to the extrapolated failure load effects, interesting comparisons can be made. For load effects 1 and 3, the extrapolated fail-ure load effects exceed the design point load effects. Therefore an elastic analysis is appropriate. Howev-er, the extrapolated failure live load effect is similar to the design point live load effect for load effect 2. In this case, a nonlinear structural model is more ap-propriate than an elastic analysis when conducting a reliability analysis, as is conventional.

Table 4. FORM analysis results.

Load Effect	1	2	3
β	5.56	5.06	5.74
p_f	13.2×10^{-9}	205×10^{-9}	4.54×10^{-9}
B_{Target}	3.8	3.8	3.8
DPLE*	1807.9 kNm	1902.2 kNm	1771.3 kNm
ECLE**	4384.9 kNm	1926.2 kNm	2244.4 kNm

* DPLE – design point live load effect.
**ECLE – extrapolated critical live load effect corresponding to a load factor of 1

6 DISCUSSION & SUMMARY

6.1 *Discussion of results*

For each of the annual maximum loading events identified, a load factor for failure was established. This load factor is dependent on numerous variables in the loading event such as, number of trucks, number of axles, axles spacing, axle weights and spacing between trucks. For instance, considering Load Effect 2 in this paper, a loading event consisting of two trucks 40 m apart would expect to require a higher load factor for failure than a similar two-truck event with a 20 m gap between vehicles.

The correlation between load factor and elastic load effect was found to be weak to strong, depending on the load effect examined. This may be due to the distribution and/or number of variables in the comprising loading events. It is clear that further analysis of the phenomenon is required.

The 1000-year load effect and load factors for each load effect type analyzed are presented in Table 2. The load factors found are well above the crucial load factor of 1 and the reliability indices are well above the target indices. These results confirm that the minimum Eurocode design resistance is safe for the traffic, bridge, and load effects analyzed. Further, since no yield was observed at the extrapolated elastic load effect, elastic structural analysis models are adequate to be used in reliability analysis of the given bridge. However, whilst this is true for the beams examined here, and most probably true for prestressed beams in general, it may not be true for reinforced concrete or steel beam-and-slab bridges.

In this work it was found that a crucial component of the nonlinear analysis is the definition of the yield and plastic moment capacities. Accurate modeling of the behavior of the structure in the inelastic and ultimate ranges is clearly required. Considering that the moment capacities of the structure generally deteriorate over time, lower load factors may result. As such, nonlinear methods may yet be well-suited to estimate the true safety in such cases.

6.2 *Summary*

A nonlinear analysis is performed on a three-span beam-and-slab structure subjected to 100 years of annual maximum traffic for three specific loading effects. The 1000-year load effects and corresponding load factors were established using an approximate method to relate the two. The strength capacity of this structure was deemed to be adequate as the extrapolated load factors were significantly greater than the critical load factor of 1.

The structural safety of the bridge was determined using a reliability analysis. Load and resistance parameters were modeled as random variables. The live load distributions were from the distribution of 100 annual maximum loading events. The dead load and resistance parameters were the same as considered for the nonlinear analysis. Statistical distributions for the variables were taken from the available literature and both the nonlinear analysis and reliability analysis indicated that the structure has adequate safety under the considered traffic.

REFERENCES

Becker, A. 2004. *An Introductory Guide to Finite Element Analysis*. Suffolk: Professional Engineering Publishing.

Chen, W., Goto, Y. & Richard Liew, J. 1996. *Stability Design of Semi-Rigid Frames*. New York: John Wiley & Son.

Choi, S.K., Grandhi, R.V. & Canfield, R.A. 2007. *Reliability - based structural design.* London: Springer

Coles, S.G. 2001. *An Introduction to Statistical Modelling of Extreme Values*. London: Springer-Verlag.

Cost 345, 2004.*Procedures Required for Assessing Highway Structures*. Available from http://cost345.zag.si/: Cordis

EC1, 2005, Eurocode 1: Actions on Structures, European Standard EN 1991-2. Brussels: European Committee for Standardisation.

EC1.2, 2003, Eurocode 1: Actions on Structures, Part 2: Traffic loads on bridges, European Standard EN 1991-2. Brussels: European Committee for Standardisation.

Ghali, A. Neville, A & Brown, T. 2009. *Structural Analysis-A unified classical and matrix approach*. London: Spon Press

Hwang, E.S., Paik, I.R., & Nguyen, S., H.2010. Reliability Analysis of Stresses in Prestressed Concrete Girder Under Service Load, *Proceedings of 11th International Conference on Applications of Statistics and Probability in Civil Engineering*, 1-4 August 2011, Zurich, Switzerland

Khaleel, M.A. & Itani, R.Y. 1993. Safety Evaluation of Existing Partially Prestressed Concrete Girder Bridge*, Journal of Computers & Structures* 48(5): 763 - 771.

Li, G.Q. & Li, J.J. 2007. *Advanced Analysis and Design of Steel Frames*. Sussex: John Wiley & Sons.

Melchers, R.E. 1999. *Structural Reliability Analysis and Prediction*. Sussex: John Wiley and Sons.

Neves, R.A., Chateauneuf, A., Venturini, W.S. & Lemaire, M. 2005. Reliability analysis of reinforced concrete grids with nonlinear material behavior, *Journal of Reliability Engineering and System Safety* 91:735-744

Nicholson, B.A.1997. *Simple Bridge Design using prestressed Beams*. Leicester: Uniskill Ltd

Nowak, A.S. & Park, C.H. 2001.Reliability analysis of prestressed concrete bridge girders: comparison of Eurocode, Spanish Norma IAP and AASHTO. *Journal of Structural Safety* 23:331-344

Owen, D.R.J. & Hinton, E.1986. *Finite Elements in Plasticity Theory and Practice*. Swansea: Pineridge Press Limited

Rackwitz, R. & Fiessler, B. 1978. Structural Reliability under Combined Random Load Sequences, *Journal of Computer and Structures* 9:489-494

Soares, R.C., Mohamed, A., Venturing, W.S. & Lemaitre, M.2001. Reliability analysis of non-linear reinforced concrete frames using the response surface method. *Journal of Reliability Engineering and System Safety* 75:1-16.

Torrii, A.J. & Machado, D.A. 2010. Reliability analysis of nonlinear reinforced concrete beams*. Proceedings for Asociacón Argentina de Mecánica Computacional Conference*, 15 - 18 November 2010, Buenos Aires, Argentina.

Val, D., Bluger, F. & Yankelevsky D.1997 Reliability evaluation in nonlinear analysis of reinforced concrete structures. *Journal of Structural Safety* 19(2):203-17.

Probabilistic Analysis of an Indeterminate Beam Subjected to Moving Loads Considering Material Nonlinearity

C.C. Caprani, L.A. McCarthy

Department of Civil & Structural Engineering, Dublin Institute of Technology, Bolton Street, Dublin 1, Ireland

Email: colin.caprani@dit.ie, liam.mccarthy@dit.ie

ABSTRACT: In the probabilistic assessment of existing bridge structures, elastic structural models are typically used. At the ultimate limit state this may not be appropriate. In this work, the response of an indeterminate beam structure subjected to static and moving loads is assessed using a one dimensional nonlinear material finite element model. A deterministic study is used to calculate the load factor required to cause structural collapse for static and moving loads. A probabilistic assessment of the structure is conducted using the first order reliability method for static loads. Importance Sampling is used for moving loads. It is found that in some cases the common assumption used to locate the load does not lead to the true collapse load factor.

KEY WORDS: Bridges; Loading; Reliability analysis; Nonlinear; Finite element; Importance sampling.

1 INTRODUCTION

1.1 Bridge Structural Safety

Bridge maintenance is an ever-growing concern due to reducing financial budgets and increasing traffic volumes. Accurate bridge assessment is now a necessity as it is no longer acceptable to assess a bridge structure using excessive conservatism. According to a recent survey, one major reason for a bridge structure to fail an assessment is "conservative or inappropriate methods of assessment" [1]

Typically, bridge failure is deemed to occur when the load effects found using an elastic structural assessment reach the resistance capacity at single location in the structure [2]. According to the Lower bound Theorem of plastic theory, this ensures safety against structural collapse. However, this ignores the structure's ability to carry further load by redistribution of bending moments. For efficient assessment, this extra reserve of strength can be accounted for when using sufficiently ductile materials and cross-sections.

1.2 Nonlinear Modelling in Reliability Analysis

Several researchers have used a nonlinear structural model in probabilistic analysis methods. These methods are grouped as follows: 1) Monte Carlo Simulations; 2) the Response Surface Method, and; 3) sensitivity-based analysis [3]. Monte Carlo simulation, including efficient sampling techniques such as Importance Sampling, produce high levels of accuracy but can require extensive simulations, especially when dealing with low probabilities of failure [4]. The response surface method uses a polynomial to approximate an unknown limit sate function, thereby allowing a closed-form probabilistic analysis such as the first order reliability method to be carried out. This method has proved to be successful [5] and [6]. However, it may be inaccurate when dealing with several modes of failure [3]. Sensitivity-based methods have a high level of accuracy [7], but are not easily adapted to practical applications [3]

This study uses the first order reliability method (FORM) to examine static loads considering material nonlinearity. When the problem is extended to a moving load, Importance Sampling combined with a nonlinear finite element model is used to determine the probability of failure. The results are compared to those established using the common assumption that locates the load according to the elastic critical location.

By incorporating a nonlinear structural model into a reliability assessment, an improved estimate of the structure's true safety level can be determined for a given traffic loading scenario. This is because a better model of material behaviour is accounted for. Consequently, this work can find practical application in safety assessment of existing highway infrastructure due to the considerable potential savings to maintenance budgets that may be realized.

2 STRUCTURAL RELIABILITY

2.1 Introduction

For a basic structural problem with a known limit state function, the probability of failure can be defined as follows:

$$p_f = \int \cdots \int_{g(x) \leq 0} f_X(x) \, dx \qquad (1)$$

where $g(x)$, is a limit state function of basic random variables x, and $f_X(x)$ is the joint probability density function of those variables.

Failure is often deemed to occur when an applied load effect (S) is greater than the structural resistance (R) giving a limit state function (g) of:

$$g = R - S \qquad (2)$$

Equation 1 can be rewritten as:

$$p_f = \int \ldots \int I\big[g(r,s) \leq 0\big] f_R(r) f_S(s) \, drds \qquad (3)$$

Where: $I[\ ]$ is an indicator function which takes on a value of unity if the term in the brackets is true, or zero if the term in the brackets is false; and f_R and f_S are the probability density functions of resistance and load.

Evaluation of the probability integration outlined above can prove difficult when a large number of random variables (the vector *X*) are involved. Generally this equation cannot be solved in closed form due to the complexity of establishing the joint probability density function. Also, the limit state can often only be evaluated using simulation models such as finite element analysis. For this reason, approximate methods such as the FORM have been developed.

2.2 First Order Reliability Method

FORM simplifies the integration process by transforming variables from their original random space (*X*-space) into a standard normal space (*U*-space). This may be done using the Rosenblatt transformation [4] to ensure the contours of the integrand $f_X(x)$ are regular and symmetric:

$$U = \Phi^{-1}\left[F_X(X)\right] = \Phi^{-1}\left[\Phi\left(\frac{X-\mu}{\sigma}\right)\right] = \frac{X-\mu}{\sigma} \qquad (4)$$

where Φ is the standard normal cumulative distribution function (cdf), Φ^{-1} is the inverse of the standard normal cdf, $F_X(.)$ is the cdf of variable X, μ is the mean value of X and σ is the standard deviation of X.

Another measure FORM takes to simplify the integration process is to linearize the limit state $g(X) = 0$. A first order Taylor series expansion is performed at the Most Probable Point (MPP); that is, the point on the limit state function which has the largest probability density (denoted $U*$). An iterative process is implemented to establish this point and the reliability index, β, can be evaluated as follows [8]:

$$\beta = \frac{g(U^*) - \sum_{i=1}^{n} \frac{\partial g(U^*)}{\partial x_i} \sigma_{x_i} u_i^*}{\sqrt{\sum_{i=1}^{n} \left(\frac{\partial g(U^*)}{\partial x_i} \sigma_{x_i}\right)^2}} \qquad (5)$$

The probability of failure and reliability index are related:

$$p_f = \Phi(-\beta) \qquad (6)$$

where β, originally defined by Cornell (1969), represents the shortest distance from the origin to the limit state function in standard normal space and Φ is the standard normal cdf.

2.3 Importance Sampling

Monte Carlo simulation can be used to estimate the probability of failure. Samples of the random variables are generated and the limit state function evaluated for each set. The probability of failure is then given by:

$$p_f = \frac{1}{N} \sum_{j=1}^{N} I\left[g(x) \le 0\right] \qquad (7)$$

where N is the total number of samples. This approach is inefficient when dealing with low probabilities of failure because a very large sample set is required.

Importance Sampling can produce an accurate estimate of the probability of failure. If sampling occurs around random variables that are more likely to contribute to the probability of failure fewer samples are required. This is achieved by using a biased sampling distribution. This bias is corrected for

by weighting the outputs of the simulation. The probability integral may be estimated as follows:

$$p_f = \int \ldots \int I\left[g(x) \le 0\right] \frac{f_X(x)}{h_v(x)} h_v(x)\, dx \qquad (8)$$

where $h_v(x)$ is the importance sampling function. It is common to use a normal distribution for h with the mean shifted to the MPP (Melchers, 1999). The above integral may be then estimated using:

$$p_f = \frac{1}{N} \sum_{i=1}^{N} \left(I\left[g(x) \le 0\right] \frac{f_x(x)}{h_v(x)} \right) \qquad (9)$$

3 NONLINEAR FINITE ELEMENT MODEL

3.1 Finite element model

One-dimensional Euler-Bernoulli elements are used to model the beams for this work. Using the element stiffness matrices end forces and moments are calculated on each element. To minimize computation but retain accuracy, a non-uniform mesh is used. A fine mesh of 0.2 m is used at critical mid-span locations while a coarse mesh of 1 m is used for the remainder of the structure.

3.2 Material nonlinearity model

The approached used to represent the nonlinear response is that established by Clough et al (1990) as outlined in [9]. The spread of plasticity through the section is traced using force recovery parameters (*R*). The force recovery parameters are established from the following yield function:

$$\Gamma = \frac{M}{M_p} \qquad (10)$$

where M is the moment currently on the cross section, and M_p is the plastic moment capacity of the section. The values of the force recovery parameters can be seen in Figure 1 at different stages of loading. When the structure is subject to loading and is behaving in an elastic manner (Stage 1) the force recovery parameters are equal to one, as no reduction in stiffness has taken place:

$$\Gamma \le \Gamma_y : \ R = 1 \qquad (11)$$

The slope of the moment rotation curve for this stage is EI, where E is the modulus of elasticity of the material and I is the second moment of area of the section.

Once the initial yield capacity (Stage 2) has been reached, the force recovery parameters and the stiffness of the structure reduce as follows:

$$\Gamma_y \le \Gamma \le \Gamma_p : \quad R = 1 - \frac{\Gamma - \Gamma_y}{\Gamma_p - \Gamma_y} \qquad (12)$$

When a plastic hinge has fully formed (Stage 3) the force recovery parameter at that location equals the value of strain hardening (*q*) of the critical material in the section. The slope of the moment rotation curve for this stage is qEI:
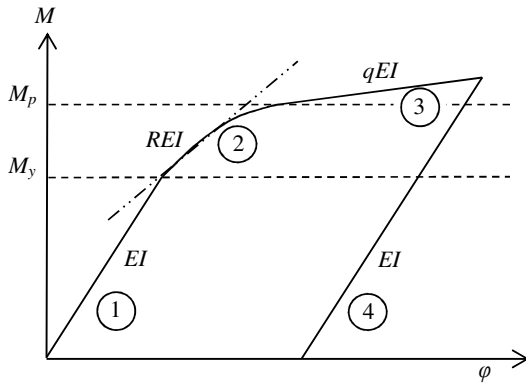
$$\Gamma \ge \Gamma_p : \ R = q \qquad (13)$$

During an unloading event at any point (Stage 4), the structure is assumed to behave elastically [9]. Hence the unloading force recovery parameter is:

$$\text{Unloading}: \qquad R = 1 \qquad (14)$$
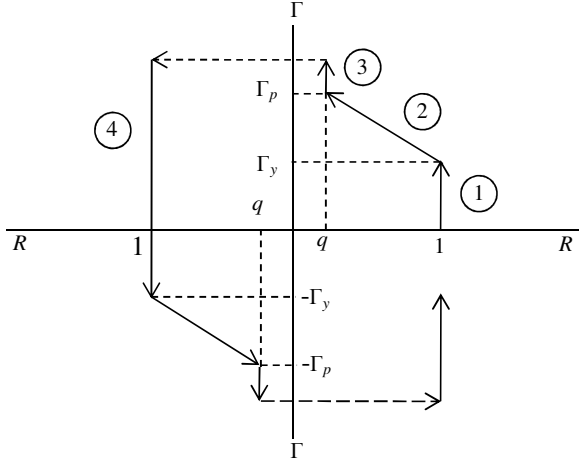
(a) Force recovery parameters under cyclic loading;

(b) Moment rotation relationship;

Figure 1. Stages in the behaviour of the cross section.

Once the force recovery parameters have been identified at each end of the element, the local stiffness matrix of each element is altered as follows:

$$R_1 \geq R_2 : \left[k_g \right] = R_2 \left[k_e \right] + \left(R_1 - R_2 \right) \left[k_2 \right] \qquad (15)$$

$$R_2 \geq R_1 : \left[k_g \right] = R_1 \left[k_e \right] + \left(R_2 - R_1 \right) \left[k_1 \right] \qquad (16)$$

in which k_g is element tangent stiffness matrix at the current state of loading. The elastic element stiffness matrix, k_e, is given by:

$$[k_e] = \frac{EI}{L^3} \begin{bmatrix} 12 & 6L & -12 & 6L \\ 6L & 4L^2 & -6L & 2L^2 \\ -12 & -6L & 12 & -6L \\ 6L & 2L^2 & -6L & 4L^2 \end{bmatrix} \qquad (17)$$

The stiffness matrix with an element with a hinge at end 1, k_1, is given by:

$$[k_1] = \frac{EI}{L^3} \begin{bmatrix} 3 & 0 & -3 & 3L \\ 0 & 0 & 0 & 0 \\ -3 & 0 & 3 & -3L \\ 3L & 0 & -3L & 3L^2 \end{bmatrix} \qquad (18)$$

The stiffness matrix with an element with a hinge at end 2, k_2, is given by:

$$[k_2] = \frac{EI}{L^3} \begin{bmatrix} 3 & 3L & -3 & 0 \\ 3L & 3L^2 & -3L & 0 \\ -3 & -3L & 3 & 0 \\ 0 & 0 & 0 & 0 \end{bmatrix} \qquad (19)$$

where EI is the flexural rigidity of the cross section and L is the element length.

3.3 Incremental Loading/Unloading Approach

The incremental loading procedure outlined in [10], [11], and [12] is implemented to model the stress history at a cross section. At each increment the equilibrium equation is formulated and solved:

$$\lambda \{F\} = \left[K_g \right] \{u\} \qquad (20)$$

where λ is the load factor, F is the external force vector, K_g is the global stiffness matrix, and u is displacement vector. The stiffness is altered after each increment using the force recovery parameters as previously outlined. At the onset of the nonlinearity the equilibrium path drifts away from the actual path. This drift can be minimized by using sufficiently small increments [12].

As extreme loads traverse the structure, plastic hinges may form and so load redistribution along the structure may occur. The incremental procedure is adapted to represent a moving load. This is implemented using a loading-unloading process, illustrated in Figure 2. The load at Position 1 unloads as the load at Position 2 loads. Hence, a residual rotation remains after plastic behaviour ensues in the beam once the load is unloaded. In this manner a true representation of the moving load is accounted for.
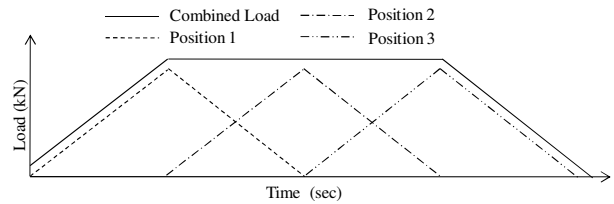

Figure 2. Incremental Loading/Unloading Procedure.

4   DETERMINISTIC ANALYSIS

4.1   Problem parameters

A two-span beam of 10 m equal spans is examined. To size the beam initially, the maximum elastic bending moment when subjected to moving 100 kN point load is used. A minimum resistance formula ignoring dead load (Nowak, 2001) is used:

$$R_{MIN} = \left[\alpha_L \left(M_L \right) \right] / \phi \qquad (21)$$

where α_L is live load factor (1.5), ϕ is the resistance factor (0.88) and M_L is the live load on the structure. The section used is a 457×152×74 hot-rolled universal beam. The steel is assumed to have yield strength of 265 N/mm^2 and a modulus of elasticity of 210 kN/mm^2.

Failure is defined to occur when the global stiffness matrix becomes singular in the nonlinear analyses [13]. This corresponds to the formation of a mechanism [14]. For comparison, a moving elastic analysis and a moving nonlinear analysis taking strain hardening into account are also presented in some cases. The strain hardening stiffness is taken to be 1.5% of the elastic stiffness [9]. This prevents the global stiffness matrix turning singular and a collapse mechanism forming. However, significant ductility and rotation of cross sections can occur numerically using this assumption. Whilst these rotations should be checked for real sections, for this work, the allowance of strain hardening identifies the residual moments in the structure and provides a comparison to an elastic analysis of the moving load

4.2 Example moving single point load analysis

A moving single point load of 100 kN is considered. To establish the collapse load factor, that is, the ratio of failure load to the working load of 100 kN, the load is increased after each complete run across the structure, and this is continued until a collapse mechanism forms. An arbitrary speed of 1 m/s is used with a time step of 1 s. It must be noted that vibration of the beam is ignored. The bending moment time-history is shown in Figure 4 at each plastic hinge location.

From Figure 4(b) and 4(c), it can be seen that a collapse mechanism forms when the point load is approximately 4 m from the left hand side. As the load traverses the structure, plastic hinges successively form at 3 m, 4 m, and 10 m. The plastic hinge formed at 3 m is not present at collapse as the load has travelled beyond this point and unloading has taken place. This is identified in Figure 4(a).

### 4.3 Collapse load factors for a single moving point load

Typically, the collapse load factor for moving load problems is found by first identifying the location of the loads that causes the maximum elastic moments. Then, a nonlinear analysis is carried out with the load(s) located statically at this location [3]. A difficulty arises in choosing what is meant by the critical elastic location. For example, in the two-span continuous beam considered here, the point load locations causing the maximum sagging moment and maximum hogging moment are different. Furthermore, the load factors corresponding to failure of the beam are different for these two different locations. However, the true collapse load factor can be found using the nonlinear moving load approach developed here.

The load factors (λ) corresponding to failure are found for three scenarios: a static nonlinear analysis is carried out with the load located at the critical elastic maximum sagging (1) and hogging (2) positions; and a moving load nonlinear analysis (3) is carried out using the procedures outlined earlier. The results for each of these scenarios are given in Table 1. It is clear from these results that the location
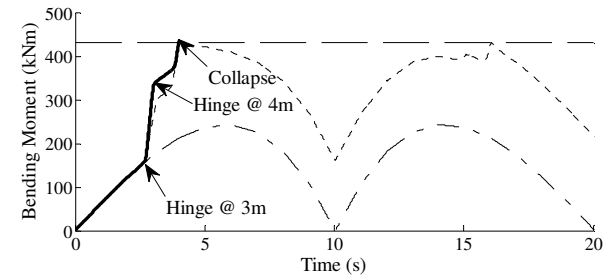
identified by the maximum elastic sagging moment is the closest to the true collapse load factor. However, it is significant that the true result (scenario (3)) is not given by either elastic means of locating the load.
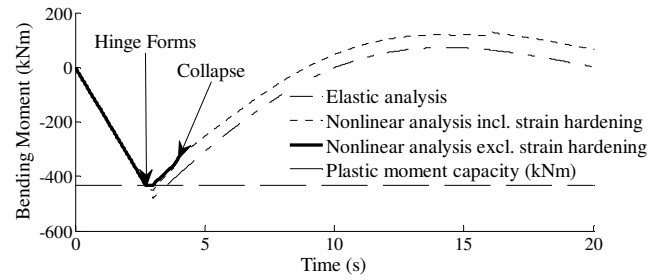
(a) Hinge formation at 3 m;
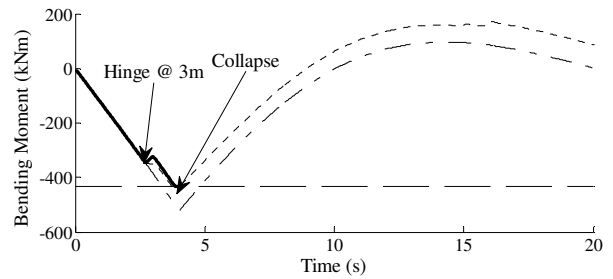
(b) Hinge formation at 4 m;

(c) Bending moment at 10 m through time;

Figure 4. Time history of bending moment.

Table 1. Failure Load Factors.

Loading scenario*	(1)	(2)	(3)
Position (m)	4.3	5.8	---
λ	2.516	2.796	2.524

* Refer to text for description of scenarios.

4.4 Collapse load factors for two point loads travelling in the same direction

A range of inter-load spacings (ILS) for two same-direction 50 kN point loads are considered. The ILS is expressed as a ratio of the spacing (x) to the length of the beam ($L = 20$ m). The elastic critical location collapse load factors (sagging position-λ(1) and hogging position-λ(2)) are found for comparison. The results are shown in Figure 5, expressed as a ratio of the true collapse load factor.

Figure 5 shows that for the majority of inter-load spacings the load factor found using sagging is close to the true collapse load factor. The collapse load factors found using

186

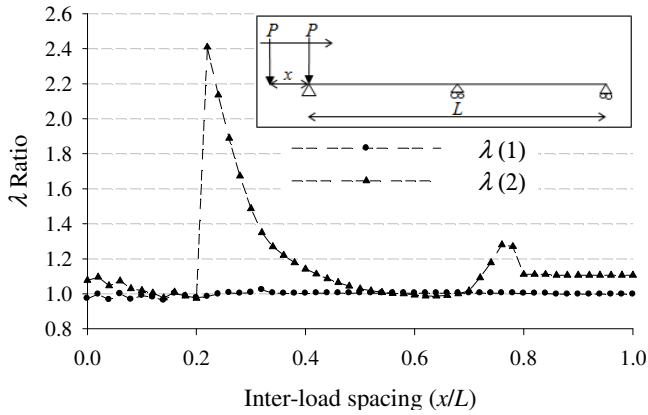hogging are often far higher than the true value, and this could lead to an unsafe assessment.

Figure 5. Two point loads moving in the same direction.

4.5 Collapse load factors for two point loads travelling in opposite directions

Two 50 kN point loads travelling in opposite directions are considered for a range of relative starting positions (again termed inter-load spacings). The results are again compared to those found using the elastic critical locations through a ratio of load factors and are shown in Figure 6.

It can be seen from Figure 6 that similar to the uni-directional case, the elastic sagging critical location generally gives load factors close to the true collapse load factor. However, for an ILS of 0.2 the elastic locations give load factors higher than the true load factors and so are unsafe. Further, for an ILS of around 0.8, the elastic hogging location gives unsafe load factors.
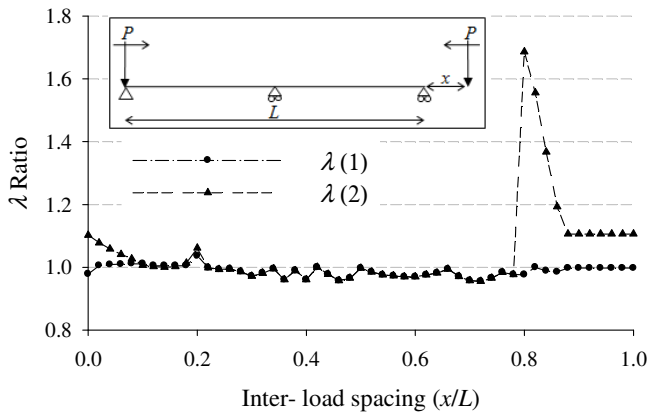

Figure 6. Two point loads moving in opposite directions.

5 PROBABILISTIC ANALYSIS

5.1 Reliability analysis of static loads

Loads located at the critical elastic sagging moment location are examined further using reliability analysis. This is to reflect common practice for bridge reliability analyses [3][15]. The results are compared to the actual failure probabilities obtained using a moving-load nonlinear analysis.

The section plastic moment capacity and the point load are the random variables of the problem and are assumed independent: all other variables are taken to be known. The

coefficients of variation (CoV) of the random variables given in Table 2 are taken from [16] and [17].

Table 2. Statistical Properties.

Variable	μ	CoV	Distribution
M_p	431.16 kNm	0.075	Normal
P	100 kN	0.25	Normal

Only flexural failures are considered and other failure mechanisms were ignored. Two limit sates are considered. An elastic limit state is used in which failure occurs when the elastic moment exceeds the plastic moment capacity:

$$g = M_p - \frac{Pab}{4L^3}\left(4L^2 - a(L+a)\right) \quad (21)$$

This in effect assumes an ideal elastic-plastic material.

Ultimate collapse due to the formation of a mechanism brought about by the formation of plastic hinges is also considered. Virtual work for the collapse mechanism (one hinge forming at the position of the point load and the other at the interior support) gives the plastic limit state function:

$$g = M_p(1+\frac{2a}{b}) - aP \quad (22)$$

5.2 First-order reliability analysis results

The FORM results are given in Table 3 for the two limit state functions of Equations (21) and (22). The functions are plotted in standard normal space (*U*-space) in Figure 6. This allows a visual comparison between reliability indices to be made.It can be seen clearly that a higher reliability index (β) can be achieved when using a less conservative limit state function. This expected result corresponds to a lower probability of failure.

Table 3. FORM Results

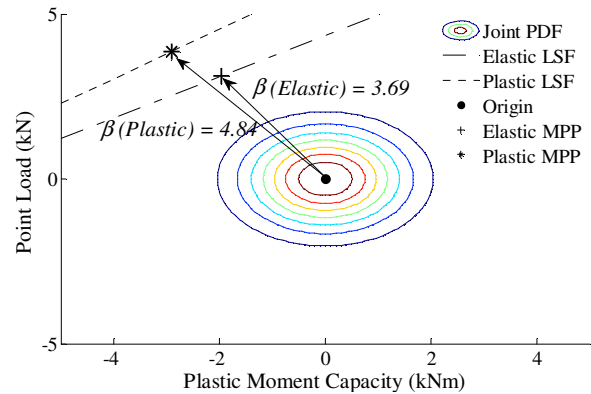|	Elastic	Plastic
β	3.69	4.84
p_f	1.121×10^{-4}	6.492×10^{-7}
M_p (design value)	337.78 kNm	178.186 kNm
P (design value)	336.93 kNm	196.54 kNm

Figure 7. Limit state comparison in standard normal space.

5.3 Importance sampling for reliability analysis of moving load

The common assumption of locating the loads at the elastic critical locations for a reliability analysis is assessed using Importance Sampling and the moving load analysis model. The design point found using the FORM analysis considering a plastic limit state function is used as the MPP for the Importance Sampling (see Section 3). Ten thousand samples are generated around this design point. Each combination of random variables is analysed using a constant speed of 1 m/s and a refined time step of 0.2 s.

A 'success' rate of approximately 50 % is found and so the estimate of MPP is reasonable. Figure 9 gives the histogram of point load locations at failure. All failures occur while the load is on the first span. Most occur when the moving load is positioned 3 metres from the left hand support.
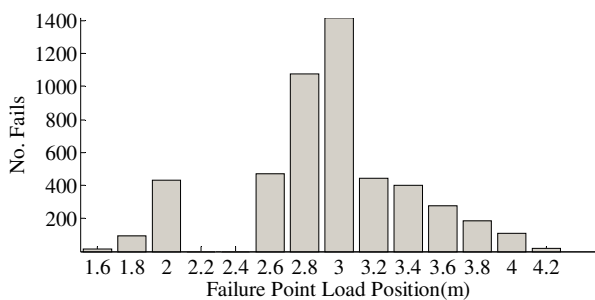

Figure 8. Number of fails at each point load position

A reliability index of 4.84 is found corresponding to a probability of failure of 6.488×10^{-7}. This is only marginally different to the probability of failure found using the plastic static critical load location (Table 3 – $p_f = 6.492 \times 10^{-7}$). This interesting result means that locating the loads using an elastic analysis may not give the true probability of failure.

6 DISCUSSION & CONCLUSIONS

A moving nonlinear analysis method is proposed in this work. The response of an indeterminate steel beam subjected to moving loads is examined and compared to that when subjected to static loads. Both deterministic and probabilistic analyses are performed.

The deterministic study is used to establish load factors causing collapse for moving loads and critically placed static loads. Static load positions were identified as positions causing maximum sagging and hogging bending moments using an elastic analysis. For this particular structure and the various loading scenarios analysed, it is established that the static load factor found using the position causing maximum sagging moment closely relates to the load factor found using the proposed moving load approach. For the majority of circumstances examined the load factor found using the maximum hogging position over-estimates the strength capacity of the structure.

A probabilistic study is presented examining a single static load, using FORM and Importance Sampling when examining a moving load. An elastic limit state function which is typically implemented in practice is analysed and compared to a plastic limit state function. The plastic limit state function has a less conservative definition of failure and produces a higher reliability index and a lower probability of failure as expected.

The reliability index found when analysing the moving load corresponded exactly to that found using a static analysis. The common assumption of locating the point load at a critical position can be deemed appropriate for this structure subjected to a single point load. However the moving load approach provides a more complete overall assessment of failure.

It can be concluded from this study that taking a less conservative definition of failure, significantly higher reliability indices can be found, more indicative of the true safety of the structure. An accurate representation of a structure's nonlinear behaviour when subjected to moving loads can be found using the proposed method. Both these findings when applied to practical problems may lead to a more accurate assessment of existing bridge structures and consequently a more informed decision on required rehabilitation measures.

REFERENCES

[1] Parsons & Brinckerhoff, (2003), A review of bridge assessment failures on the motorway and trunk road network. *Final Project Report prepared for the Highways Agency. Parsons Brinckerhoff Ltd.*

[2] Imhof,D. (2004). *Risk Assessment of Existing Bridge Structures*. Ph.D Thesis. King's College, UK.

[3] Wisniewski D.F., Casas J.R. & Ghosn M, (2009). Simplified probabilistic non-linear assessment of existing railway bridges. *Structure and Infrastructure Engineering: Maintenance, Management, Life-Cycle Design and Performance*. 5, 6, 439-453.

[4] Melchers, R.E., *Structural Reliability Analysis and Prediction*. Sussex: John Wiley and Sons, 1999

[5] Soares, R.C., Mohamed, A., Venturing, W.S. & Lemaitre, M., (2001), Reliability analysis of non-linear reinforced concrete frames using the response surface method. *Journal of Reliability Engineering and System Safety*, 75, 1-16.

[6] Neves, R.A., Chateauneuf, A., Venturini, W.S. & Lemaire, M. (2005), Reliability analysis of reinforced concrete grids with nonlinear material behavior, *Journal of Reliability Engineering and System Safety*. 91,735-744.

[7] Torrii, A.J. & Machado, D.A., (2010), Reliability analysis of nonlinear reinforced concrete beams. *Proceedings for Asociacón Argentina de Mecánica Computacional Conference*, Buenos Aires, Argentina.

[8] Choi, S.K., Grandhi, R.V. & Canfield, R.A., *Reliability - based structural design*. London: Springer, 2007.

[9] Li, G.Q. & Li, J.J., *Advanced Analysis and Design of Steel Frames*. Sussex: John Wiley & Sons, 2007.

[10] Ghali, A. Neville, A & Brown, T., *Structural Analysis-A unified classical and matrix approach*. London: Spon Press, 2009.

[11] Becker, A., *An Introductory Guide to Finite Element Analysis*. Suffolk: Professional Engineering Publishing, 2004.

[12] Chen, W., Goto, Y. & Richard Liew, J., *Stability Design of Semi-Rigid Frames*. New York: John Wiley & Son, 1996.

[13] Val, D., Bluger, F. & Yankelevsky D., (1997), Reliability evaluation in nonlinear analysis of reinforced concrete structures. *Journal of Structural Safety, 19, 2,203-21*.

[14] Ghosn, M & Moses, F., Redundancy in highway bridge superstructures. NCHRP Report. 406, TRB - Transportation Research Board, Washington D.C., 1998.

[15] Biondini, F., Bontempi, F., Frangopol, D., & Melerba, P.,(2004), Reliability of material and geometrically non-linear reinforced and prestressed concrete structures, *Computers and Structures* 82, 1021 - 1031.

[16] Ellingwood, B.R. and Galambos,T.V.,(1982), Probability -based criteria for structural design, *Journal of Structural Safety*,1, 15 - 26

[17] Nowak, A.S. & Park, C.H. (2001), R*eliability analysis of prestressed concrete bridge g*irders: comparison of Eurocode, Spanish Norma IAP and AASHTO. *Journal of Structural Safety* 23,331-344.